

NOAA Technical Report NOS CS 9

THREE-DIMENSIONAL HYDRODYNAMIC MODEL DEVELOPMENTS FOR A GALVESTON BAY NOWCAST/FORECAST SYSTEM

Silver Spring, Maryland
November 2000



noaa National Oceanic and Atmospheric Administration

U.S. DEPARTMENT OF COMMERCE
National Ocean Service
Coast Survey Development Laboratory
Marine Modeling and Analysis Programs

Office of Coast Survey
National Ocean Service
National Oceanic and Atmospheric Administration
U.S. Department of Commerce

The Office of Coast Survey (CS) is the Nation's only official chartmaker. As the oldest United States scientific organization, dating from 1807, this office has a long history. Today it promotes safe navigation by managing the National Oceanic and Atmospheric Administration's (NOAA) nautical chart and oceanographic data collection and information programs.

There are four components of CS:

The Coast Survey Development Laboratory develops new and efficient techniques to accomplish Coast Survey missions and to produce new and improved products and services for the maritime community and other coastal users.

The Marine Chart Division collects marine navigational data to construct and maintain nautical charts, Coast Pilots, and related marine products for the United States.

The Hydrographic Surveys Division directs programs for ship and shore-based hydrographic survey units and conducts general hydrographic survey operations.

The Navigation Services Division is the focal point for Coast Survey customer service activities, concentrating predominantly on charting issues, fast-response hydrographic surveys and Coast Pilot updates.

THREE-DIMENSIONAL HYDRODYNAMIC MODEL DEVELOPMENTS FOR A GALVESTON BAY NOWCAST/FORECAST SYSTEM

Richard A. Schmalz, Jr.
November 2000



noaa National Oceanic and Atmospheric Administration

U.S. DEPARTMENT
OF COMMERCE
Norman Y. Mineta, Secretary

National Oceanic and
Atmospheric Administration
D. James Baker, Under Secretary

National Ocean Service
Margaret A. Davidson
Acting Assistant Administrator

Office of Coast Survey
Captain David MacFarland

Coast Survey Development
Laboratory
Bruce Parker

NOTICE

Mention of a commercial company or product does not constitute an endorsement by NOAA. Use for publicity or advertising purposes of information from this publication concerning proprietary products or the tests of such products is not authorized.

TABLE OF CONTENTS

LIST OF FIGURES	iv
LIST OF TABLES	xi
GALVESTON BAY BASE MAP	xiii
EXECUTIVE SUMMARY	xvii
1. INTRODUCTION	1
2. BAY AND CHANNEL MODEL DEVELOPMENTS	3
2.1. Bottom Emergence/Submergence Scheme	3
2.2. Salinity Flux Corrected Transport Scheme	4
2.3. Atmospheric Heat Flux Formulation	5
2.4. Barnes Interpolation of Meteorological Variables	9
2.5. Channel Model Grid Resolution Considerations	18
2.6. Composite Channel Grid Generation	18
2.7. One-way Channel Coupling Algorithm	19
3. BAY MODEL HINDCASTS	27
3.1. Initial Conditions	27
3.2. Boundary Conditions	27
3.3. Simulation Results	32
4. BAY MODEL WATER LEVEL SENSITIVITY ANALYSIS	75
4.1. Experiment Set 1	75
4.2. Experiment Set 2	94
5. ONE-WAY COUPLED BAY AND CHANNEL MODEL HINDCAST	107
5.1. Galveston Bay Model	107
5.2. Houston Ship Channel Model	114
5.3. Coupling Mechanism Assessment	119
5.4. Error Budget	122
6. CONCLUSIONS AND RECOMMENDATIONS	163
ACKNOWLEDGEMENTS	164
REFERENCES	165

LIST OF FIGURES

Galveston Bay Base Map	xiii
PORTS Base Map	xiv
Tide Gauge Base Map	xv
Current Meter Base Map	xvi
Figure 2.1. Interpolation Meteorological Station Locations	11
Figure 2.2. JD 167.0 1995 One-step Barnes Interpolated Wind Speed (m/s) over Galveston Bay	12
Figure 2.3. JD 167.0 1995 $1/r^2$ Interpolated Wind Speed (m/s) over Galveston Bay	13
Figure 2.4. JD 167.0 1995 One-step Barnes Interpolated Windfield (m/s) over Galveston Bay	14
Figure 2.5. JD 167.0 1995 $1/r^2$ Interpolated Windfield (m/s) over Galveston Bay	15
Figure 2.6. JD 167.0 1995 One-step Barnes Interpolated Sea-level Atmospheric Pressure (mb) over Galveston Bay	16
Figure 2.7. JD 167.0 1995 $1/r^2$ Barnes Interpolated Sea-level Atmospheric Pressure (mb) over Galveston Bay	17
Figure 2.8. Houston Ship Channel Model Subgrid 1: Bay Entrance Section	20
Figure 2.9. Houston Ship Channel Model Subgrid 2: Bay Entrance to Morgans Point	21
Figure 2.10. Houston Ship Channel Model Subgrid 3: Above Morgans Point	22
Figure 2.11. Houston Ship Channel Model Composite Computational Grid	23
Figure 2.12. Galveston Bay Model Bathymetry (m relative to MTL)	24
Figure 2.13. Houston Ship Channel Model Bathymetry (m relative to MTL) In the Vicinity of the Entrance to Galveston Bay	25
Figure 3.1. Texas Water Development Board Salinity and Temperature Station Locations	38
Figure 3.2. Initial Near-surface Salinity Field (PSU) 1 January 1995	39
Figure 3.3. Initial Near-bottom Salinity Field (PSU) 1 January 1995	39
Figure 3.4. Initial Near-surface Salinity Field (PSU) 1 October 1994	40
Figure 3.5. Initial Near-bottom Salinity Field (PSU) 1 October 1994	40
Figure 3.6. Initial Near-surface Temperature Field (°C) 1 January 1995	41
Figure 3.7. Initial Near-bottom Temperature Field (°C) 1 January 1995	41
Figure 3.8. Initial Near-surface Temperature Field (°C) 1 October 1994	42
Figure 3.9. Initial Near-bottom Temperature Field (°C) 1 October 1994	42
Figure 3.10. USGS Average Daily Flows Buffalo Bayou at Piney Point, TX in January 1995	43
Figure 3.11. USGS Average Daily Flows Trinity River at Romayor, TX in January 1995	43

LIST OF FIGURES

Figure 3.12. USGS Average Daily Flows San Jacinto River near Sheldon, TX in January 1995	44
Figure 3.13. USGS Average Daily Flows Buffalo Bayou at Piney Point, TX in October 1994	44
Figure 3.14. USGS Average Daily Flows Trinity River at Romayor, TX in October 1994	45
Figure 3.15. USGS Average Daily Flows San Jacinto River near Sheldon, TX in October 1994	45
Figure 3.16. JD 1 (1995) Barnes Interpolation Windfield	46
Figure 3.17. JD 1 (1995) Barnes Interpolation Windspeed Contours	47
Figure 3.18. JD 11 (1995) Barnes Interpolation Windfield	48
Figure 3.19. JD 11 (1995) Barnes Interpolation Windspeed Contours	49
Figure 3.20. JD 21 (1995) Barnes Interpolation Windfield	50
Figure 3.21. JD 21 (1995) Barnes Interpolation Windspeed Contours	51
Figure 3.22. JD 274 (1994) Barnes Interpolation Windfield	52
Figure 3.23. JD 274 (1994) Barnes Interpolation Windspeed Contours	53
Figure 3.24. JD 284 (1994) Barnes Interpolation Windfield	54
Figure 3.25. JD 284 (1994) Barnes Interpolation Windspeed Contours	55
Figure 3.26. JD 294 (1994) Barnes Interpolation Windfield	56
Figure 3.27. JD 294 (1994) Barnes Interpolation Windspeed Contours	57
Figure 3.28. Galveston Pleasure Pier Subtidal Water Level Signal during January 1995	58
Figure 3.29. Galveston Pleasure Pier Subtidal Water Level Signal during October 1994	58
Figure 3.30. Galveston Pleasure Pier Simulated vs Observed Water Level Comparison during January 1995	59
Figure 3.31. Galveston Pier 21 Simulated vs Observed Water Level Comparison during January 1995	59
Figure 3.32. Christmas Bay Simulated vs Observed Water Level Comparison during January 1995	60
Figure 3.33. Port Bolivar Simulated vs Observed Water Level Comparison during January 1995	60
Figure 3.34. Eagle Point Simulated vs Observed Water Level Comparison during January 1995	61
Figure 3.35. Clear Lake Simulated vs Observed Water Level Comparison during January 1995	61
Figure 3.36. Morgans Point Simulated vs Observed Water Level Comparison during January 1995	62
Figure 3.37. Round Point Simulated vs Observed Water Level Comparison during January 1995	62
Figure 3.38. Rollover Pass Simulated vs Observed Water Level Comparison during January 1995	63

LIST OF FIGURES

Figure 3.39. High Island Point Simulated vs Observed Water Level Comparison during January 1995	63
Figure 3.40. Galveston Pleasure Pier Simulated vs Observed Water Level Comparison during October 1994	64
Figure 3.41. Galveston Pier 21 Simulated vs Observed Water Level Comparison during October 1994	64
Figure 3.42. Port Bolivar Simulated vs Observed Water Level Comparison during October 1994	65
Figure 3.43. Eagle Point Simulated vs Observed Water Level Comparison during October 1994	65
Figure 3.44. Clear Lake Simulated vs Observed Water Level Comparison during October 1994	66
Figure 3.45. Morgans Point Simulated vs Observed Water Level Comparison during October 1994	66
Figure 3.46. Dollar Point Simulated vs Observed Salinity Comparison during January 1995	67
Figure 3.47. Trinity Bay (DBC) Simulated vs Observed Salinity Comparison during January 1995	67
Figure 3.48. Hannah Reef Point Simulated vs Observed Salinity Comparison during January 1995	68
Figure 3.49. Red Bluff Simulated vs Observed Salinity Comparison during January 1995	68
Figure 3.50. Port Bolivar Simulated vs Observed Salinity Comparison during October 1994	69
Figure 3.51. Trinity Bay (DBC) Simulated vs Observed Salinity Comparison during October 1994	69
Figure 3.52. Dollar Point Simulated vs Observed Salinity Comparison during October 1994	70
Figure 3.53. Red Bluff Simulated vs Observed Salinity Comparison during October 1994	70
Figure 3.54. Dollar Point Bolivar Simulated vs Observed Temperature Comparison during January 1995	71
Figure 3.55. Trinity Bay (DBC) Simulated vs Observed Temperature Comparison during January 1995	71
Figure 3.56. Hannah Reef Simulated vs Observed Temperature Comparison during January 1995	72
Figure 3.57. Red Bluff Simulated vs Observed Temperature Comparison during January 1995	72
Figure 3.58. Port Bolivar Simulated vs Observed Temperature Comparison during October 1994	73
Figure 3.59. Trinity Bay (DBC) Simulated vs Observed Temperature Comparison during October 1994	73

LIST OF FIGURES

Figure 3.60. Dollar Point Simulated vs Observed Temperature Comparison during October 1994	74
Figure 3.61. Red Bluff Simulated vs Observed Temperature Comparison during October 1994	74
Figure 4.1. Galveston Bay - Bay, Shelf, and Gulf of Mexico Windfield Definition	80
Figure 4.2. Galveston Bay Water Level Sensitivity Analysis Station Locations	81
Figure 4.3. Experiment Set 1 Experiment 1 Water Level Time Series Response Comparisons at Morgans Point	82
Figure 4.4. Experiment Set 1 Experiment 1 Water Level Time Series Response Comparisons at Galveston Pier 21	83
Figure 4.5. Experiment Set 1 Experiment 1 Water Level Time Series Response Comparisons at Galveston Pleasure	84
Figure 4.6. Experiment Set 1 Experiment 2 Water Level Time Series Response Comparisons at Morgans Point	85
Figure 4.7. Experiment Set 1 Experiment 2 Water Level Time Series Response Comparisons at Galveston Pier 21	86
Figure 4.8. Experiment Set 1 Experiment 2 Water Level Time Series Response Comparisons at Galveston Pleasure	87
Figure 4.9. Experiment Set 1 Experiment 4 Water Level Time Series Response Comparisons at Morgans Point	88
Figure 4.10. Experiment Set 1 Experiment 4 Water Level Time Series Response Comparisons at Galveston Pier 21	89
Figure 4.11. Experiment Set 1 Experiment 4 Water Level Time Series Response Comparisons at Galveston Pleasure Pier	90
Figure 4.12. Experiment Set 1 Experiment 5 Water Level Time Series Response Comparisons at Morgans Point	91
Figure 4.13. Experiment Set 1 Experiment 5 Water Level Time Series Response Comparisons at Galveston Pier 21	92
Figure 4.14. Experiment Set 1 Experiment 5 Water Level Time Series Response Comparisons at Galveston Pleasure Pier	93
Figure 4.15. Experiment Set 2 Experiment 1 Water Level Time Series Response Comparisons at Morgans Point	97
Figure 4.16. Experiment Set 2 Experiment 1 Water Level Time Series Response Comparisons at Galveston Pier 21	98
Figure 4.17. Experiment Set 2 Experiment 1 Water Level Time Series Response Comparisons at Galveston Pleasure Pier	99
Figure 4.18. Experiment Set 2 Experiment 2 Water Level Time Series Response Comparisons at Morgans Point	100
Figure 4.19. Experiment Set 2 Experiment 2 Water Level Time Series Response Comparisons at Galveston Pier 21	101

LIST OF FIGURES

Figure 4.20. Experiment Set 2 Experiment 2 Water Level Time Series Response Comparisons at Galveston Pleasure Pier	102
Figure 4.21. Experiment Set 2 Experiment 4 Water Level Time Series Response Comparisons at Morgans Point	103
Figure 4.22. Experiment Set 2 Experiment 4 Water Level Time Series Response Comparisons at Galveston Pier 21	104
Figure 4.23. Experiment Set 2 Experiment 4 Water Level Time Series Response Comparisons at Galveston Pleasure Pier	105
Figure 5.1. Initial Near-surface Salinity Field 1 April 1996	127
Figure 5.2. Initial Near-bottom Salinity Field 1 April 1996	127
Figure 5.3. Initial Near-surface Temperature Field 1 April 1996	128
Figure 5.4. Initial Near-bottom Temperature Field 1 April 1996	128
Figure 5.5. USGS Average Daily Flows Buffalo Bayou at Piney Point, TX in April 1996	129
Figure 5.6. USGS Average Daily Flows Trinity River at Romayor, TX in April 1996	129
Figure 5.7. JD 101 Barnes Interpolation Windfield	130
Figure 5.8. JD 101 Barnes Interpolation Windspeed Contours	131
Figure 5.9. JD 111 Barnes Interpolation Windfield	132
Figure 5.10. JD 111 Barnes Interpolation Windspeed Contours	133
Figure 5.11. JD 121 Barnes Interpolation Windfield	134
Figure 5.12. JD 121 Barnes Interpolation Windspeed Contours	135
Figure 5.13. Galveston Pleasure Pier Subtidal Water Level Signal during April 1996	136
Figure 5.14. GBM: Galveston Pleasure Pier Simulated vs Observed Water Level Comparison during April 1996	136
Figure 5.15. GBM: Galveston Pier 21 Simulated vs Observed Water Level Comparison during April 1996	137
Figure 5.16. GBM: Port Bolivar Simulated vs Observed Water Level Comparison during April 1996	137
Figure 5.17. GBM: Eagle Point Simulated vs Observed Water Level Comparison during April 1996	138
Figure 5.18. GBM: Clear Lake Simulated vs Observed Water Level Comparison during April 1996	138
Figure 5.19. GBM: Morgans Point Simulated vs Observed Water Level Comparison during April 1996	139
Figure 5.20. GBM: Umbrella Point Simulated vs Observed Water Level Comparison during April 1996	139
Figure 5.21. GBM: Lynchburg Landing Simulated vs Observed Water Level Comparison during April 1996	140
Figure 5.22. GBM: Manchester Dock 2 Simulated vs Observed Water Level Comparison during April 1996	140

LIST OF FIGURES

Figure 5.23. GBM: Bolivar Roads (PORTS) Simulated vs Observed Principal Component Direction Current Comparison during April 1996	141
Figure 5.24. GBM: Redfish Bar (PORTS) Simulated vs Observed Principal Component Direction Current Comparison during April 1996	142
Figure 5.25. GBM: Morgans Point (PORTS) Simulated vs Observed Principal Component Direction Current Comparison during April 1996	143
Figure 5.26. GBM: Trinity Bay (DBC) Simulated vs Observed Salinity Comparison during April 1996	144
Figure 5.27. GBM: Hannah Reef Simulated vs Observed Salinity Comparison during April 1996	144
Figure 5.28. GBM: Red Bluff Simulated vs Observed Salinity Comparison during April 1996	145
Figure 5.29. GBM: Port Bolivar Simulated vs Observed Salinity Comparison during April 1996	145
Figure 5.30. GBM: Trinity Bay (DBC) Simulated vs Observed Temperature Comparison during April 1996	146
Figure 5.31. GBM: Hannah Reef Simulated vs Observed Temperature Comparison during April 1996	146
Figure 5.32. GBM: Red Bluff Simulated vs Observed Temperature Comparison during April 1996	147
Figure 5.33. GBM: Port Bolivar Simulated vs Observed Temperature Comparison during April 1996	147
Figure 5.34. HSCM: JD 101 Barnes Interpolation Windfield	148
Figure 5.35. HSCM: JD 101 Barnes Interpolation Windspeed Contours	149
Figure 5.36. HSCM: JD 111 Barnes Interpolation Windfield	150
Figure 5.37. HSCM: JD 111 Barnes Interpolation Windspeed Contours	151
Figure 5.38. HSCM: JD 121 Barnes Interpolation Windfield	152
Figure 5.39. HSCM: JD 121 Barnes Interpolation Windspeed Contours	153
Figure 5.40. HSCM: Galveston Pier 21 Simulated vs Observed Water Level Comparison during April 1996	154
Figure 5.41. HSCM: Port Bolivar Simulated vs Observed Water Level Comparison during April 1996	154
Figure 5.42. HSCM: Eagle Point Simulated vs Observed Water Level Comparison during April 1996	155
Figure 5.43. HSCM: Morgans Point Simulated vs Observed Water Level Comparison during April 1996	155
Figure 5.44. HSCM: Lynchburg Landing Simulated vs Observed Water Level Comparison during April 1996	156
Figure 5.45. HSCM: Manchester Dock 2 Simulated vs Observed Water Level Comparison during April 1996	156

LIST OF FIGURES

Figure 5.46. HSCM: Bolivar Roads (PORTS) Simulated vs Observed Principal Component Direction Current Comparison during April 1996	157
Figure 5.47. HSCM: Redfish Bar (PORTS) Simulated vs Observed Principal Component Direction Current Comparison during April 1996	158
Figure 5.48. HSCM: Morgans Point (PORTS) Simulated vs Observed Principal Component Direction Current Comparison during April 1996	159
Figure 5.49. HSCM: Port Bolivar Simulated vs Observed Salinity Comparison during April 1996	160
Figure 5.50. HSCM: Red Bluff Simulated vs Observed Salinity Comparison during April 1996	160
Figure 5.51. HSCM: Port Bolivar Simulated vs Observed Temperature Comparison during April 1996	161
Figure 5.52. HSCM: Red Bluff Simulated vs Observed Temperature Comparison during April 1996	161

LIST OF TABLES

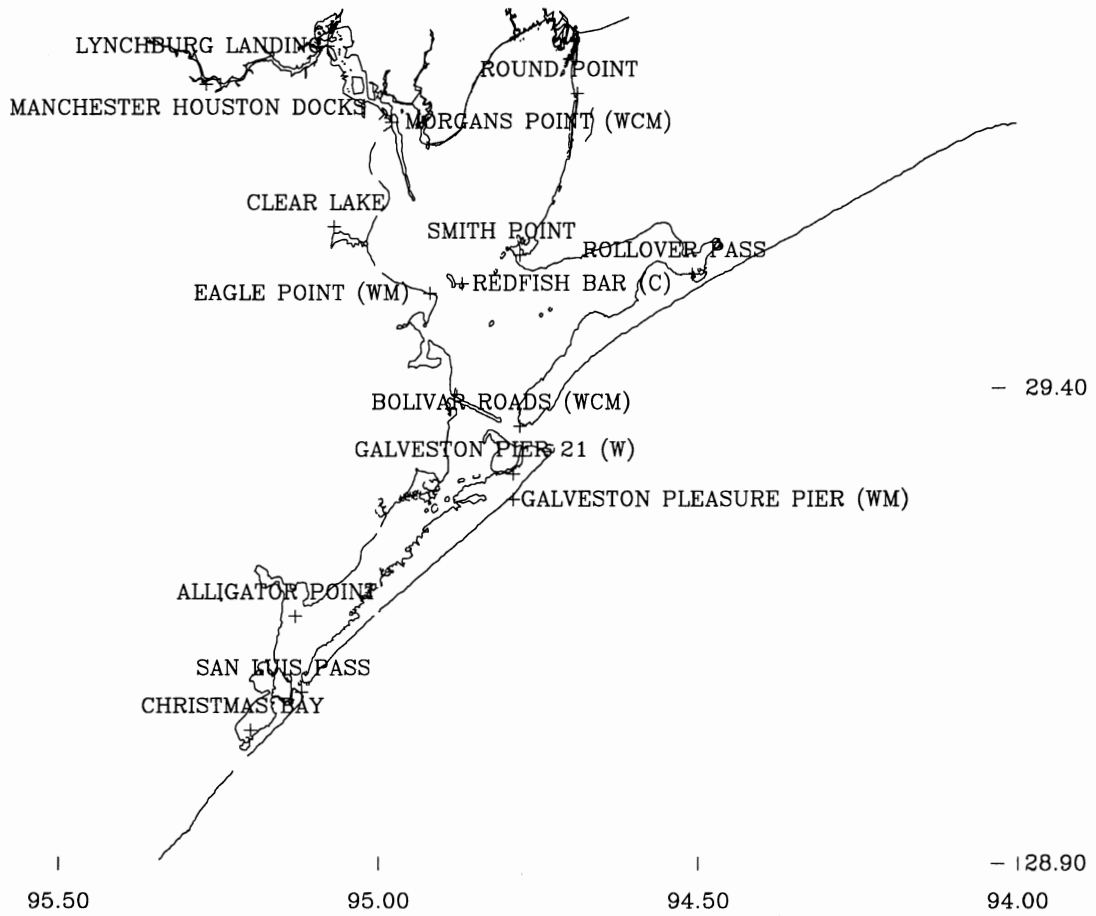
Table 2.1. Emergence/Submergence Scheme Flux Adjustments	5
Table 3.1. January 1995 Galveston Bay Model Barnes Interpolation Summary	30
Table 3.2. October 1994 Galveston Bay Model Barnes Interpolation Summary	31
Table 3.3. January 1995 Hindcast Water Surface Elevation Comparisons	33
Table 3.4. October 1994 Hindcast Water Surface Elevation Comparisons	34
Table 3.5. January 1995 Mid-depth Salinity Comparisons	36
Table 3.6. October 1994 Mid-depth Salinity Comparisons	36
Table 3.7. January 1995 Mid-depth Temperature Comparisons	37
Table 3.8. October 1994 Mid-depth Temperature Comparisons	37
Table 4.1. January 1995 Sensitivity Analysis Experiment Set 1	76
Table 4.2. Experiment Set 1 Water Level Response RMS and Relative Error Statistics	78
Table 4.3. Experiment Set 1 Mean Water Level Response	79
Table 4.4. October 1994 Sensitivity Analysis Experiment Set 2	94
Table 4.5. Experiment Set 2 Water Level Response RMS and Relative Error Statistics	96
Table 4.6. Experiment Set 2 Mean Water Level Response	96
Table 5.1. April 1996 Galveston Bay Model Barnes Interpolation Summary	109
Table 5.2. Galveston Bay Model April 1996 Hindcast Water Surface Elevation Comparisons	110
Table 5.3. Galveston Bay Model April 1996 Principal Flood Direction Comparisons	112
Table 5.4. Galveston Bay Model April 1996 Principal Component Direction Current Comparisons	112
Table 5.5. Galveston Bay Model April 1996 Mid-depth Salinity Comparisons	113
Table 5.6. Galveston Bay Model April 1996 Mid-depth Temperature Comparisons	113
Table 5.7. April 1996 Houston Ship Channel Model Barnes Interpolation Summary	115
Table 5.8. Houston Ship Channel Model April 1996 Hindcast Water Surface Elevation Comparisons	116
Table 5.9. Houston Ship Channel Model April 1996 Principal Flood Direction Comparisons	117
Table 5.10. Houston Ship Channel Model April 1996 Principal Component Direction Current Comparisons	118
Table 5.11. Houston Ship Channel Model April 1996 Mid-depth Salinity Comparisons	118

LIST OF TABLES

Table 5.12. Houston Ship Channel Model April 1996 Mid-depth Temperature Comparisons	119
Table 5.13. Demeaned Water Level GBM and HSCM Model April 1996 Comparisons	120
Table 5.14. Galveston Bay Model vs Houston Ship Channel Model April 1996 Principal Component Direction Comparisons	120
Table 5.15. Galveston Bay Model vs Houston Ship Channel Model April 1996 Principal Component Direction Current at Prediction Depth Comparisons	121
Table 5.16. Galveston Bay Model vs Houston Ship Channel Model Bathymetry Comparisons	121
Table 5.17. Galveston Bay Model Offshore, West Bay, and East Bay 29-day Harmonic Analysis Summary	123
Table 5.18. Galveston Bay Model Water Surface Elevation 29-day Harmonic Analysis Summary	124
Table 5.19. Galveston Bay Model vs Houston Ship Channel Model Water Surface Elevation 29-day Harmonic Analysis Comparison	124
Table 5.20. April 1996 Water Surface Elevation RMS Error Budget	125
Table 5.21. Galveston Bay Model vs Houston Ship Channel Model Principal Component Direction Current at Prediction Depth 29-day Harmonic Analysis Comparison	126
Table 5.22. April 1996 Principal Component Direction Current at Prediction Depth RMS Error Budget	126

GALVESTON BAY BASE MAP

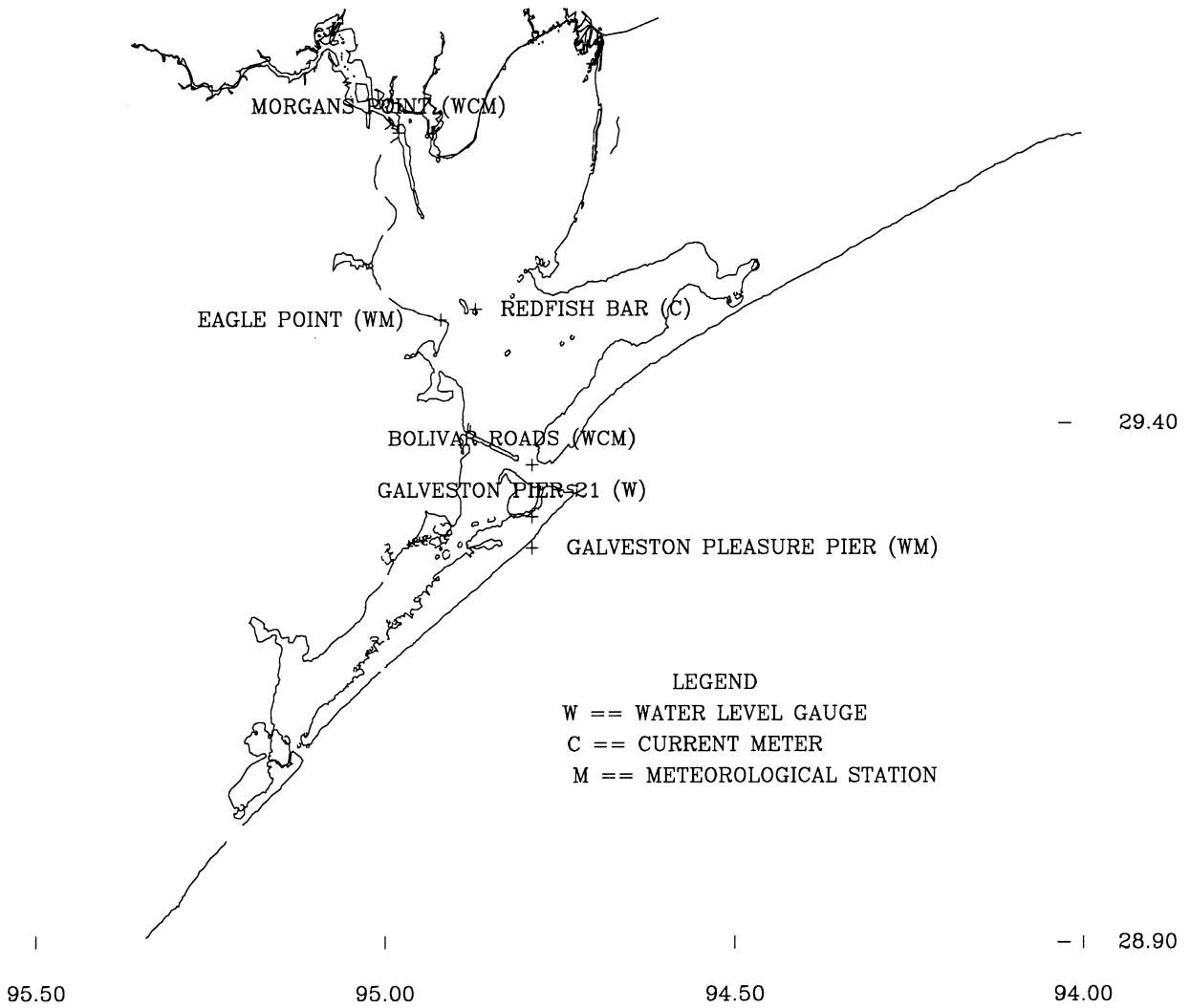
- 29.90



Galveston Bay Base Map

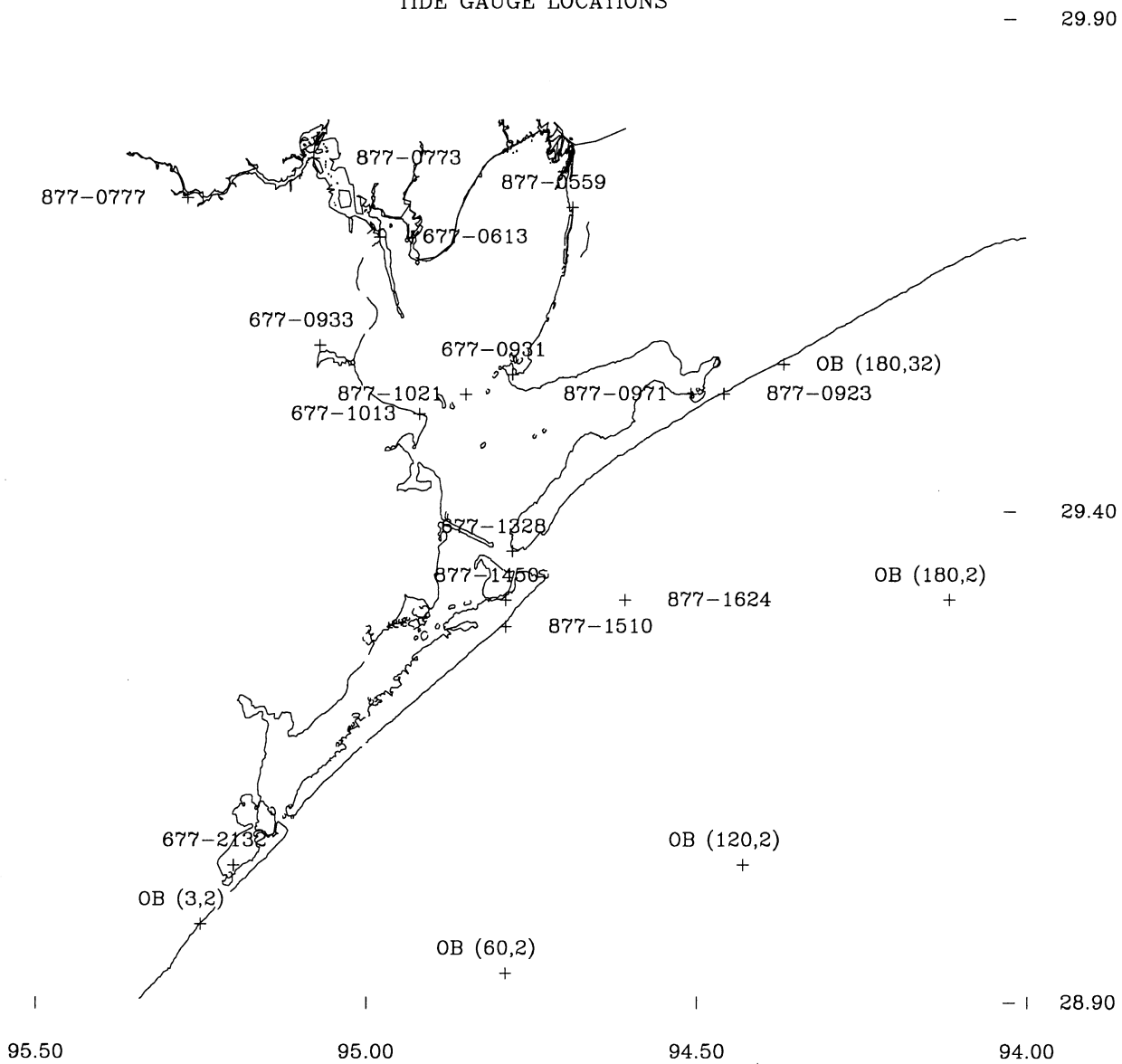
PORTS LOCATIONS

- 29.90



PORTS Base Map

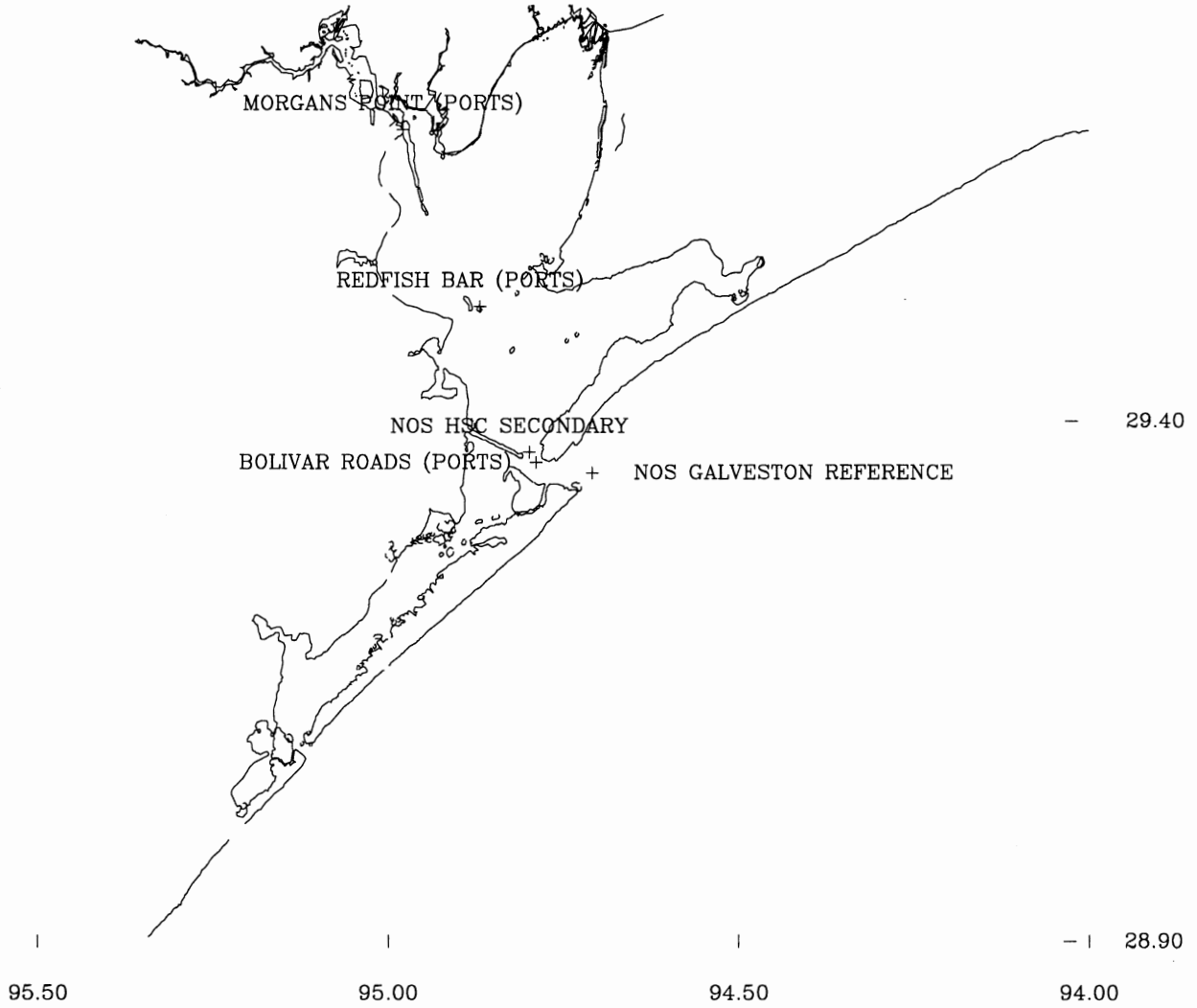
TIDE GAUGE LOCATIONS



Tide Gauge Base Map

CURRENT METER LOCATIONS

- 29.90



Current Meter Base Map

EXECUTIVE SUMMARY

The National Oceanic and Atmospheric Administration installed a Physical Oceanographic Real Time System (PORTS) in June 1996 in Galveston Bay. Water surface elevation, currents at prediction depth (4.6m) as well as near-surface and near-bottom temperature and salinity, and meteorological information are available at six-minute intervals. To complement the PORTS a nowcast/forecast system is being developed. The hydrodynamic model component is based on the NOS three-dimensional Galveston Bay hydrodynamic model (Schmalz, 1996) developed in the NOS Partnership Program to support Differential Global Positioning System hydrographic surveys. Based on nowcast/forecast requirements the model has been extended to include a bottom emergence/submergence algorithm, a Flux Corrected Transport (FCT) salinity scheme, and atmospheric heat flux routines. In addition, the $1/r^2$ interpolation procedure of meteorological fields has been enhanced by the implementation of a multi-step Barnes (1973) interpolation method.

This refined Bay model was applied to the October 1994 flood of record and demeaned simulated water levels were in agreement with demeaned observations to order 8 cm in standard deviation (SD). Initial salinity and temperature fields were based on adjustment of climatology. The adjustment could only be performed in an average sense due to the lack of observations. The salinity field adjustment time length is a function of previous freshwater inflow patterns. In the case of the October 1994 flood, the effect of the initial conditions was removed immediately within a single day after the flooding. The after flood simulated salinity response exhibited no over- or under-shooting and was positive definite, and was in excellent agreement with observations indicating the effectiveness of the FCT scheme in handling the large horizontal salinity gradients.

The refined Bay model was then applied to the January 1995 "Northers", during which observed water depths at Round Point went to zero. While simulated water depths remained nonzero, demeaned simulated water levels were in agreement with demeaned observations to order 8 cm in SD. Additional hindcast studies are needed to further evaluate the bottom emergence/submergence scheme and to aid in the potential development of a overland flooding scheme. The errors in the initial salinity field persisted throughout the simulation period, which represented a period of modest freshwater inflow.

Both the October 1994 and January 1995 hindcast water temperatures appeared to be order 2 to 3 °C cooler than observations. An area of further research is the incoming solar radiation mechanics in particular the transmissivity of the earth's atmosphere.

A water level sensitivity analysis of winds and freshwater inflows was performed using the Galveston Bay Model. NOS windfield interpolation techniques are consistent with those developed at Texas A&M University and provide reasonably accurate nowcast windfields; e.g., demeaned water levels are generated in agreement with demeaned observations in the Upper Bay to order 10 cm in SD. The pursuit of additional improvements in Bay windfields using local high resolution atmospheric models is warranted based on the sensitivities shown here. Based on the sensitivity tests performed, it appears that the Galveston Bay nowcast/forecast system represents an extremely challenging problem. Accurate subtidal water level forecasts, Bay windfield forecasts, and streamflow forecasts are all necessary requirements for the system.

EXECUTIVE SUMMARY

The National Oceanic and Atmospheric Administration installed a Physical Oceanographic Real Time System (PORTS) in June 1996 in Galveston Bay. Water surface elevation, currents at prediction depth (4.6m) as well as near-surface and near-bottom temperature and salinity, and meteorological information are available at six-minute intervals. To complement the PORTS a nowcast/forecast system is being developed. The hydrodynamic model component is based on the NOS three-dimensional Galveston Bay hydrodynamic model (Schmalz, 1996) developed in the NOS Partnership Program to support Differential Global Positioning System hydrographic surveys. Based on nowcast/forecast requirements the model has been extended to include a bottom emergence/submergence algorithm, a Flux Corrected Transport (FCT) salinity scheme, and atmospheric heat flux routines. In addition, the $1/r^2$ interpolation procedure of meteorological fields has been enhanced by the implementation of a multi-step Barnes (1973) interpolation method.

This refined Bay model was applied to the October 1994 flood of record and demeaned simulated water levels were in agreement with demeaned observations to order 8 cm in standard deviation (SD). Initial salinity and temperature fields were based on adjustment of climatology. The adjustment could only be performed in an average sense due to the lack of observations. The salinity field adjustment time length is a function of previous freshwater inflow patterns. In the case of the October 1994 flood, the effect of the initial conditions was removed immediately within a single day after the flooding. The after flood simulated salinity response exhibited no over- or under-shooting and was positive definite, and was in excellent agreement with observations indicating the effectiveness of the FCT scheme in handling the large horizontal salinity gradients.

The refined Bay model was then applied to the January 1995 "Northers", during which observed water depths at Round Point went to zero. While simulated water depths remained nonzero, demeaned simulated water levels were in agreement with demeaned observations to order 8 cm in SD. Additional hindcast studies are needed to further evaluate the bottom emergence/submergence scheme and to aid in the potential development of a overland flooding scheme. The errors in the initial salinity field persisted throughout the simulation period, which represented a period of modest freshwater inflow.

Both the October 1994 and January 1995 hindcast water temperatures appeared to be order 2 to 3 °C cooler than observations. An area of further research is the incoming solar radiation mechanics in particular the transmissivity of the earth's atmosphere.

A water level sensitivity analysis of winds and freshwater inflows was performed using the Galveston Bay Model. NOS windfield interpolation techniques are consistent with those developed at Texas A&M University and provide reasonably accurate nowcast windfields; e.g., demeaned water levels are generated in agreement with demeaned observations in the Upper Bay to order 10 cm in SD. The pursuit of additional improvements in Bay windfields using local high resolution atmospheric models is warranted based on the sensitivities shown here. Based on the sensitivity tests performed, it appears that the Galveston Bay nowcast/forecast system represents an extremely challenging problem. Accurate subtidal water level forecasts, Bay windfield forecasts, and streamflow forecasts are all necessary requirements for the system.

A fine resolution Houston Ship Channel Model was developed and one-way coupled to the Galveston Bay hindcast model. The two models combined are used to form the initial hydrodynamic component of an experimental nowcast/forecast system. They were applied using a SST specification to the April 1996 PORTS beta test period to simulate water levels and currents. Simulated water temperatures were within 1 to 2 °C RMS of observations. The SST specification appears to be sufficient for the nowcast/forecast studies, thereby eliminating the need for further calibration of the heat flux algorithm. Water level standard deviations were order 8 cm. Principal flood directions errors were order 25 degrees, while current speed errors were order 15 to 25 cm/s in both models. However, the current speeds are improved in the Channel model above Redfish Bar. There is some indication that the bathymetry used in the Channel model may be inappropriate through the lower Bay. The more recent 1988 hydrographic datasets for Galveston Bay should be used to update both model bathymetries.

Water level errors are summarized in Table 1 and meet the standard deviation target of order 10 cm. At Galveston Pleasure Pier on the Gulf coast the standard deviation to mean diurnal range ratio was near 10%. Due to the reduced tidal ranges within the lower and upper Galveston Bay regions, the ratios approached 20 to 30%.

Prediction depth principal component errors are summarized in Table 2a for directions and in Table 2b for current strengths. Direction errors are order 25 degrees; equal to the target set. RMS error in current speeds were order 20 cm/s; below the 0.5 kt target. The ratios of the RMS error to mean diurnal range were from 10 to 25%.

A significant portion of the water level and current errors are in the astronomical tidal component in both models, based upon the results of the error budget analysis reported here. As a result, additional experiments should be performed focusing on improving the tidal response. Refined tidal boundary conditions and further adjustment of bottom friction should be considered. Since the Galveston Bay Model appears to be damped, an increase of tidal amplitude of order 10 percent may be investigated in the future. Additional work on specifying the subtidal signal along the Galveston Bay Model open boundary may also be undertaken. There is some indication that a smoothing of the subtidal signal would reduce the oscillations in simulated coastal water levels. Within the Houston Ship Channel Model, a velocity/transport boundary condition might be explored in addition to further adjustments of the present internal mode radiation scheme.

Of concern is the availability of measurements to assess these three-dimensional models. For water surface elevation, this may be less of a problem than for currents and density. One approach towards alleviating this concern would be to broaden the PORTS system philosophy. Several mobile instrument packs (Mobile-PORTS) might be incorporated to allow for the acquisition of additional data throughout the system in non realtime. The basic navigational sensors (Navigational-PORTS) would be stationary and could of course be increased, but the mobile sensors would be used to continually obtain additional data and to assess future additional navigational sensor sites. As the model development and PORTS matured, the Mobile-PORTS sensors would either migrate into the Navigational-PORTS or be discontinued for use elsewhere.

Table 1. Galveston Bay Model (GBM) and Houston Ship Channel Model (HSCM) Hindcast Water Surface Elevation Errors. Note the standard deviation refers to the demeaned differences between observed and simulated six-minute water levels. Mean Diurnal Range is the average difference between MHHW and MLLW. Average Relative Error as defined by Willmott et al. (1985) ranges from 0 to 1, with 0 being no error.

Station Name	Mean Diurnal Range (MDR) (cm)	Standard Deviation (SD) (cm)	SD/MDR Ratio (%)	Average Relative Error (-)
Galveston Pleasure Pier GBM-1/95 GBM-10/94 GBM- 4/96	67	8.5 7.7 9.2	12.6 11.5 13.7	0.02 0.04 0.06
Galveston Pier 21 GBM-1/95 GBM-10/94 GBM- 4/96 HSCM-4/96	43	6.2 5.3 7.2 7.6	14.4 12.3 16.7 17.7	0.02 0.03 0.06 0.06
Port Bolivar GBM-1/95 GBM-10/94 GBM- 4/96 HSCM-4/96	43	10.5 10.8 7.3 7.5	24.4 25.1 17.0 17.4	0.06 0.11 0.06 0.06
Eagle Point GBM-1/95 GBM-10/94 GBM- 4/96 HSCM-4/96	30	7.6 8.5 4.8 4.7	25.3 28.3 16.0 15.7	0.03 0.07 0.02 0.02
Clear Lake GBM-1/95 GBM-10/94 GBM- 4/96	28	6.8 8.1 6.9	24.2 28.9 24.6	0.02 0.04 0.04
Morgans Point GBM-1/95 GBM-10/94 GBM- 4/96 HSCM-4/96	30	7.4 9.3 5.4 5.4	24.6 31.0 18.0 18.0	0.02 0.04 0.02 0.02

Table 2a. Galveston Bay Model (GBM) and Houston Ship Channel Model (HSCM) Principal Flood Direction Errors during April 1996.

PORTS Station	Observed Principal Flood Direction (deg T)	Model Principal Flood Direction (deg T)	Model - Observed Principal Flood Direction (deg)
Bolivar Roads GBM HSCM	322	342 321	20 -1
Redfish Bar GBM HSCM	322	336 331	14 9
Morgans Point GBM HSCM	341	313 318	-28 -23

Table 2b. Galveston Bay Model/Houston Ship Channel Model Principal Component Direction Current Errors during April 1996. Mean diurnal range corresponds to the sum of average maximum flood and ebb speeds over each tidal cycle. It is estimated as 1.3 times sum of average tidal cycle flood and ebb speeds. Average Relative Error as defined by Willmott et al. (1985) ranges from 0 to 1, with 0 being no error.

PORTS Station Start-End Days	Mean Diurnal Range (MDR) (cm/s)	RMS Error (RMSE) (cm/s)	RMSE/MDR Ratio (%)	Average Relative Error (-)
Bolivar Roads 1-10 11-20 21-30	194	21.3/27.4 21.1/26.1 25.7/30.2	11.0/14.1 10.8/13.5 13.2/15.6	0.04/0.08 0.04/0.07 0.07/0.10
Redfish Bar 1-10 11-20 21-28	130	13.3/17.0 13.8/15.5 11.7/13.5	10.2/13.1 10.6/11.9 0.9/10.4	0.04/0.07 0.05/0.07 0.04/0.06
Morgans Point 1-10 11-20 21-30	66	17.9/12.7 15.9/13.2 16.4/14.4	27.1/19.2 24.1/20.0 24.8/21.8	0.39/0.10 0.27/0.11 0.33/0.15

1. INTRODUCTION

The National Oceanic and Atmospheric Administration installed a Physical Oceanographic Real Time System (PORTS) patterned after Bethem and Frey (1991) in June 1996 to monitor Galveston Bay. In the present system, water surface elevation, currents at prediction depth (4.6m) as well as near-surface and near-bottom temperature and salinity, and meteorological information are available at six-minute intervals (Appell et al., 1994) at locations shown in PORTS Base Map. To complement the PORTS a nowcast/forecast system (Parker, 1996) is being developed based on the National Ocean Service (NOS) Galveston Bay three-dimensional hydrodynamic model (Schmalz, 1996) and the National Weather Service (NWS) Aviation atmospheric model. To simulate currents within the Houston Ship Channel (HSC), a finer resolution three-dimensional HSC model has been developed. The Galveston Bay model is used to provide Bay wide water level and near entrance current forecasts as well as to directly provide water levels, density, and turbulence quantities to the HSC model for use in a one-way coupling. Tide gauge (refer to the Galveston Bay Base Map) and current meter station locations for hindcast assessment are as shown in Tide Gauge and Current Meter Base Maps, respectively.

To initially determine nowcast/forecast water level requirements, we examined January 1994 - December 1995 six-minute water level time series at Morgans Point (877-0613, in the upper Galveston Bay), Galveston Pier 21 (877-1450, in the lower Galveston Bay), and at Galveston Pleasure Pier (877-1510, nearshore Gulf south of the entrance to Galveston Bay) and June 1994 - May 1995 six-minute water level time series at Round Point (877-0559, head of Trinity Bay). The need to extend the NOS Galveston Bay model to include emergence/submergence to account for the effect of the observed drying of Trinity Bay during strong northerly winds was identified. Mid-depth salinity measurements obtained from the Texas Water Development Board at Morgans Point and Bolivar Roads indicated the need for a positive definite flux corrected salinity transport scheme to treat the observed large horizontal gradients. To utilize potential point meteorological forecasts, a surface heat flux capability was identified. In addition, a Barnes (1973) interpolation of meteorological fields as an alternative to the $1/r^2$ method, which tended to produce "bull's eyes" at measurement locations (Schmalz, 1996) was considered. Discussions with the Houston Galveston Navigation Safety Advisory Committee (HOGANSAC) revealed the need to provide accurate nowcast and forecast currents at both Bolivar Roads and Morgans Point. To improve Galveston Bay Model (GBM) current predictions, a high resolution Houston Ship Channel Model (HSCM) was developed. Prior to conducting forecasts, monthly hindcasts were performed. The following objectives were sought: 1) agreement in standard deviation of demeaned water levels order 10 cm, 2) rms errors in principal component current direction of order 25 degrees, and 3) rms error in principal component current strength order 20 cm/s (< 0.5 kt).

In Chapter 2, the GBM extensions to include emergence/submergence, flux-corrected transport (FCT), and heat flux are presented. It should be noted that the emergence/submergence scheme allows regions of the Bay system, which were originally wet, to dry. No overland flooding capability is presently built in. Next the development of the high resolution HSCM are presented in the context of grid resolution requirements and available computational resources. It should be noted, that the emergence/submergence scheme, FCT scheme, and heat flux algorithms have all been incorporated within the HSCM. The present one-way boundary coupling between the GBM to the HSCM allows

emergence/submergence effects to propagate through the boundary from the GBM to the HSCM. Hindcast results for the extended GBM are presented for the October 1994 flood, to examine the FCT scheme, and the January 1995 "Northers", to evaluate the emergence/submergence scheme. In both hindcasts the heat flux algorithm is used. In Chapter 4, GBM water level sensitivities to freshwater inflow, and Bay, Shelf, and Gulf winds are presented. Of particular interest is to: 1) identify the role of the Bay winds in influencing water levels at Morgans Point and 2) to investigate the influence of large volume inflows greater than 2,000 m³/s on water levels throughout the Bay system. In Chapter 5, the one-way coupled GBM and HSCM are used to hindcast the April 1996 PORTS beta test month. Hindcast water levels and prediction depth principal component direction currents as well as salinity and temperature are compared with PORTS observations. For water levels and currents an error budget is developed to identify the tidal and nontidal error components in each model. The ability of the HSCM to provide improved current predictions at Morgans Point is demonstrated. In Chapter 6, conclusions are drawn and recommendations made to further improve model performance. A coordinated increase in the availability of measurements to evaluate the three-dimensional models is advanced.

2. BAY AND CHANNEL MODEL DEVELOPMENTS

Based on preliminary nowcast/forecast requirements, the NOS Galveston Bay Model (Blumberg and Mellor, 1987; Schmalz, 1996) was substantially modified. Developments included the incorporation of an emergence/submergence scheme, a flux-corrected salinity transport, and heat flux algorithms. In addition, a two-step Barnes interpolation procedure was implemented to provide meteorological fields to drive the model.

To improve simulated currents within the Houston Ship Channel (HSC), a fine resolution channel model (HSCM) over the entire channel length was developed. It was envisioned, that by improving the resolution, channel currents would be more accurately represented, particularly in the very irregular channel regions in the vicinity of Morgans Point. The HSCM also includes the FCT and emergence/submergence, and heat flux algorithms used in the GBM. Each of these developments is discussed in turn below followed by discussions on the HSCM grid resolution, composite grid generation and one-way coupling scheme.

2.1. Bottom Emergence/Submergence Scheme

The scheme developed by Hess (1994) in Tampa Bay is modified for application in Galveston Bay to simulate winter time "Northerners", during which northerly winds of up to 40 knots associated with cold front passages persist over the Bay. An x-direction flow width reduction factor, $wx_{i,j}$ based on upstream vertically integrated velocity, $u_{i,j}^n$, and cell depth, $d_{i,j}^n$, is computed at the beginning of each external mode time step using the relation:

$$\begin{aligned}
 wx_{i,j} &= \min(1, \max(0, (d_{i-1,j}^n - d_u) / d_T)) & u_{i,j}^n \geq 0 \\
 wx_{i,j} &= \min(1, \max(0, (d_{i,j}^n - d_u) / d_T)) & u_{i,j}^n < 0 \\
 \text{Note } wx_{i,j} &\in (0,1) \text{ for } d_{*,j} \in (d_u, d_T + d_u), & \text{where } * = (i, i-1).
 \end{aligned} \tag{2.1}$$

An analogous relationship is used to specify the y-direction flow width reduction. In the Galveston Bay model application, $d_u = 0.25\text{m}$ and $d_T = 0.5\text{m}$. Since the model is written in horizontal area format, one multiplies the x-direction flow width, $dx = 0.5(dx_{i,j} + dx_{i-1,j})$ by $wx_{i,j}$ and the analogous expression for dy by $wy_{i,j}$ to reduce the horizontal fluxes at each sigma level. Fluxes given in Table 2.1, with their associated subroutines (refer to Mellor, 1996), are adjusted based on flow width reductions. The above linear cell depth relationship is used to reduce cell face flow widths when cell water depths drop below 0.75m and to fully eliminate flow paths when water depths drop below 0.25m. For water depths greater than 0.75m no reduction in flow width is made. A five day wind loading test case, in which winds out of the north were ramped from 0 to 40 kts during day one, held constant at 40 kts for the next two days, then ramped to zero over the fourth day, and held at zero over the final day was used. May 1-5, 1995 astronomical tide conditions were specified with a -50 cm subtidal water level ramped analogously to the wind. A large section of Trinity Bay dried and then reflooded after the wind and subtidal water level signal went to zero. In addition to the flood

width reduction, it is necessary for stability to reduce the wind stress over cells with small water depths. The following approach was utilized for the above test case and in subsequent simulations.

$$r_t = \min(1, \max(0, (\bar{d}_* - d_0)/(d_1 - d_0))) \quad * \equiv (x,y) \quad (2.2)$$

where $\bar{d}_x = 0.5(d_{i,j}^n + d_{i-1,j}^n)$ and $\bar{d}_y = 0.5(d_{i,j}^n + d_{i,j-1}^n)$

The factor r_t was applied to the surface wind stress terms in Subroutines PROFU and PROFV, and in the Mainline external mode horizontal momentum equations with $d_0=0.5\text{m}$ and $d_1=1.5\text{m}$, respectively. In general, the constants d_u and d_T in the cell width reduction formulas and d_0 and d_1 in the wind stress reduction relationship must be determined based on wind event strength, estuarine tidal range, bathymetry, and morphology. The scheme fails if a negative water depth is computed.

2.2. Salinity Flux Corrected Transport Scheme

A second order van Leer-type upstream-biased transport scheme (Lin et al., 1994) has been implemented to treat the very sharp horizontal salinity gradients in Galveston Bay. The Fortran coded scheme was obtained from Dr. Sirpa Hakkinen, NASA-GSFC, and modified for application to the shallow water Galveston Bay region. Consider the following parameter, $f_{i,j,k}^m$, to represent grid cell salinity at internal model time level m . The scheme corrects the flux based on grid cell upstream velocity, $u_{i,j,k}^m$, x-direction cell width, $dx_{i,j}$, and internal mode time step length, ΔT , in the following manner.

$$\begin{aligned} fdif &= 0.5(f_{i+1,j,k}^m - f_{i-1,j,k}^m) \\ fmin &= \min(f_{i-1,j,k}^m, f_{i,j,k}^m, f_{i+1,j,k}^m) \\ fmax &= \max(f_{i-1,j,k}^m, f_{i,j,k}^m, f_{i+1,j,k}^m) \\ \Delta \bar{F}_{i,j,k}^m &= \text{sign}(fdif) * \min[|fdif|, 2(fmax - f_{i,j,k}^m), 2(f_{i,j,k}^m - fmin)] \\ co &= 0.5(1 - u_{i,j,k}^m \Delta T / dx_{i-1,j}) \quad u_{i,j,k}^m > 0 \\ co &= 0.5(1 + u_{i,j,k}^m \Delta T / dx_{i,j}) \quad u_{i,j,k}^m \leq 0 \\ XFLUX &= u_{i,j,k}^m (f_{i-1,j,k}^m + co \Delta \bar{F}_{i-1,j,k}^m) \quad u_{i,j,k}^m > 0 \\ XFLUX &= u_{i,j,k}^m (f_{i,j,k}^m + co \Delta \bar{F}_{i,j,k}^m) \quad u_{i,j,k}^m \leq 0 \end{aligned} \quad (2.3)$$

Analogous relationships hold for the y-direction, YFLUX, and sigma direction, ZFLUX. The XFLUX and YFLUX terms are multiplied by $\bar{d}_x = 0.5(d_{i,j}^m + d_{i+1,j}^m)wx_{i,j}$ and $\bar{d}_y = 0.5(d_{i,j}^m + d_{i,j+1}^m)wy_{i,j}$. The XFLUX, YFLUX, and ZFLUX terms replace the original quantities used in Subroutine ADVT (refer to Mellor, 1996). Note the scheme employs a single increment from time level m to level $m+1$ and hence, the diffusion terms are evaluated at time level m in the standard manner.

Table 2.1. Emergence/Submergence Scheme Flux Adjustments

<u>Subroutine</u>	<u>Flux Description</u>	<u>Variable Name</u>
ADVAVE	Horizontal Vertically Integrated Velocity Advection and Viscosity	FLUXUA, FLUXVA
ADVQ	Horizontal Turbulent Kinetic Energy and Length Scale Advection and Diffusion	XFLUX, YFLUX
ADVS	Horizontal Salinity Advection and Diffusion	XFLUX, YFLUX
ADVT	Horizontal Temperature Advection and Diffusion	XFLUX, YFLUX
ADVU	Horizontal U-velocity fluxes Advection and Diffusion Coriolis (modified for curvilinear terms) Water Surface Elevation Gradient	XFLUX, YFLUX CURV EG
ADV V	Horizontal V-velocity fluxes Advection and Diffusion Coriolis (modified for curvilinear terms) Water Surface Elevation Gradient	XFLUX, YFLUX CURV EG
BAROPG	Baroclinic Pressure Gradient	DRHOX, DRHOY
VERTVL	Horizontal Velocity Fluxes	XFLUX, YFLUX
MAINLINE	External Mode Horizontal Vertically Integrated Fluxes in EL Coriolis terms in UA and VA Water surface elevation gradient in UA and VA	FLUXUA, FLUXVA CURV2D EL

2.3. Atmospheric Heat Flux Formulation

A set of heat flux routines were obtained from Mr. Paul Martin, Naval Research Laboratory, and was implemented in the Galveston Bay Model. The total incoming solar radiation at the top of the atmosphere, Q_0 , is determined by the following formula (List, 1951, p. 417).

$$Q_0 = \frac{J_0}{r^2} \cos z \quad , \quad \text{where } \cos z = \sin \phi \sin \delta + \cos \phi \cos \delta \cos h \quad (2.4)$$

- $\phi \equiv$ Latitude
- $\delta \equiv$ Solar declination
- $r \equiv$ Radius vector of the earth
- $h \equiv$ Solar hour angle ($h = 2\pi(H - 0.5)$)
- $H \equiv$ Hour of the day divided by 24
- $J_0 \equiv$ Solar constant ($1.94 \text{ cal cm}^{-2} \text{ min}^{-1}$)

At the earth's surface, the transmissivity of the atmosphere must be considered in addition to the effect of diffuse sky radiation. The so-called "Clear Sky Formula" of Fritz is used (List, 1951, p. 420) as given below.

$$\begin{aligned} D &= Q_0 a^{\sec z} & S &= Q_0(0.91 - a^{\sec z}) & (2.5) \\ Q_r &= D + S/2 = Q_0(0.5 a^{\sec z} + 0.455) \end{aligned}$$

- $Q_0 \equiv$ Total solar radiation at the top of the atmosphere
- $D \equiv$ Direct solar radiation at the earth's surface
- $S \equiv$ Diffuse sky radiation at the earth's surface
- $a \equiv$ Transmissivity of the earth's atmosphere

The albedo of the Bay surface, Al , is based on the solar altitude and atmospheric transmittance and is taken from Payne (1972). To determine the other fluxes, it is necessary to determine several

$$\begin{aligned} e &= 6.1121e^{17.502T/(240.97+T)}(1.0007 + 3.46 \times 10^{-6}P)(1. - 5.37 \times 10^{-4}S) \\ r &= 0.62197e/(P-e) & h &= r/(1+r) & (2.6) \end{aligned}$$

- $e \equiv$ Saturation vapor pressure (mb)
- $T \equiv$ Temperature ($^{\circ}\text{C}$)
- $S \equiv$ Salinity (PSU)
- $P \equiv$ Atmospheric Pressure (mb)
- $r \equiv$ Mixing ratio
- $h \equiv$ Specific humidity

supplemental variables. The saturation vapor pressure is needed for moist air at 10m and at the water surface. Equation (2.6) based on Buck (1981) and List (1951, p. 373) is used. Mixing ratio and specific humidity are also given.

If $P = P_a$, sea-level atmospheric pressure, $T = T_w$, surface water temperature, and $S = S_s$, surface salinity, then $e = e_w$, $r = r_w$, $h = h_w$, the saturation vapor pressure, mixing ratio, and specific

humidity, respectively, at the water surface. If $P = P_{10} = P_a$, atmospheric pressure at 10m, $T = T_a$, air (wet bulb) temperature at 10m, then $e = e_{a'}$, the saturation vapor pressure at 10m. To adjust the saturation vapor pressure to the vapor pressure of moist air, the following psychrometric relation (List, 1951, p. 366) is used.

$$e_a = e_{a'} - 0.000660(1 + 0.00115T_a)P_a(T_a - T_{a'}) \quad (2.7)$$

- $e_a \equiv$ Moist air vapor pressure at T_a
- $e_{a'} \equiv$ Saturation vapor pressure at $T_{a'}$
- $P_a \equiv$ Atmospheric pressure at 10m
- $T_a \equiv$ dry bulb temperature
- $T_{a'} \equiv$ wet bulb temperature

Then one recomputes r_a and h_a , accordingly, using e_a .

The air density, ρ_a , is computed based on List (1951, p. 290 and p. 295) using a virtual temperature, $T_v = (T_a + 273.16)(1 + 1.60779r_a)/(1 + r_a)$, in the following relation, $\rho_a = 3.4838 \times 10^{-4} P_a / T_v$ (gm/cm³). The neutral condition exchange coefficient for latent and sensible heats, C_E and C_H , are set to 1.4×10^{-3} . Following Kondo (1975) the following method is used to develop the ratio of the exchange coefficient for diabatic conditions to that for neutral conditions based on T_w , T_a , u , the windspeed in (cm/s).

$$C = C_0 |C_0| / (|C_0| + 0.01) \quad C_0 = (T_w - T_a)u^{-2} \quad (2.8)$$

- For stable conditions $T_w < T_a$ $C_{HD}/C_H = C_{ED}/C_E = \max(0, 0.1 + 0.03C + 0.9e^{4.8C})$.
- For unstable conditions $T_a < T_w$ $C_{HD}/C_H = C_{ED}/C_E = 1.0 + 0.63C^{0.5}$.

We are now in a position to develop the long wave radiation heat fluxes shown in the following aerodynamic bulk formulas.

$$\begin{aligned}
Q_E &= -\rho_a C_{ED} H (h_w - h_a) u \quad \text{where, } H = 597.8 - 0.573 T_w & (2.9) \\
Q_S &= -\rho_a C_{SD} C_p (T_w - T_a) u \\
Q_b &= -\sigma \epsilon \theta_w^3 [(0.39 - 0.05 e_a^{0.5}) (1 - 0.6 C^2) \theta_w + 4(T_w - T_a)]
\end{aligned}$$

Q_E \equiv Latent (evaporative) heat flux (cal/cm²/s)

Q_S \equiv Sensible heat flux (cal/cm²/s)

Q_b \equiv Backscattered heat flux (cal/cm²/s)

C_p \equiv Specific heat of water at constant pressure (0.24 cal/gm/°C)

σ \equiv Stephan-Boltzmann constant (1.3553×10^{-12} cal/cm²/s)

ϵ \equiv Black body emissivity (0.96)

C \equiv Fractional cloud cover

θ_w \equiv Absolute surface water temperature ($T_w + 273.16$)

To convert to model MKS units, 1 cal/cm²/day = 0.484433 watts/m². In the present Bay model, the Large and Pond (1981) neutral condition wind stress momentum exchange coefficient might be adjusted as appropriate from neutral to diabatic conditions based on stability considerations, similarly as in Equation (2.8) above. The short wave radiation is given by $q_s = -Q_r (1 - Al)$, while the long wave radiation is $q_l = -(Q_E + Q_S + Q_b)$. The flux sign convention is such that a positive sign represents transfer from the water to the air. To include the effects of the surface heat fluxes in the hydrodynamics, the following temperature equation surface boundary condition is implemented.

$$\frac{K_H \partial T}{H \partial \sigma} = \frac{-q_s}{\rho C_p} \quad \sigma = 0 \quad (2.10)$$

T \equiv Water temperature

K_H \equiv Diffusivity for heat

σ \equiv sigma vertical coordinate

H \equiv Water depth

q_s \equiv Short wave radiation

ρ \equiv Water density

C_p \equiv Specific heat of water at constant pressure

In Galveston Bay, a Jerlov type 2 condition representative of turbid coastal waters is considered appropriate with short wave transmission coefficient, $T_r = 0.310$, and extinction coefficient, $k = 0.420$. The following equation is considered (Mellor, 1996).

$$\frac{DT}{dt} = \mathfrak{D}(T) - kT_r q_s \frac{e^{k\sigma H}}{\rho C_p} \quad (2.11)$$

$T \equiv$ Water temperature

$t \equiv$ Time

$\sigma \equiv$ sigma vertical coordinate

$H \equiv$ Water depth

$\frac{D(\)}{dt} \equiv$ Substantive derivative

$\mathfrak{D}(\) \equiv$ Three-dimensional Diffusion operator

$k \equiv$ Extinction coefficient

$T_r \equiv$ Short wave radiation transmittance coefficient

The extinction coefficient must be of sufficient magnitude such that all flux is transmitted to the water column in shallow regions. For the present value used in Galveston Bay, we note that for the value of the exponent to equal -3, the depth, H , must be at least 7m. For shallower regions of order 2m depth in the Bay, some of the short-wave radiation will be lost in the present scheme. To correct this, one might employ the following depth dependent and thereby spatially variable extinction coefficient, $k' = \max(k, 3/H)$.

2.4. Barnes Interpolation of Meteorological Variables

Consider a meteorological variable (wind components, sea-level atmospheric pressure, cloud cover, dry bulb and wet bulb temperature) with the set of observations, $(O_k, k=1, N)$, at N stations. The task of the interpolation procedure is to assign a value of the meteorological variable at the center of each grid cell of the hydrodynamic model (Bay or Channel) computational grid. For each station, the distance, $d_{i,j,k}$, to the center of cell (i,j) , is determined. Next, the pair of indices $(i(k), j(k))$ is determined to be the grid cell closest to station $k \ni \min_{i,j} d_{i,j,k} = d_{i(k),j(k),k}$.

The Barnes (1973) interpolation procedure applied to Galveston Bay is governed by a length scale, $l=40$ km, and a convergence parameter, $\gamma=0.4$. The interpolation is usually performed in two independent steps based upon the use of exponential station weighting factors in the following manner.

$$\begin{aligned} wi^1_{i,j,k} &= e^{-(d_{i,j,k}/l)^2} & wsi^1_{i,j} &= \sum_{k=1}^N wi^1_{i,j,k} \\ wi^2_{i,j,k} &= e^{-(d_{i,j,k}/\gamma l)^2} & wsi^2_{i,j} &= \sum_{k=1}^N wi^2_{i,j,k} \\ wf^1_{i,j,k} &= wi^1_{i,j,k}/wsi^1_{i,j} & wf^2_{i,j,k} &= wi^2_{i,j,k}/wsi^2_{i,j} \end{aligned} \quad (2.12)$$

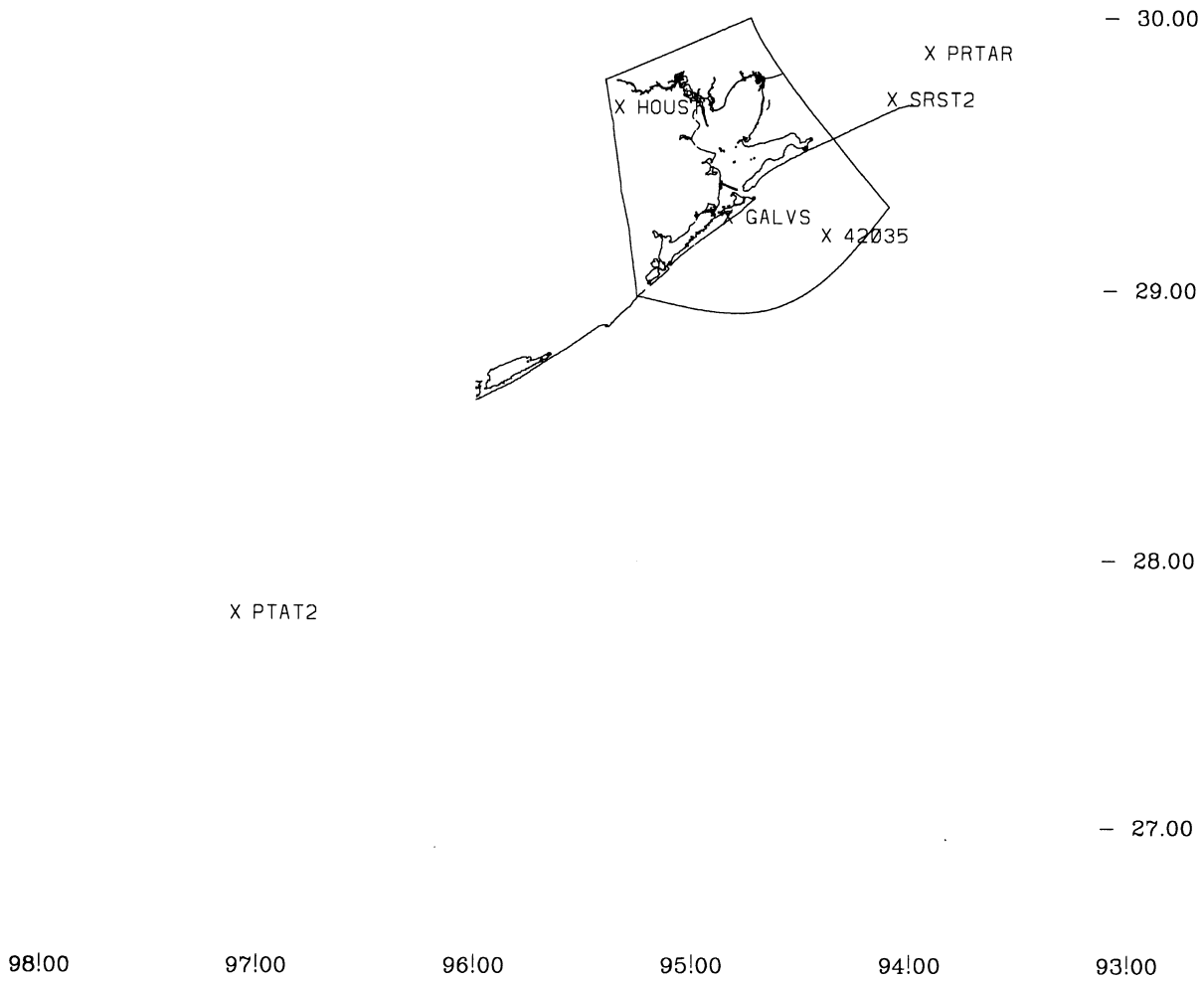
The interpolation for step one is given by $V^1_{i,j} = \sum_{k=1}^N wf^1_{i,j,k} O_k$. Usually a second step is performed

by using the residuals and proceeds as follows.

$$R_k = O_k - V_{i(k),j(k)}^1 \quad (2.13)$$

$$V_{ij}^2 = \sum_{k=1}^N w f_{ij,k}^2 R_k$$

Then $V_{ij} = V_{ij}^1 + mV_{ij}^2$. For a two step interpolation, $m=1$, while if only a single step interpolation is performed, $m=0$. To illustrate the properties of the Barnes interpolation, we compare results based on observations at the stations shown in Figure 2.1 using one step with a $1/r^2$ interpolation for 16 June 1995 (JD 167) of 10 m windspeed in Figures 2.2-2.3, 10m wind vectors in Figures 2.4-2.5, and sea-level atmospheric pressure in Figures 2.6-2.7, respectively. The "bull's eye" effect associated with the $1/r^2$ interpolation at observation station locations for scalars is eliminated in the Barnes procedure. For vector fields based on interpolation of scalar components, as shown in Figures 2.4-2.5, the interpolations are nearly identical. For the distribution of measurement locations, 0.4 convergence parameter, and 40 km length scale, the results of the one and two-step interpolations are very similar.



42020 = SE of PTAT2 slightly below 27 °N

Figure 2.1. Interpolation Meteorological Station Locations

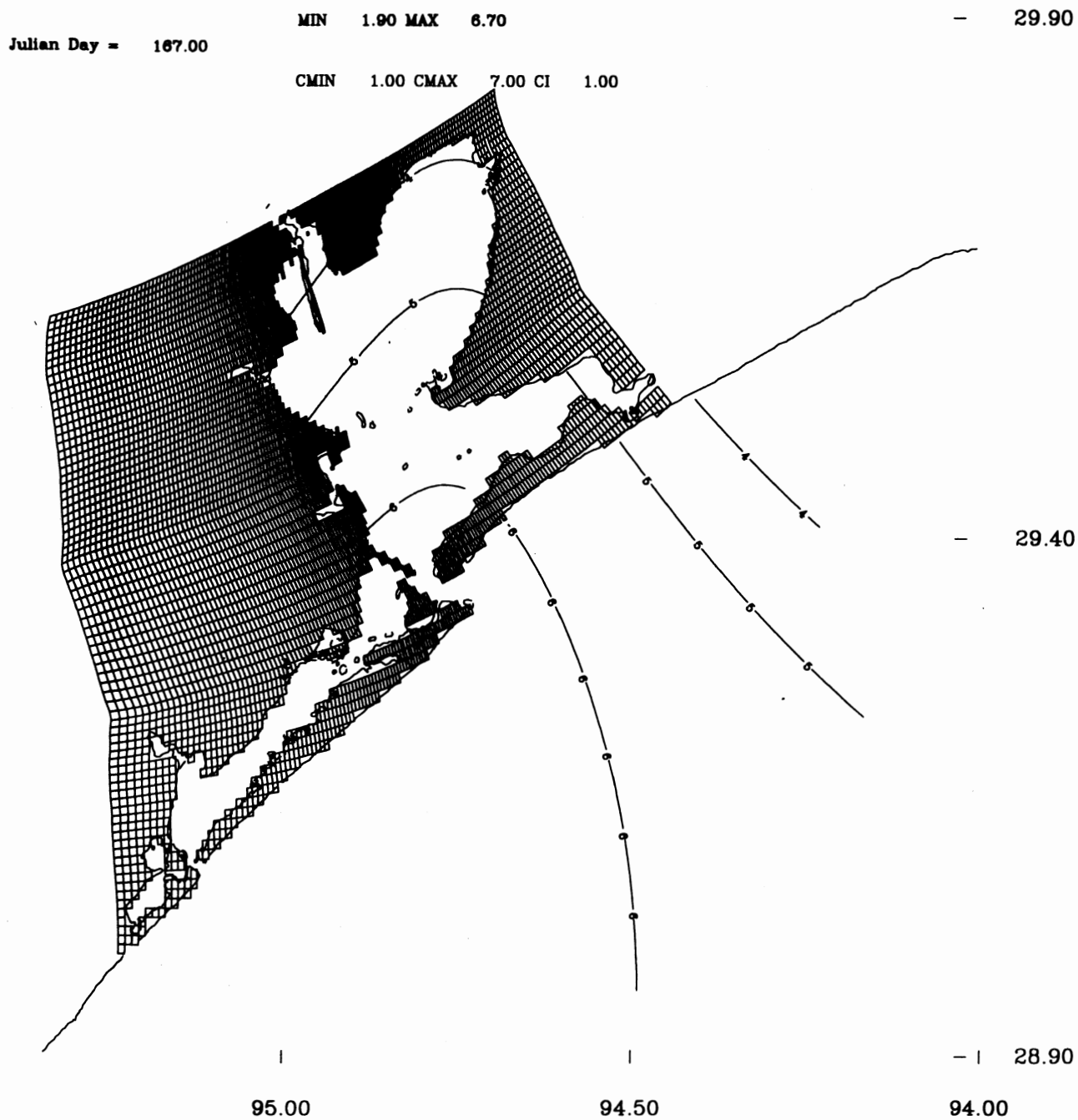


Figure 2.2. JD 167.0 1995 One-step Barnes Interpolated Wind Speed (m/s) over Galveston Bay

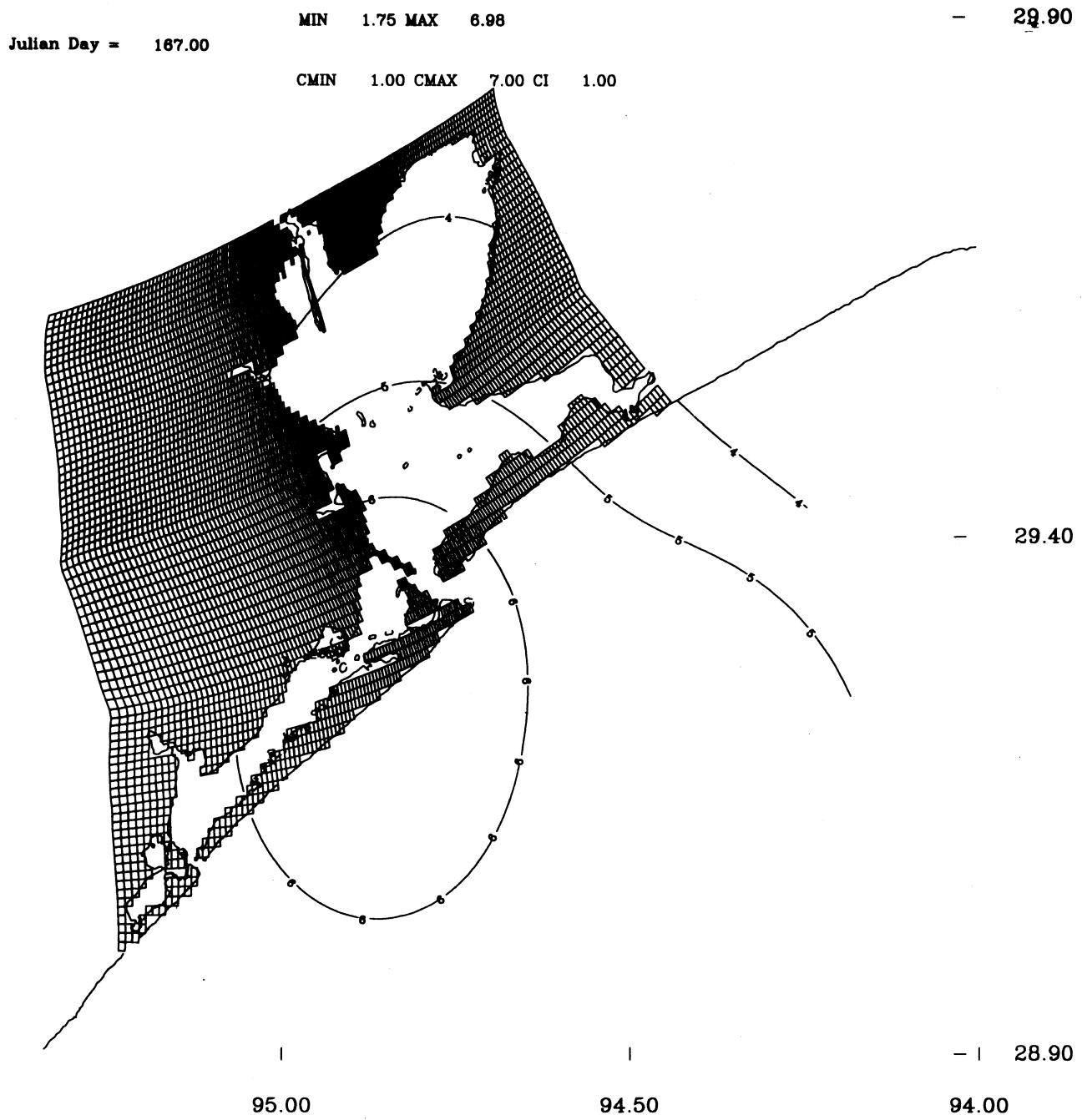


Figure 2.3. JD 167.0 1995 $1/r^2$ Interpolated Wind Speed (m/s) over Galveston Bay

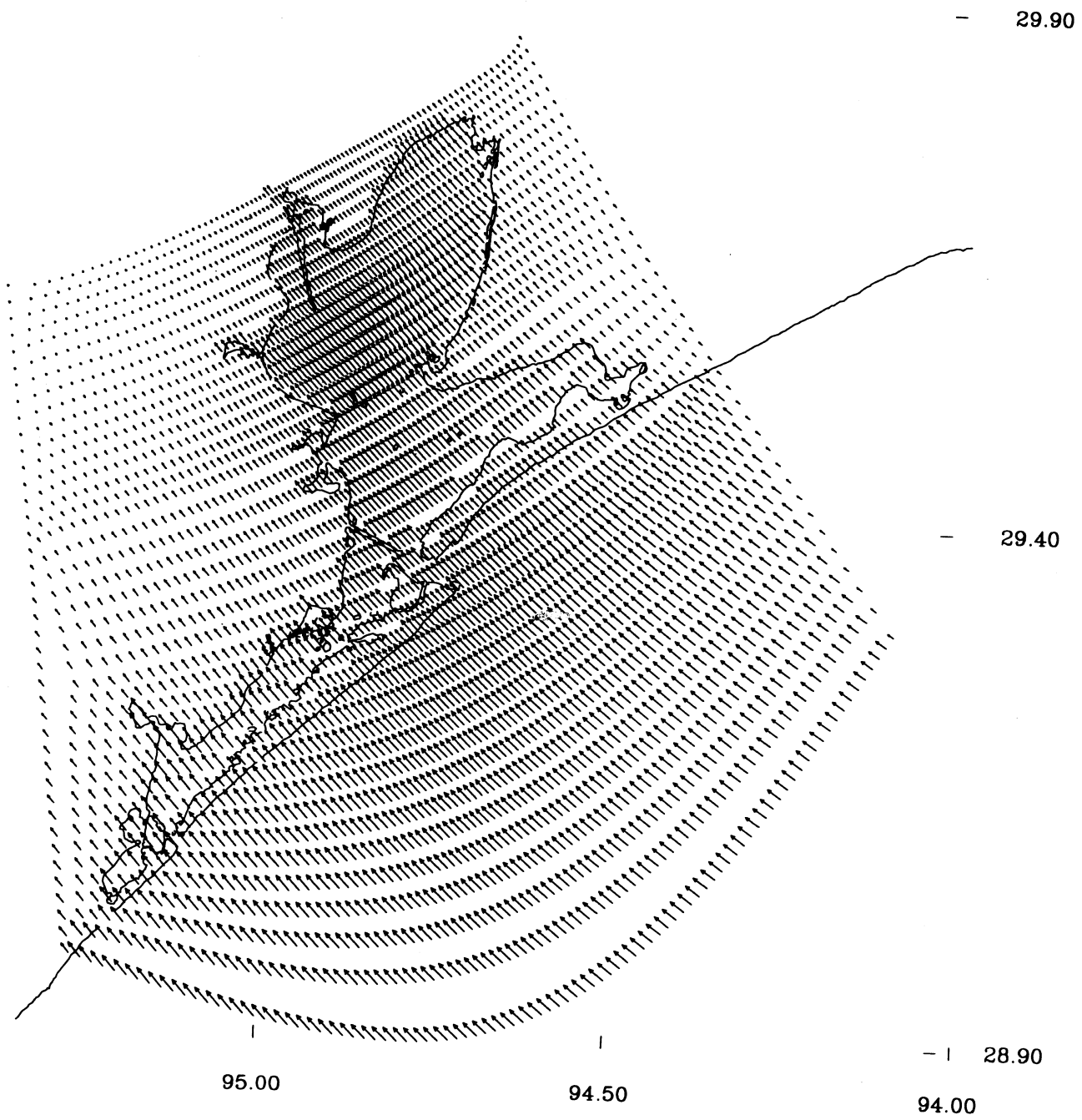


Figure 2.4. JD 167.0 1995 One-step Barnes Interpolated Windfield (m/s) over Galveston Bay

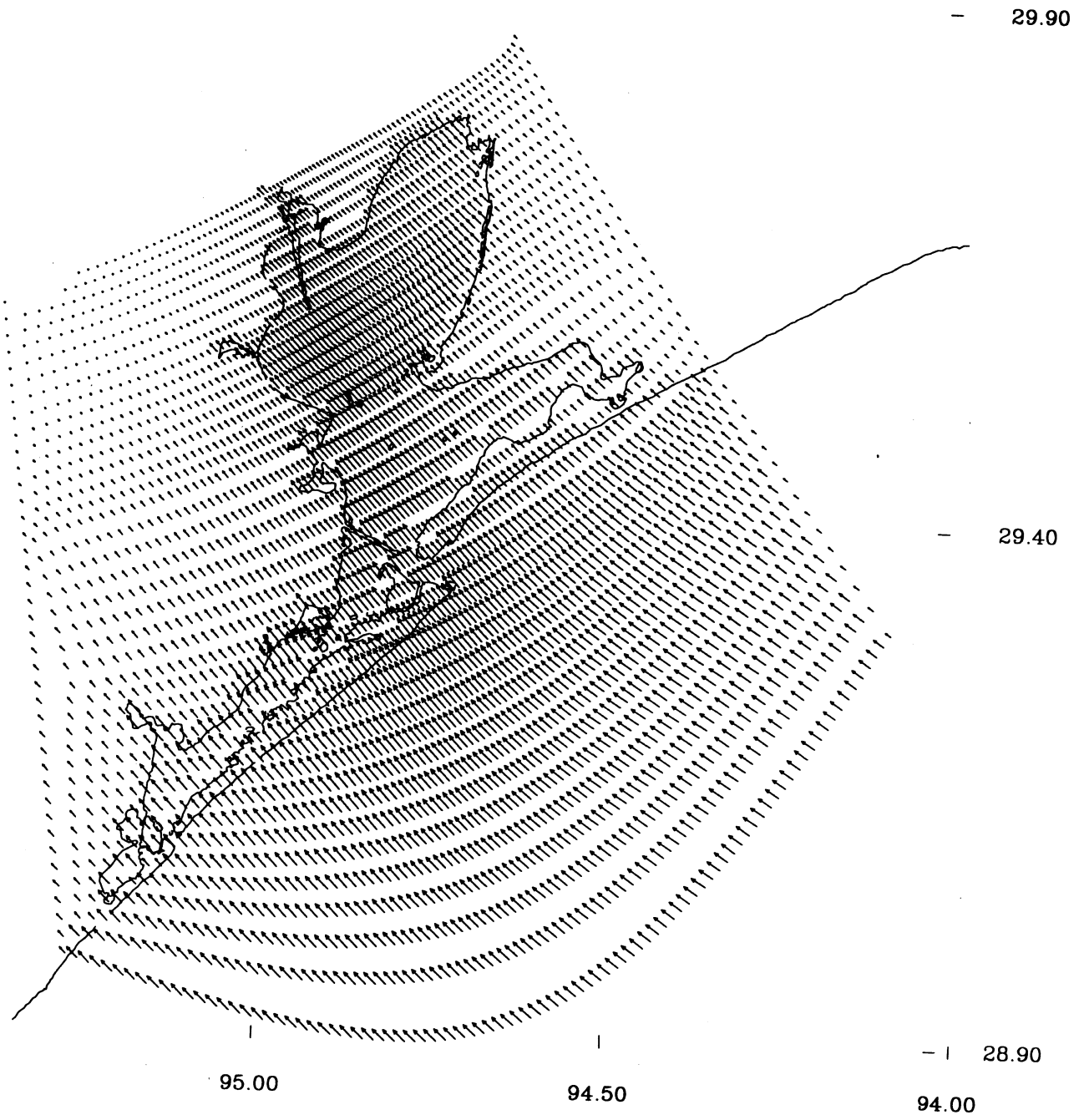


Figure 2.5. JD 167.0 1995 $1/r^2$ Interpolated Windfield (m/s) over Galveston Bay

Julian Day = 167.00

MIN 1017.48 MAX 1018.82

— 29.90

CMIN 1016.00 CMAX 1020.00 CI 0.50

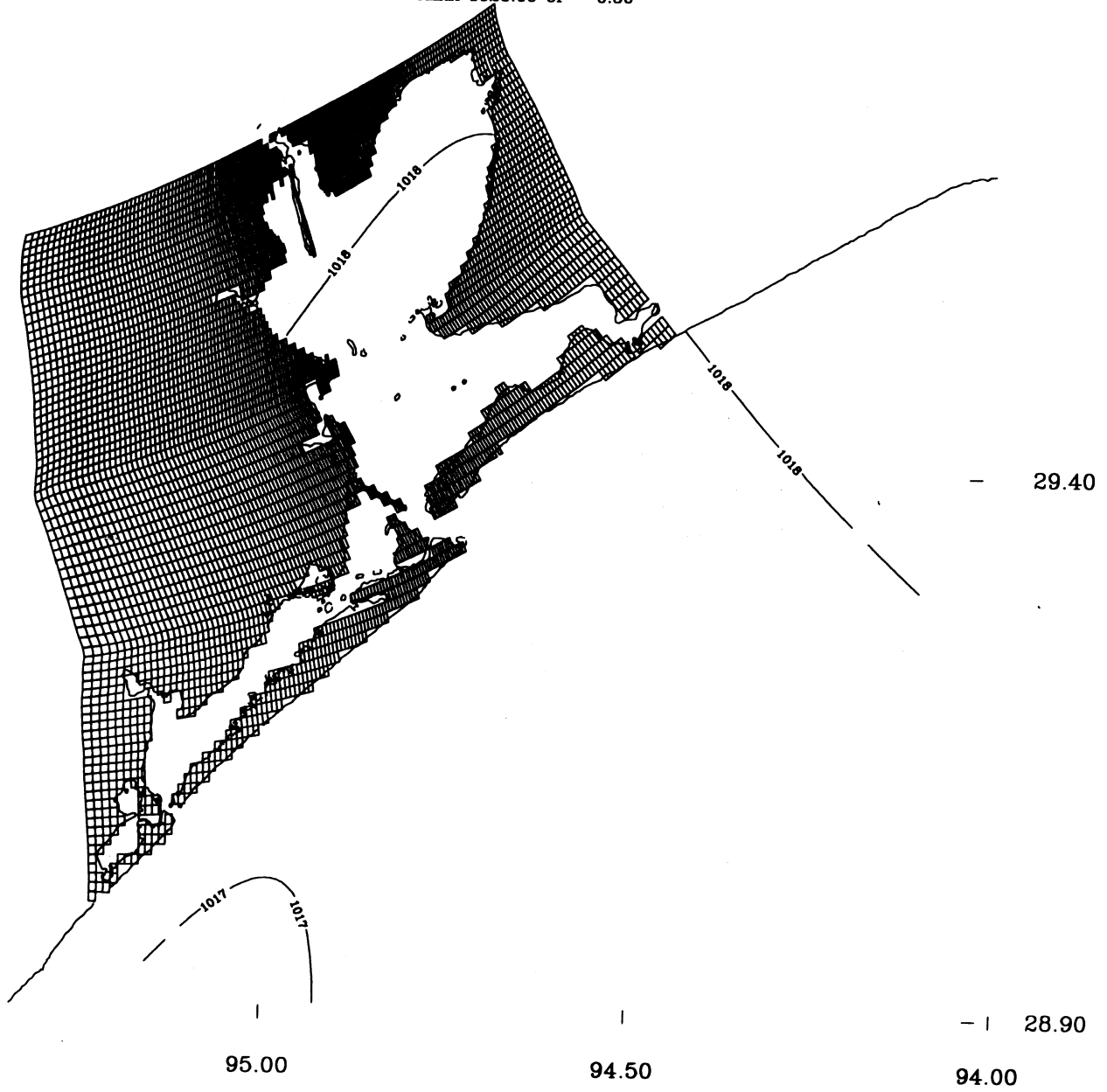


Figure 2.6. JD 167.0 1995 One-step Barnes Interpolated Sea-level Atmospheric Pressure (mb) over Galveston Bay

Julian Day = 167.00

MIN 1017.40 MAX 1018.86

— 29.90

CMIN 1016.00 CMAX 1019.00 CI 0.50

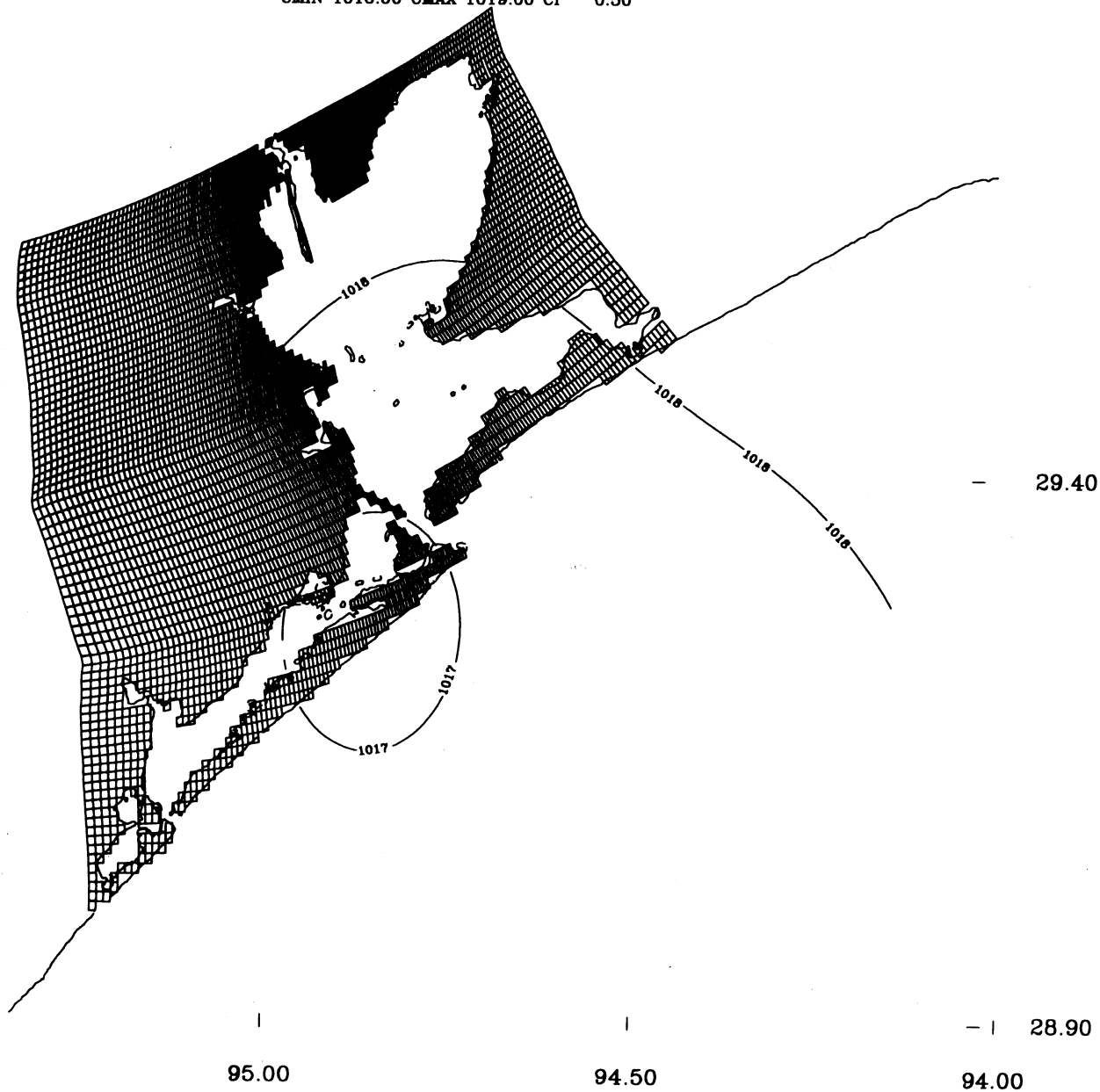


Figure 2.7. JD 167.0 1995 $1/r^2$ Barnes Interpolated Sea-level Atmospheric Pressure (mb) over Galveston Bay

2.5. Channel Model Grid Resolution Considerations

The Houston Ship Channel (HSC) is the major navigation channel in Galveston Bay extending from the Bay Entrance to the Port of Houston, a distance of order 50 km. The depth of the channel is maintained by U.S. Army Corps of Engineers (USACOE) at a design width of 122m (400 feet) and project depth of 12.2 m (40 feet). Design channel side slopes are 1:2.5. Along the majority of channel length, the Bay is extremely shallow, approximately 2m in depth, so that the transition from the approximate 12m design depth at a 1:2.5 side slope occurs over a 25m horizontal extent on each side of the channel. The present Galveston Bay Model (GBM) grid is focused to provide maximum resolution along the navigation channel with along channel resolutions (order 0.5 to 2.5km) at and a maximum cross channel resolution of 250m; e.g., the channel and side slopes are not fully resolved.

Since horizontal salinity gradients are large during the wet season, the potential exists for intense gravitational circulation during this period. To numerically investigate the role of the gravitational circulation on channel currents, a fine resolution grid is required. To resolve the across channel current shear approximately 10 cells over the channel width would be required; e.g., a cross-channel resolution of order 12m and an along-channel resolution of 25m to maintain a 2:1 aspect ratio. On each side of the channel side slope transition region, a further transition out to a distance of order 0.5 km would be required if the assumption is made that channel circulation influences are negligible outside this area. With presently available computational resources, grid resolutions of this scale are not economically feasible to construct along the entire 50km channel. A 100 x 4200 horizontal grid would be required. If only the portion of the channel above Morgans Point, a distance of approximately 15km, is considered, the horizontal grid size would still be 100 x 1260.

In this study, a fine resolution channel grid over the entire channel length was developed at twice the across-channel resolution of the GBM. This will allow for a combined 60 hour nowcast/forecast to be simulated by using 1 and 2 hours of total time on the 8-CPU SGI Origin 2000 for the GBM and Houston Ship Channel Model (HSCM), respectively.

2.6. Composite Channel Grid Generation

The refined channel grid was developed in three subgrids based on the Wilken (1988) elliptic grid generation program patterned after Ives and Zacharais (1987). In their procedure, grid cell center boundary locations are specified along the bottom and left-hand side of each grid. An interpolation procedure is used to specify grid cell center locations along the two opposite boundaries prior to the solution of the elliptic boundary value problem. Therefore to preserve orthogonality, it was necessary to write out the top boundary locations for subgrid 1 shown in Figure 2.8 as input to the bottom boundary for subgrid 2. Spacings along the left-hand side boundary of composite grid 2 were input. Similarly, the top spacings of subgrid 2 in Figure 2.9 were written to a file to serve as the bottom boundary grid cell center locations for composite grid 3 shown in Figure 2.10. Each subgrid consisted of 71 x 71 grid cell center locations and was linked in order to develop the final composite channel grid shown in Figure 2.11 consisting of 71 x 211 horizontal cells ($dx=63-1007m$, $dy=133-1268m$). The same five sigma levels (-0.1667, -0.4167, -0.5833, -0.7643, -0.9167) used in the Galveston Bay Model were used.

NOS 15 sec gridded bathymetry based on historical hydrographic surveys (NGDC, 1987) was used to determine grid cell depths with respect to tidal epoch Mean Lower Low Water (MLLW). A $1/r^2$ interpolation was used to adjust the MLLW values to tidal epoch Mean Tide Level (MTL) based on shoreline station tidal datums. The Houston Ship Channel bathymetry was specified based on USACOE channel survey data as listed on nautical charts 11324, 11327, and 11329. Galveston Bay Model bathymetry is shown in Figure 2.12 with the corresponding Galveston Bay Entrance section of the Houston Ship Channel Model shown in Figure 2.13. Both bathymetries were not smoothed. The major navigation channels are represented in a consistent manner, but there may be some differences outside the channel areas.

2.7. One-way Channel Coupling Algorithm

The two models (GBM and HSCM) were then nested in a one-way coupling scheme. Boundary and initial condition specifications for the HSCM are presented in turn.

Open lateral boundary coupling geometry is accomplished by first specifying open boundary cells external to the Houston Ship Channel and then locating the corresponding (nearest neighbor) open boundary cells on the Bay grid. At GBM grid cell locations corresponding to HSCM open boundary cells, the GBM water surface elevation, salinity, temperature, turbulent kinetic energy, and turbulent length scale time histories were saved at 6-minute intervals. For the external mode of the HSCM, these water surface elevations are specified directly (in contrast to a velocity specification) and the vertically integrated currents are computed from the boundary specified water surface elevations as in the GBM. In the internal mode, for salinity, temperature, turbulent kinetic energy, and turbulent length scale, a one-dimensional (normal to the boundary) advection equation is used. On inflow GBM values are advected into the HSCM grid domain, while on outflow HSCM internal cell values are advected through the boundary. For the internal mode velocity, the same radiation scheme used in the GBM is employed.

Lateral flow boundary coupling is achieved by specifying river inflow cells on the Houston Ship Channel grid and by using the corresponding flow and salinity and temperature boundary signals. Inflows and salinity and temperature boundary conditions are the same as in the GBM for Buffalo Bayou and San Jacinto rivers, while the Trinity River is not included in the HSCM.

Surface boundary coupling is accomplished by placing the SST field on the HSCM grid via nearest neighbor interpolation from the GBM grid. Wind and atmospheric pressure fields are directly determined on the HSCM grid via the 2-step Barnes (1973) interpolation.

HSCM salinity and temperature initial conditions are determined from corresponding interpolation of the GBM initial fields. A nearest neighbor sigma coordinate to depth translation is first performed followed by a depth to depth interpolation to the HSCM grid. Finally, the depth based fields on the HSCM are converted to sigma levels to minimize density field errors.

The basic idea to the coupling is that the HSCM looks no different than the GBM. The same approach is used to specify boundary and initial conditions. Under this approach, there is no coupling or feedback from the GBM to the HSCM. As a result, it is necessary to place the boundaries of the HSCM well outside the navigation channel areas.



Figure 2.8. Houston Ship Channel Model Subgrid 1: Bay Entrance Section

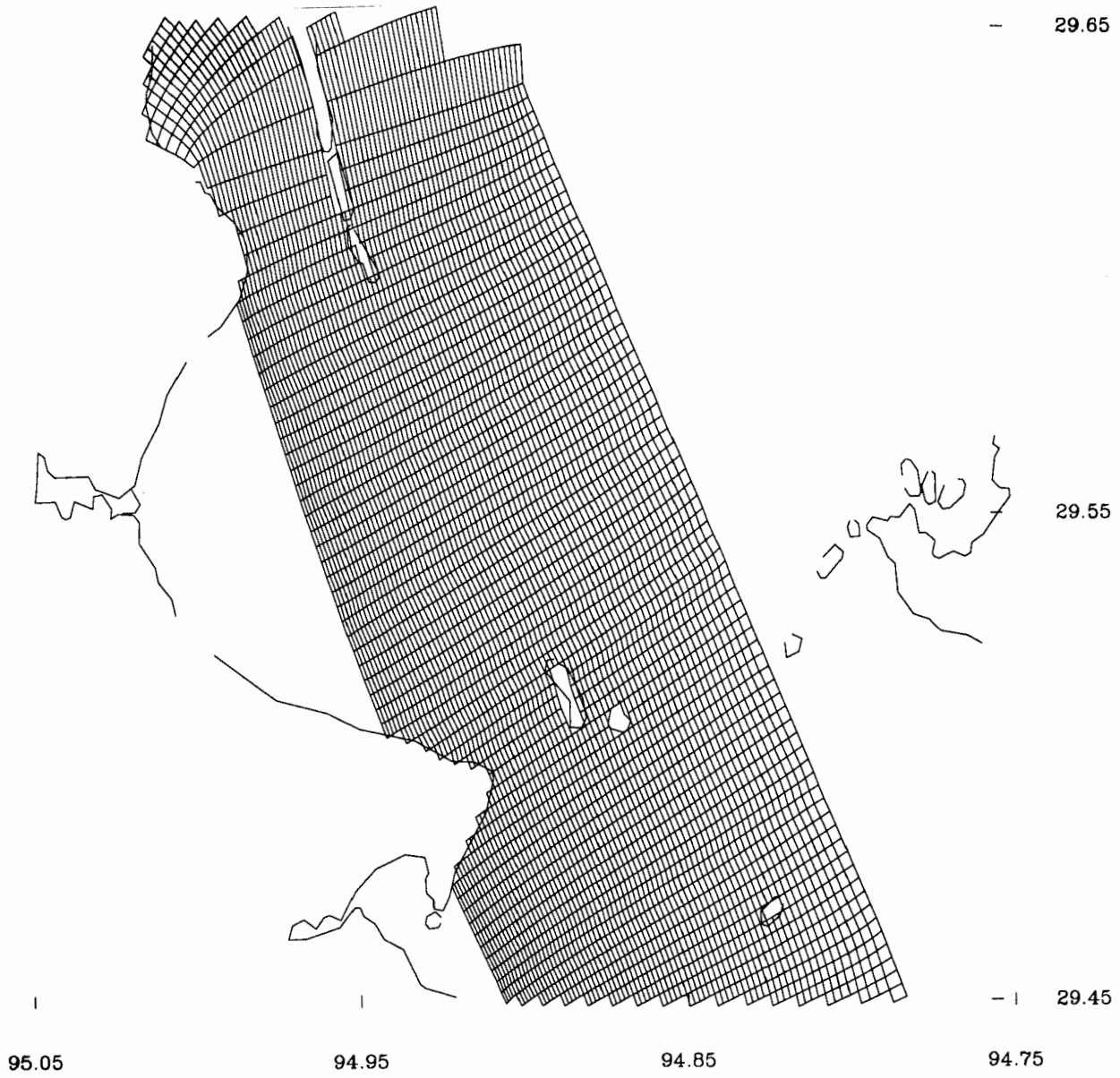


Figure 2.9. Houston Ship Channel Model Subgrid 2: Bay Entrance to Morgans Point

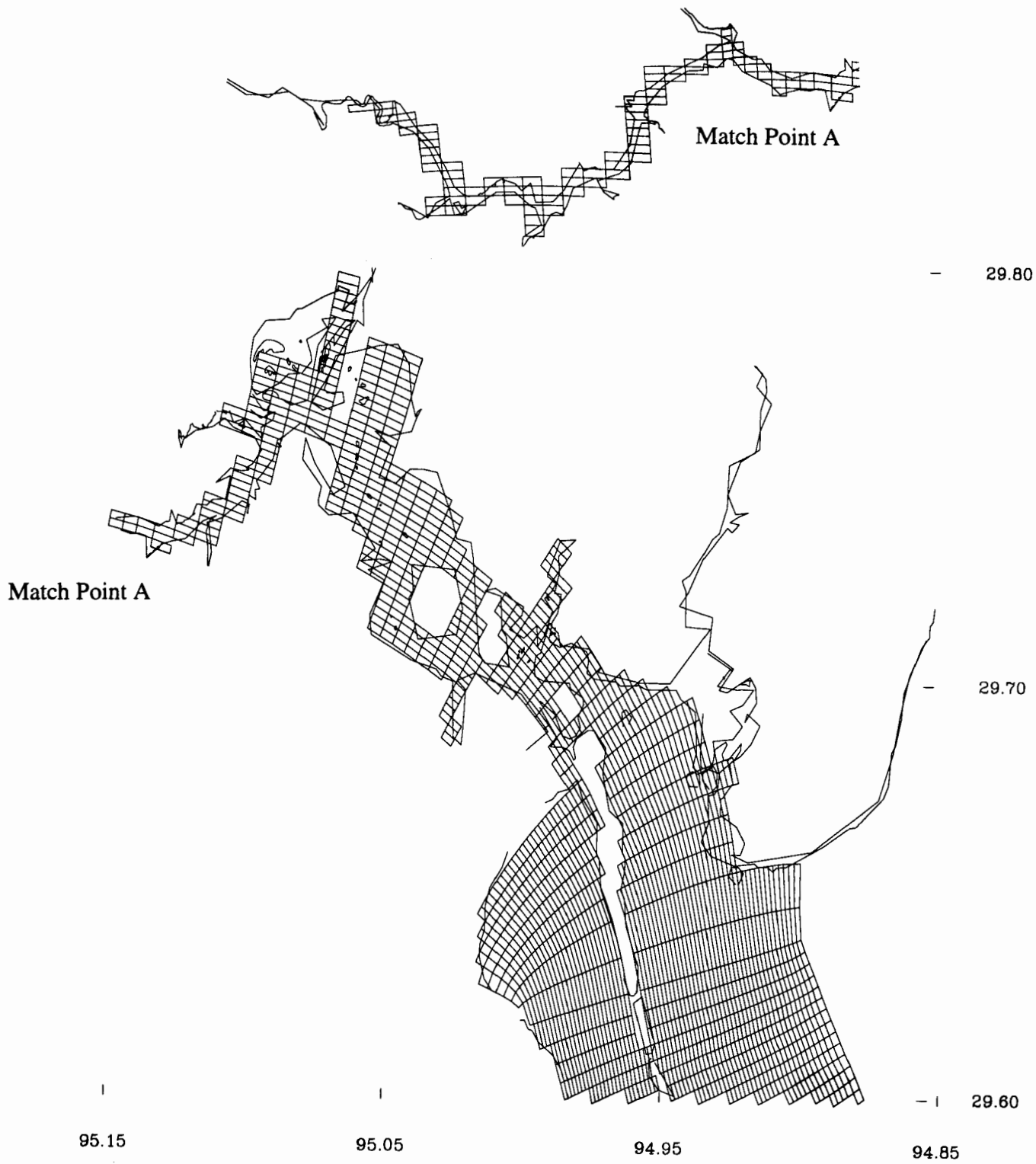


Figure 2.10. Houston Ship Channel Model Subgrid 3: Above Morgans Point

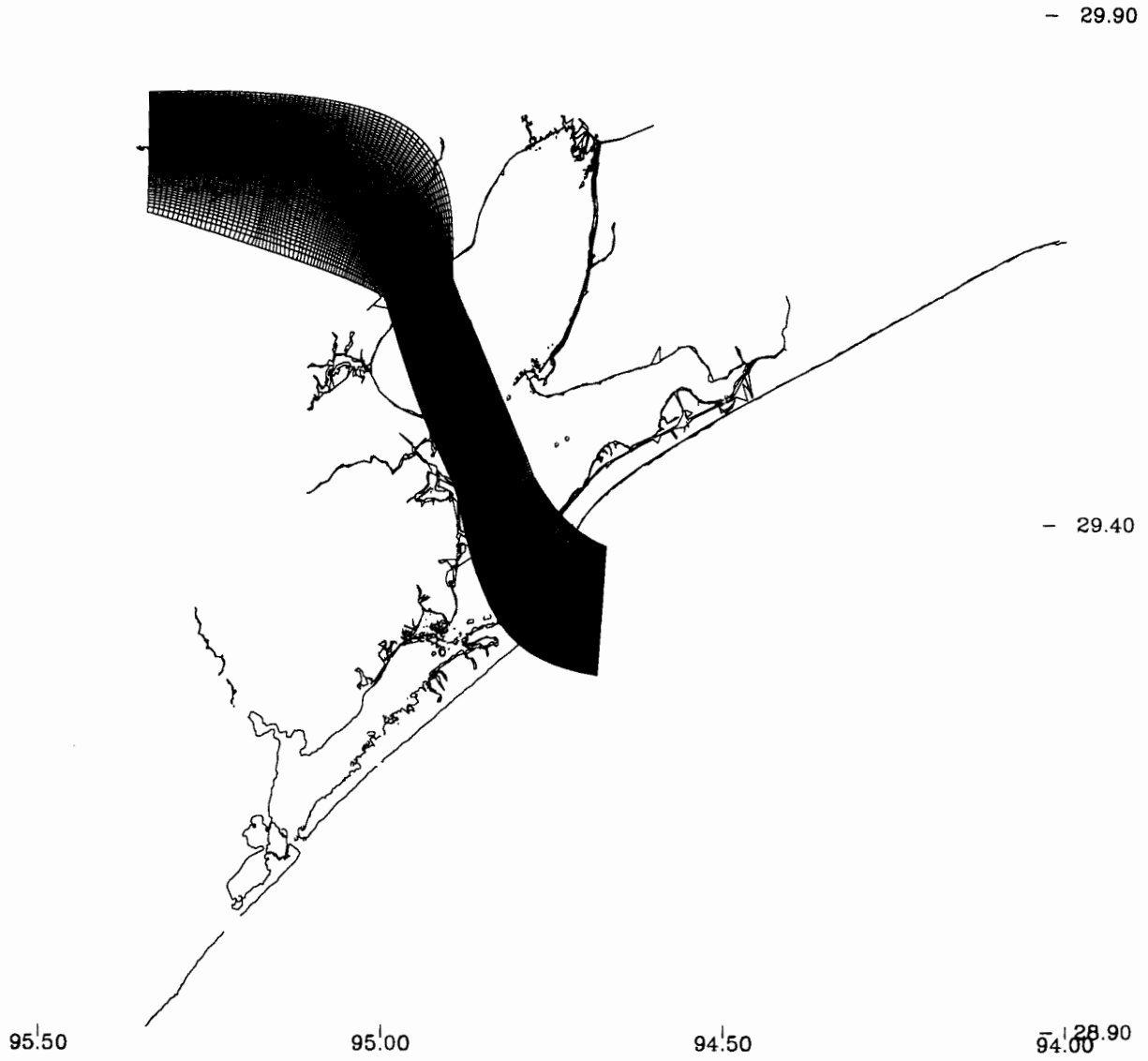


Figure 2.11. Houston Ship Channel Model Composite Computational Grid

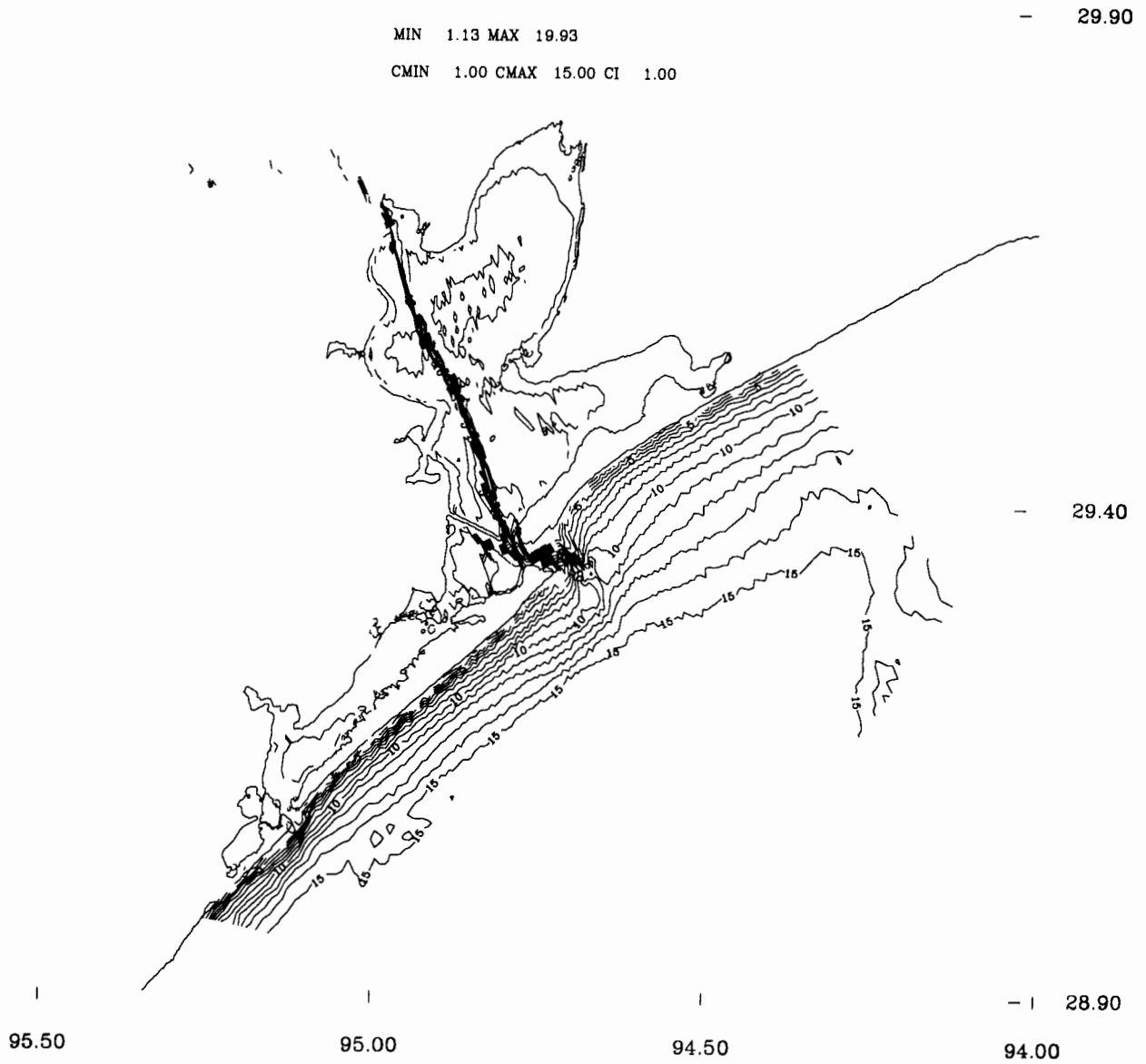


Figure 2.12. Galveston Bay Model Bathymetry (m relative to MTL)

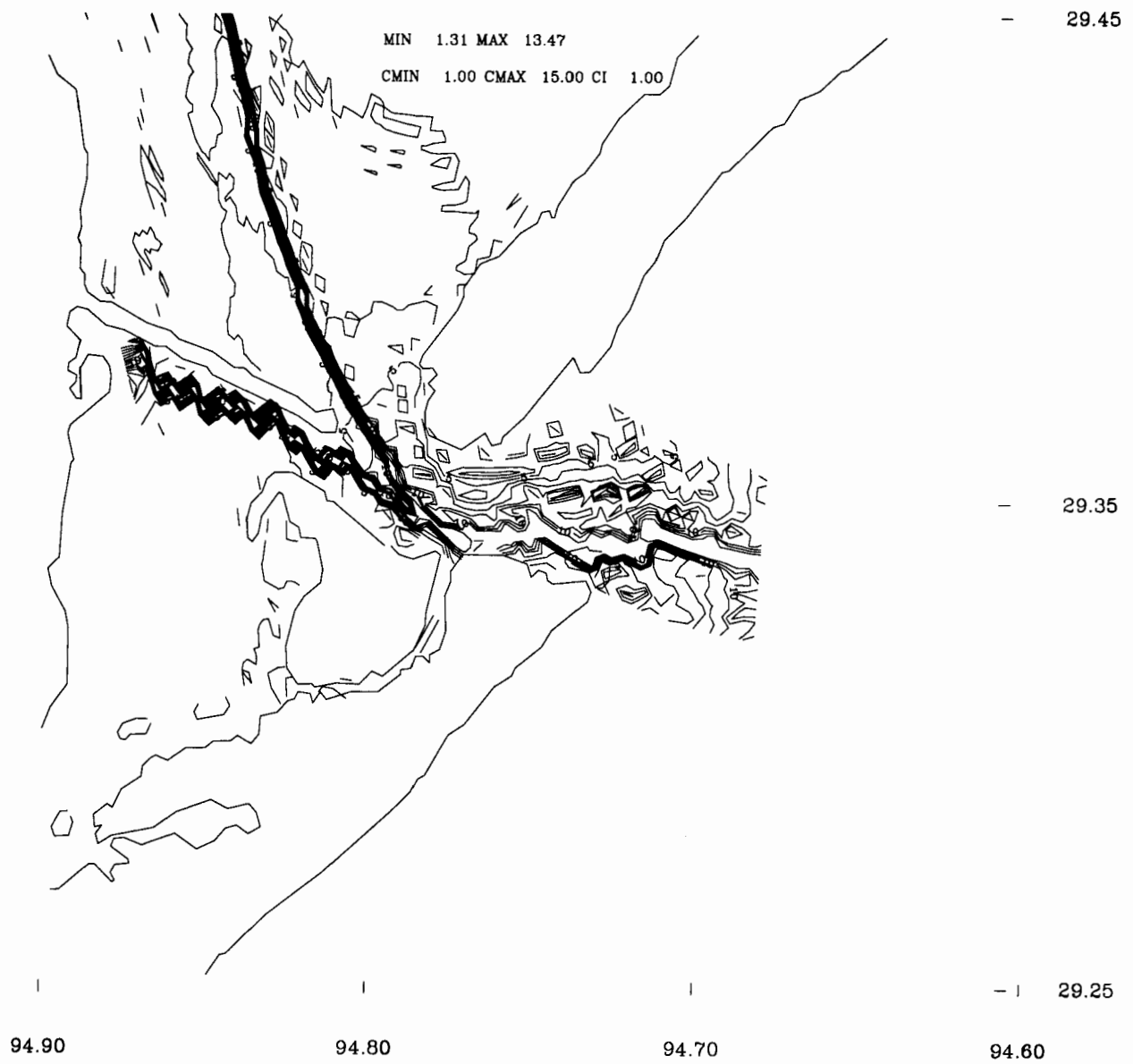


Figure 2.13. Houston Ship Channel Model Bathymetry (m relative to MTL)
 In the Vicinity of the Entrance to Galveston Bay

3. BAY MODEL HINDCASTS

To test the drying/wetting algorithm, the January 1995 period was considered, during which several "Northers" occurred and portions of Trinity Bay near Round Point dried. The October 1994 freshet period was considered to further evaluate the flux corrected transport scheme and to test the ability of the Bay model to simulate major inflow conditions. This period represented an extreme condition for freshwater inflows with the flood of record on the San Jacinto and Trinity Rivers occurring on 18-19 October.

Bottom roughness, z_0 , was set at 1 cm and the Smagorinsky horizontal eddy viscosity coefficient, C_H , set at 0.005 for the both simulations (see Mellor, 1996). To place the hindcast results in context, initial and boundary condition development are discussed first for each month. Next simulation results for each hindcast are presented for water levels, salinity, and temperature.

3.1. Initial Conditions

Velocities and water surface elevations were set to zero. Texas Water Development Board (TWDB) salinity and temperature data were available at 90 minute intervals at approximately mid-depth at the locations shown in Figure 3.1. These data were melded with tidal cycle average climatological salinity and temperature data (Temple et al., 1977 ; Orlando et al., 1993) to form the initial salinity and temperature fields using a horizontal patch-oriented interpolation scheme (Schmalz, 1994). Since the climatological fields represent tidal cycle average conditions, the salinity and temperature contours contain an uncertainty in location equal to the tidal excursion length. This is the best that can be presently accomplished in the absence of additional measurements. The problem is most severe in specifying the initial salinity field, which contains large horizontal gradients.

January 1995: Initial near surface salinity as shown in Figure 3.2 ranges from 0.0 to 32.0 PSU while near bottom initial salinity shown in Figure 3.3 ranges from 0.0 to 34.2 PSU with a vertical stratification of order 2 PSU. Initial near surface temperature fields are well mixed and are shown near the surface in Figure 3.4 (11.8 to 16.0 °C) and near the bottom in Figure 3.5 (11.8 to 16.0 °C), respectively.

October 1994: Initial near surface salinity as shown in Figure 3.6 ranges from 6.2 to 31.1 PSU while near bottom initial salinity shown in Figure 3.7 ranges from 6.3 to 31.5 PSU indicating well mixed conditions. Initial near surface temperature fields are also well mixed and are shown near the surface in Figure 3.8 (25.2 to 26.1 °C) and near the bottom in Figure 3.9 (25.2 to 26.2 °C), respectively.

3.2. Boundary Conditions

River inflows, wind and atmospheric pressure fields, and water level residual forcings were all included. Each of these effects is discussed in terms below.

Flows

Average daily flows were obtained from USGS, Houston Office, for Buffalo Bayou at Piney Point, TX (USGS Gauge 0807 3700), for the Trinity River at Romayor, TX (USGS Gauge 0806 6800), and for Lake Houston near Sheldon, TX (USGS Gauge 0807 2000). The Buffalo Bayou streamflow

contains a major portion of the City of Houston stormwater runoff and can be very flashy in nature. Flow event durations appear to be order 5 days on the San Jacinto. At station 0807 2000 Lake Houston near Sheldon, TX a stage vs discharge relation is used to convert measured stage to discharge. At stream inflow locations salinity is assumed zero, while temperature is set equal to the temperature of the inflow point.

January 1995: The Buffalo Bayou streamflow is shown in Figure 3.10. Flow events of JD 13, JD 24, JD 27, and JD 30 are to be noted. The observed mean of 780 cfs exceeds the climatological flow of 560 cfs by over 200 cfs. In Figure 3.11, the Trinity River at Romayor, TX streamflow is shown. Note the rising limb of the flow event occurs from JD 17 to 19 and recedes during the period JD 19 to 26. This flow event duration is order 7 days on the Trinity River. On JD 19 (19 January) the average daily streamflow exceeds 50,000 cfs. At station 0807 2000 Lake Houston near Sheldon, TX the released discharge is as shown in Figure 3.12. For the San Jacinto River, flow events on JD 14, 21, and 28 are to be noted.

October 1994: Buffalo Bayou streamflows are given in Figure 3.13. From JD 290 to 291 represents the rising portion of the flood, which recedes during JD 291 to 293. Note on JD 291 (18 October) the large inflow of over 4000 cfs. The climatological flow is order only 200 cfs for October and is substantially exceeded from JD 287 on. In Figure 3.14, the Trinity River at Romayor, TX streamflow during October is shown. Note the rising limb of the flood occurs from JD 291 to 292 and recedes during the period JD 292 to 296. The flood duration is order 7 days on the Trinity River. On JD 292 (19 October) the average daily streamflow is 120,000 cfs and represents the average daily flow of record. At Lake Houston near Sheldon, TX a stage vs discharge relation is used to convert water surface elevation at Lake Houston to released discharge as shown in Figure 3.15. For the San Jacinto River, the flood ascends during JD 291 to 292 and recedes over the next three days. On JD 292 (19 October) the average daily streamflow is 350,000 cfs and represents the average daily flow of record. The flood duration is thus of order 5 days on the San Jacinto.

Wind, Sea level Atmospheric Pressure, and Surface Heat Flux

NDBC buoy 42020 (3m Discus) and 42035 (3m Discus) and C-MAN station S-2 Sabine and S-4 Port Aransas, TX observations were obtained, along with NWS surface weather observations at Houston IAH, Port Arthur, and WSO Galveston, TX. Refer to Figure 2.1 for station locations. Wind and sea-level atmospheric pressure fields were developed at 3 hour intervals over the model domain via the one-step Barnes (1973) interpolation procedure discussed in Chapter 2. Prior to performing the interpolation, all winds are adjusted to 10m. At overwater stations (42035, Galveston) wind speeds are converted to land values by inverting the formula given by Hsu (1988). At Galveston the conversion from overwater to overland wind is not performed if wind directions are greater than 225 and less than 45 degrees True; e.g., the winds are blowing overland. The interpolation is then performed on overland winds. The formula of Hsu (1988) and the Galveston Bay Model land/water mask are then used to adjust the overland values to overwater values for all water cells.

The surface heat flux formulation developed by Martin (1985) reported in Chapter 2 was used. As input, one-step Barnes interpolations of the dry bulb temperature, wet bulb temperature, and cloud cover at the above meteorological stations to all Galveston Bay Model grid cells were performed.

January 1995: Daily average (8 fields per day) Galveston Bay Model grid cell minimum and maximum windspeed and atmospheric pressure are given in Table 3.1 for the resulting interpolations. Maximum wind strengths are order 25 kts. By reviewing the minimum atmospheric pressure column, one notes storm occurrences on January 6, 13 - 14, 18 and 22. Windfields at hour zero CST on JD 1, 11, and 21 are shown in Figures 3.16, 3.18, and 3.20, respectively, with corresponding windspeed contours shown in Figures 3.17, 3.19, and 3.21, respectively. On JD 1 hour zero CST, winds are directed offshore at 15 kts with a small segment of shelf southeast of Galveston over which winds come from the east and decrease in strength to 10 kts. On JD 21 hour zero CST winds are directed onshore at 10 to 15 kts. On JD 21 hour zero CST the winds are directed along shore to the northeast at less than 10 kts.

October 1994: Daily average (8 fields per day) Galveston Bay Model grid cell minimum and maximum windspeed and atmospheric pressure are given in Table 3.2 for the resulting interpolations. Maximum wind strengths are of order 25 kts. By reviewing the minimum atmospheric pressure column, one notes storm occurrences on October 7, 15 - 19, and 25. Windfields at hour zero CST on JD 274, 284, and 294 are shown in Figures 3.22, 3.24, and 3.26, respectively, with corresponding windspeed contours shown in Figures 3.23, 3.25, and 3.27, respectively. On JD 274 hour zero CST, winds are out of the east and turn to out of the northeast south of Galveston Bay. Windspeeds increase as the winds turn. On JD 284 hour zero CST winds are directed offshore and increase in magnitude as one proceeds offshore. On JD 294 hour zero the winds are directed onshore and decrease in strength as one proceeds onshore. These three windfields are representative of the three major types of windfields seen; e.g., onshore, offshore, and turning.

Subtidal Water Level

The observed subtidal water level at Galveston Pleasure Pier is obtained by detiding the observed water levels based on the harmonic constant set given in Schmalz (1996). We assume that the near-shelf wind response is small and that the subtidal water level at Galveston Pleasure Pier is nearly equal to that found on the near-shelf at a depth of 20m.

Observed subtidal water level at Galveston Pleasure Pier during January 1995 with mean 14 cm and standard deviation of 20 cm is given in Figure 3.28. Major events occur on JD 6, 14, 18, and 23, with excursions in subtidal water levels of up to 1.0 m associated with strong "Northers". For October 1994 as shown in Figure 3.29 the observed subtidal water level mean is 21 cm with a standard deviation of 11cm.

In each simulation, the observed subtidal water level at Galveston Pleasure Pier was added to the astronomical tide at each cell along the entire GBM open boundary. Despite the fact that the open boundary signals were not ramped, system depths are shallow enough (less than 20m) to damp out initial transients over a single day.

Salinity and Temperature

For the salinity and temperature open boundary conditions, climatological values consistent with the above initial conditions were used and the salinity and temperature fields were prognostically computed immediately at the simulation start. The assumption made was that the initial and

Table 3.1. January 1995 Galveston Bay Model Barnes Interpolation Summary

Day	Wind Speed Minimum (m/s)	Wind Speed Maximum (m/s)	Air Pressure Minimum (mb)	Air Pressure Maximum (mb)
1	6.27	9.61	1021.92	1025.92
2	5.61	10.04	1027.50	1030.21
3	5.31	8.64	1024.70	1026.93
4	6.56	11.89	1027.27	1029.98
5	6.85	10.47	1022.71	1027.90
6	5.36	10.46	1007.58	1011.65
7	3.72	7.11	1017.62	1021.66
8	2.84	6.53	1021.76	1023.41
9	2.31	6.14	1021.37	1022.54
10	4.39	8.49	1018.16	1020.17
11	4.93	9.84	1014.72	1016.49
12	4.63	9.55	1010.53	1013.26
13	3.63	10.41	1004.60	1007.40
14	7.26	11.25	1008.32	1010.80
15	3.74	8.05	1014.35	1016.84
16	4.22	8.18	1013.52	1015.60
17	4.90	8.95	1010.12	1012.48
18	6.49	11.87	1007.14	1010.47
19	5.70	10.27	1017.58	1020.98
20	3.54	6.29	1020.71	1022.56
21	2.09	5.83	1019.83	1021.44
22	3.85	8.60	1014.28	1017.77
23	5.62	11.28	1020.86	1025.78
24	2.93	6.31	1027.33	1028.68
25	4.59	7.87	1025.37	1027.27
26	5.43	9.02	1018.61	1021.73
27	5.75	8.60	1010.02	1012.38
28	6.00	8.70	1010.65	1012.75
29	5.50	8.95	1017.47	1020.48
30	5.67	8.62	1022.78	1025.23
31	3.02	6.54	1021.50	1023.42

Table 3.2. October 1994 Galveston Bay Model Barnes Interpolation Summary

Day	Wind Speed Minimum (m/s)	Wind Speed Maximum (m/s)	Air Pressure Minimum (mb)	Air Pressure Maximum (mb)
1	5.21	8.36	1006.40	1008.91
2	4.24	6.98	1003.40	1005.09
3	2.07	4.94	1007.98	1010.28
4	3.65	6.30	1014.96	1017.51
5	3.10	5.53	1015.19	1016.94
6	5.26	8.80	1011.86	1013.52
7	6.70	10.01	1008.41	1012.80
8	4.22	9.13	1010.98	1013.20
9	7.10	11.86	1015.07	1018.15
10	5.97	10.05	1016.24	1018.39
11	5.35	8.27	1015.03	1016.47
12	4.02	6.82	1013.19	1014.57
13	3.52	6.27	1014.54	1016.47
14	4.31	8.00	1014.57	1016.51
15	5.35	9.00	1009.10	1011.40
16	5.75	9.10	1010.34	1012.38
17	5.00	9.63	1011.40	1013.49
18	3.10	7.31	1012.42	1014.05
19	2.78	5.79	1014.16	1015.75
20	3.11	6.21	1015.43	1016.85
21	3.66	6.79	1012.03	1013.95
22	2.81	6.92	1010.39	1011.61
23	2.90	6.46	1013.71	1015.77
24	3.09	5.99	1015.35	1016.82
25	3.49	7.11	1014.82	1016.94
26	6.97	10.26	1019.42	1022.54
27	4.62	7.46	1020.12	1022.07
28	3.76	6.96	1016.52	1018.24
29	3.79	6.15	1014.88	1016.49
30	2.87	5.78	1015.53	1017.21
31	2.49	6.96	1013.45	1015.33

boundary conditions were sufficient to allow the density field to dynamically adjust to a representative value over a single day. This condition was not in general met for salinity. The salinity adjustment time length is a function of previous freshwater inflow histories. For low to moderate inflows such as occurred during January 1995, a very accurate initial state is required to obtain reasonable salinity levels and any error is felt over the entire one month simulation period. After high inflows during mid-October 1994, the effect of initial condition errors was eliminated.

3.3. Simulation Results

Simulated hydrodynamics are discussed in terms of water surface elevation, salinity, and temperature responses in turn below. For water levels both observed and simulated time series were demeaned. For salinity and temperature no demeaning was performed. As a result, error measures are expressed in terms of standard deviation (SD) for water levels and in terms of root mean square error (RMSE) for salinity and temperature. Note on all water surface elevation plots RMS ERROR corresponds to SD. The Willmott et al. (1985) dimensionless (0-1) average relative error (ARE) is also used to express the agreement in shape. For no error, this relative error is zero.

Water Surface Elevation

After the one-day spin-up period, simulated water levels were demeaned and are compared with demeaned observations in terms of standard deviation SD and the Willmott et al. (1985) dimensionless average relative error, ARE. The observed water level means are with respect to mean tide level adjusted to a tidal epoch based on only a single year's worth of data at the majority of stations. Only the two Galveston stations have a full 19 year data record to determine a true epoch mean tide level. Marmer (1951) notes that the error in deriving a epoch mean tide level based on a single year's data is order 1.5 cm. The simulated means are with respect to model datum, which represents a surface through the mean tide level; e.g., all model depths are adjusted to mean tide level. In addition, offsets from 3 to 4 cm have been added to the boundary reconstructed tidal signals to represent a northerly directed surface current. Refer to Schmalz (1996) for further details on tidal datums and mean determination.

January 1995: If one again assumes that the model datum approximates a true equipotential surface or geoid over Galveston Bay, we note from Table 3.3 that the mean water level rises by 6 cm from Galveston Pleasure Pier to Morgans Point and 4 cm from Galveston Pleasure Pier to Round Point at the head of Trinity Bay with a 3 cm rise through the Galveston Bay Entrance indicated by the difference in the two Galveston stations. With this in mind, we note that observed means indicate only a 1 cm rise over the Bay occurring through the Entrance. Assuming epoch mean tide levels do constitute an equipotential surface (subsidence issues aside), the difference in the two surfaces is order 5 to 10 cm as one moves up Galveston Bay.

Note the level of agreement in terms of SD is order 10 cm or better at most stations, with the exception of Rollover Pass. Agreement in shape, expressed in terms of average relative error, is order 0.05 except at Rollover Pass. The demeaned simulated water level response at Galveston Pleasure Pier is compared with demeaned observations at six-minute intervals in Figure 3.30. One notes high frequency oscillations (noise) in the simulated water level on JD 3, 6, 7, 12, 15, 19, and during JD 24 to 26.

Table 3.3. January 1995 Hindcast Water Surface Elevation Comparisons. Both model and observation time series are demeaned and the standard deviation (SD) is computed and compared with mean diurnal range (MDR).

Station Name	Observed Mean (cm)	Simulated Mean (cm)	SD, MDR (cm, cm)	ARE (-)
Galveston Pleasure Pier	-2	-2	8.5, 67	0.02
Galveston Pier 21	-1	1	6.2, 43	0.02
Christmas Bay	-1	5	7.3, 28	0.03
Port Bolivar	1	0	10.5, 43	0.06
Eagle Point	-1	4	7.6, 30	0.03
Clear Lake	-3	5	6.8, 28	0.02
Morgans Point	-1	4	7.4, 30	0.02
Round Point	-6	2	8.9, 30	0.03
Rollover Pass	-3	0	11.4, 41	0.08
High Island	-5	-7	9.2, 67	0.02

Time series of demeaned simulated and observed water levels at Galveston Pier 21 are shown in Figure 3.31. Noise in the simulated water level response is present at the times exhibited offshore at Galveston Pleasure Pier. The observed reduction in tidal amplitude through the Galveston Bay Entrance seems to be well replicated in the model. In Figure 3.32, the water level response at Christmas Bay is examined. No noise in simulated water levels is present and the agreement with observations suggest that the West Bay influence on water levels has been reasonably treated.

The water level response at Port Bolivar is examined in Figure 3.33. Noise in simulated water levels is present at the same times as at Galveston Pier 21. In Figure 3.34 the demeaned simulated water levels are compared with demeaned observations at Eagle Point. No noise is present in the simulated water level response.

At Clear Lake shown in Figure 3.35, the agreement is 7 cm RMS with no cell width reduction factor applied in the grid cell at the entrance to Clear Lake. At Morgans Point the simulated water level response in Figure 3.36 is similar to that at Clear Lake.

Simulated water level responses at Round Point are compared with observations in Figure 3.37. Note the absence of low water on JD 14,15,19,23,24,29, and 30. The simulated water levels are in general agreement with the observations except that no loss of low water is indicated in the model and the cell width flow reduction factors remain greater than zero. Additional knowledge on the spatial extent of the wetting/drying region is needed to further evaluate the drying/wetting algorithm.

At Rollover Pass in Figure 3.38 and High Island in Figure 3.39, noise in simulated water levels is present at the same times as at Galveston Pleasure Pier. Oscillations evident in the simulated Galveston Bay water level response are not present in the simulated water level responses at stations above Eagle Point. It appears that the noise in water level response may be induced from the clamped water surface elevation offshore boundary condition (no radiation condition is applied) and propagates through the Galveston Bay entrance channel and is damped out in lower to middle Galveston Bay.

October 1994: Simulated demeaned water level are compared with demeaned observations in terms of SD and the Willmott et al. (1985) dimensionless average relative error as given in Table 3.4. If one assumes that the model datum approximates a true equipotential surface or geoid over Galveston Bay, we note that the mean water level rises by order 10 cm from Galveston Pleasure Pier to Morgans Point and a 5 cm rise through the Galveston Bay Entrance. With this in mind, we note that the observed means indicate only a 3 cm rise over the Bay and only a 1 cm rise through the Entrance. If one ignores subsidence effects and assumes that the epoch mean tide levels do constitute an equipotential surface, then the difference between the two surfaces is order 7 cm.

Table 3.4. October 1994 Hindcast Water Surface Elevation Comparisons. Both model and observation time series are demeaned and the standard deviation (SD) is computed and compared with mean diurnal range (MDR).

Station Name	Observed Mean (cm)	Simulated Mean (cm)	SD, MDR (cm, cm)	ARE (-)
Galveston Pleasure Pier	37	46	7.7, 67	0.04
Galveston Pier 21	38	51	5.3, 43	0.03
Christmas Bay	38	54	4.6, 28	0.04
Port Bolivar	37	50	10.8, 43	0.11
Eagle Point	37	55	8.5, 30	0.07
Clear Lake	41	56	8.1, 28	0.04
Morgans Point	40	56	9.3, 30	0.04

Note the level of agreement in terms of SD is order 10 cm or better at most stations, with the exception of Port Bolivar. Agreement in shape expressed in terms of average relative error is order 0.05 except at Port Bolivar.

The demeaned simulated water level response at Galveston Pleasure Pier is compared with demeaned observations at six-minute intervals in Figure 3.40. One notes high frequency oscillations (noise) in the simulated water level during JD 282 to 284 and on JD 300. Time series of demeaned simulated and observed water levels at Galveston Pier 21 are shown in Figure 3.41. Noise in the simulated water level response is again present during JD 282 to 284 and on JD 300. The observed reduction in tidal amplitude through the Galveston Bay Entrance again seems to be well replicated in the model. At Christmas Bay no noise in simulated water levels is present and the agreement with observations suggest that the West Bay influence on water levels has been reasonably treated.

The water level response at Port Bolivar is examined in Figure 3.42. During the first week, JD 275 to 282, the demeaned simulated water levels exceed the demeaned observation. Noise in simulated water levels is present at JD 282 to 284 and on JD 300. Good agreement between demeaned simulated vs demeaned observed water levels is achieved during the periods JD 284 to 292 and JD 302 to 305. During the period JD 292 to 303, the demeaned simulated water levels are lower than the demeaned observations.

In Figure 3.43 the demeaned simulated water levels are compared with demeaned observations at Eagle Point. During the peak flood period JD 290 to 294, the simulated water levels exceed the observations. No high frequency oscillations are present in the simulated water level response. At Clear Lake, shown in Figure 3.44, during the peak flood period the situation is reversed, with the

simulated water levels less than observations. It is possible that the entrance to Clear Lake in reality is more restricted than in the model. No cell width reduction factor has been applied in the grid cell at the entrance to Clear Lake.

At Morgans Point the simulated water level response in Figure 3.45 is similar to that at Eagle Point and opposite to that at Clear Lake; e.g., during the peak flood period, the simulated water level response is higher than observations. Two factors may contribute to this behavior: 1) the timing of the Trinity River inflow and 2) the inability of the model to treat overland flooding of low lying marsh areas. The presence of the noise during JD 300 in the simulated water level response is noted.

Noise in simulated water level response at Galveston Pleasure Pier is not present in the simulated water level responses at stations above Eagle Point. It appears that the high frequency oscillations (noise) in water level response are a Galveston Bay entrance phenomena and may be induced from the clamped water surface elevation offshore boundary condition. Wind-induced oscillations over the Shelf region of the grid are reflected from the open boundary since a radiation boundary condition is not used.

Salinity

January 1995: Simulated mid-depth (level 3) salinity time series are compared with TWDB datasonde observed salinities in Table 3.5 in terms of root mean square error (RMSE) and ARE. Observed means differ from simulated means by as little as 0.5 PSU at Trinity Bay-DBC to over 4.0 PSU at Hannah Reef. The difference in means contributes substantially to the RMSEs. AREs are above 0.25 indicating substantial disagreement agreement in shape.

If one considers the time series at Dollar Point in Figure 3.46, at Trinity Bay-DBC in Figure 3.47, at Hannah Reef in Figure 3.48, and at Red Bluff in Figure 3.49, one notes a problem with the initial condition determination. Model initial conditions are in general higher than observations by order 3 to 10 PSU.

At Dollar Point in Figure 3.46, the simulated sinusoidal response at tidal period, indicative of the advection of a large horizontal salinity gradient, is in general agreement with the observations. The salinity response at Trinity Bay-DBC shown in Figure 3.47 appears to be primarily influenced by the Trinity River inflow. During this period it is essentially fresh, in agreement with observations.

The simulated salinity response at Hannah Reef, shown in Figure 3.48, diverges from the observations particularly during JD 17 to 20, during which the inflow of saline water appears not to have been captured by the model. At Red Bluff, shown in Figure 3.49, the model trend exhibits a decrease of over 10 PSU over the month, while the observations show a near constant mean of order 6 PSU.

It appears that streamflows are sufficient to maintain a large horizontal salinity gradient, which is at its maximum in lower Galveston Bay and in East Bay. Station data are insufficient (Port Bolivar data not available) to resolve the gradient structure in the initial conditions and along the near-shelf boundary such that a close agreement in model and observed salinity response can be obtained over Galveston Bay.

Table 3.5. January 1995 Mid-depth Salinity Comparisons

TWDB Station	Observed Mean (PSU)	Simulated Mean (PSU)	RMSE (PSU)	ARE (-)
Dollar Point	11.0	12.6	5.5	0.26
Trinity Bay-DBC	0.1	0.6	0.8	0.70
Hannah Reef	9.5	5.1	5.8	0.53
Red Bluff	8.8	6.2	4.6	0.60

October 1994: Simulated mid-depth (level 3) salinity time series are compared with TWDB datasonde observations (refer to Figure 3.1) in Table 3.6. Observed means are lower than simulated means by 1.5 to 3.5 PSU, which is the order of the RMS errors. Relative errors are order 0.05 indicating excellent agreement in shape.

If one considers the time series at Port Bolivar in Figure 3.50, at Trinity Bay-DBC in Figure 3.51, at Dollar Point in Figure 3.52, and at Red Bluff in Figure 3.53, one notes a problem with the initial condition based on an average tidal cycle determination. Model initial conditions are in general higher than observations by order 3 to 10 PSU.

At Port Bolivar in Figure 3.50, the simulated sinusoidal response at tidal period, indicative of the advection of a large horizontal salinity gradient, is in excellent agreement with the observations. The simulated time of occurrence of the drop in salinity associated with the freshwater flood pulse is in excellent agreement with observations. This flood pulse wipes out the influence of the initial conditions and after the flood pulse, the correspondence in the simulated and observed salinity response is excellent. There is no under or overshooting in the simulated salinity response, which is also positive definite. This behavior indicates that the FCT salinity transport algorithm is very effective in handling the large horizontal salinity gradients present.

The salinity response at Trinity Bay-DBC is shown in Figure 3.51. Based on its location shown in Figure 3.1, it appears that this station at the head of Trinity Bay is primarily influenced by the Trinity River inflow. In the simulation, the Trinity River flows measured at Romayor, TX at river mile 94.3, were directly input with no time lag to represent the freshwater inflow from the Trinity River. Based on the timing of the freshwater influence indicated by the observations, it appears that these flows should be lagged by order 2 to 3 days.

The initial condition error is order 10 PSU at Dollar Point (Figure 3.52) and 5 PSU at Red Bluff (Figure 3.53). However, after the freshwater flood pulse, the agreement between simulated and observed salinities is much improved.

Table 3.6. October 1994 Mid-depth Salinity Comparisons

TWDB Station	Observed Mean (PSU)	Simulated Mean (PSU)	RMSE (PSU)	ARE (-)
Port Bolivar	17.4	21.0	4.4	0.06
Trinity Bay-DBC	9.4	7.9	3.4	0.07
Dollar Point	12.3	15.4	4.8	0.07
Red Bluff	10.3	11.7	2.2	0.02

Temperature

January 1995: Simulated mid-depth (level 3) temperature time series are compared with TWDB datasonde observed salinities in Table 3.7. Refer to Figure 3.1 for station locations. Observed means are lower than simulated means by order 2 °C. RMS errors are order 4.0 to 5.0 °C and Willmott (1985) average relative errors are greater than 0.5.

Simulated temperature responses are compared with observations at Dollar Point in Figure 3.54, at Trinity Bay-DBC in Figure 3.55, at Hannah Reef in Figure 3.56, and at Red Bluff in Figure 3.57. Note the absence of any large horizontal gradients in temperature in the observations, which would be suggested by sinusoidal behavior at tidal period. At all observation stations, there is a slight warming over the period of order 1 to 2 °C. However, a decrease in temperatures over the month of order 3 °C is exhibited in the model response at all stations. A review of the incoming short wave radiation mechanics would appear to be warranted with a focus on the representation of the transmissivity of the earth's atmosphere.

Table 3.7. January 1995 Mid-depth Temperature Comparisons

TWDB Station	Observed Mean (deg C)	Simulated Mean (deg C)	RMSE (deg C)	ARE (-)
Dollar Point	12.7	8.4	4.7	0.66
Trinity Bay-DBC	12.2	8.1	4.8	0.58
Hannah Reef	12.5	7.6	5.2	0.61
Red Bluff	13.0	7.2	6.3	0.69

October 1994: Simulated mid-depth (level 3) temperature time series are compared with TWDB datasonde observed temperatures in Table 3.8. Refer to Figure 3.1 for station locations. Observed means are higher than simulated means by order 2 °C. RMS errors are order 2.5 to 3.0 °C and relative errors are order 0.25.

Simulated temperature responses are compared with observations at Port Bolivar in Figure 3.58, at Trinity Bay-DBC in Figure 3.59, at Dollar Point at Figure 3.60, and at Red Bluff in Figure 3.61. At Port Bolivar (Figure 3.58) the observed sinusoidal response at tidal period during JD 300 to 305, indicative of the advection of a large horizontal temperature gradient, is well represented by the model. At all stations, the general cooling over the period JD 284 to 287 and warming over the period JD 287 to 293 in the observations is well represented. Consistent with results obtained for the January 1995 hindcast discussed above, the discrepancy in the magnitudes of the cooling and warming again suggest a review of the incoming short wave radiation mechanics.

Table 3.8. October 1994 Mid-depth Temperature Comparisons

TWDB Station	Observed Mean (deg C)	Simulated Mean (deg C)	RMSE (deg C)	ARE (-)
Port Bolivar	23.5	21.7	2.3	0.28
Trinity Bay-DBC	22.7	20.0	2.9	0.22
Dollar Point	23.2	20.9	2.6	0.24
Red Bluff	23.3	20.4	3.3	0.33

TWDB DATASONDE LOCATIONS

- 29.90

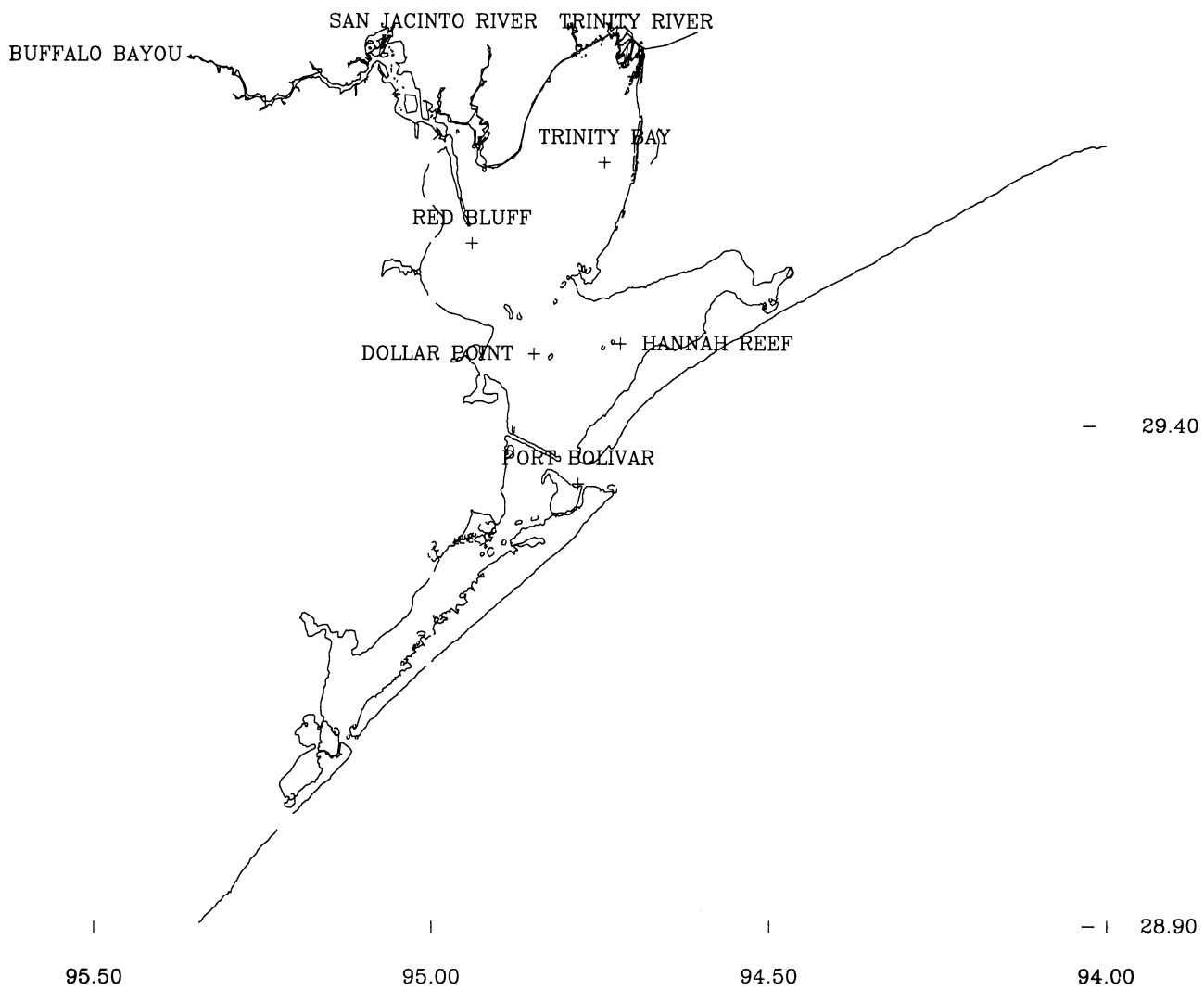


Figure 3.1. Texas Water Development Board Salinity and Temperature Station Locations

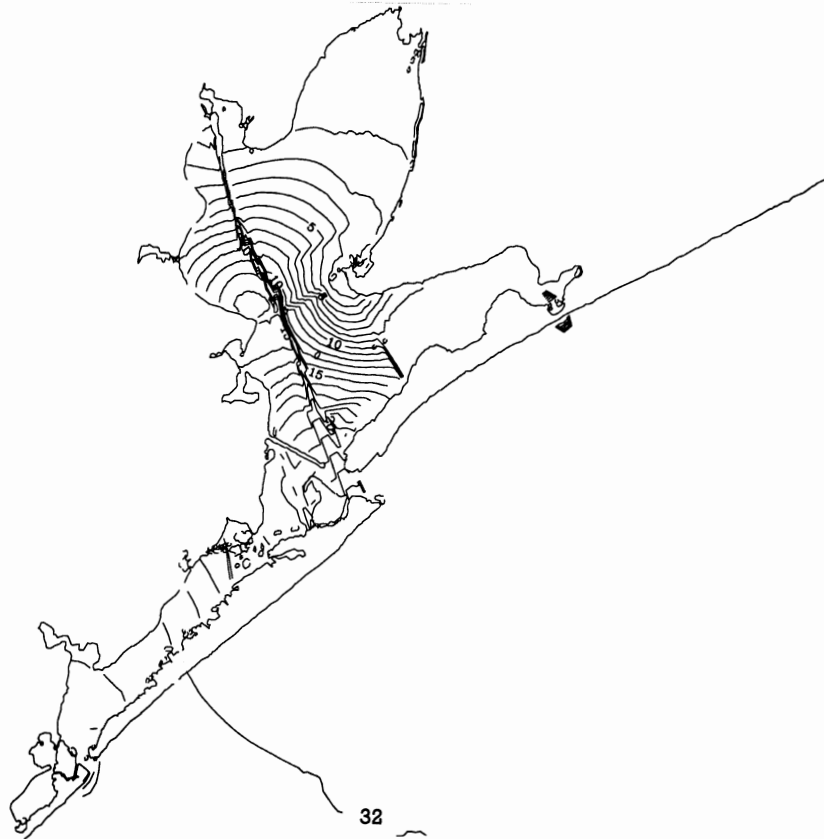


Figure 3.2. Initial Near-surface Salinity Field (PSU) 1 January 1995

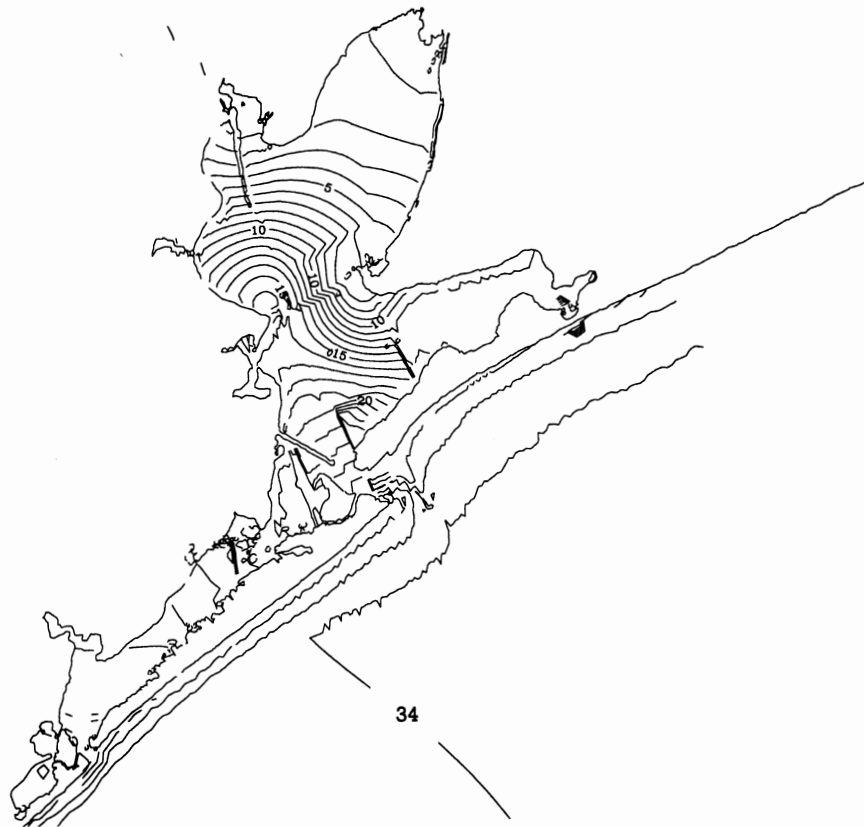


Figure 3.3. Initial Near-bottom Salinity Field (PSU) 1 January 1995



Figure 3.4. Initial Near-surface Temperature Field (°C) 1 January 1995

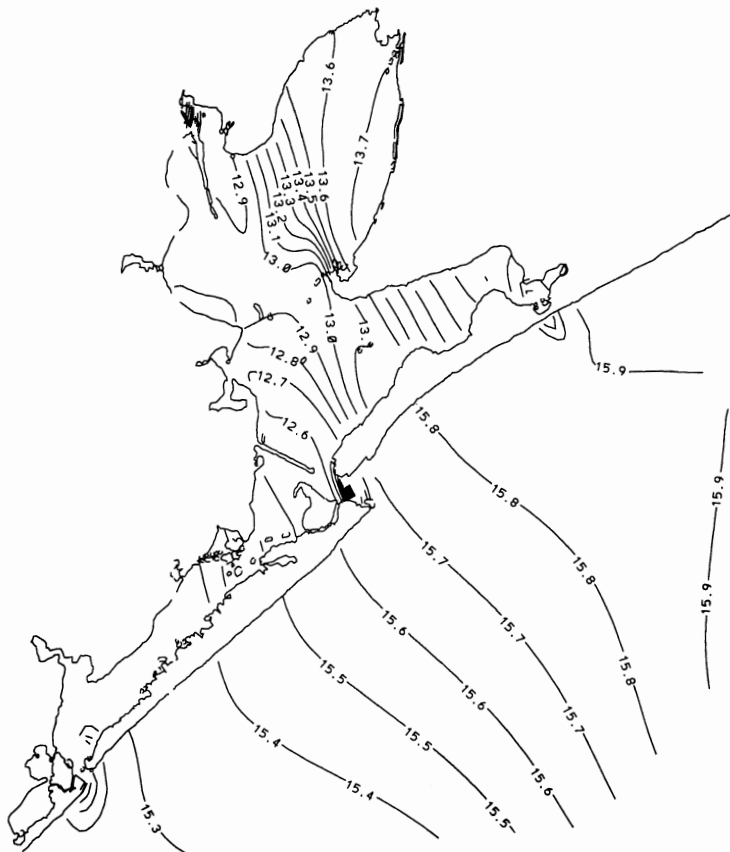


Figure 3.5. Initial Near-bottom Temperature Field (°C) 1 January 1995

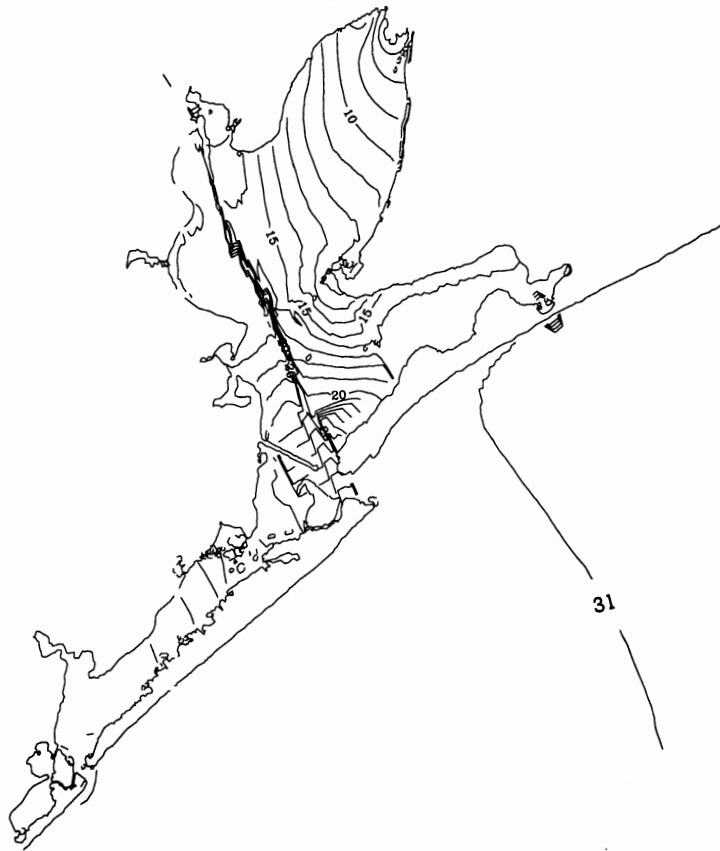


Figure 3.6. Initial Near-surface Salinity Field (PSU) 1 October 1994

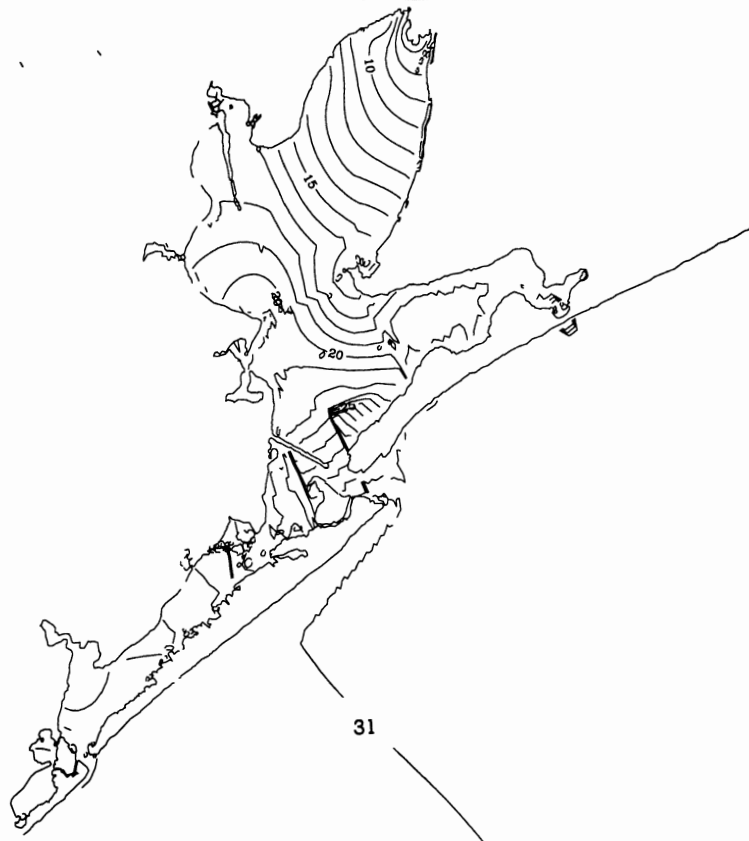


Figure 3.7. Initial Near-bottom Salinity Field (PSU) 1 October 1994



Figure 3.8. Initial Near-surface Temperature Field (°C) 1 October 1994

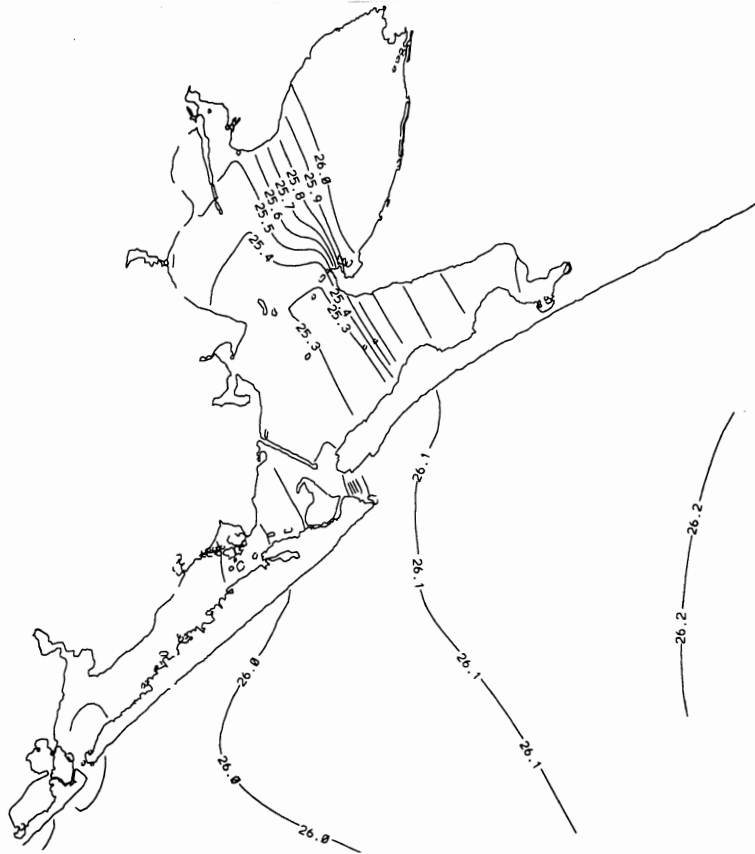


Figure 3.9. Initial Near-bottom Temperature Field (°C) 1 October 1994

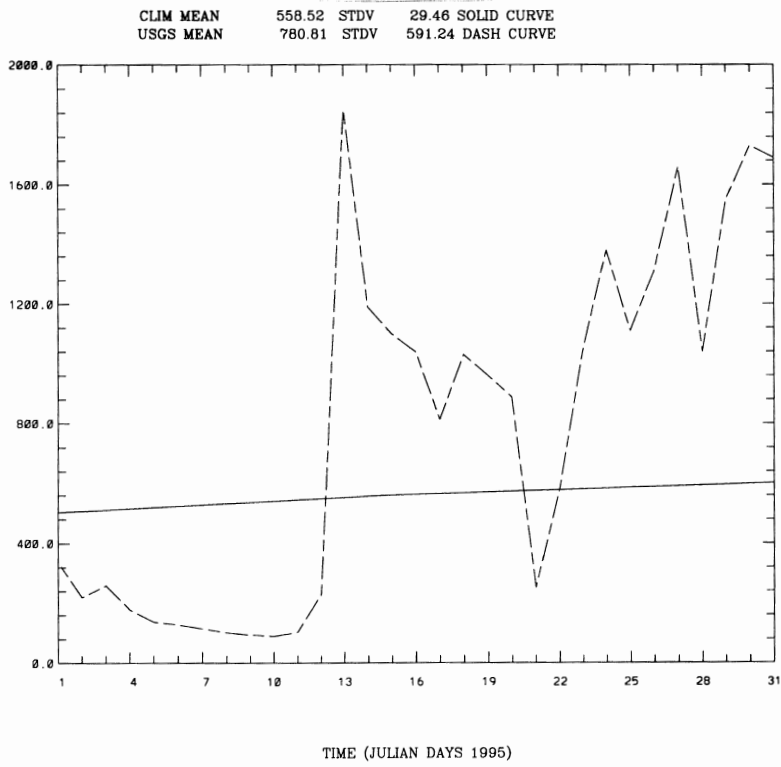


Figure 3.10. USGS Average Daily Flows (Cfs) Buffalo Bayou at Piney Point, TX in January 1995

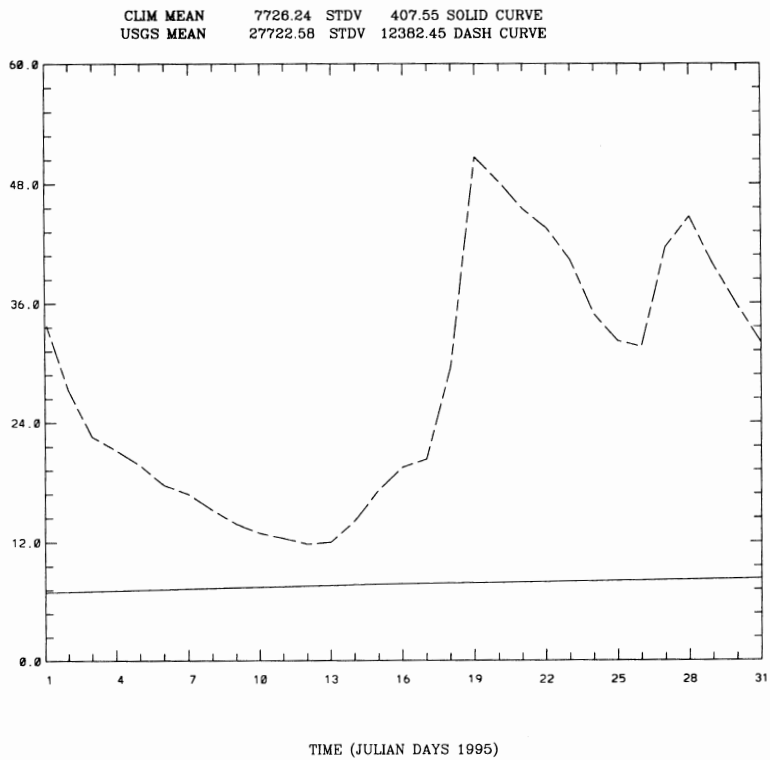


Figure 3.11. USGS Average Daily Flows (10^{-3} Cfs) Trinity River at Romayor, TX in January 1995

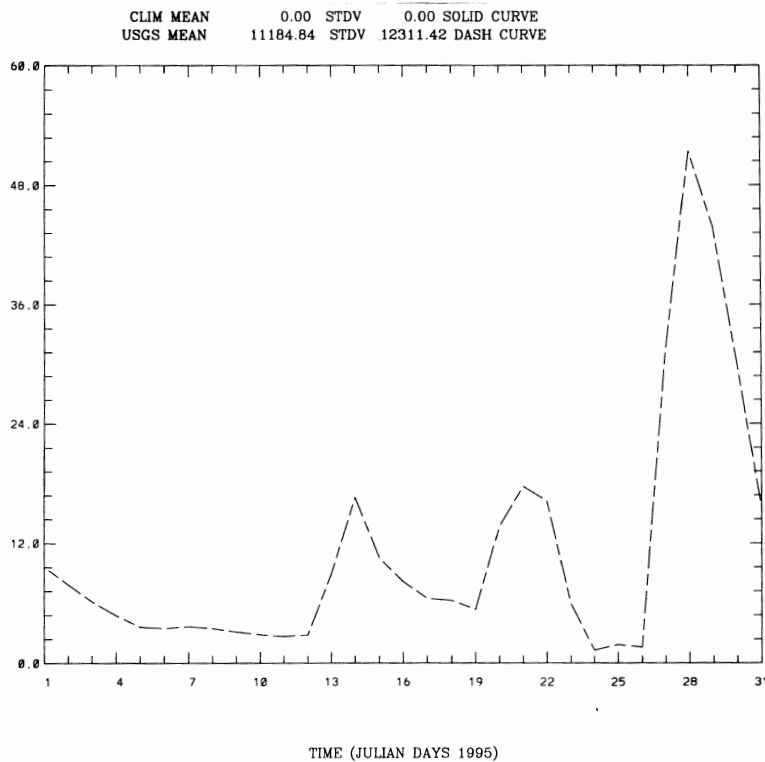


Figure 3.12. USGS Average Daily Flows (10^3 Cfs) San Jacinto River near Sheldon, TX in January 1995

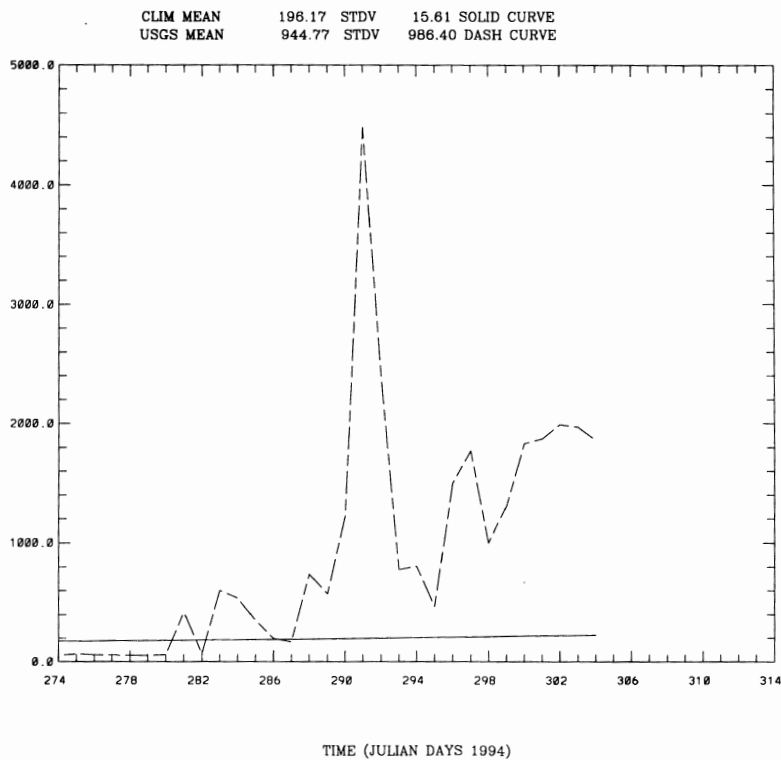


Figure 3.13. USGS Average Daily Flows (Cfs) Buffalo Bayou at Piney Point, TX in October 1994

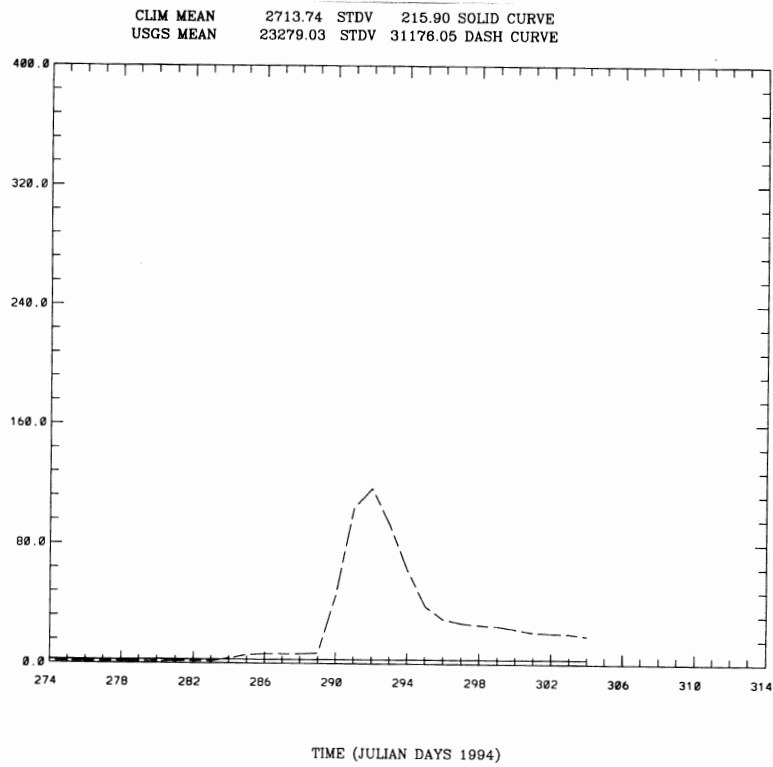


Figure 3.14. USGS Average Daily Flows Trinity River (10^3 Cfs) at Romayor, TX in October 1994

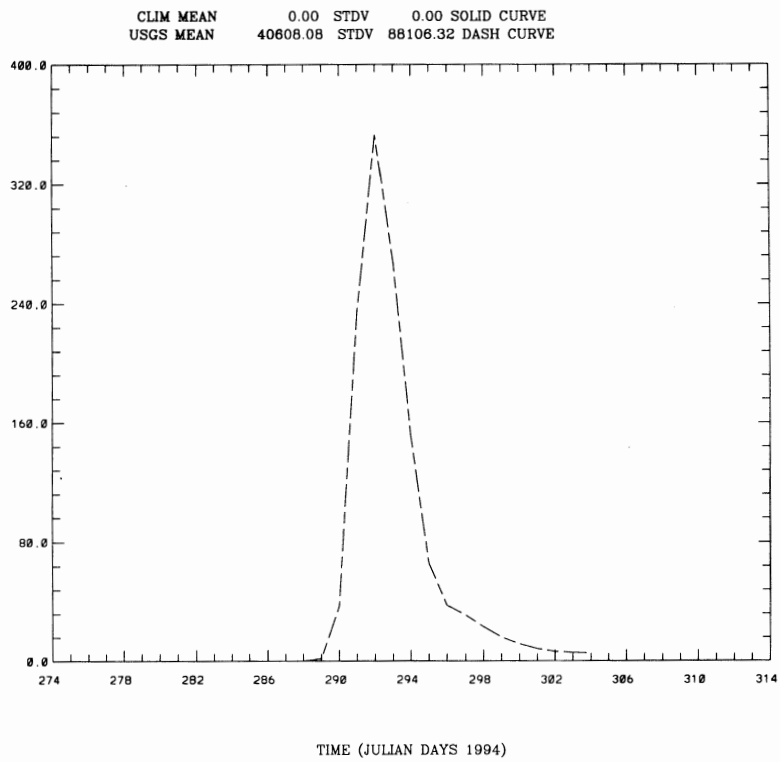


Figure 3.15. USGS Average Daily Flows San Jacinto River (10^3 Cfs) near Sheldon, TX in October 1994

WIND

Data Source NOS
wmin = 4.10 wmax = 8.53
Julian Date = 1.000
January 1 1995

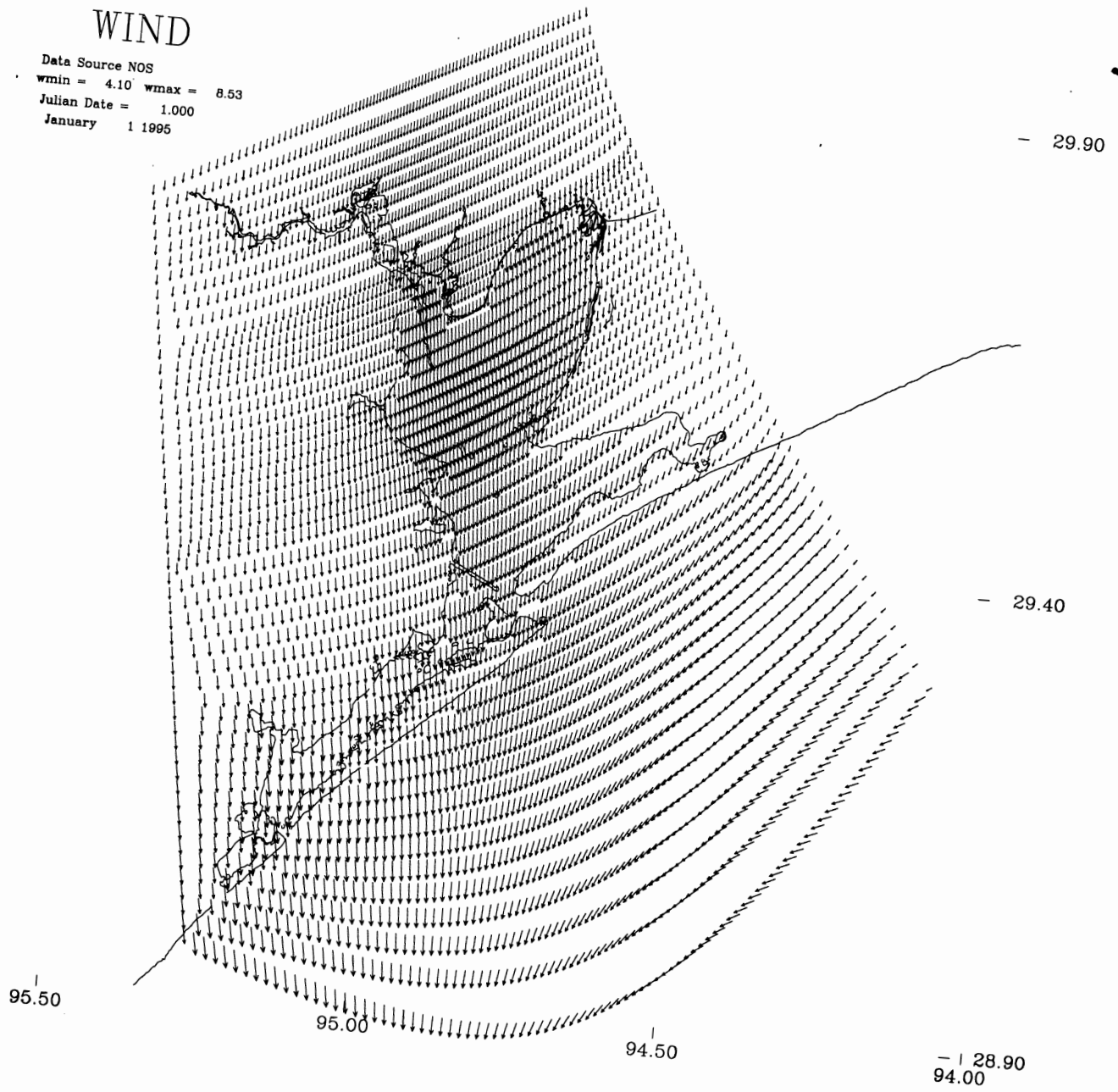


Figure 3.16. JD 1 (1995) Barnes Interpolation Windfield

WIND SPEED (M/S)

Data Source NOS

cmin = 2.00, cmax = 12.00, contour interval = 0.50

- 29.90

Julian Date = 1.000

January 1 1995

wmin = 4.10, wmax = 8.53

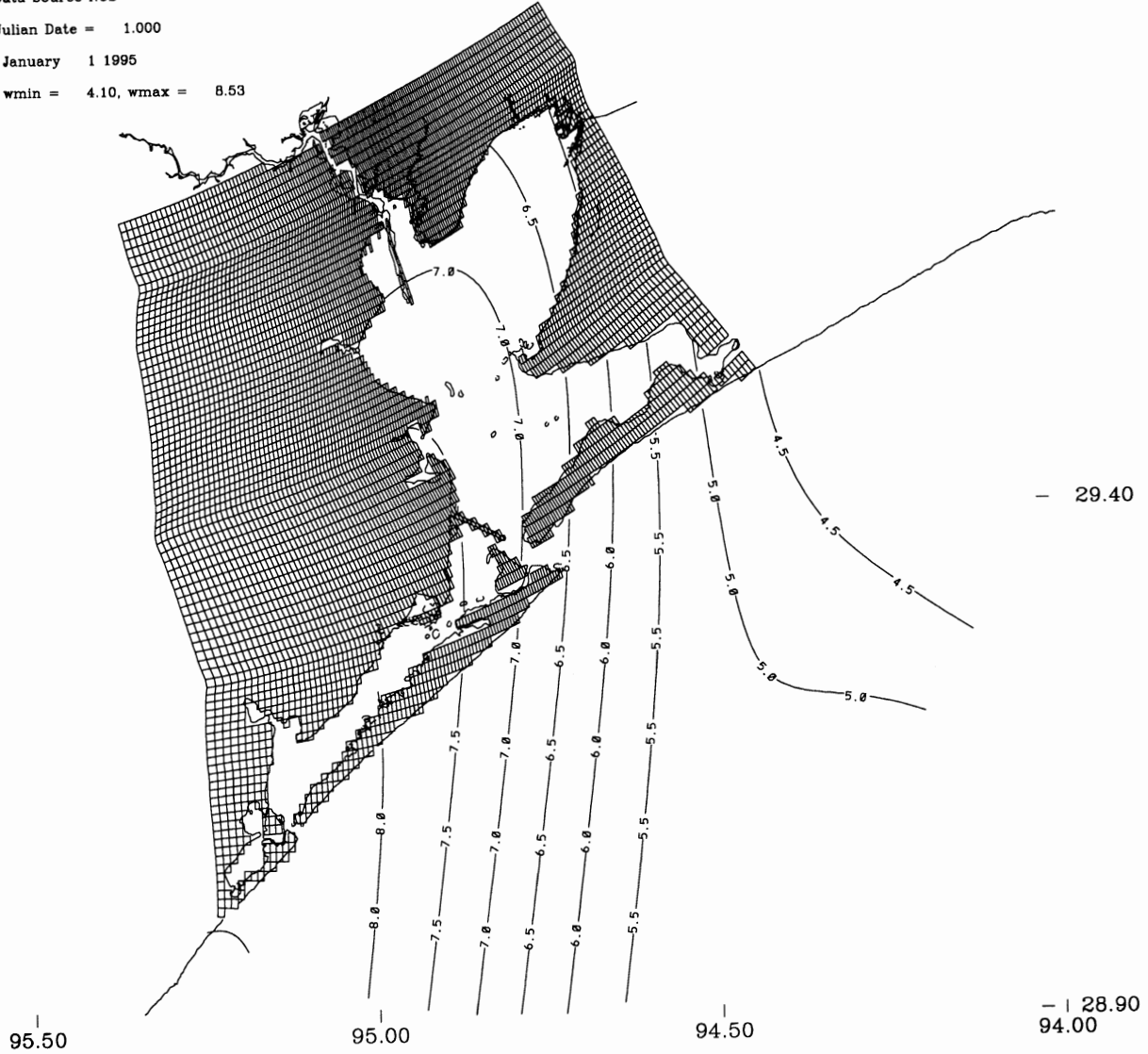


Figure 3.17. JD 1 (1995) Barnes Interpolation Windspeed Contours

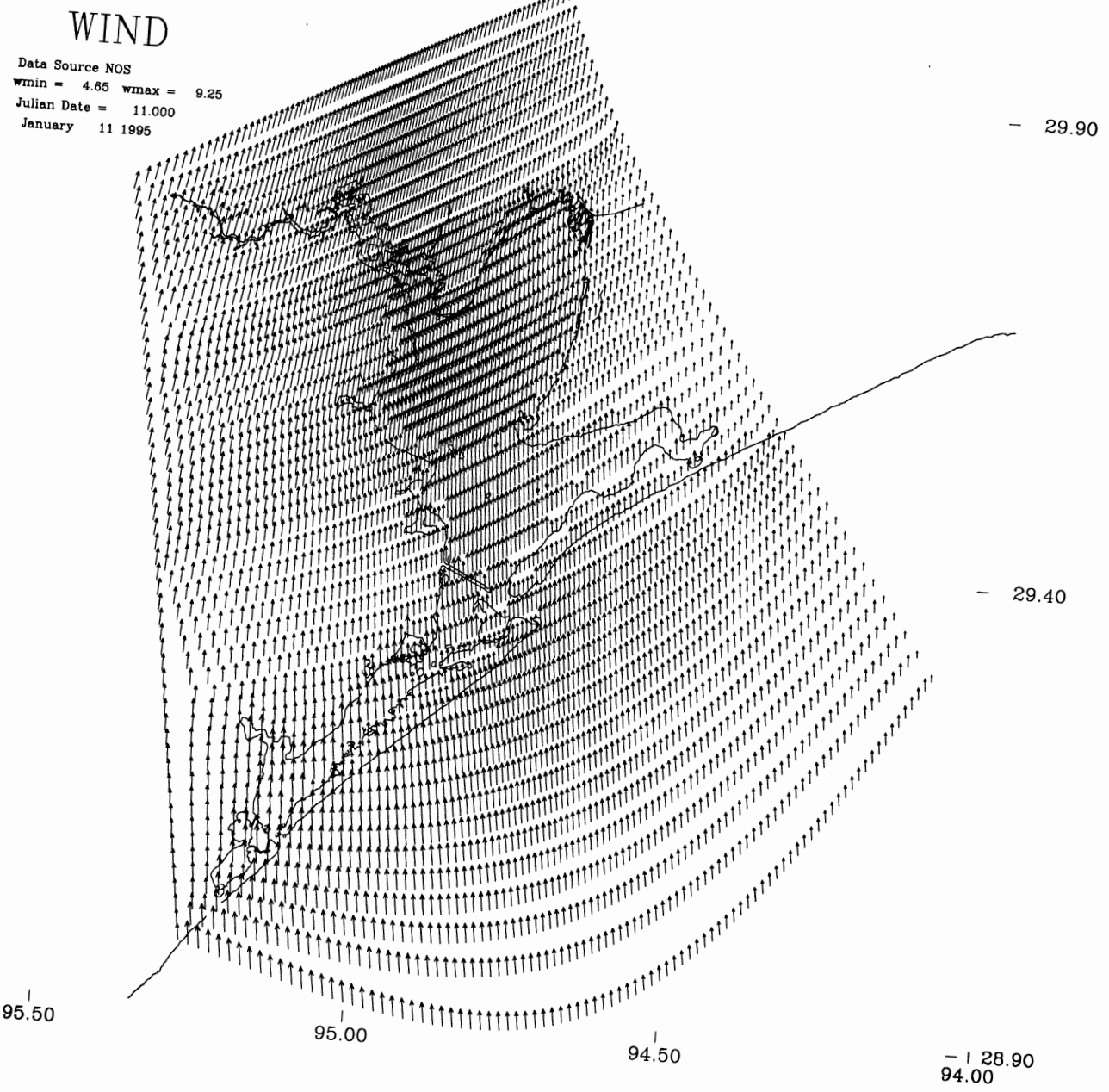


Figure 3.18. JD 11 (1995) Barnes Interpolation Windfield

WIND SPEED (M/S)

Data Source NOS

cmin = 2.00, cmax = 12.00, contour interval = 0.50

— 29.90

Julian Date = 11.000

January 11 1995

wmin = 4.65, wmax = 9.25

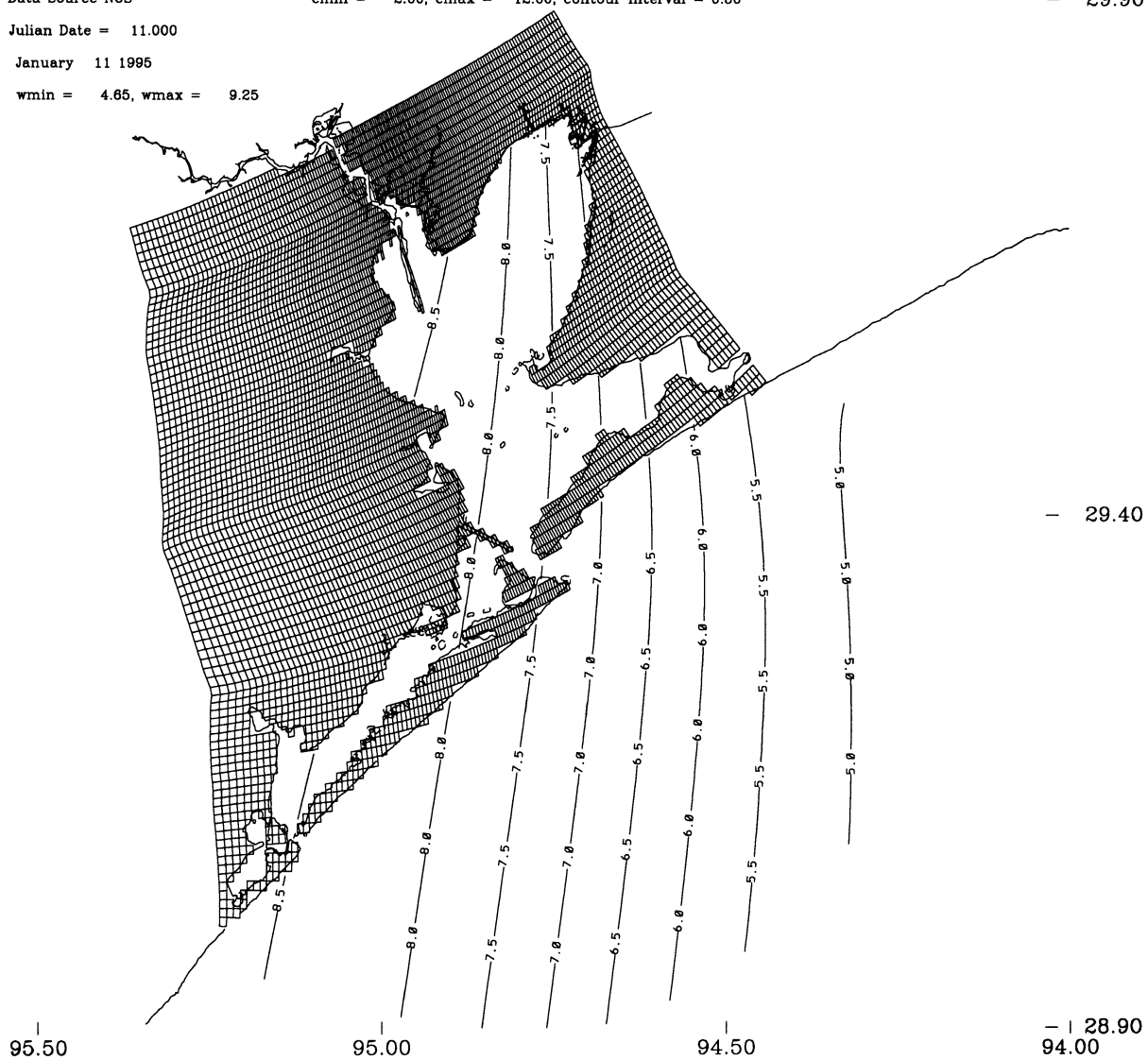


Figure 3.19. JD 11 (1995) Barnes Interpolation Windspeed Contours

WIND

Data Source NOS
wmin = 1.90 wmax = 5.48
Julian Date = 21.000
January 21 1995

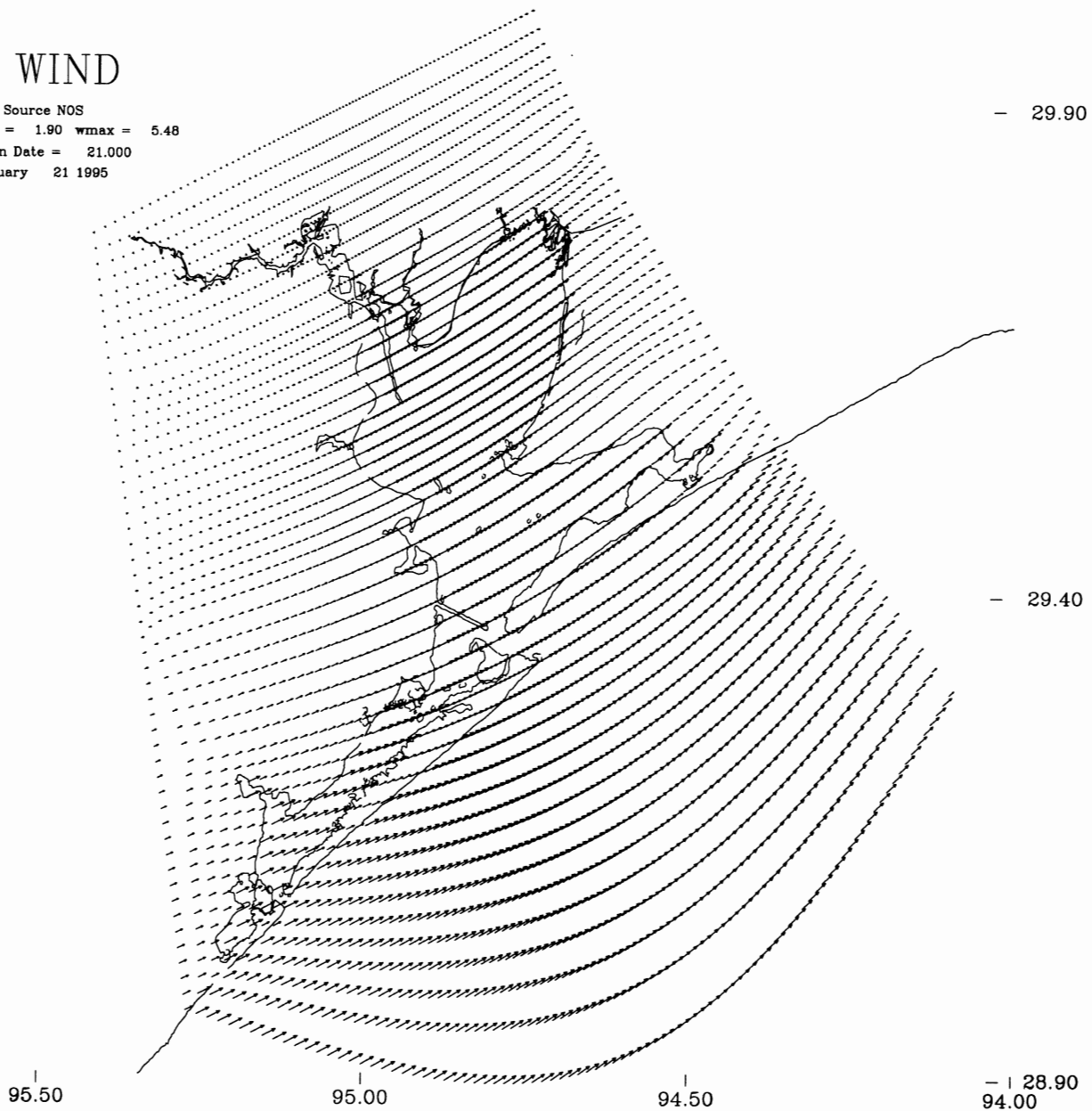


Figure 3.20. JD 21 (1995) Barnes Interpolation Windfield

WIND SPEED (M/S)

Data Source NOS

cmin = 2.00, cmax = 12.00, contour interval = 0.50

— 29.90

Julian Date = 21.000

January 21 1995

wmin = 1.90, wmax = 5.48

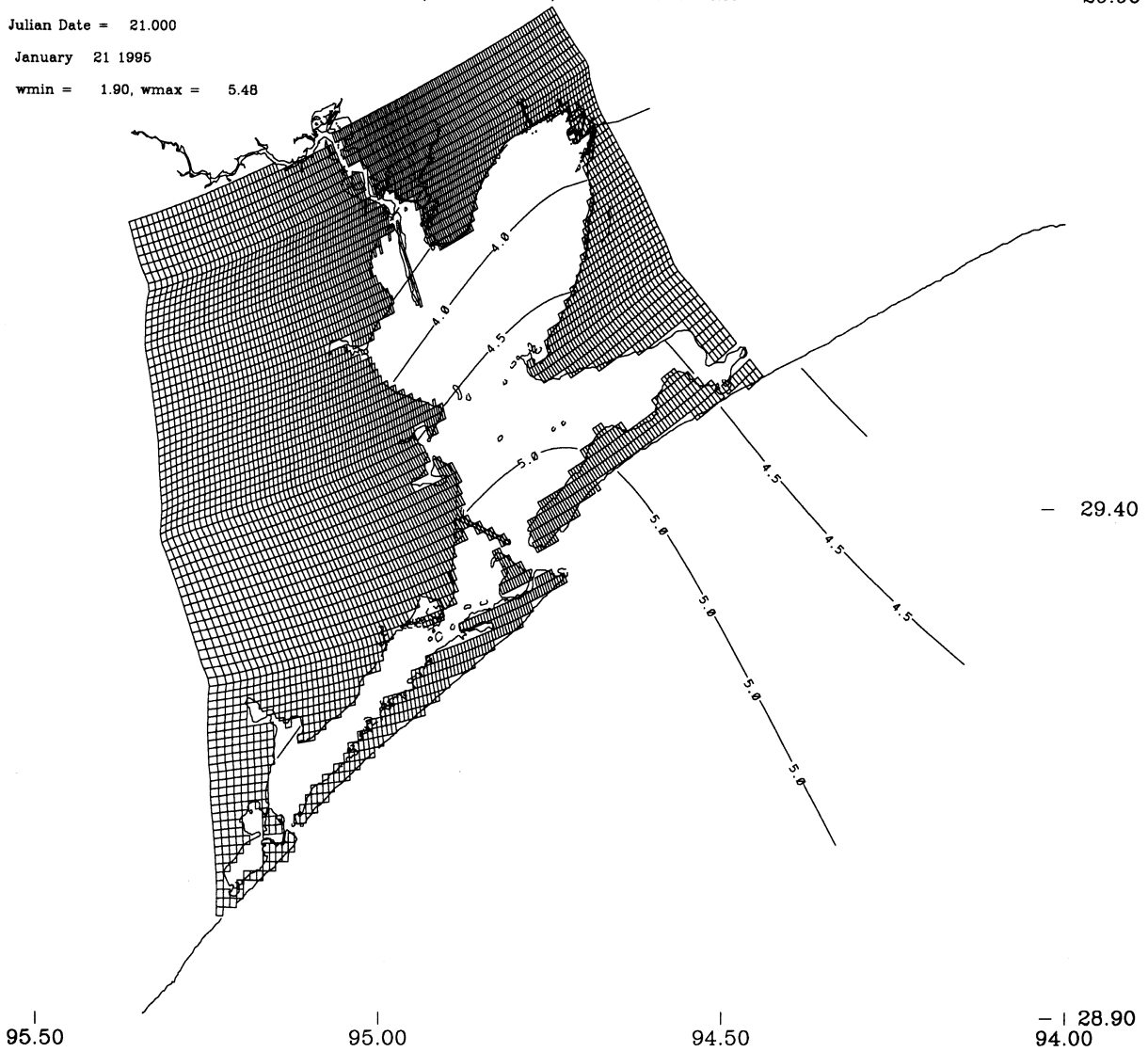


Figure 3.21. JD 21 (1995) Barnes Interpolation Windspeed Contours

WIND

Data Source NOS
wmin = 3.24 wmax = 6.82
Julian Date = 274.000
October 1 1994

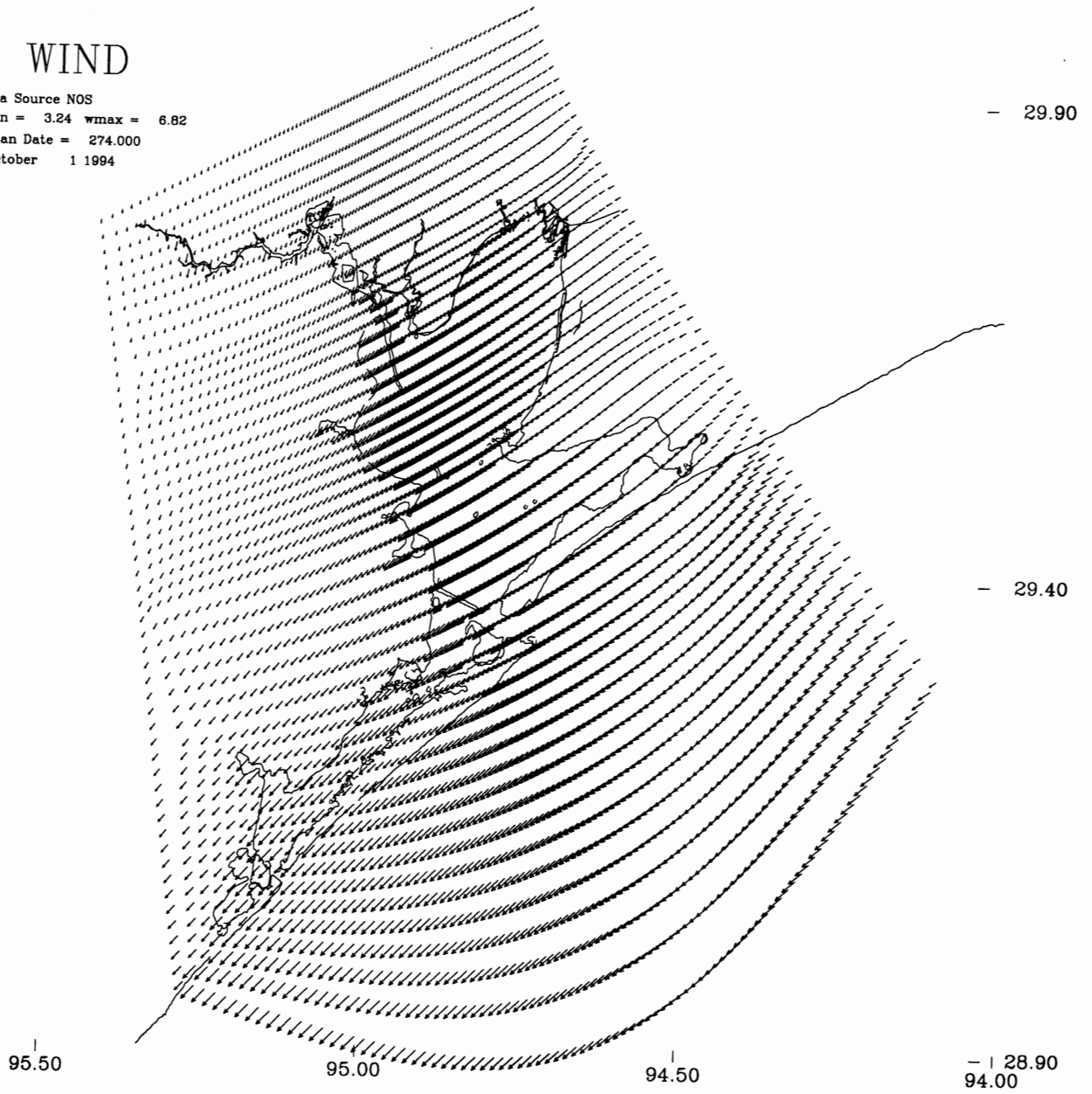


Figure 3.22. JD 274 (1994) Barnes Interpolation Windfield

WIND SPEED (M/S)

Data Source NOS

Julian Date = 274.000

October 1 1994

wmin = 3.24, wmax = 6.82

cmin = 2.00, cmax = 12.00, contour interval = 0.50

- 29.90

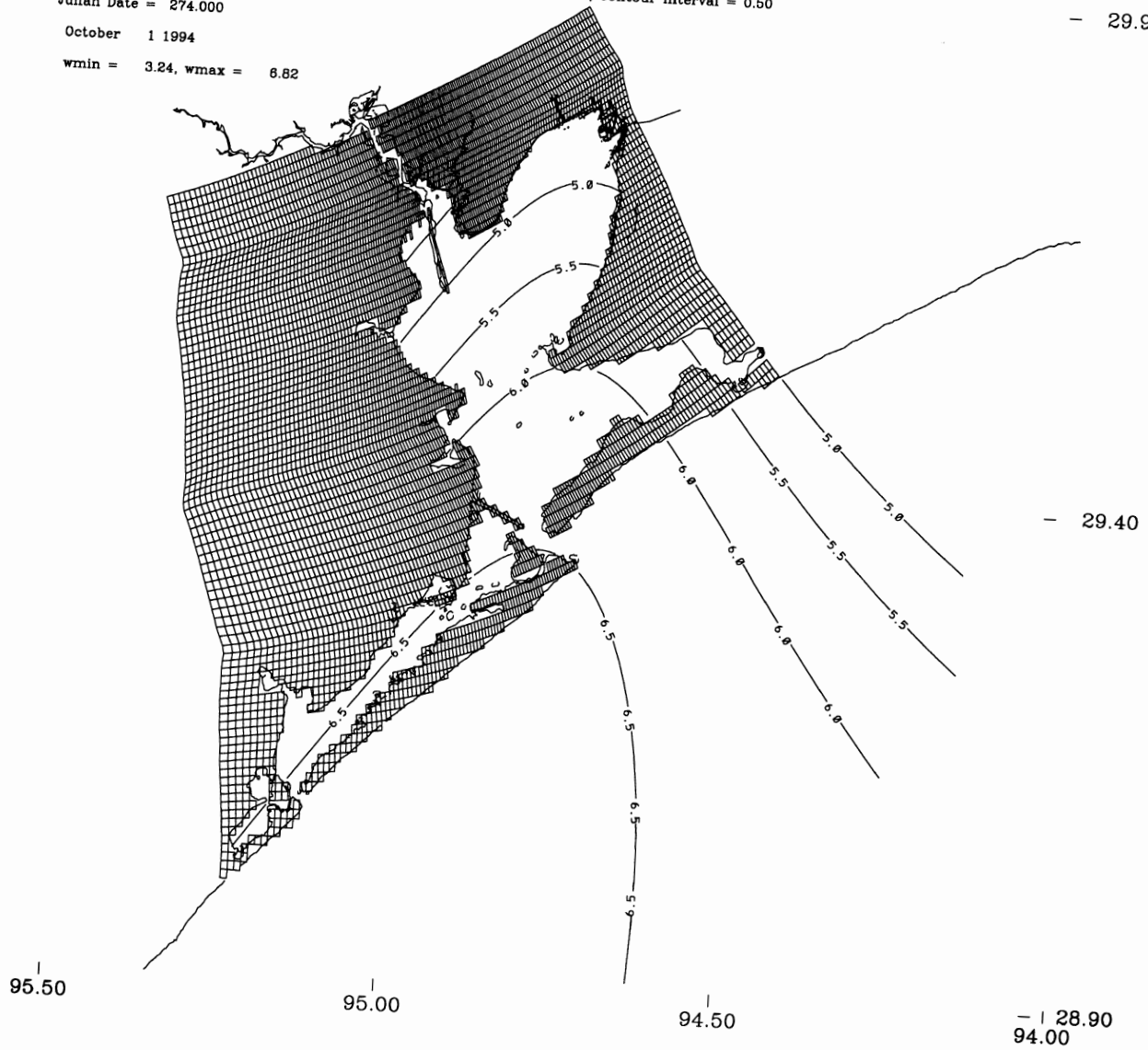


Figure 3.23. JD 274 (1994) Barnes Interpolation Windspeed Contours

WIND

Data Source NOS
wmin = 5.17 wmax = 8.52
Julian Date = 284.000
October 11 1994

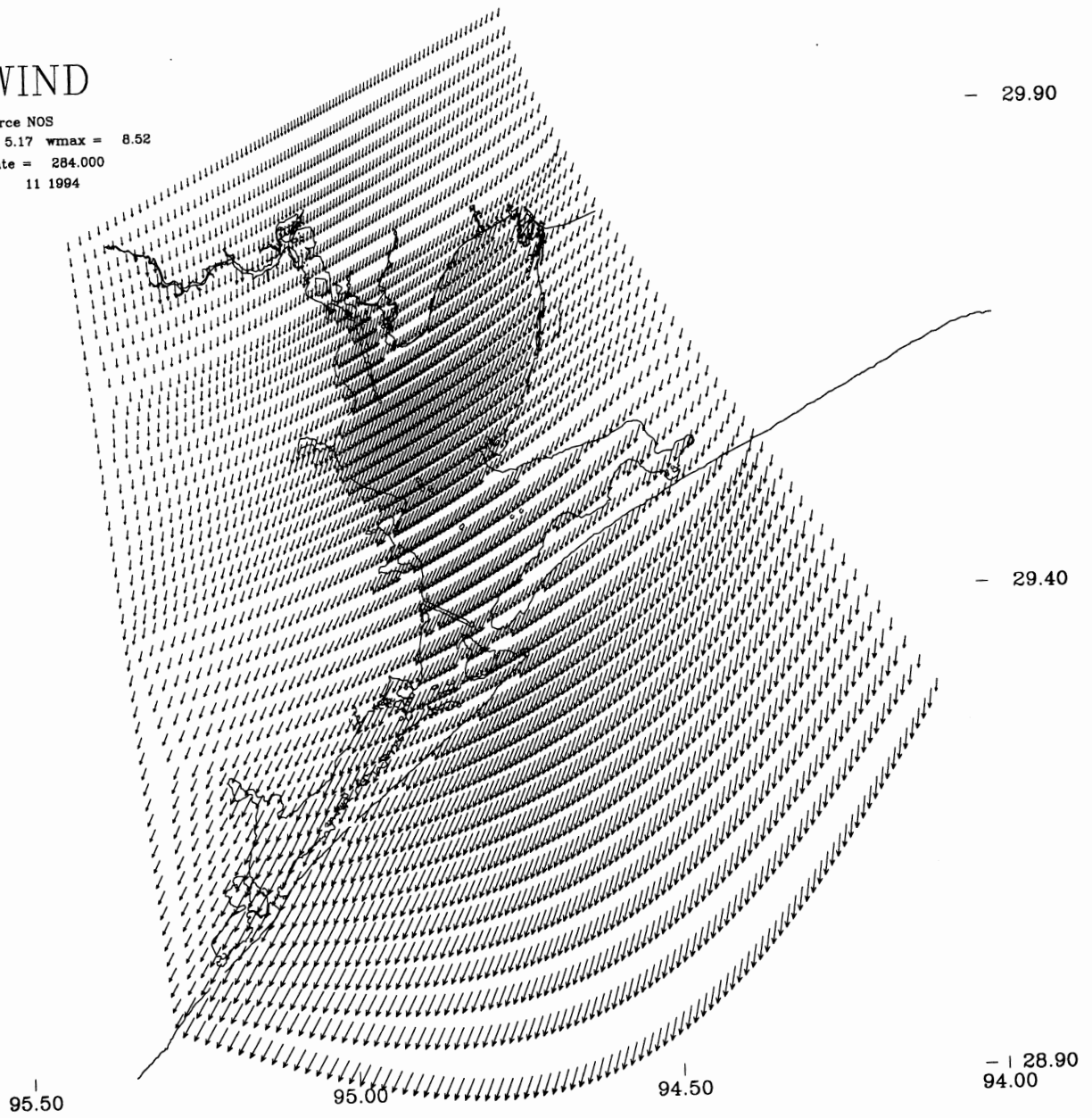


Figure 3.24. JD 284 (1994) Barnes Interpolation Windfield

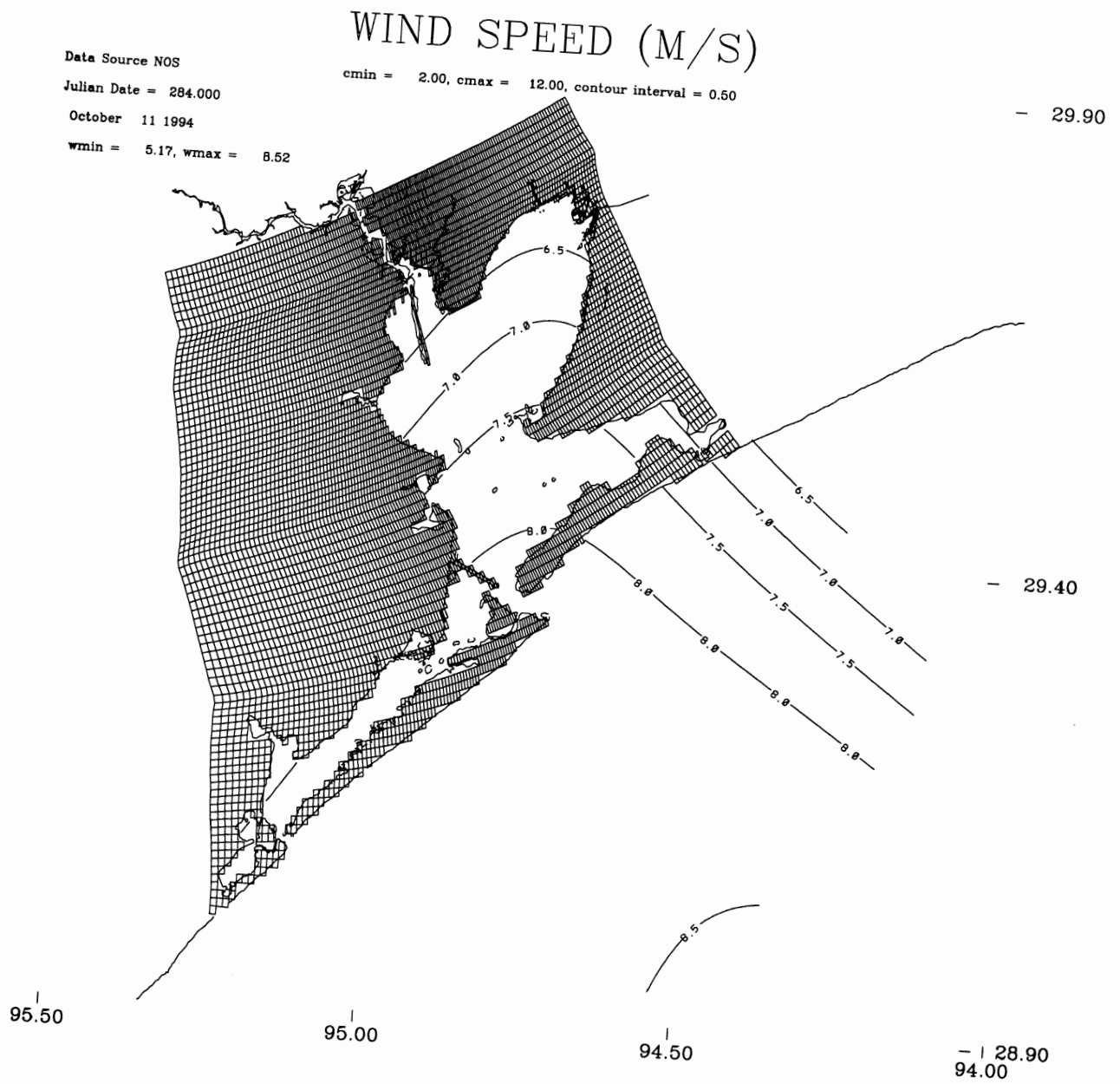


Figure 3.25. JD 284 (1994) Barnes Interpolation Windspeed Contours

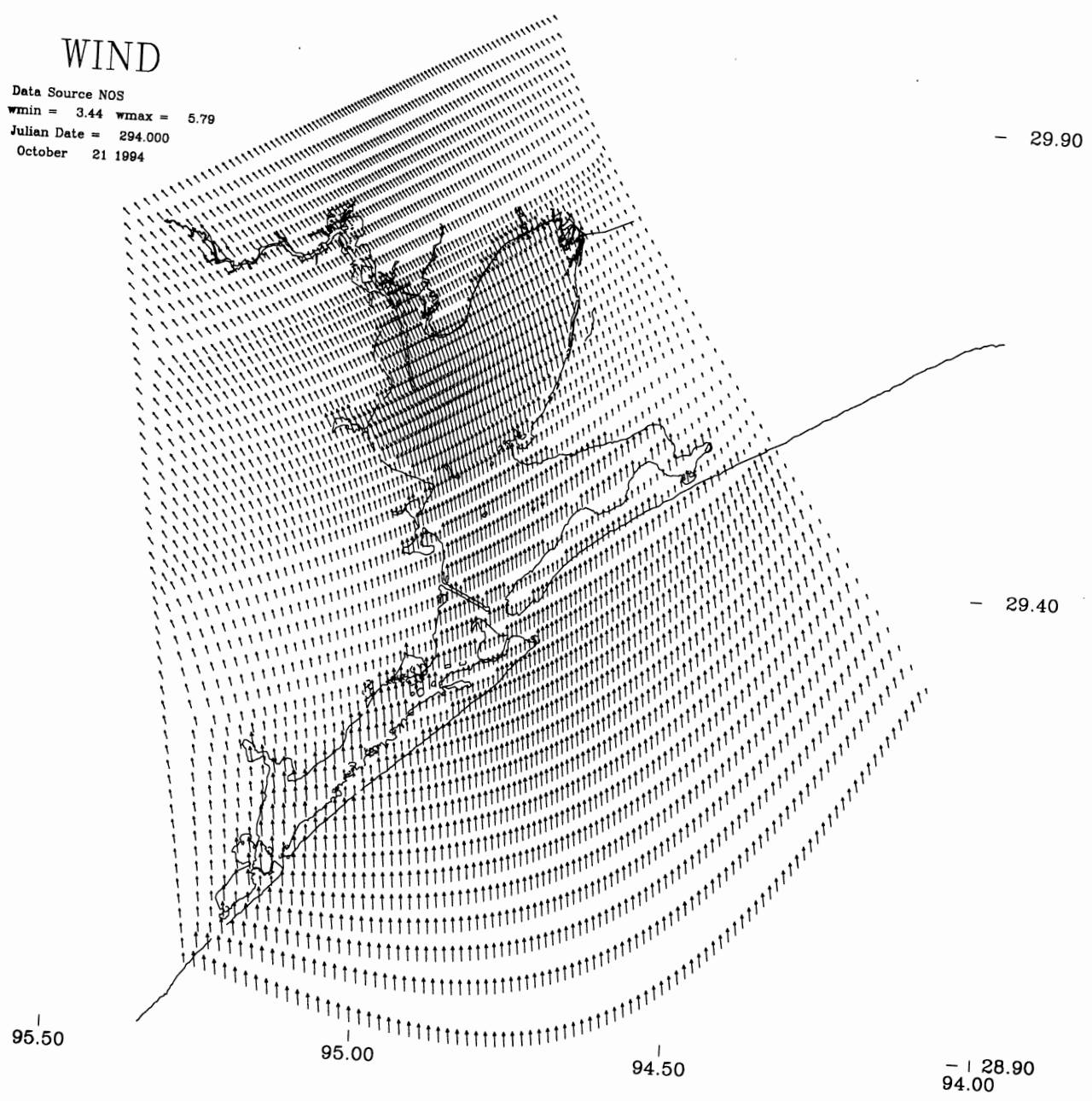


Figure 3.26. JD 294 (1994) Barnes Interpolation Windfield

WIND SPEED (M/S)

Data Source NOS

cmin = 2.00, cmax = 12.00, contour interval = 0.50

— 29.90

Julian Date = 294.000

October 21 1994

wmin = 3.44, wmax = 5.79

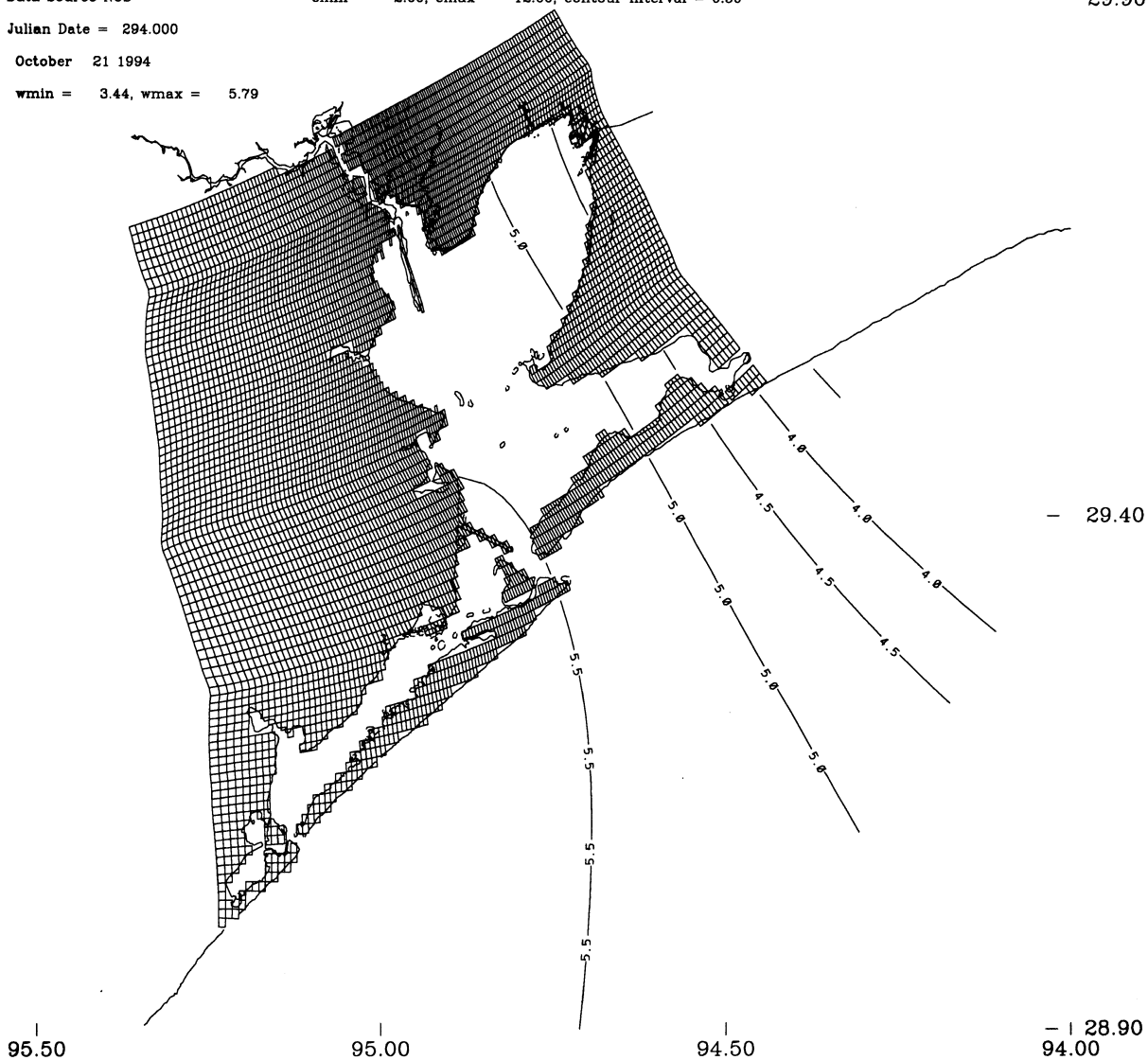


Figure 3.27. JD 294 (1994) Barnes Interpolation Windspeed Contours

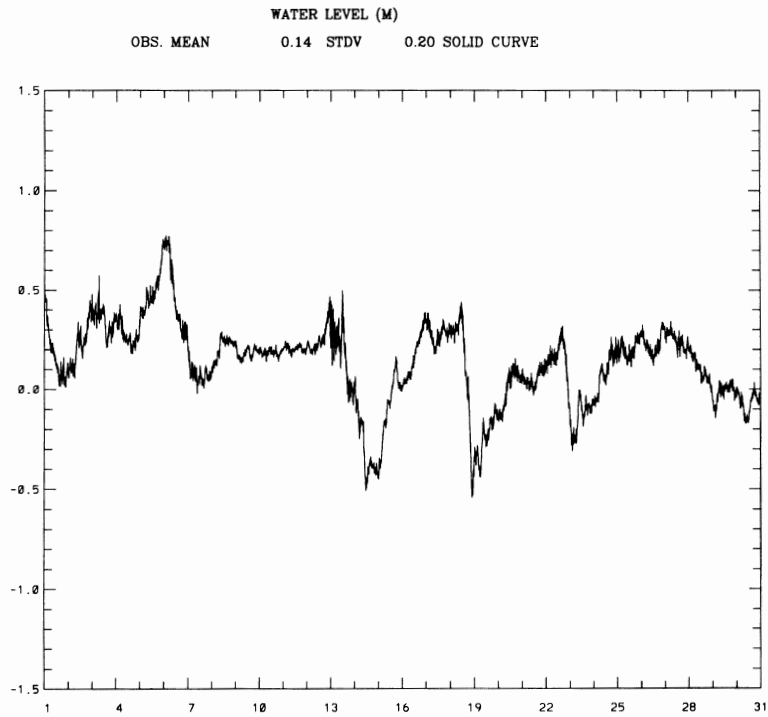


Figure 3.28. Galveston Pleasure Pier Subtidal Water Level Signal during January 1995

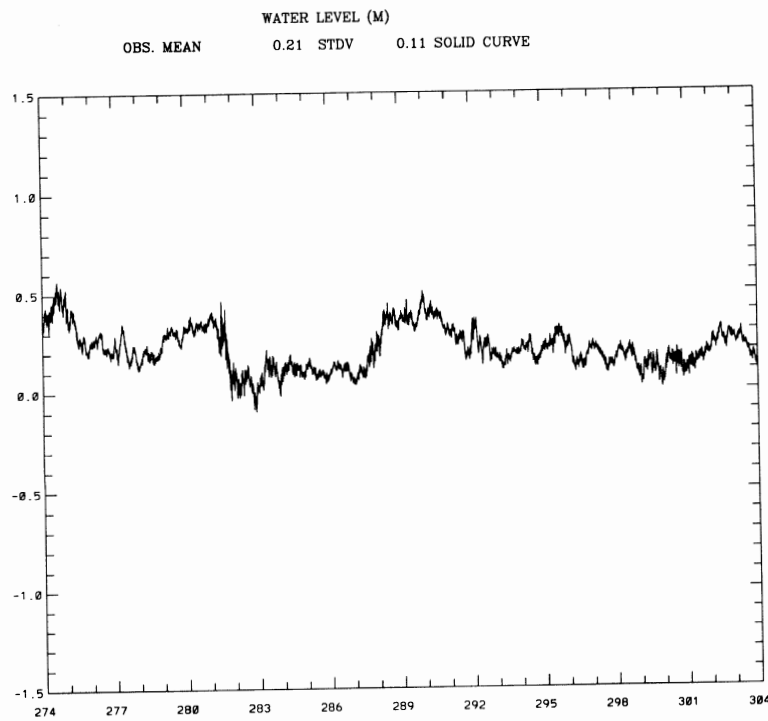


Figure 3.29. Galveston Pleasure Pier Subtidal Water Level Signal during October 1994

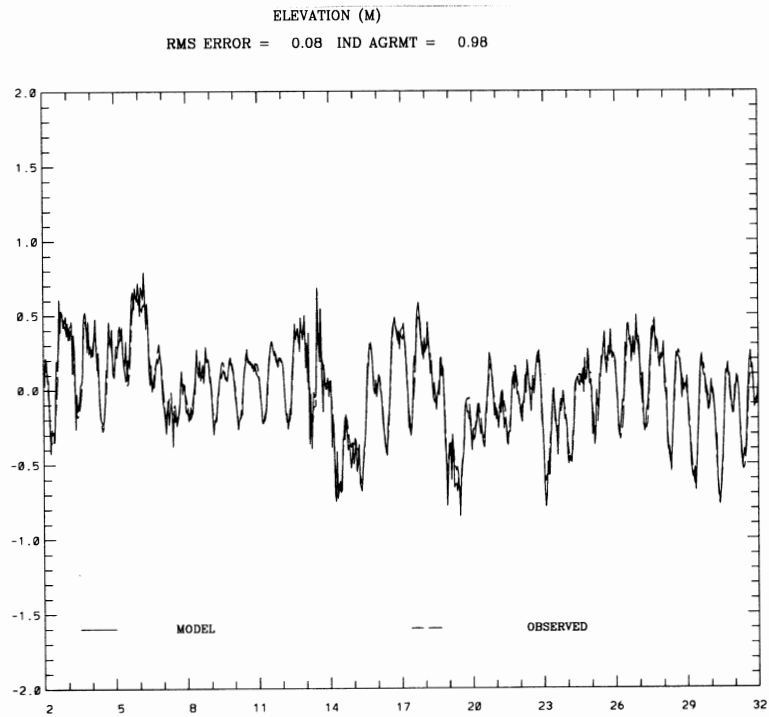


Figure 3.30. Galveston Pleasure Pier Simulated vs Observed Water Level Comparison during January 1995

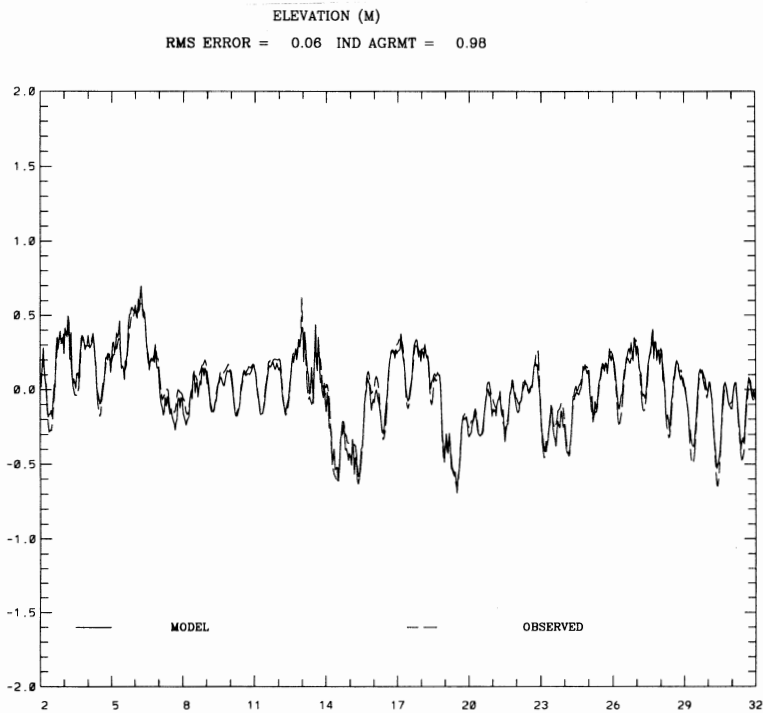


Figure 3.31. Galveston Pier 21 Simulated vs Observed Water Level Comparison during January 1995

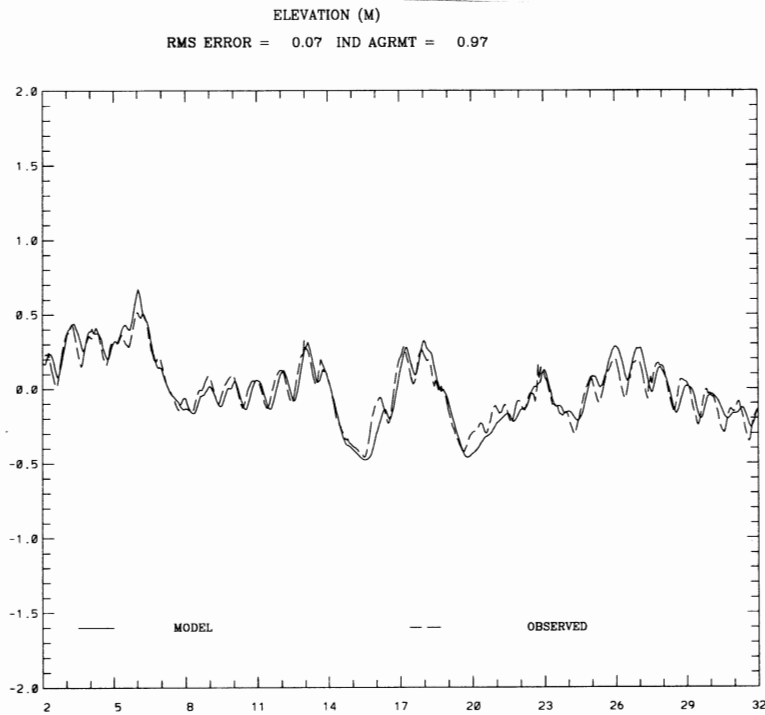


Figure 3.32. Christmas Bay Simulated vs Observed Water Level Comparison during January 1995

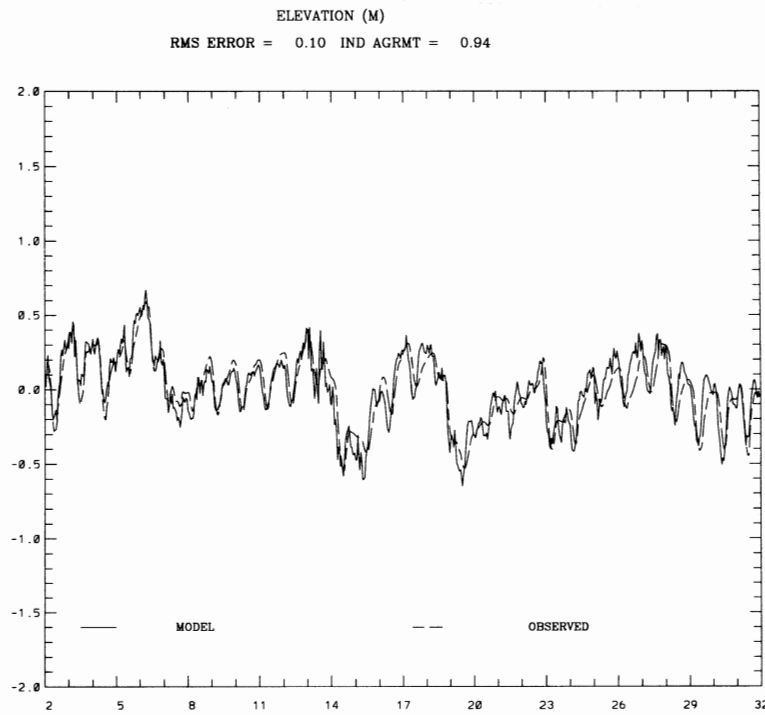


Figure 3.33. Port Bolivar Simulated vs Observed Water Level Comparison during January 1995

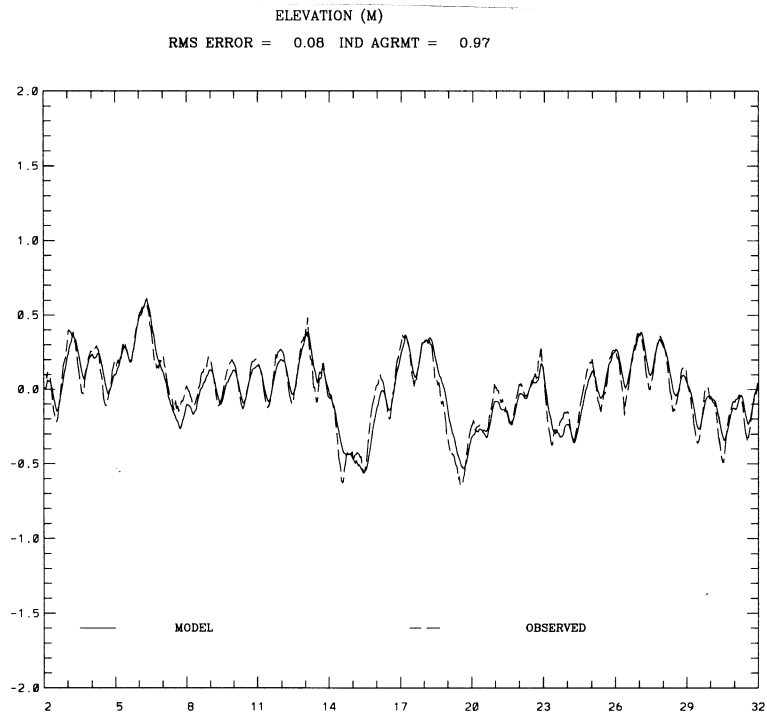


Figure 3.34. Eagle Point Simulated vs Observed Water Level Comparison during January 1995

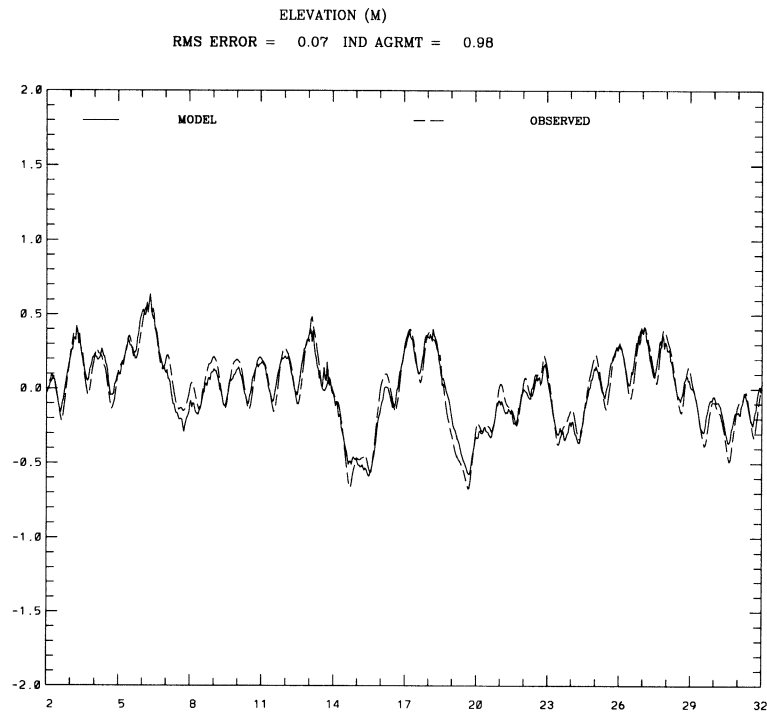


Figure 3.35. Clear Lake Simulated vs Observed Water Level Comparison during January 1995

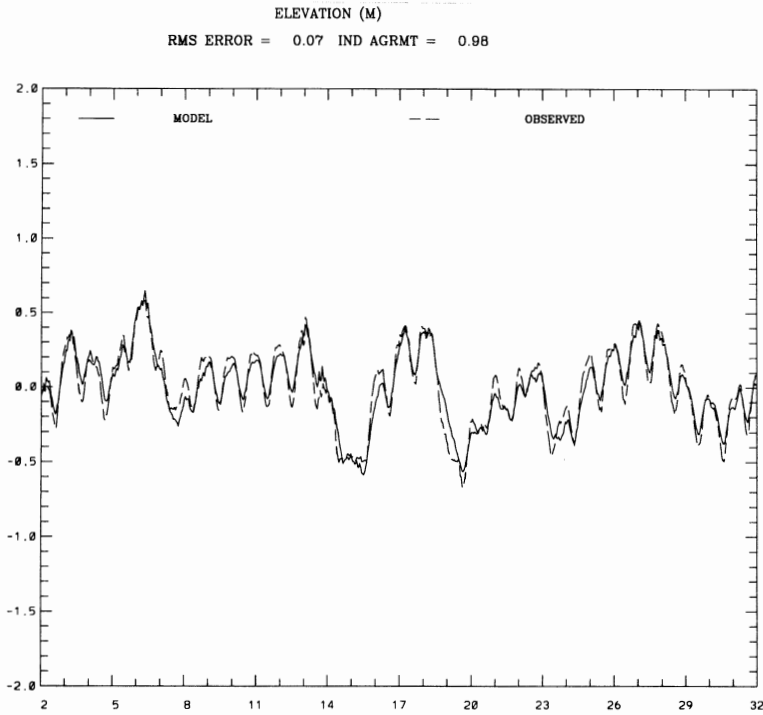


Figure 3.36. Morgans Point Simulated vs Observed Water Level Comparison during January 1995

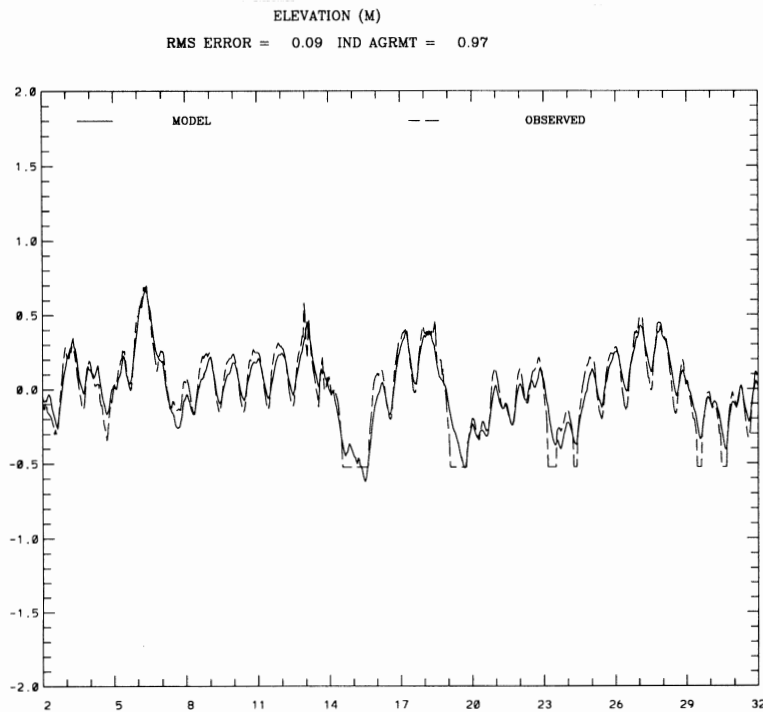


Figure 3.37. Round Point Simulated vs Observed Water Level Comparison during January 1995

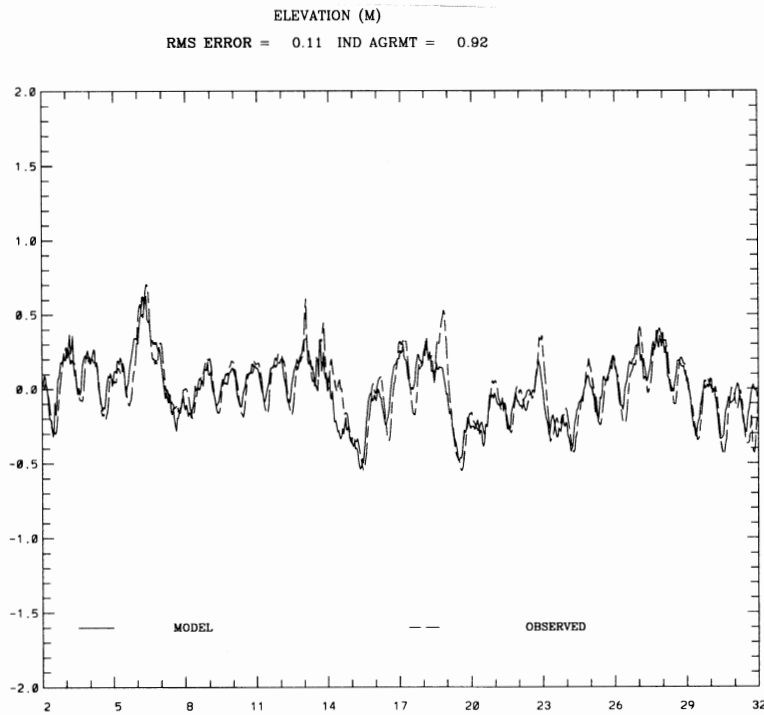


Figure 3.38. Rollover Pass Simulated vs Observed Water Level Comparison during January 1995

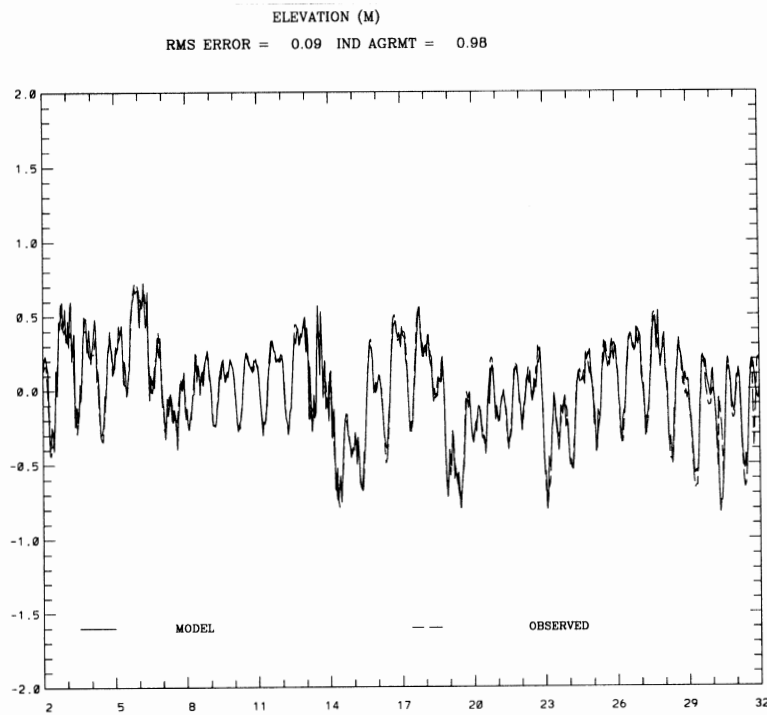


Figure 3.39. High Island Point Simulated vs Observed Water Level Comparison during January 1995

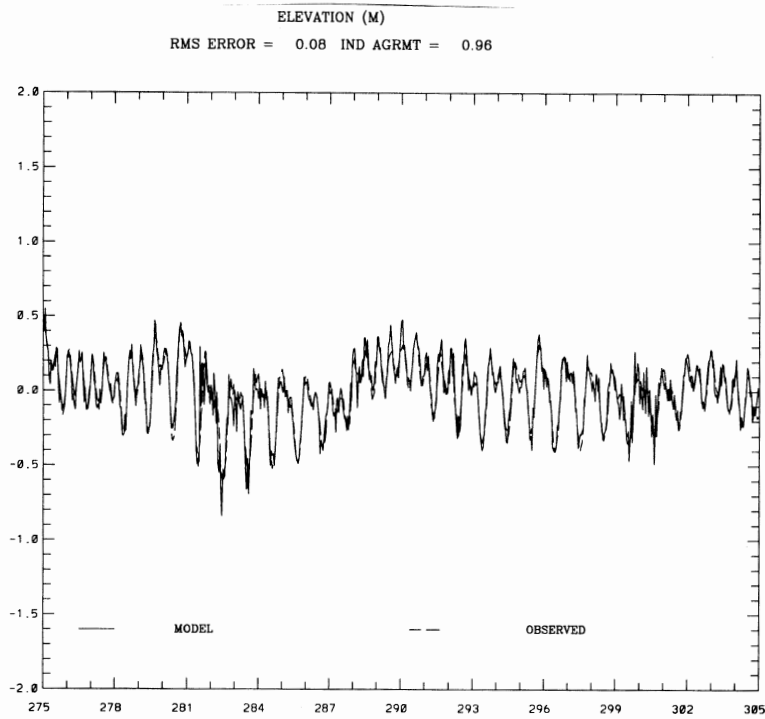


Figure 3.40. Galveston Pleasure Pier Simulated vs Observed Water Level Comparison during October 1994

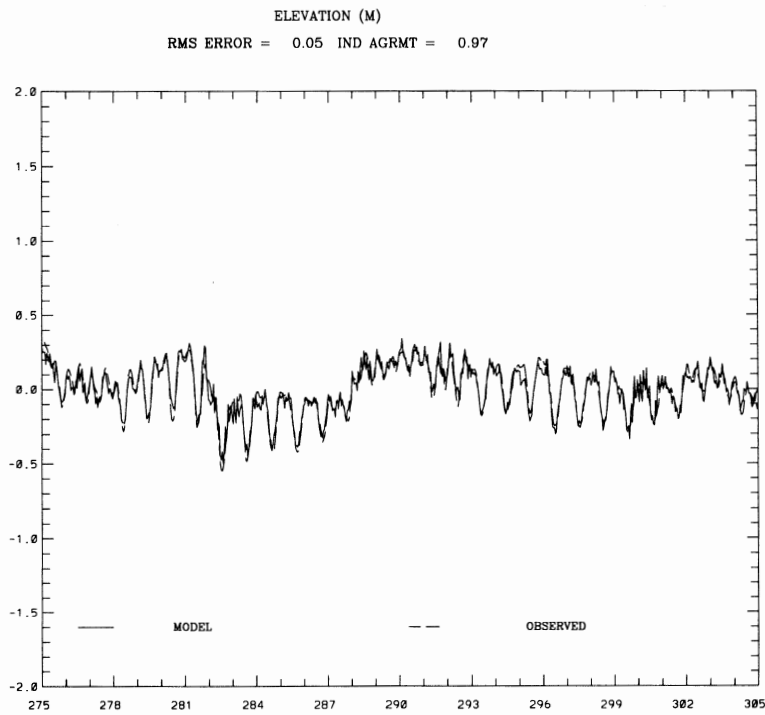


Figure 3.41. Galveston Pier 21 Simulated vs Observed Water Level Comparison during October 1994

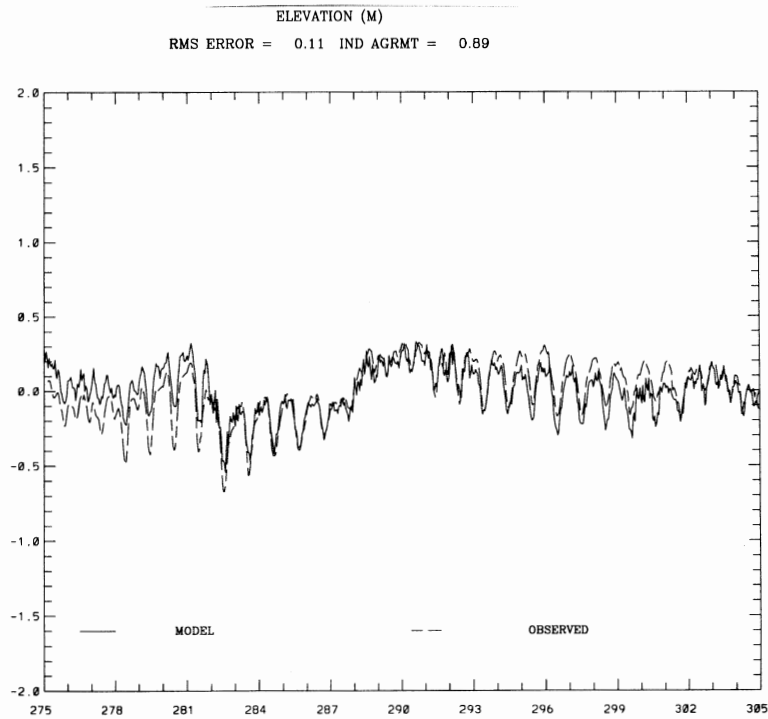


Figure 3.42. Port Bolivar Simulated vs Observed Water Level Comparison during October 1994

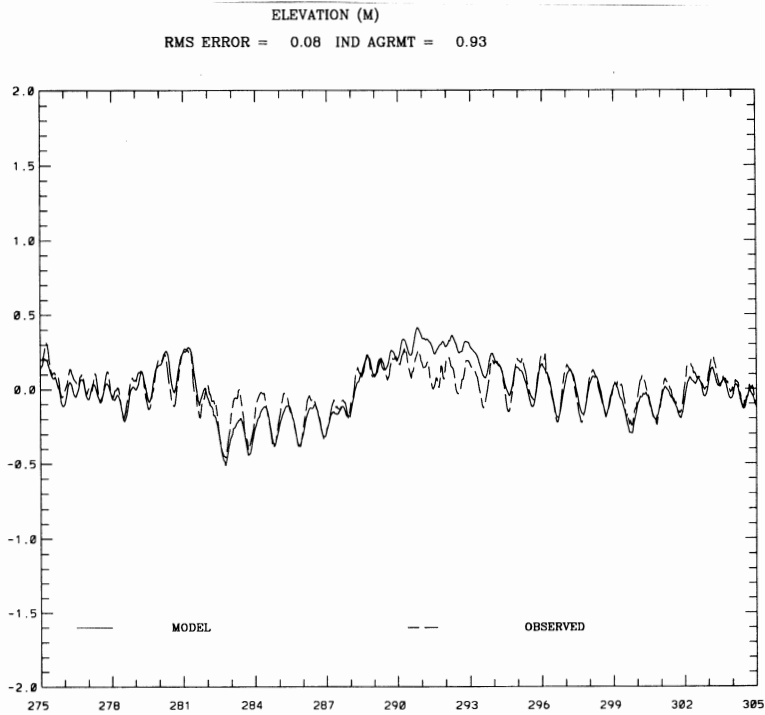


Figure 3.43. Eagle Point Simulated vs Observed Water Level Comparison during October 1994

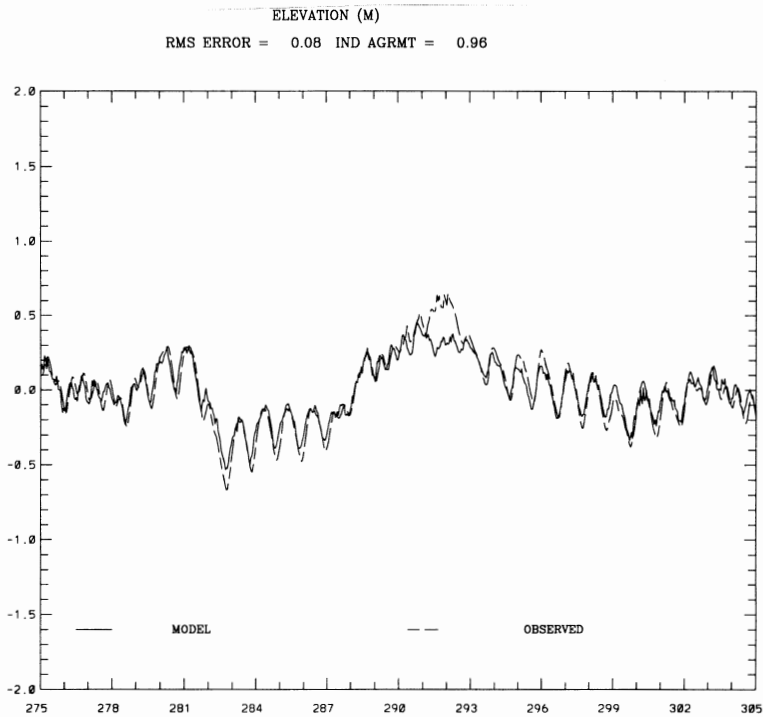


Figure 3.44. Clear Lake Simulated vs Observed Water Level Comparison during October 1994

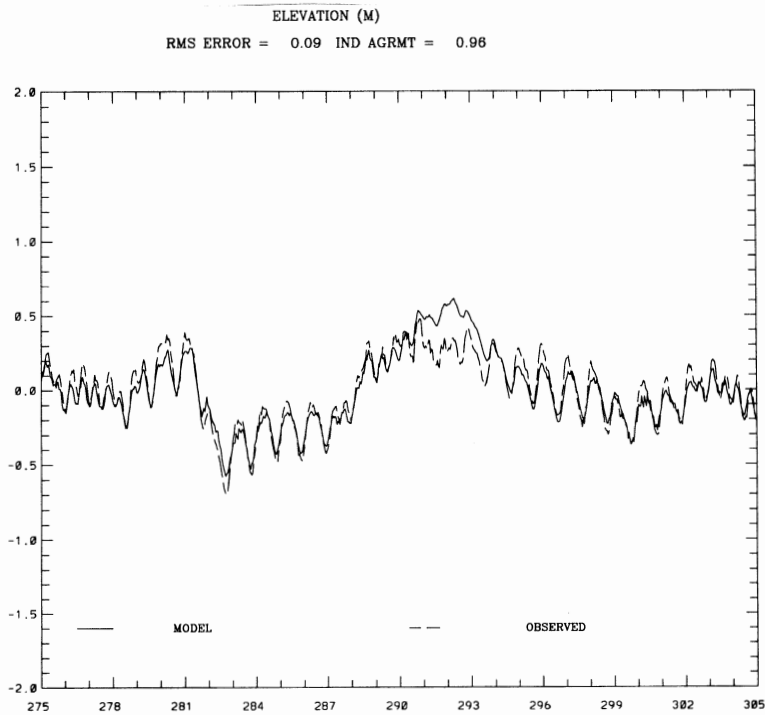


Figure 3.45. Morgans Point Simulated vs Observed Water Level Comparison during October 1994

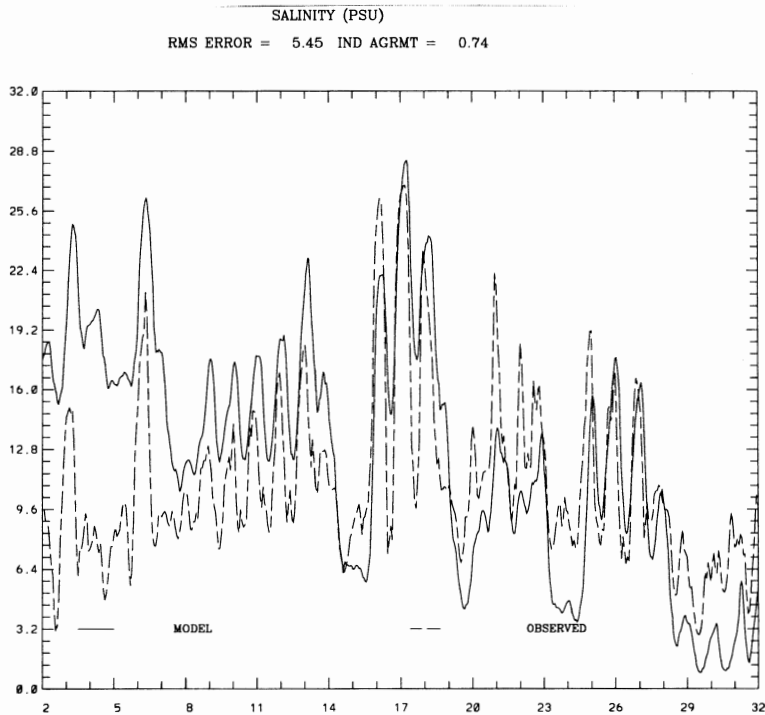


Figure 3.46. Dollar Point Simulated vs Observed Salinity Comparison during January 1995

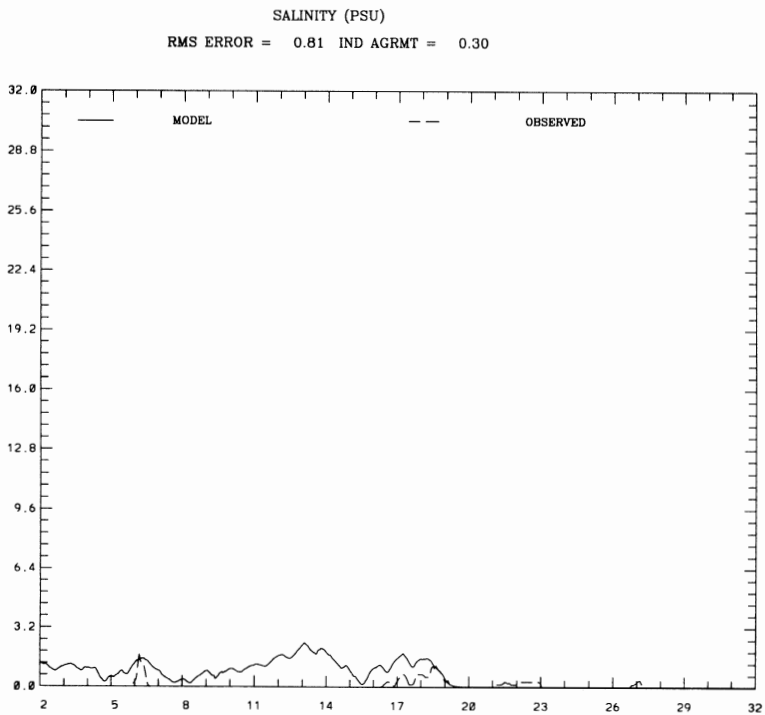


Figure 3.47. Trinity Bay (DBC) Simulated vs Observed Salinity Comparison during January 1995

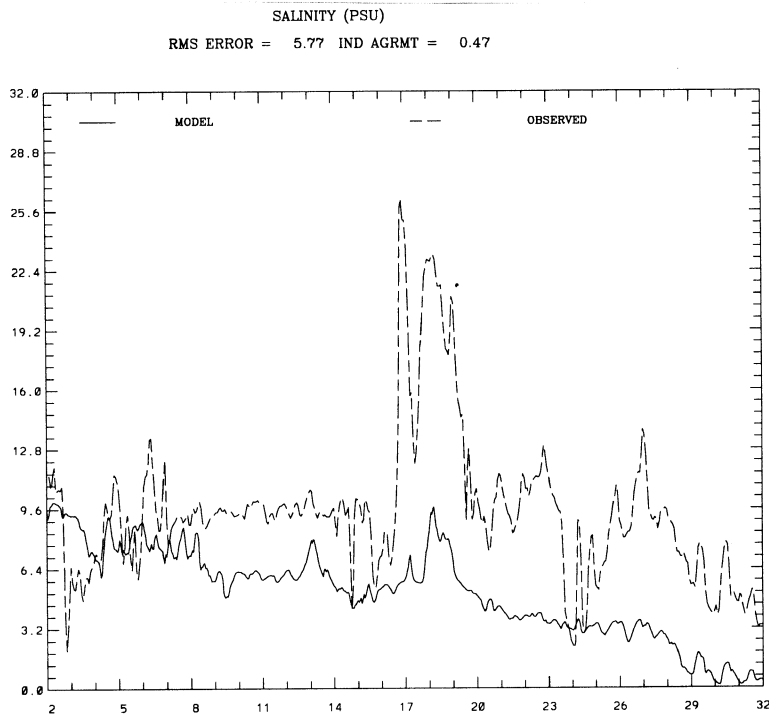


Figure 3.48. Hannah Reef Point Simulated vs Observed Salinity Comparison during January 1995

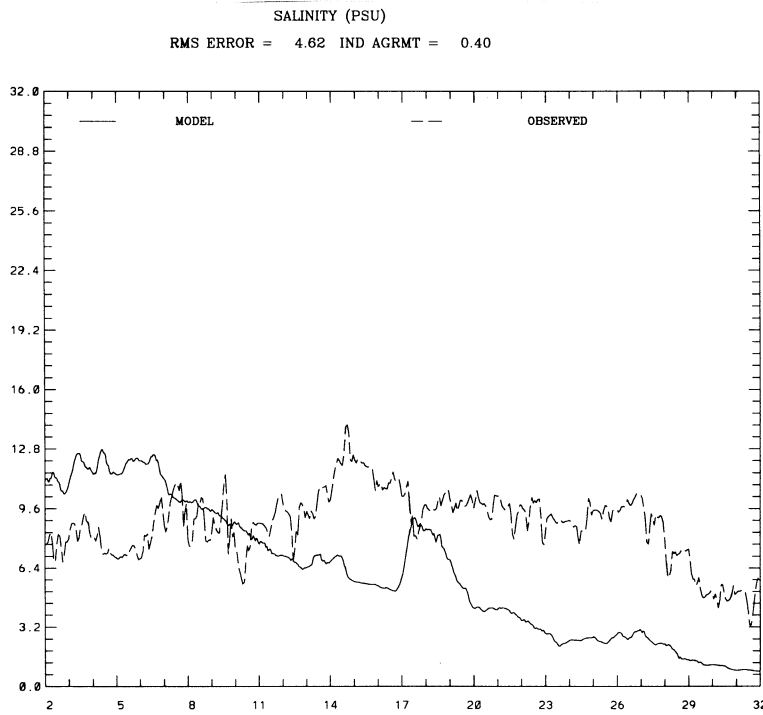


Figure 3.49. Red Bluff Simulated vs Observed Salinity Comparison during January 1995

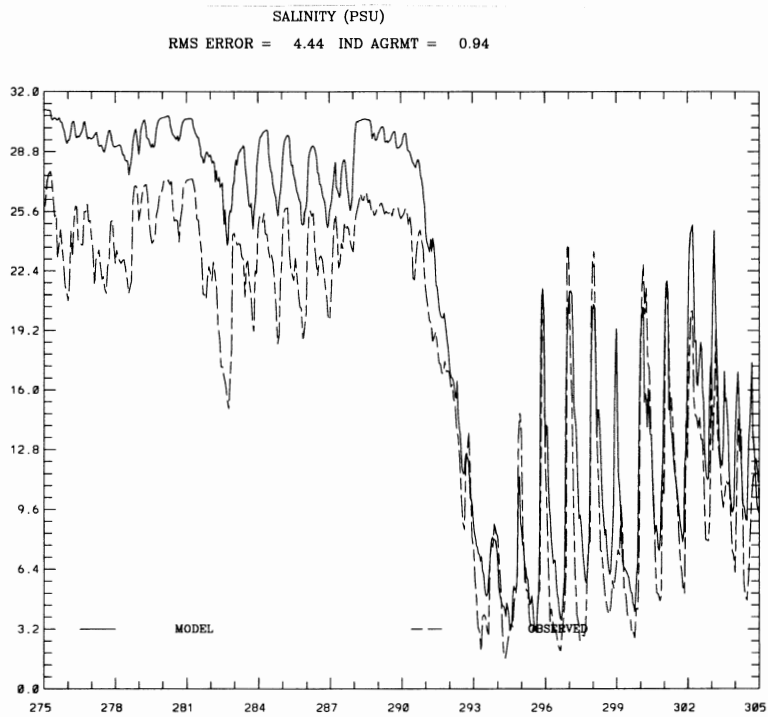


Figure 3.50. Port Bolivar Simulated vs Observed Salinity Comparison during October 1994

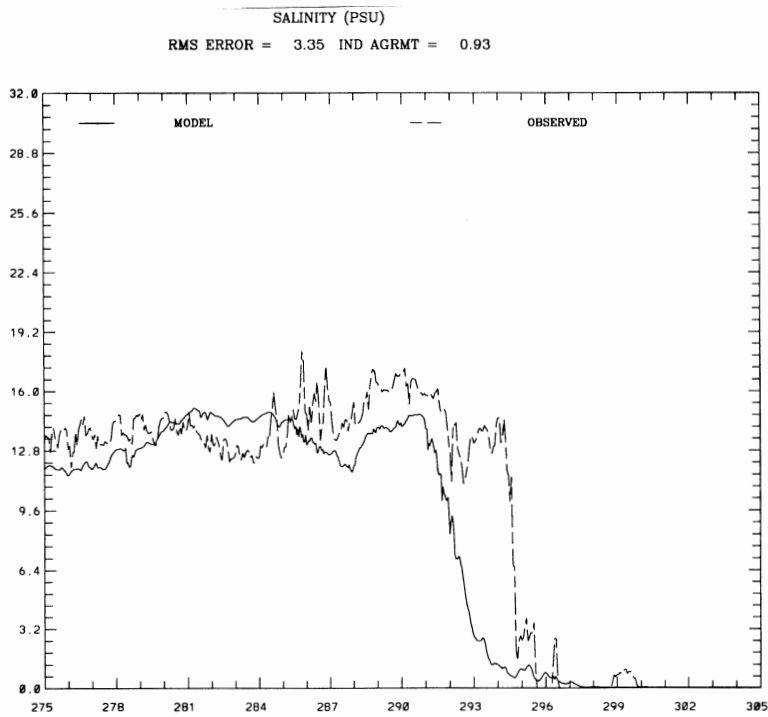


Figure 3.51. Trinity Bay (DBC) Simulated vs Observed Salinity Comparison during October 1994

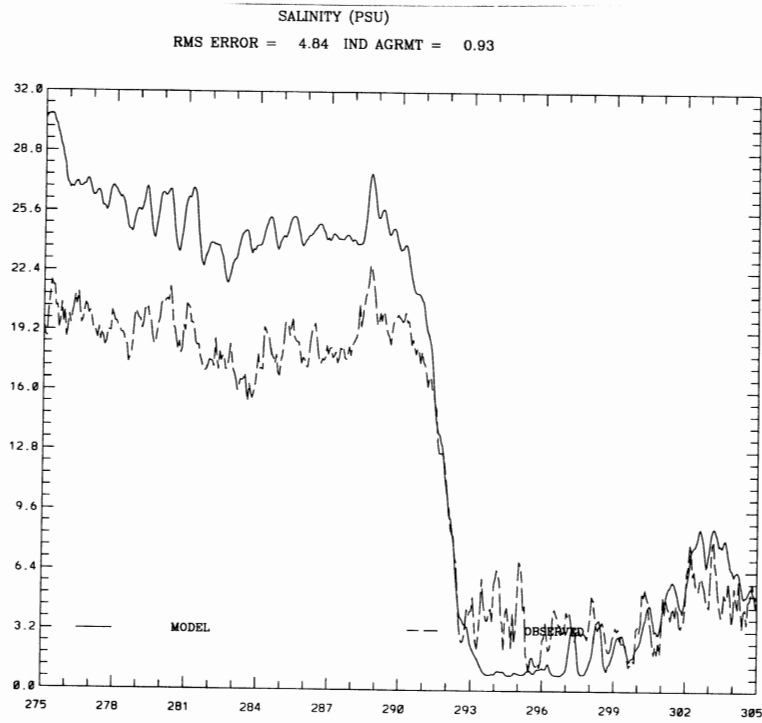


Figure 3.52. Dollar Point Simulated vs Observed Salinity Comparison during October 1994

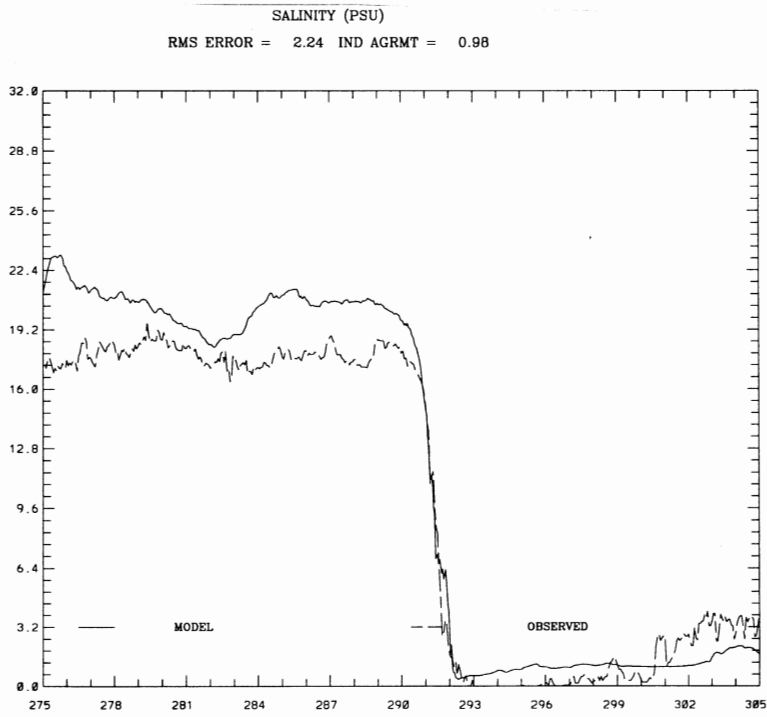


Figure 3.53. Red Bluff Simulated vs Observed Salinity Comparison during October 1994

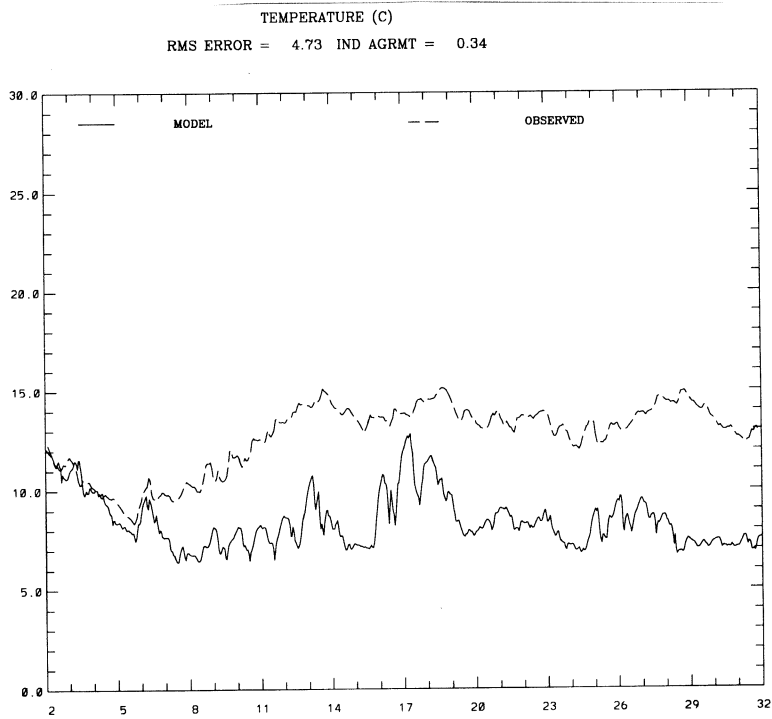


Figure 3.54. Dollar Point Bolivar Simulated vs Observed Temperature Comparison during January 1995

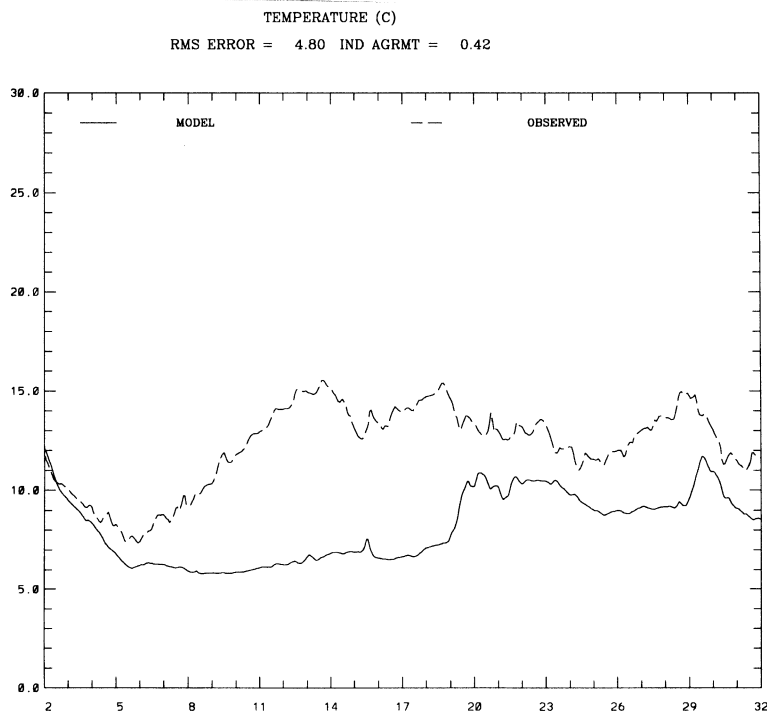


Figure 3.55. Trinity Bay (DBC) Simulated vs Observed Temperature Comparison during January 1995

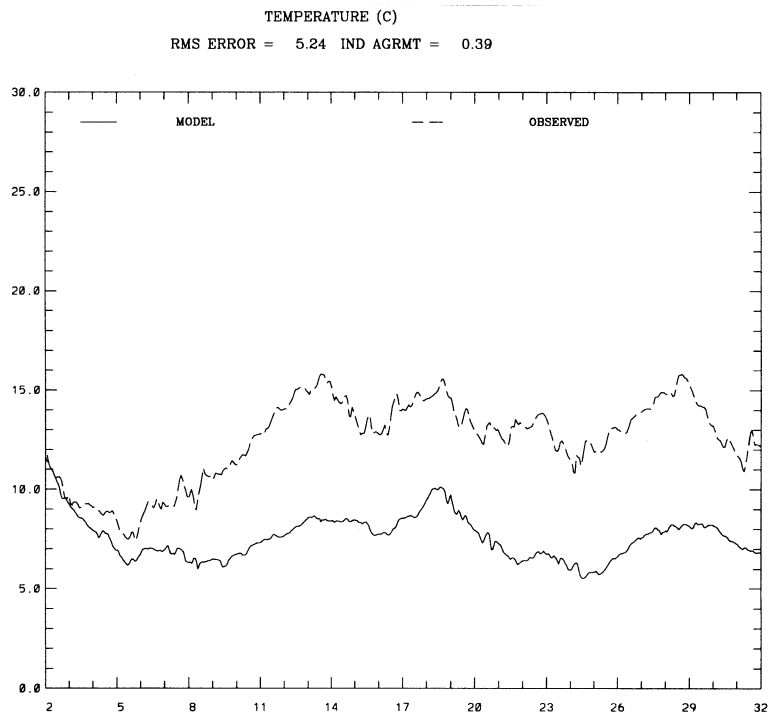


Figure 3.56. Hannah Reef Simulated vs Observed Temperature Comparison during January 1995

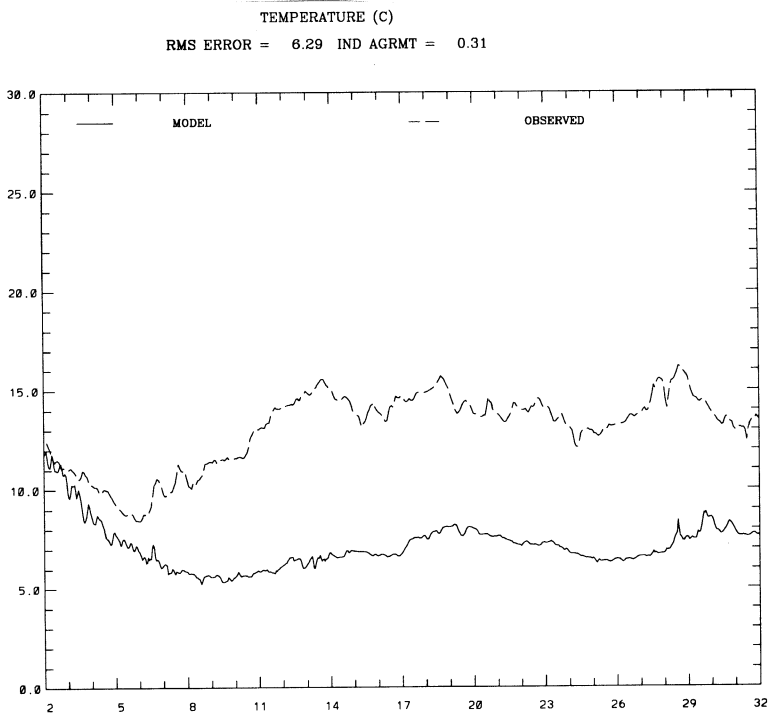


Figure 3.57. Red Bluff Simulated vs Observed Temperature Comparison during January 1995

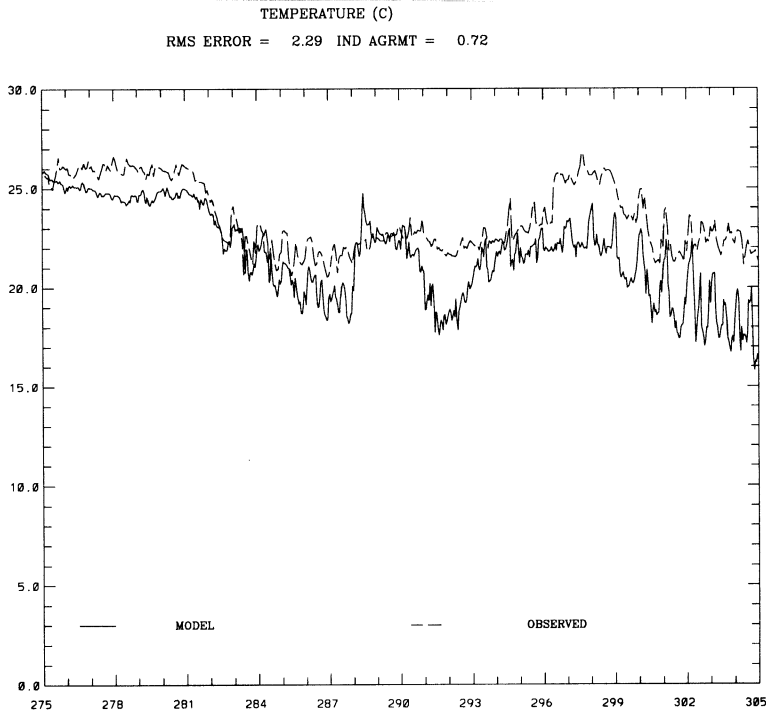


Figure 3.58. Port Bolivar Simulated vs Observed Temperature Comparison during October 1994

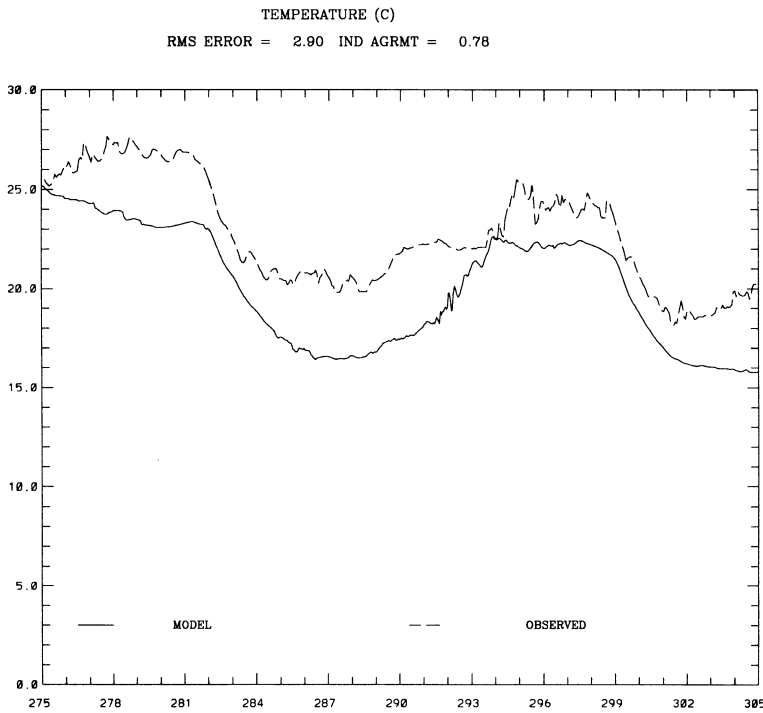


Figure 3.59. Trinity Bay (DBC) Simulated vs Observed Temperature Comparison during October 1994

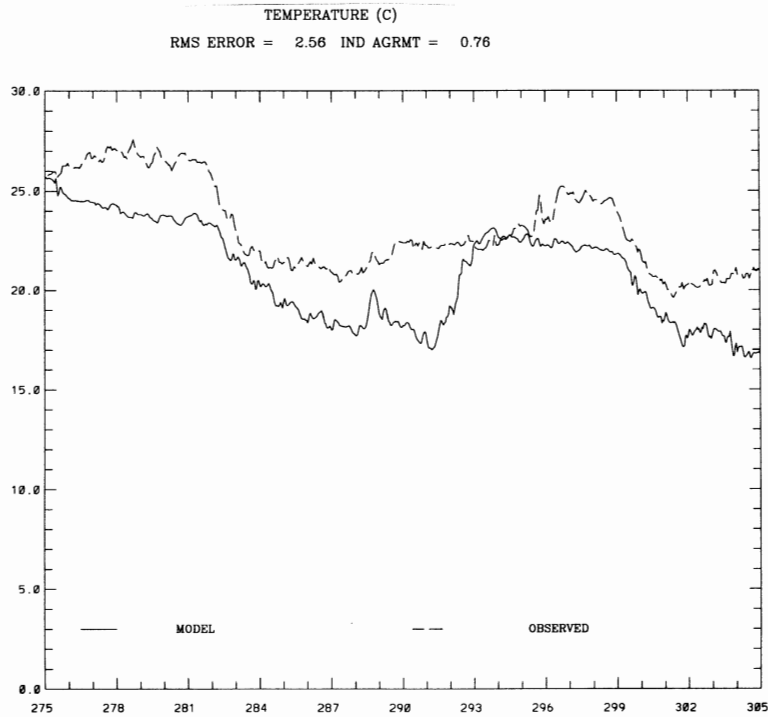


Figure 3.60. Dollar Point Simulated vs Observed Temperature Comparison during October 1994

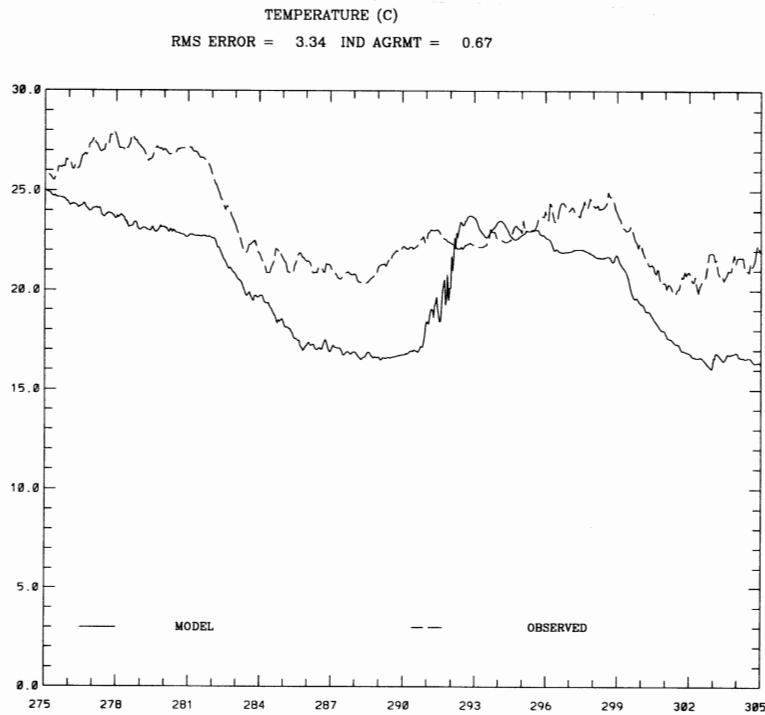


Figure 3.61. Red Bluff Simulated vs Observed Temperature Comparison during October 1994

4. BAY MODEL WATER LEVEL SENSITIVITY ANALYSIS

A sensitivity analysis was performed in two experiment sets to investigate the sensitivity of water levels throughout the Galveston Bay system to Bay, Shelf, and Gulf of Mexico winds and to freshwater inflow. The Bay windfield was specified over Galveston, Trinity, West, and East Bays, which comprised all grid cells interior to the barrier island system as shown in Figure 4.1. Shelf winds were specified over the grid cells exterior to the barrier island system. Gulf of Mexico wind effects were assumed to be the major component of the subtidal water level signal specified along the open boundary of the grid. Note other components of this subtidal signal include Loop Current, Mississippi River, and atmospheric pressure gradient effects. The subtidal water level signal was assumed to be spatially uniform and equal to the subtidal water level at Galveston Pleasure Pier.

The processing of each experiment's water level signal was performed in the same manner as for the hindcast. The monthly mean of the simulated signal was determined and compared with the observed monthly mean. Note the observed means are with respect to estimated tidal epoch mean tide level and are not on a vertical datum. Subsidence and record length issues can cause significant differences at individual stations. Simulated means are with respect to model datum, which constitutes an equipotential surface fit through mean tide level.

Due to the difference in vertical datums, observed and simulated means can disagree substantially from station to station. Thus, the monthly signal was demeaned and compared with the demeaned observed water level signal in terms of a root mean square error (RMSE) and a dimensionless (0-1) average relative error (ARE) derived by Willmott et al. (1985), which is zero for no error. Since both series are demeaned, the RMSE is equivalent to the standard deviation (SD) of the difference between the two demeaned series. Thus in comparing the monthly responses of each experiment, one initially considers the difference in means between the experiment and hindcast. Then the differences in the SD (demeaned simulation minus observation series) for the experiment and hindcast are considered.

In comparing a times series of experiment and hindcast water level signals, one notes the difference in means between the experiment and hindcast and appropriately shifts the ordinate of the experiment time series. One next observes the difference between the series and the observation at a common time to assess the impact of the experiment on the water level. If the means are nearly equal, which is often the case, one needs to make no shift in ordinate for the experiment. It is thus possible to assess the difference between the experiment and hindcast water level response in terms of a difference in means, SD of the differences between the demeaned simulated signals and the demeaned observations, and as absolute water level differences during portions of the month.

4.1. Experiment Set 1

In experiment set one, the January 1995 'Northers' period (refer to Chapter 3) was considered to assess the impact of the windfields on water level response. The subtidal water level signal at Galveston Pleasure Pier had a 14 cm mean and 20 cm standard deviation, with large excursions on 5, 13, 18, and 22 January. Mean average daily discharges on the Trinity River at Romayor, TX, San Jacinto near Sheldon, TX, and Buffalo Bayou at Piney Point, TX were 28,000 cfs, 11,000 cfs, and 780 cfs, respectively, with associated standard deviations of 7700 cfs, 12,300 cfs, and 590 cfs. Peak

average daily flows exceeded 48,000 cfs on both the Trinity and San Jacinto Rivers.

The experiments shown in Table 4.1 were conducted. The results of each experiment are discussed by comparing the water level response with the January 1995 hindcast, which was produced by using a one-step Barnes interpolation for wind and sea-level atmospheric pressure fields as discussed in Chapter 2. The comparisons are developed in terms of tabulated means, SD and ARE. Time series plots at Morgans Point (Upper Galveston Bay), Galveston Pier 21 (Lower Galveston Bay), and Galveston Pleasure Pier (Gulf of Mexico) as shown in Figure 4.2. In these plots, RMS ERROR corresponds to SD since both series have been demeaned.

Table 4.1. January 1995 Experiment Set 1

Experiment 1	Bay and Gulf of Mexico winds (Shelf winds neglected)
Experiment 2	Shelf and Gulf of Mexico winds (Bay winds neglected)
Experiment 3	Gulf of Mexico winds (Bay and Shelf wind neglected)
Experiment 4	Bay and Shelf winds (Gulf of Mexico winds neglected)
Experiment 5	Texas A&M University (TAMU) objective analysis windfield

Experiment Set 1 Experiment 1

In this experiment, Shelf winds are set to zero. With Bay and Gulf of Mexico winds the water level response is in close agreement with the hindcast as shown in Table 4.2. RMS and relative error values with respect to observations are nearly identical. From Table 4.3 one notes that, winds over the area of the Shelf influence coastal water levels 1 cm in the monthly mean. Water level time series responses are shown (in the top half for this experiment and in the lower half for the hindcast) at Morgans Point, Galveston Pier 21, and Galveston Pleasure Pier in Figures 4.3 - 4.5, respectively, and are nearly the same for both experiment and hindcast. The indicator of agreement (IND AGRMT) shown in the plots is equal to one minus the relative error. Based on these results, there appears to be no significant double-counting of Shelf wind response by imposing the subtidal water level signal at Galveston Pleasure Pier along the offshore model boundary.

Experiment Set 1 Experiment 2

In this experiment, Bay winds are set to zero and Shelf and Gulf of Mexico wind effects are considered. SD and ARE statistics are given in Table 4.2. SD water level differences between the hindcast and this experiment are 3 cm at Morgans Point and 1 cm at Clear Lake, which indicates the strongest region of influence on Bay winds is over the Upper Bay. Mean water level differences shown in Table 4.3 are 3 cm at Round Point and 1 cm at Morgans Point. At Christmas Bay (West

Bay) and Rollover Pass (East Bay) mean water level differences are 2 and 1 cm, respectively. Time series of water level response are compared with the hindcast at Morgans Point, Galveston Pier 21, and Galveston Pleasure Pier in Figures 4.6 - 4.8, respectively. During the periods 9 - 12 and 24 - 31 January, experiment and hindcast water levels at Morgans Point differ by order 10 cm. At Galveston Pier 21 and at Galveston Pleasure Pier water levels are nearly identical to those of the hindcast. The effect of the Bay winds during January 1995 is felt primarily over the Upper Galveston Bay and East Bay. The wind effect is reduced in Lower Galveston Bay and on the Shelf.

Experiment Set 1 Experiment 3

In this experiment, Bay and Shelf winds are set to zero and only Gulf of Mexico wind effects are considered via specification of the subtidal water level signal at Galveston Pleasure Pier along the Bay model's open boundary. SD and ARE statistics are given in Table 4.2 and water level means are given in Table 4.3. Time series of water level response were compared with the hindcast at Morgans Point, Galveston Pier 21, and Galveston Pleasure Pier. Results of this experiment are nearly identical to those of experiment 2, indicating that Shelf winds have no effect on Bay water levels and minor (order 1 cm or less in monthly mean) on coastal water levels.

Experiment Set 1 Experiment 4

In this experiment, Gulf of Mexico winds are neglected by setting the subtidal water level signal to zero along the model open boundary. Bay and Shelf winds are both considered. SD and ARE statistics are given in Table 4.2. SDs differ by order 10 cm. In Table 4.3 mean water levels throughout the system differ by 13 cm, which is approximately equal to the neglected open boundary 14 cm subtidal water level mean. Time series of water level response are compared with the hindcast at Morgans Point, Galveston Pier 21, and Galveston Pleasure Pier in Figures 4.9 - 4.11, respectively. On 6, 14, and 20 January the water level differences between the experiment and hindcast at all three stations are order 50 cm. Results of this experiment indicate that the subtidal water level plays a major role in water level response throughout the system during January 1995.

Experiment Set 1 Experiment 5

In this experiment, TAMU objectively analyzed windfields are used. Atmospheric pressure anomalies are set to zero. Due to system disk problems, this experiment was run for 29.8 days. SD and ARE error statistics in Table 4.2 and mean water levels in Table 4.3, indicate that TAMU windfields and NOS windfields produce similar (nearly identical means and RMS differences order 1 cm) water level responses. Time series of water level response are compared with the hindcast using NOS windfields at Morgans Point, Galveston Pier 21, and Galveston Pleasure Pier in Figures 4.12 - 4.14, respectively. TAMU wind generated water level signals at Galveston Pier 21 (Lower Bay) and Galveston Pleasure Pier (Shelf) have greater noise (oscillations) than those generated using NOS wind. However, during 8 - 14 and 20 - 31 January at Morgans Point (Upper Bay), TAMU wind generated water levels are in closer agreement to observations.

Experiment Set 1 Results Summary

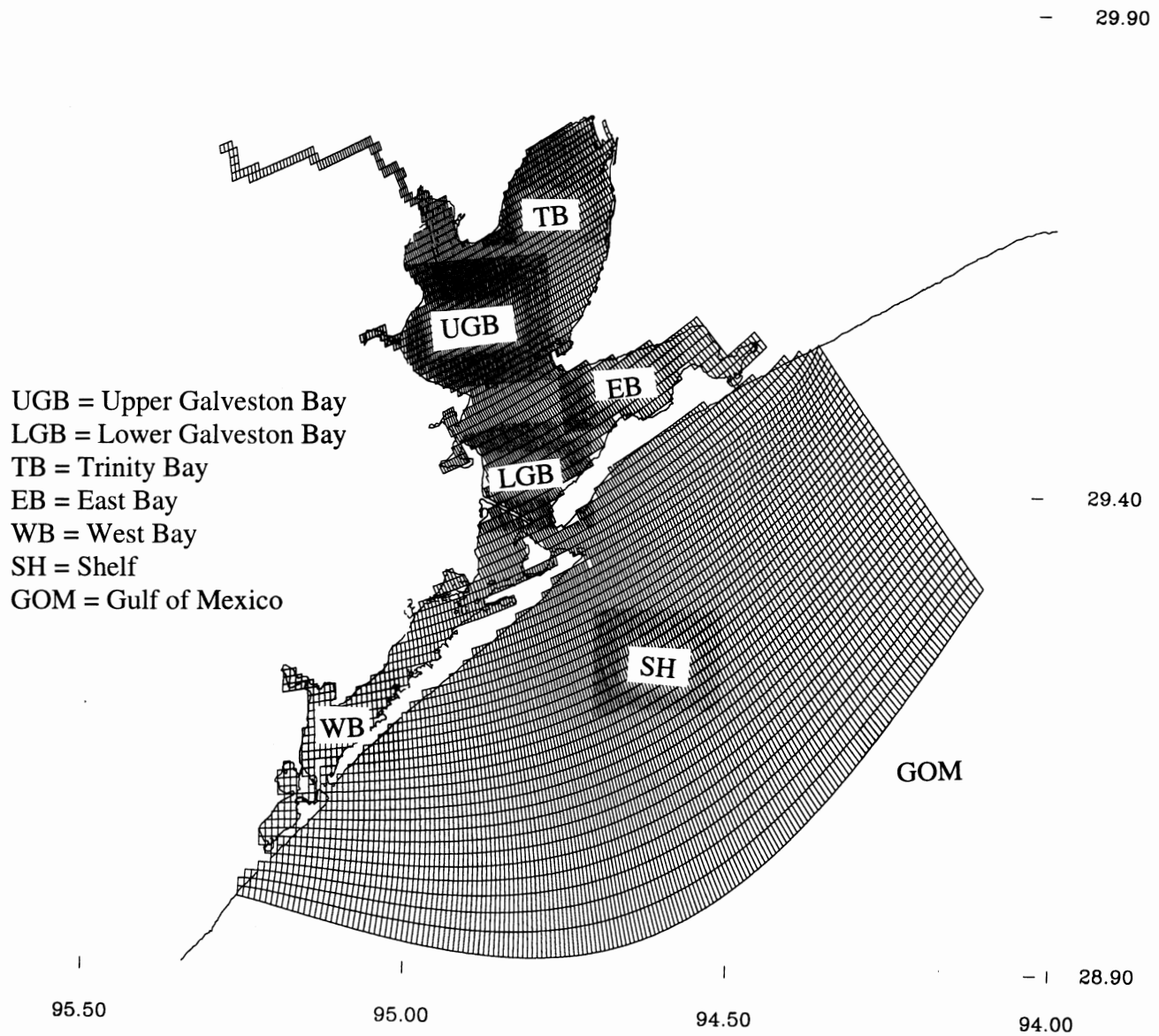
Based on these experiments, the order 10 cm influence of the Bay windfield on Bay water levels during several portions of the month cannot be ignored. The nowcast/forecast system must use accurate Bay windfields. The subtidal water level influence on Bay water levels can be order 50 cm during portions of the month and appears to be the major influence. Therefore, the nowcast/forecast system is highly dependent on an accurate representation of the subtidal water level signal along the computational Bay model open boundary during both nowcast and forecast periods.

Table 4.2. Experiment Set One Water Level Response SD (cm)/ ARE (-) Statistics

Station	Hindcast	Exp. 1	Exp. 2	Exp. 3	Exp. 4	Exp. 5
Galveston Pleasure Pier	8/0.02	8/0.02	8/0.02	8/0.02	18/0.17	9/0.03
Galveston Pier 21	6/0.02	6/0.02	6/0.02	6/0.02	18/0.25	7/0.02
Morgans Point	7/0.02	7/0.03	10/0.04	10/0.05	18/0.25	5/0.01
Clear Lake	7/0.02	7/0.02	8/0.03	9/0.04	18/0.28	6/0.02
Eagle Point	8/0.03	8/0.03	8/0.03	8/0.04	18/0.31	5/0.01
Port Bolivar	10/0.06	10/0.06	10/0.06	10/0.06	19/0.37	10/0.06
Christmas Bay	7/0.03	7/0.03	8/0.04	8/0.05	15/0.26	6/0.02
Round Point	9/0.03	9/0.04	12/0.07	13/0.08	20/0.29	8/0.03
Rollover Pass	11/0.08	11/0.08	14/0.12	14/0.11	20/0.40	11/0.07
High Island	9/0.02	9/0.03	9/0.02	9/0.02	22/0.21	8/0.02

Table 4.3. Experiment Set One Water Level Means (cm)

Station	Hindcast/ Observed	Exp. 1	Exp. 2	Exp. 3	Exp. 4	Exp. 5
Galveston Pleasure Pier	-2/-2	-3	-2	-3	-15	-2
Galveston Pier 21	1/-1	0	1	0	-12	0
Morgans Point	4/-1	4	5	5	-9	4
Clear Lake	5/-3	5	5	4	-8	3
Eagle Point	4/-1	4	4	4	-9	3
Port Bolivar	0/1	0	1	0	-12	0
Christmas Bay	5/-1	5	3	2	-8	3
Round Point	2/-6	1	5	5	-12	4
Rollover Pass	0/-3	0	1	1	-14	1
High Island	-7/-5	-6	-6	-6	-20	-6



Bay Winds == UGB + LGB + TB + EB + WB
 Shelf Winds == SH
 Gulf of Mexico Winds === GOM (Galveston Pleasure Pier subtidal water level signal)

Figure 4.1. Galveston Bay - Bay, Shelf, and Gulf of Mexico Windfield Definition

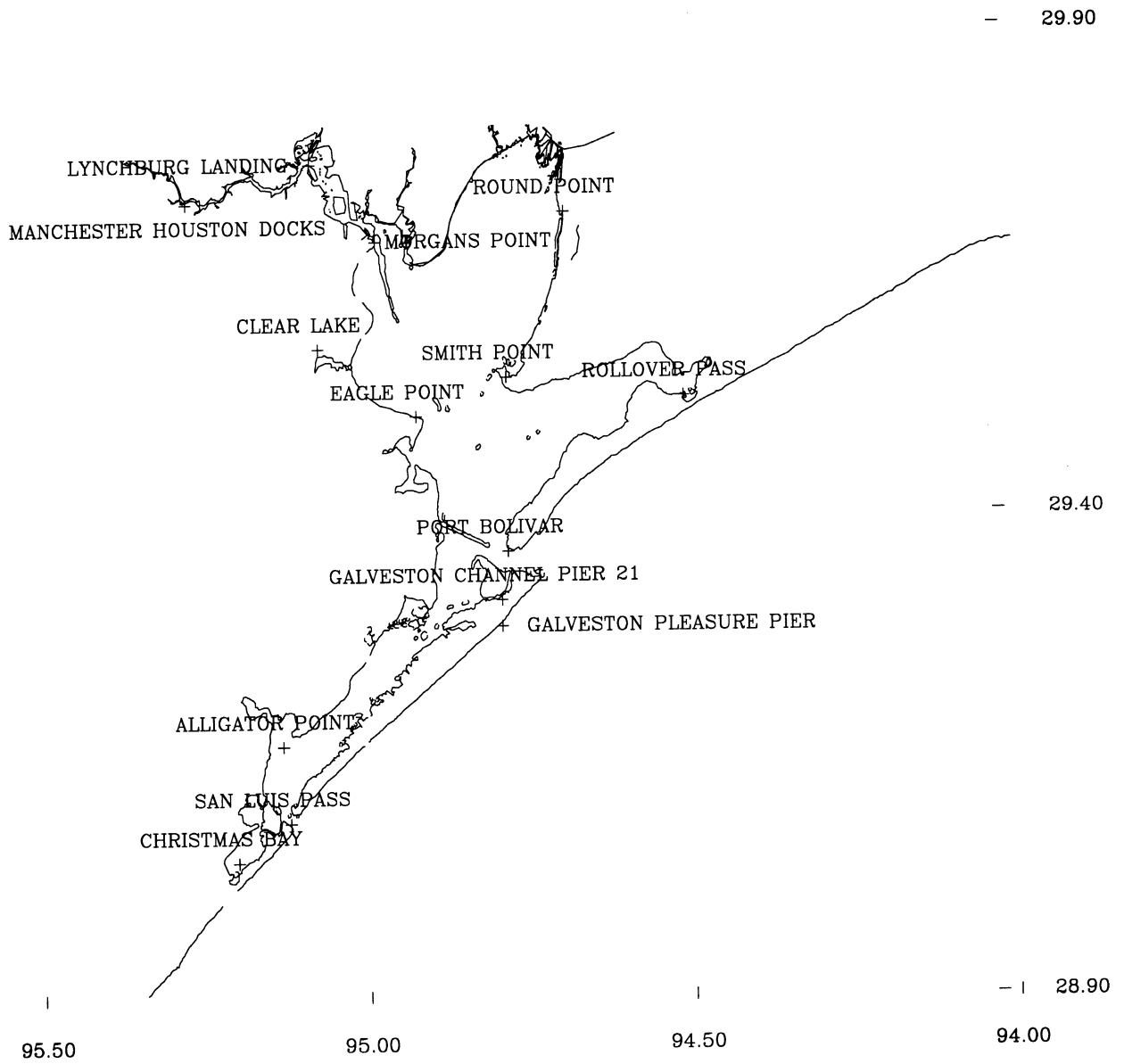
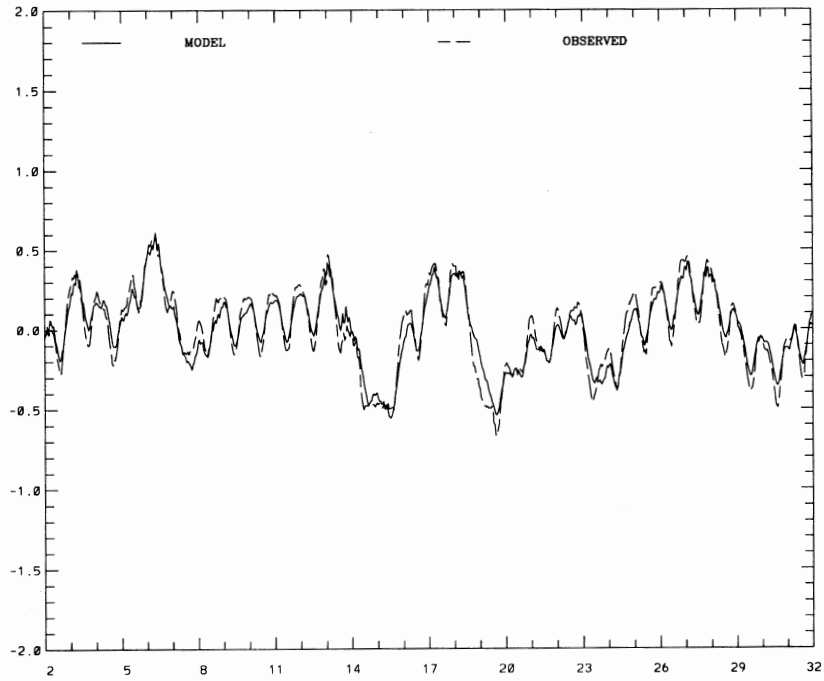


Figure 4.2. Galveston Bay Water Level Sensitivity Analysis Station Locations

NOS HINDCAST (BAY + GOM WINDS) JANUARY 1995 MORGANS POINT

ELEVATION (M)

RMS ERROR = 0.07 IND AGRMT = 0.97



NOS HINDCAST JANUARY 1995 MORGANS POINT

ELEVATION (M)

RMS ERROR = 0.07 IND AGRMT = 0.98

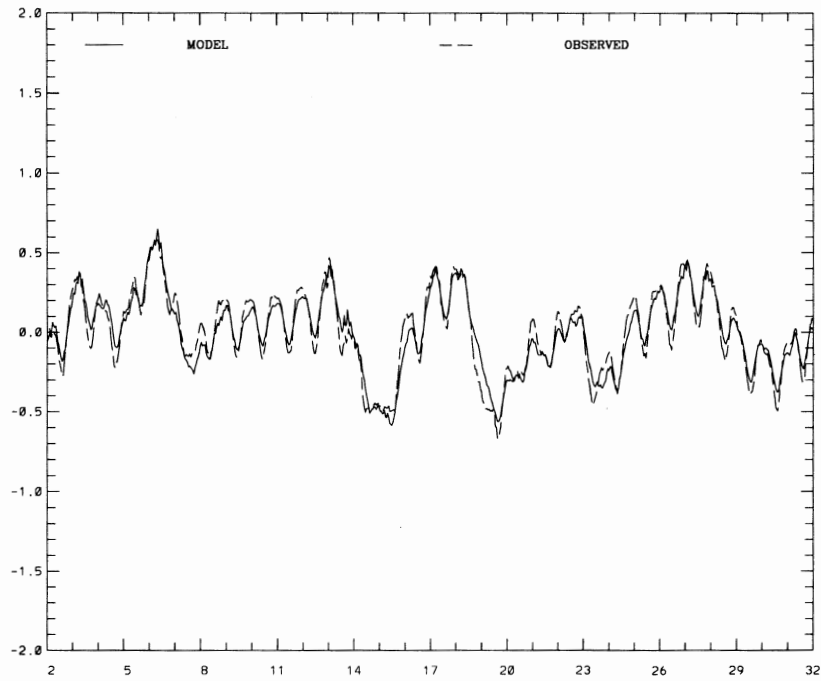
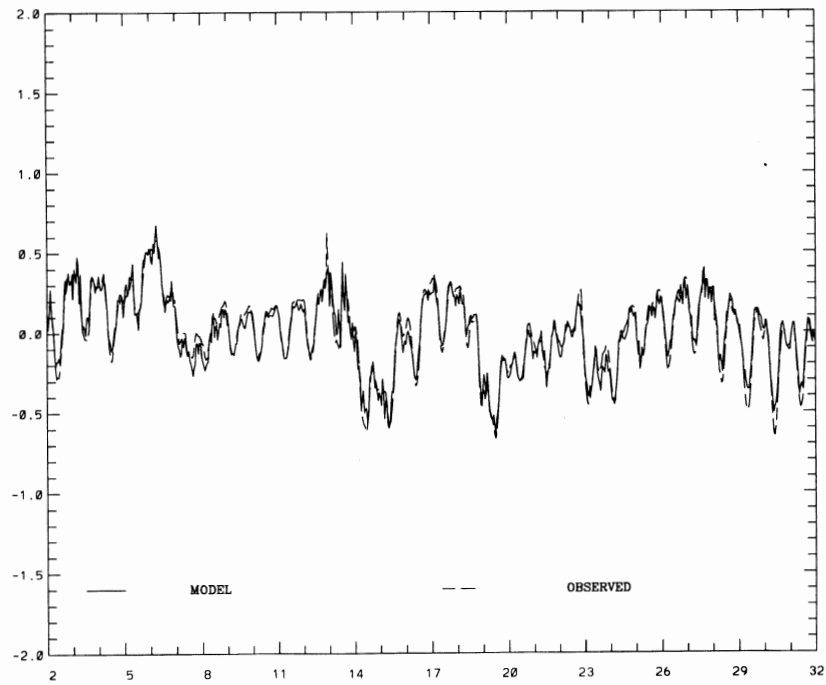


Figure 4.3. Experiment Set 1 Experiment 1 Water Level Time Series Response Comparisons at Morgans Point

NOS HINDCAST (BAY + GOM WINDS) JANUARY 1995 GALVESTON CHANNEL PIER 21

ELEVATION (M)

RMS ERROR = 0.06 IND AGRMT = 0.98



NOS HINDCAST JANUARY 1995 GALVESTON CHANNEL PIER 21

ELEVATION (M)

RMS ERROR = 0.06 IND AGRMT = 0.98

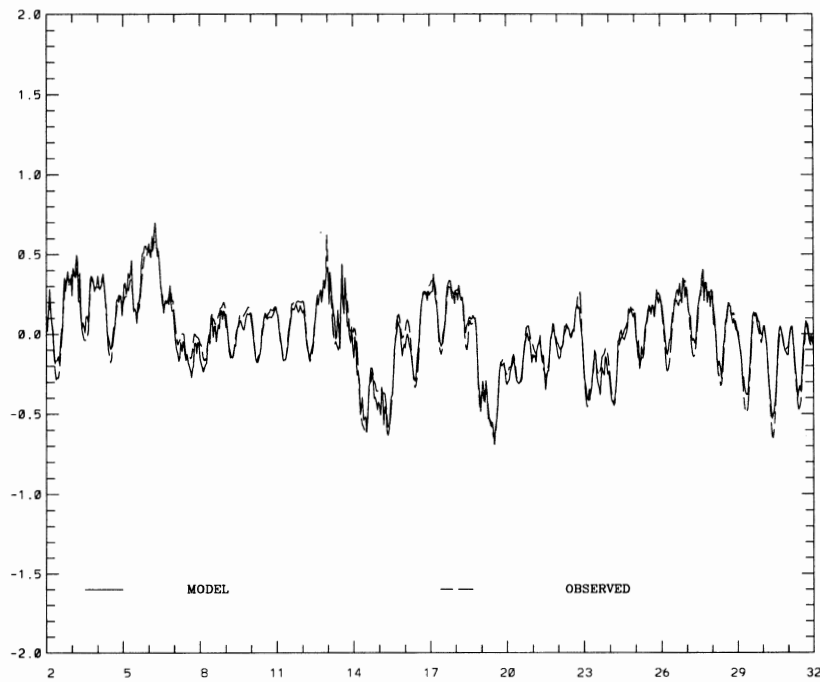
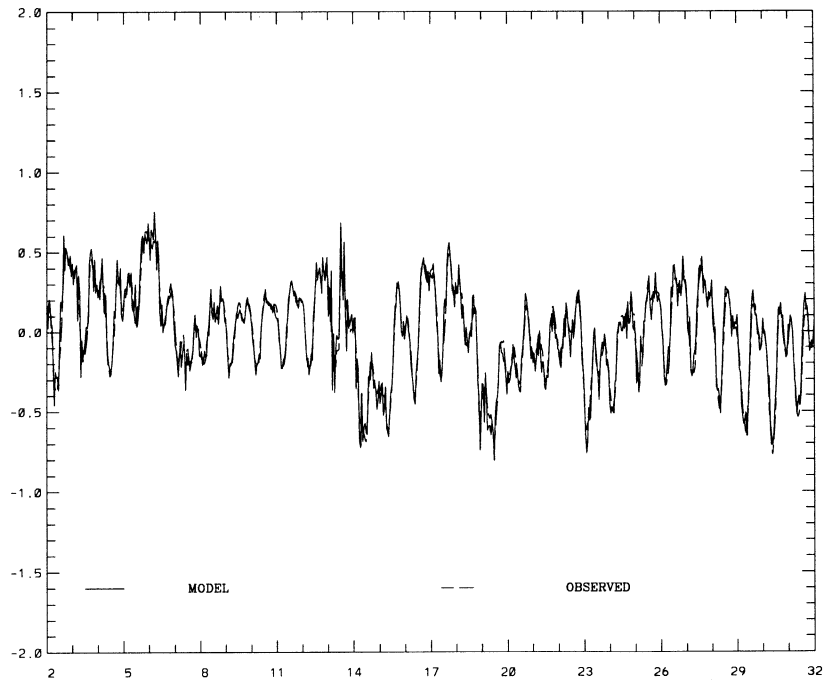


Figure 4.4. Experiment Set 1 Experiment 1 Water Level Time Series Response Comparisons at Galveston Pier 21

NOS HINDCAST (BAY + GOM WINDS) JANUARY 1995 GALVESTON PLEASURE PIER

ELEVATION (M)

RMS ERROR = 0.08 IND AGRMT = 0.98



NOS HINDCAST JANUARY 1995 GALVESTON PLEASURE PIER

ELEVATION (M)

RMS ERROR = 0.08 IND AGRMT = 0.98

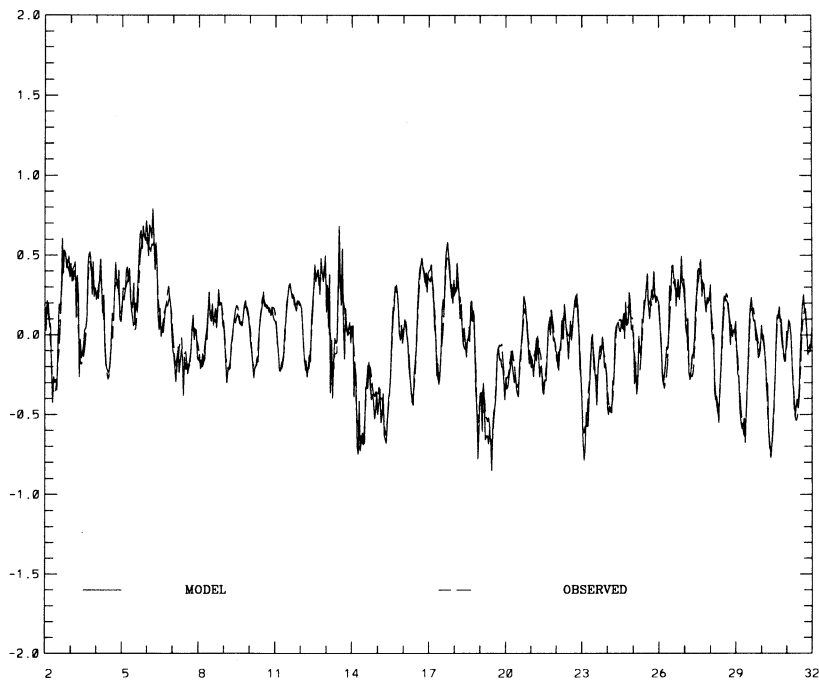
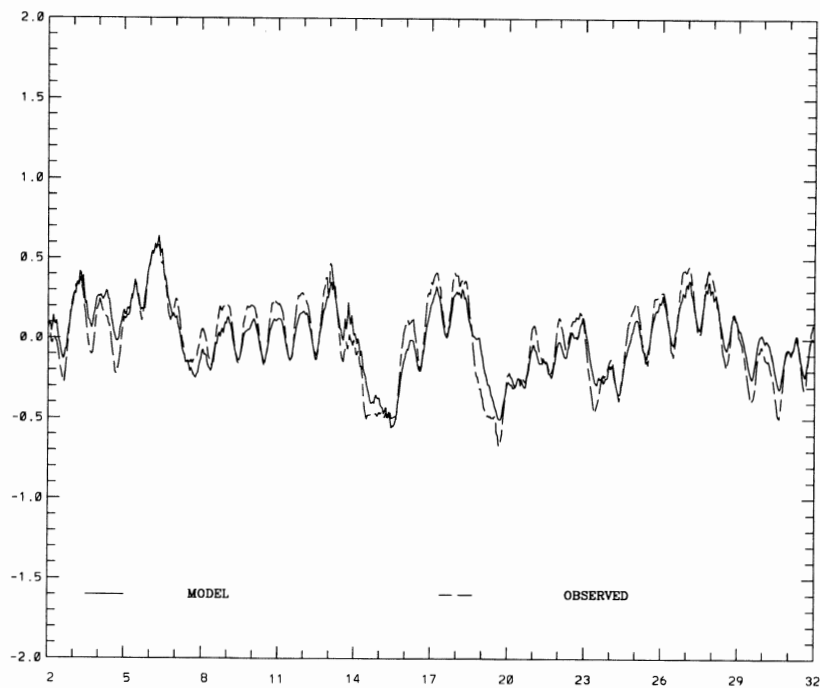


Figure 4.5. Experiment Set 1 Experiment 1 Water Level Time Series Response Comparisons at Galveston Pleasure Pier

NOS HINDCAST (SHELF+GOM WINDS) JANUARY 1995 MORGANS POINT

ELEVATION (M)

RMS ERROR = 0.10 IND AGRMT = 0.96



NOS HINDCAST JANUARY 1995 MORGANS POINT

ELEVATION (M)

RMS ERROR = 0.07 IND AGRMT = 0.98

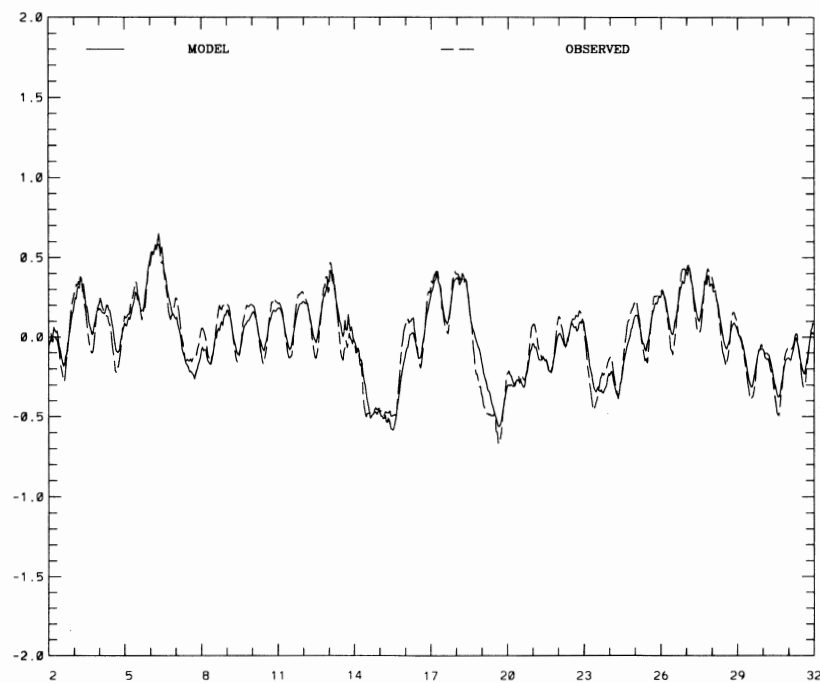
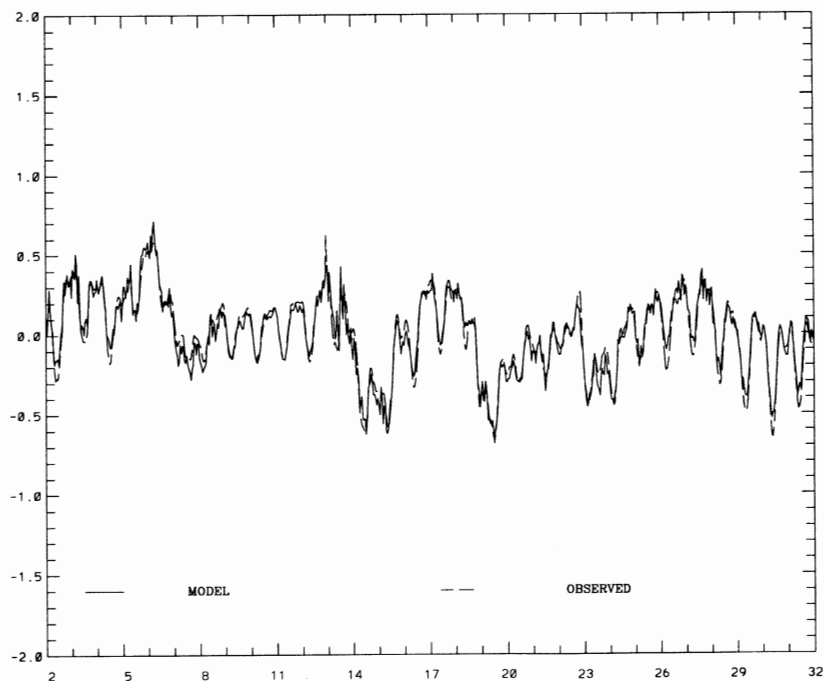


Figure 4.6. Experiment Set 1 Experiment 2 Water Level Time Series Response Comparisons at Morgans Point

NOS HINDCAST (SHELF+GOM WINDS) JANUARY 1995 GALVESTON CHANNEL PIER 21

ELEVATION (M)

RMS ERROR = 0.06 IND AGRMT = 0.98



NOS HINDCAST JANUARY 1995 GALVESTON CHANNEL PIER 21

ELEVATION (M)

RMS ERROR = 0.06 IND AGRMT = 0.98

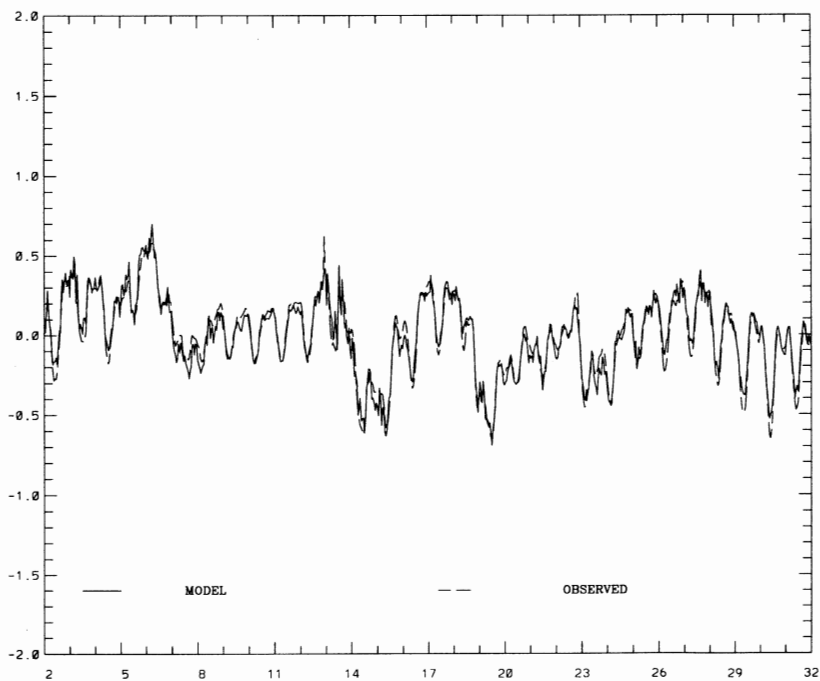
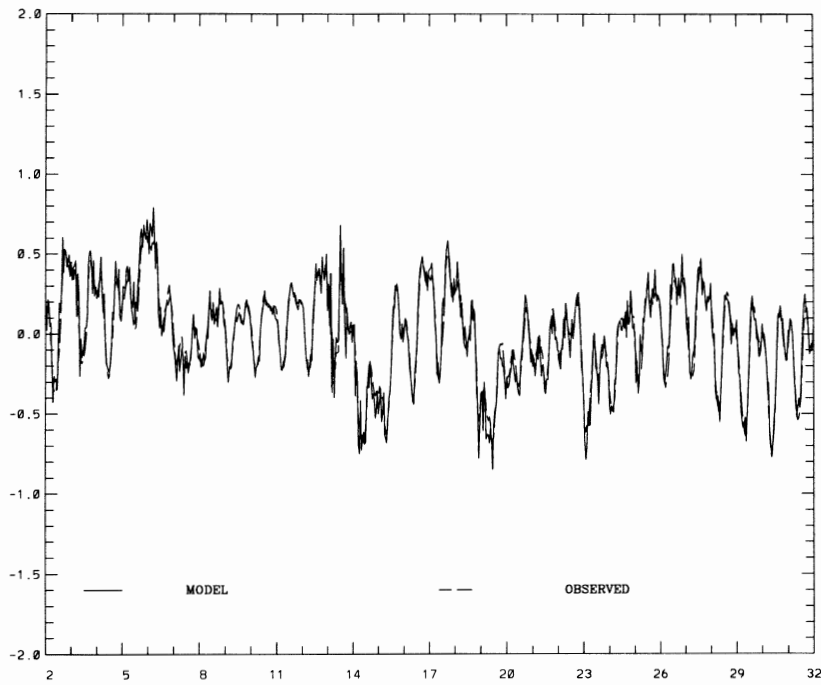


Figure 4.7. Experiment Set 1 Experiment 2 Water Level Time Series Response Comparisons at Galveston Pier 21

NOS HINDCAST (SHELF+GOM WINDS) JANUARY 1995 GALVESTON PLEASURE PIER

ELEVATION (M)

RMS ERROR = 0.08 IND AGRMT = 0.98



NOS HINDCAST JANUARY 1995 GALVESTON PLEASURE PIER

ELEVATION (M)

RMS ERROR = 0.08 IND AGRMT = 0.98

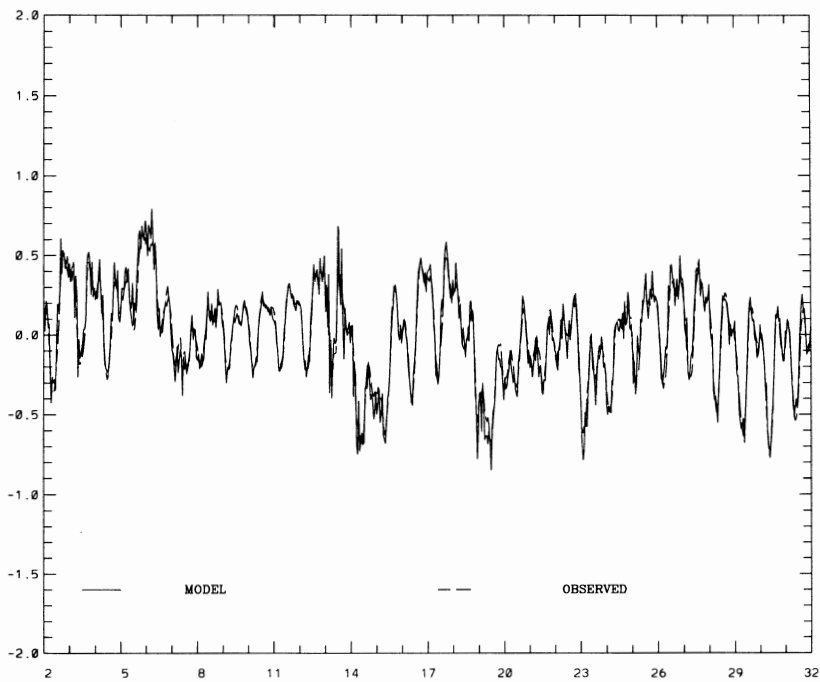
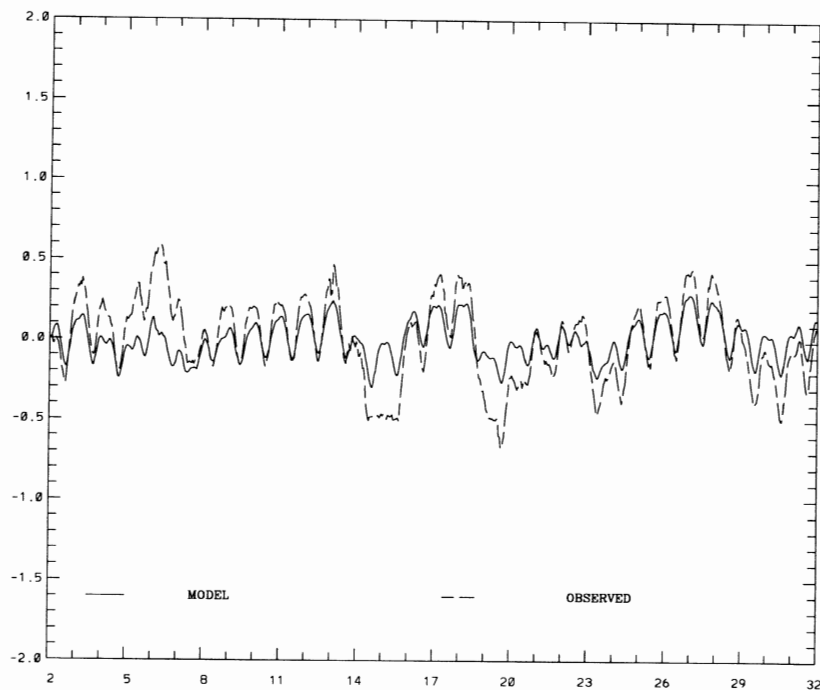


Figure 4.8. Experiment Set 1 Experiment 2 Water Level Time Series Response Comparisons at Galveston Pleasure Pier

NOS HINDCAST (-GOM WIND) JANUARY 1995 MORGANS POINT

ELEVATION (M)

RMS ERROR = 0.18 IND AGRMT = 0.75



NOS HINDCAST JANUARY 1995 MORGANS POINT

ELEVATION (M)

RMS ERROR = 0.07 IND AGRMT = 0.98

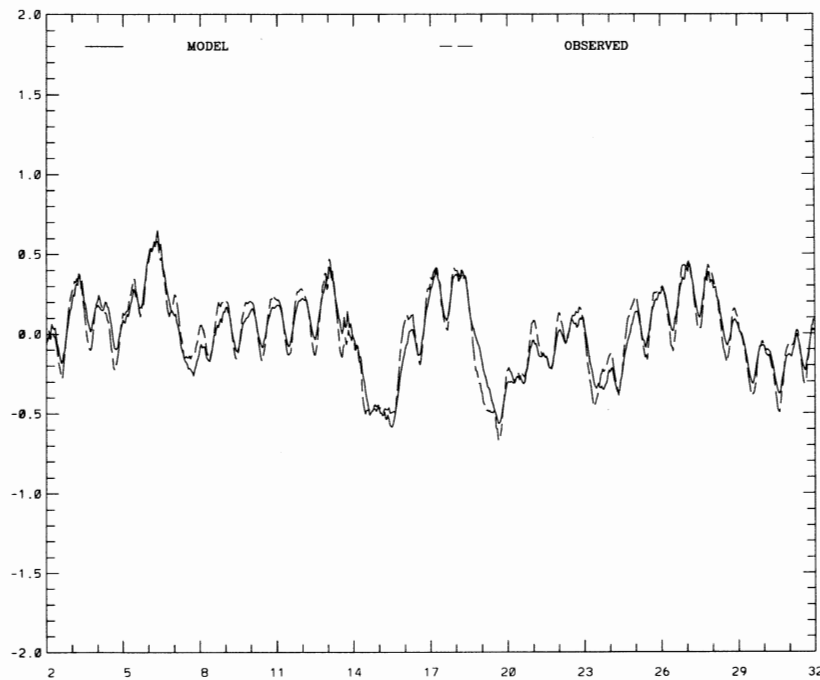
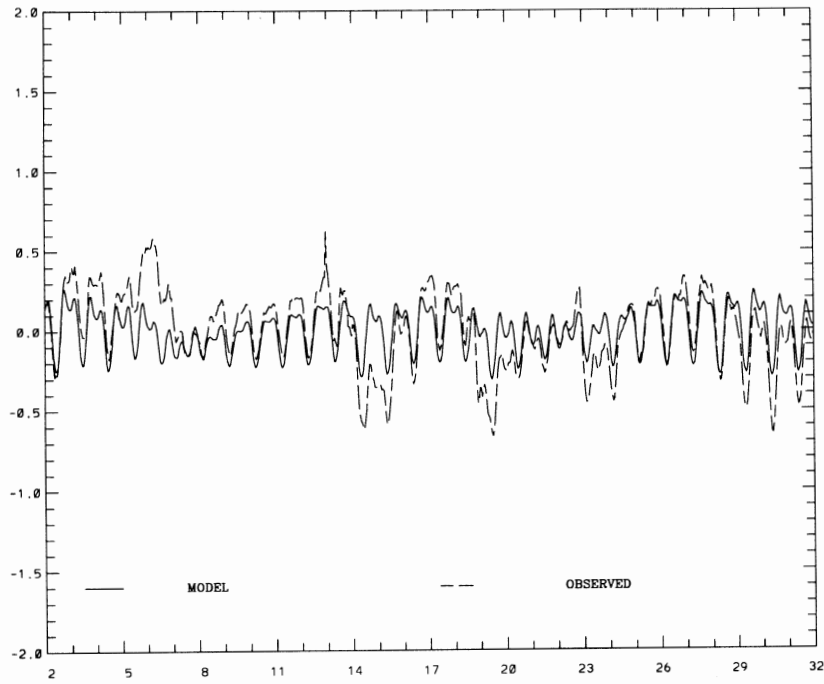


Figure 4.9. Experiment Set 1 Experiment 4 Water Level Time Series Response Comparisons at Morgans Point

NOS HINDCAST (-GOM WIND) JANUARY 1995 GALVESTON CHANNEL PIER 21

ELEVATION (M)

RMS ERROR = 0.18 IND AGRMT = 0.75



NOS HINDCAST JANUARY 1995 GALVESTON CHANNEL PIER 21

ELEVATION (M)

RMS ERROR = 0.06 IND AGRMT = 0.98

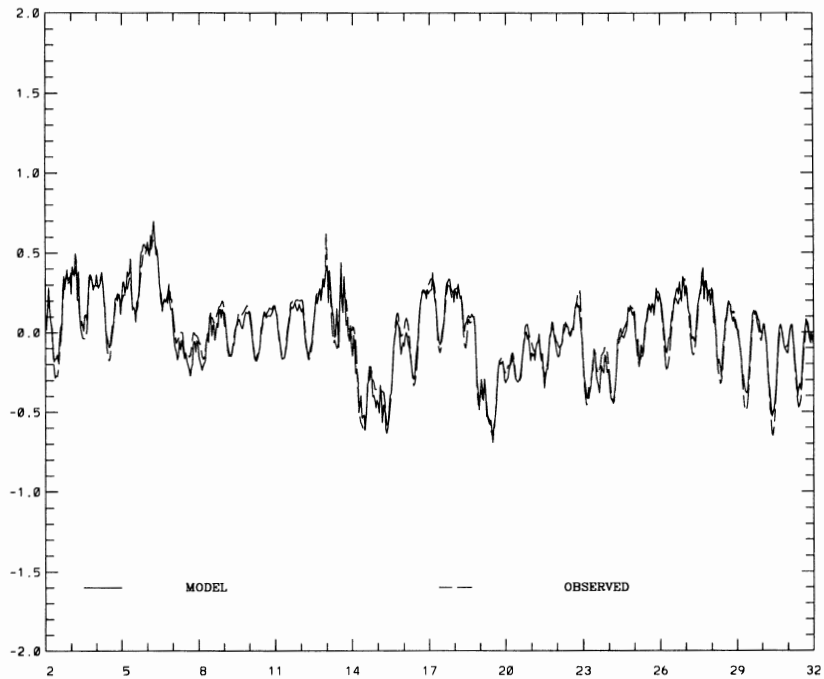
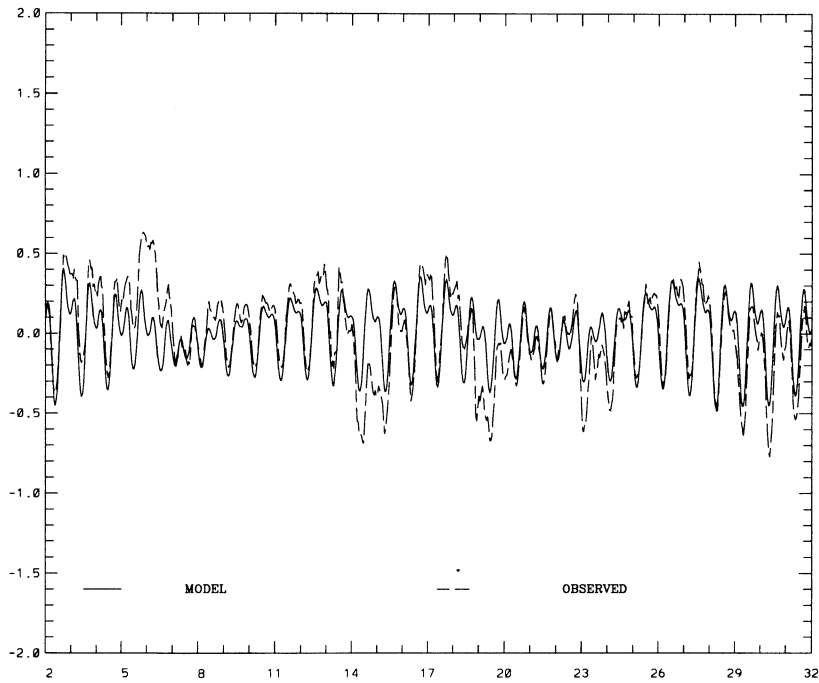


Figure 4.10. Experiment Set 1 Experiment 4 Water Level Time Series Response Comparisons at Galveston Pier 21

NOS HINDCAST (-GOM WIND) JANUARY 1995 GALVESTON PLEASURE PIER

ELEVATION (M)

RMS ERROR = 0.18 IND AGRMT = 0.83



NOS HINDCAST JANUARY 1995 GALVESTON PLEASURE PIER

ELEVATION (M)

RMS ERROR = 0.08 IND AGRMT = 0.98

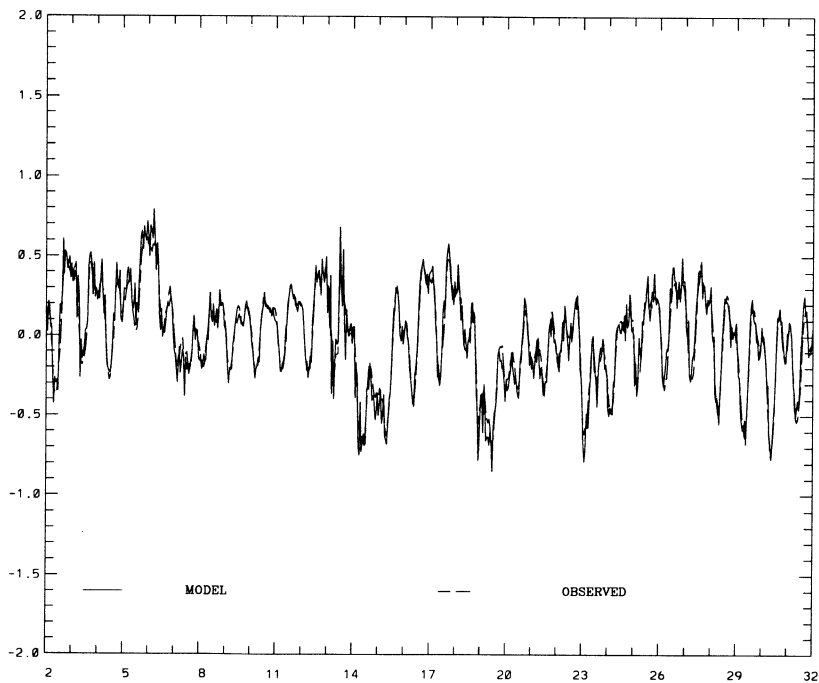
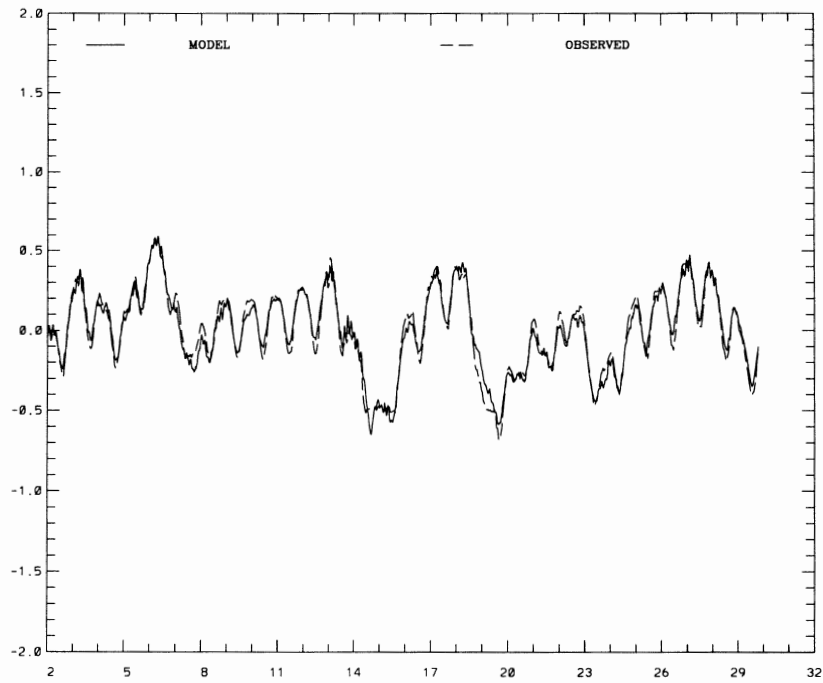


Figure 4.11. Experiment Set 1 Experiment 4 Water Level Time Series Response Comparisons at Galveston Pleasure Pier

NOS HINDCAST (TAMU WINDS) JANUARY 1995 MORGANS POINT

ELEVATION (M)

RMS ERROR = 0.05 IND AGRMT = 0.99



NOS HINDCAST JANUARY 1995 MORGANS POINT

ELEVATION (M)

RMS ERROR = 0.07 IND AGRMT = 0.98

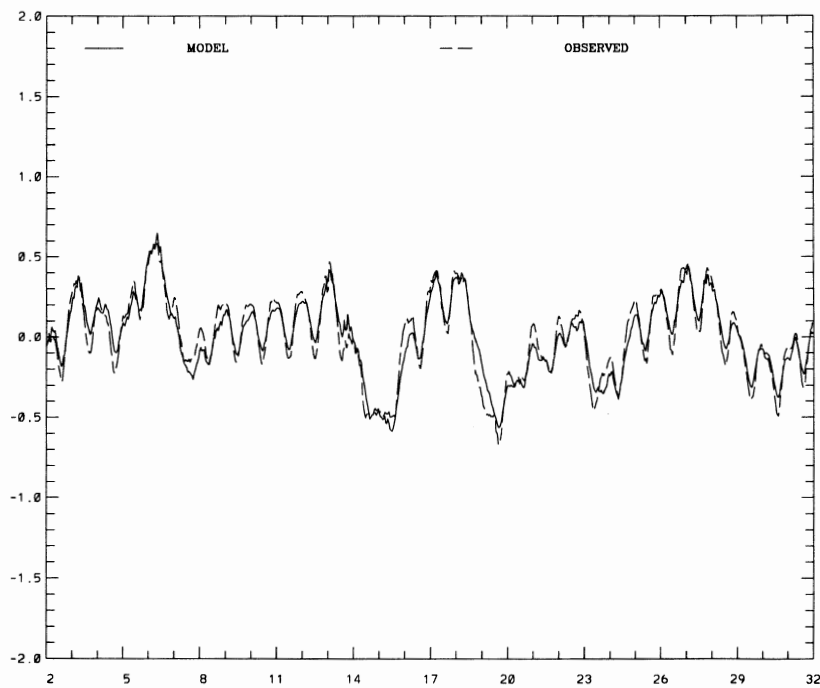
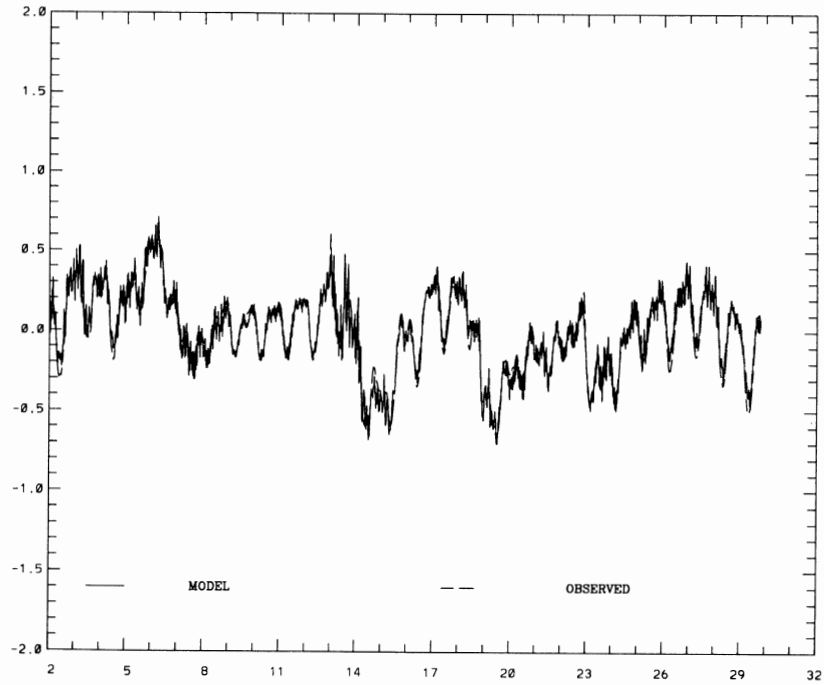


Figure 4.12. Experiment Set 1 Experiment 5 Water Level Time Series Response Comparisons at Morgans Point

NOS HINDCAST (TAMU WINDS) JANUARY 1995 GALVESTON CHANNEL PIER 21

ELEVATION (M)

RMS ERROR = 0.07 IND AGRMT = 0.98



NOS HINDCAST JANUARY 1995 GALVESTON CHANNEL PIER 21

ELEVATION (M)

RMS ERROR = 0.06 IND AGRMT = 0.98

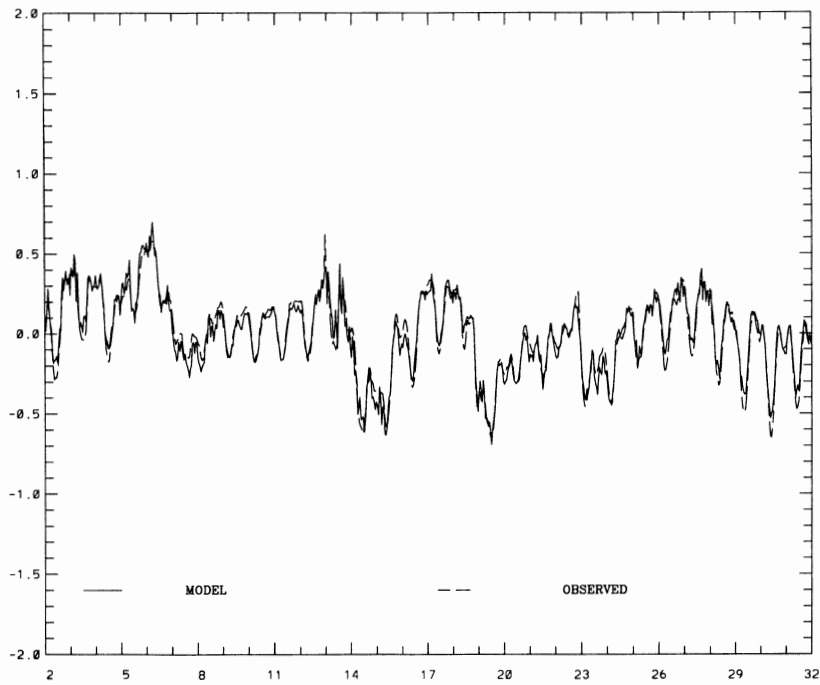
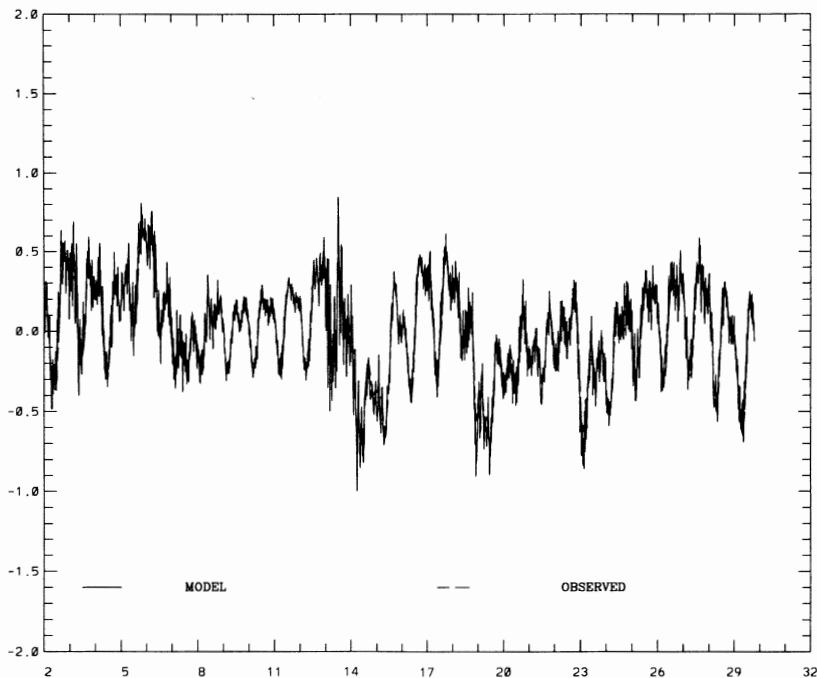


Figure 4.13. Experiment Set 1 Experiment 5 Water Level Time Series Response Comparisons at Galveston Pier 21

NOS HINDCAST (TAMU WINDS) JANUARY 1995 GALVESTON PLEASURE PIER

ELEVATION (M)

RMS ERROR = 0.09 IND AGRMT = 0.97



NOS HINDCAST JANUARY 1995 GALVESTON PLEASURE PIER

ELEVATION (M)

RMS ERROR = 0.08 IND AGRMT = 0.98

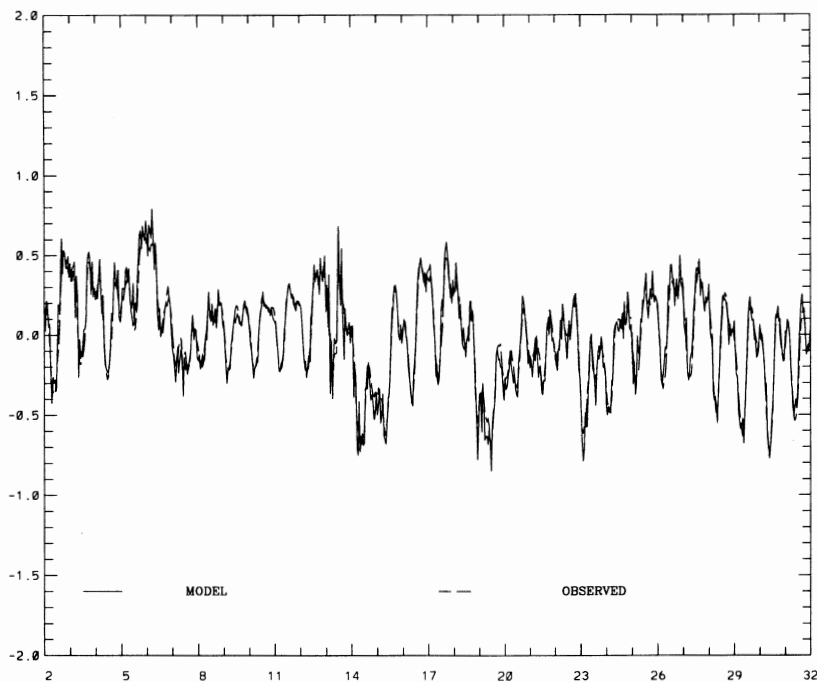


Figure 4.14. Experiment Set 1 Experiment 5 Water Level Time Series Response Comparisons at Galveston Pleasure Pier

4.2. Experiment Set 2

In experiment set two, the October 1994 ‘freshet’ period (refer to Chapter 3) was considered to assess the impact of river inflows on water level response. The effect of Bay winds was evaluated with this experiment set as well. Record average daily flows of 130,000 cfs and 350,000 cfs occurred on the Trinity and San Jacinto Rivers, respectively, during 18 - 19 October (JD 291-292). The subtidal water level mean at Galveston Pleasure Pier was 21 cm with a standard deviation of 11 cm. The experiments shown in Table 4.4 were conducted.

Table 4.4. October 1994 Experiment Set 2

Experiment 1	1 percent of inflow with all winds included
Experiment 2	1 percent of inflow with Gulf of Mexico winds (Bay and Shelf winds neglected)
Experiment 3	Bay and Shelf winds neglected
Experiment 4	Texas A&M University (TAMU) objective analysis windfield

Results of each experiment are discussed in turn below by comparing the water level response with the October 1994 hindcast, which was produced by using the NOS two-step Barnes interpolation for wind and sea-level atmospheric pressure fields. The comparisons are made by examining tabulated SD differences and means and time series plots at Morgans Point (Upper Galveston Bay), Galveston Pier 21 (Lower Galveston Bay), and Galveston Pier 21 (Gulf of Mexico) as done previously. Note in the plots, since both series are demeaned RMS ERROR is equivalent to SD.

Experiment Set 2 Experiment 1

In this experiment, freshwater inflows are reduced by a factor of 100 (peak flows are now on the order of 1,000 - 3,000 cfs). SD differences in water level differ by 1 cm at Morgans Point, 7 cm at Clear Lake, and 2 cm at Port Bolivar as shown in Table 4.5. Mean monthly water levels differ by order 8 cm throughout the Upper Bay and by order 3 cm in the Lower Bay and in the West Bay as given in Table 4.6. Water level time series responses at Morgans Point, Galveston Pier 21, and Galveston Pleasure Pier are shown in Figures 4.15 - 4.17, respectively. During the peak flow period on 18-19 October (JD 291-292), water levels between the experiment and hindcast differ by order 50 cm, 10 cm, and less than 2 cm, at Morgans Point (Upper Bay), Galveston Pier 21 (Lower Bay), and Galveston Pleasure Pier (Shelf), respectively.

Experiment Set 2 Experiment 2

In this experiment, freshwater inflows are as reduced in experiment 1 and Bay and Shelf winds are neglected. SD differences in water level differ by 2 cm at Galveston Pier 21 and 4 cm at Morgans Point as given in Table 4.5. Mean monthly water levels in Table 4.6 differ by order 9 cm in the Upper Bay and by order 4 cm in the Lower Bay and by 8 cm in the West Bay. By comparing water level time series responses at Morgans Point, Galveston Pier 21, and Galveston Pleasure Pier shown

in Figures 4.18 - 4.20, respectively, with those in Figures 4.15 - 4.17 for experiment one, and noting the experiment means are nearly the same, one notes that at Morgans Point, the Bay wind influence is order 10 cm during 9 - 14 October (JD 282-287), while at the other stations it is minor.

Experiment Set 2 Experiment 3

In this experiment, freshwater inflows are not reduced but Bay and Shelf winds are neglected. SD differences in water level differ by 1 cm at Galveston Pier 21 and 2 cm at Morgans Point as given in Table 4.5. Mean monthly water levels differ by less than 1 cm in the Upper Bay and by order 2 cm in the Lower Bay and by 6 cm in the West Bay as shown in Table 4.6. Water level time series responses at Morgans Point, Galveston Pier 21, and Galveston Pleasure Pier indicate the influence of the wind at Morgans Point (Upper Bay) and minor influence at Galveston Pier 21 (Lower Bay) to be the same as in experiment 2.

Experiment Set 2 Experiment 4

In this experiment, TAMU objectively analyzed windfields are used. Atmospheric pressure anomalies are set to zero. SD and ARE statistics in Table 4.5 and mean water levels in Table 4.6 indicate that TAMU windfields produce similar water level responses (mean order 2 cm and nearly identical RMS and relative error) to the NOS windfields. Time series of water level response are compared with the hindcast at Morgans Point, Galveston Pier 21, and Galveston Pleasure Pier in Figures 4.21 - 4.23, respectively. TAMU wind generated water level signals exhibit more oscillation in the Lower Bay and on the Shelf as noted previously during January 1995.

Experiment Set 2 Results Summary

Based on these experiments, freshwater influences on the Bay water levels may be as large as 50 cm during major flooding events (order 100,000 cfs on the Trinity River and 300,000 cfs on the San Jacinto River). If we assume a linear relationship between streamflow and water level response, flows order 50,000 cfs on both rivers, and an equal influence, then one might expect an influence on Bay water levels of order 10-20 cm. Thus flows of order 20,000 cfs, which are prevalent during the wet season (October - May), would appear to be significant at the 5 cm level. As a result, the nowcast/forecast system must use accurate streamflows to produce realistic water levels in the Upper Bay. Experiments 2 and 3 confirmed the influence of the Bay windfields on Bay water levels to be order 10 cm during periods of October 1994 as well as was found previously during periods of January 1995.

Table 4.5. Experiment Set Two Water Level Response SD (cm)/ ARE (-) Statistics

Station	Hindcast	Exp. 1	Exp. 2	Exp. 3	Exp. 4
Galveston Pleasure Pier	8/0.04	8/0.04	8/0.04	8/0.04	8/0.04
Galveston Pier 21	5/0.03	7/0.05	7/0.05	6/0.03	6/0.03
Morgans Point	9/0.04	10/0.07	13/0.13	11/0.07	6/0.02
Clear Lake	8/0.04	15/0.14	16/0.20	10/0.06	9/0.05
Eagle Point	8/0.07	7/0.05	6/0.05	7/0.06	7/0.04
Port Bolivar	11/0.11	13/0.17	14/0.18	11/0.12	11/0.11
Christmas Bay	5/0.04	5/0.06	6/0.06	6/0.06	5/0.04

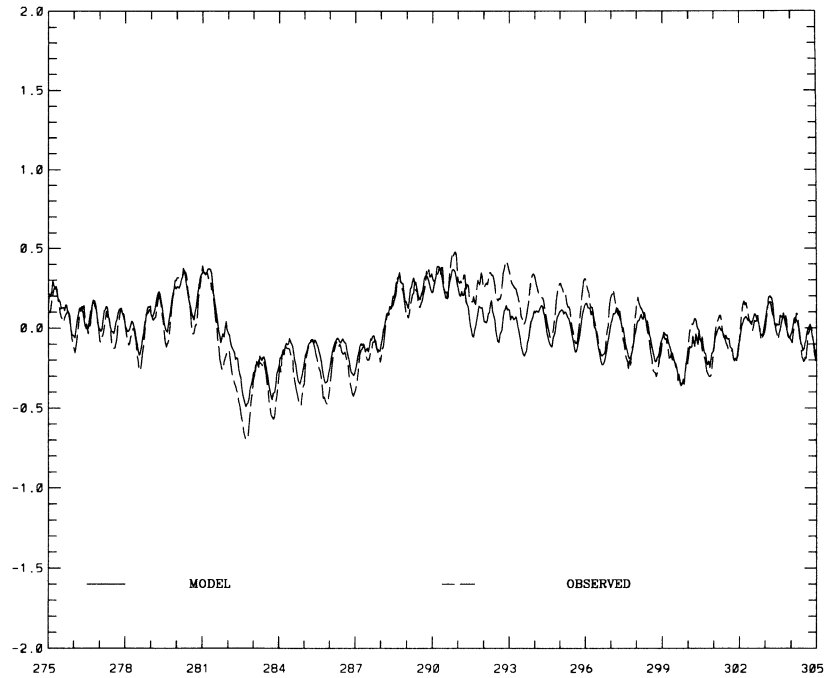
Table 4.6. Experiment Set Two Water Level Means (cm)

Station	Hindcast/ Observed	Exp. 1	Exp. 2	Exp. 3	Exp. 4
Galveston Pleasure Pier	45/37	46	45	46	47
Galveston Pier 21	47/38	51	46	49	50
Morgans Point	48/40	56	47	56	55
Clear Lake	49/41	56	47	53	54
Eagle Point	48/37	55	47	53	53
Port Bolivar	47/37	50	46	49	50
Christmas Bay	51/38	54	46	48	51

NOS HINDCAST (0.01 FLOW) OCTOBER 1994 MORGANS POINT

ELEVATION (M)

RMS ERROR = 0.10 IND AGRMT = 0.93



NOS HINDCAST OCTOBER 1994 MORGANS POINT

ELEVATION (M)

RMS ERROR = 0.09 IND AGRMT = 0.96

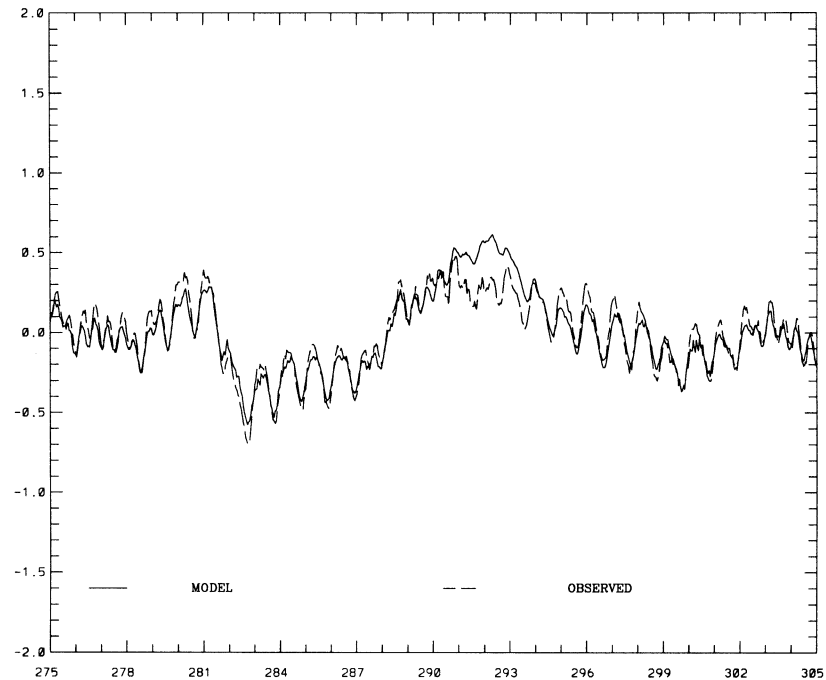
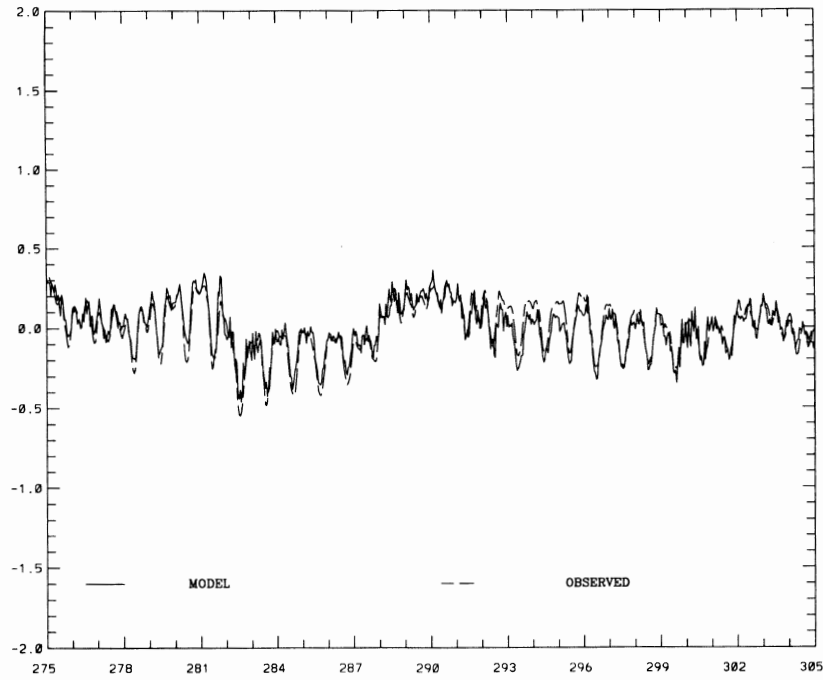


Figure 4.15. Experiment Set 2 Experiment 1 Water Level Time Series Response Comparisons at Morgans Point

NOS HINDCAST (0.01 FLOW) OCTOBER 1994 GALVESTON CHANNEL PIER 21

ELEVATION (M)

RMS ERROR = 0.07 IND AGRMT = 0.95



NOS HINDCAST OCTOBER 1994 GALVESTON CHANNEL PIER 21

ELEVATION (M)

RMS ERROR = 0.05 IND AGRMT = 0.97

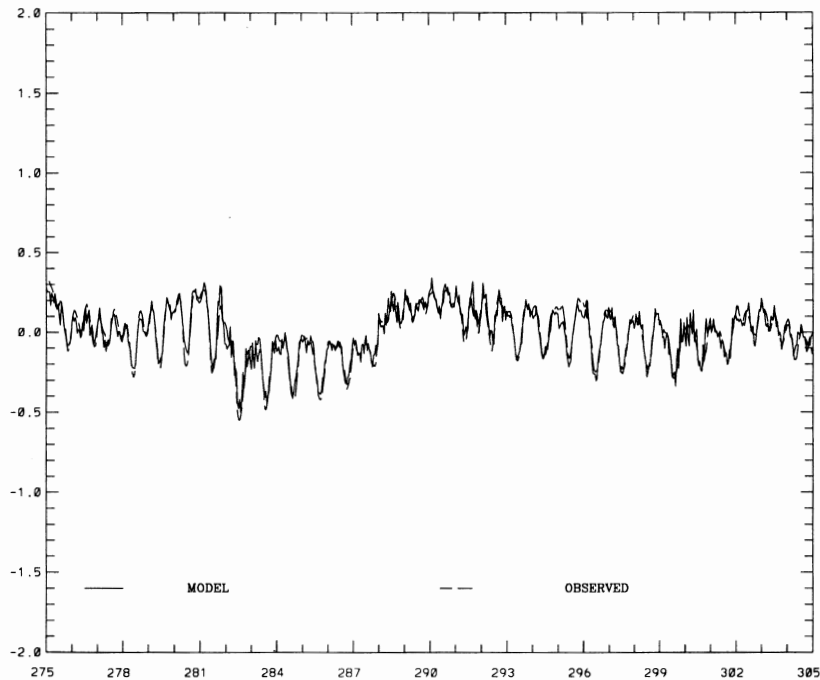
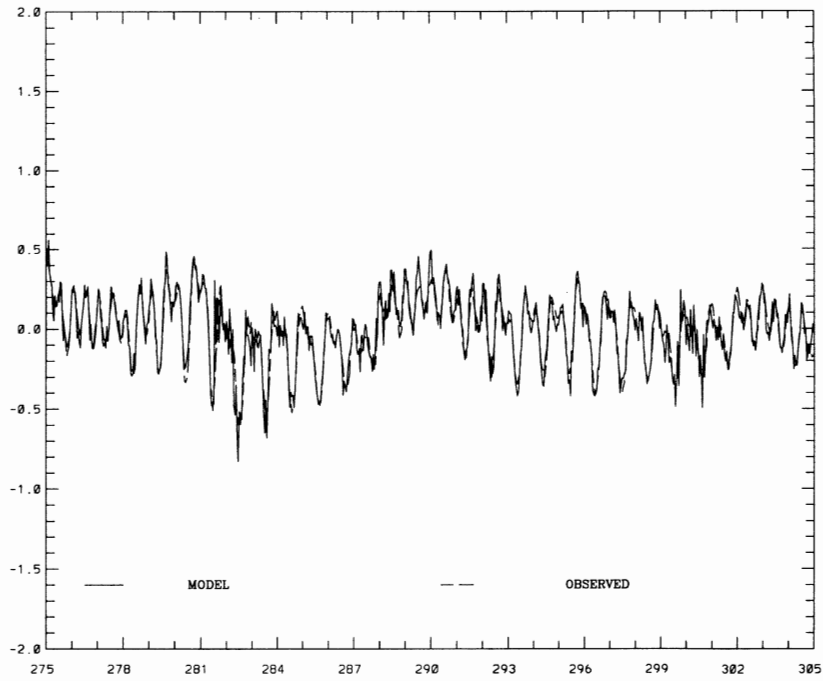


Figure 4.16. Experiment Set 2 Experiment 1 Water Level Time Series Response Comparisons at Galveston Pier 21

NOS HINDCAST (0.01 FLOW) OCTOBER 1994 GALVESTON PLEASURE PIER

ELEVATION (M)

RMS ERROR = 0.08 IND AGRMT = 0.96



NOS HINDCAST OCTOBER 1994 GALVESTON PLEASURE PIER

ELEVATION (M)

RMS ERROR = 0.08 IND AGRMT = 0.96

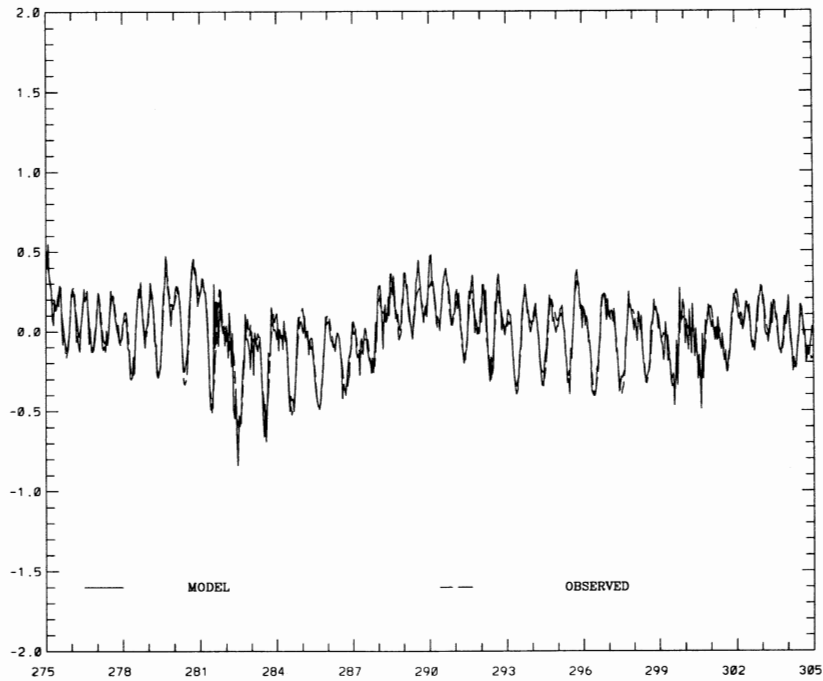
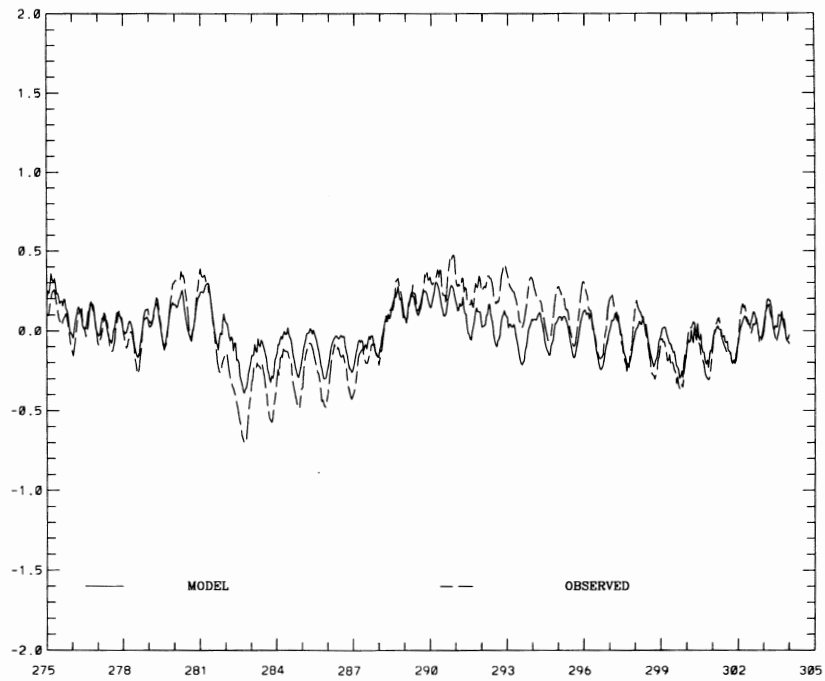


Figure 4.17. Experiment Set 2 Experiment 1 Water Level Time Series Response Comparisons at Galveston Pleasure Pier

NOS HINDCAST (0.01 FLOW + GOM) OCTOBER 1994 MORGANS POINT

ELEVATION (M)

RMS ERROR = 0.13 IND AGRMT = 0.87



NOS HINDCAST OCTOBER 1994 MORGANS POINT

ELEVATION (M)

RMS ERROR = 0.09 IND AGRMT = 0.96

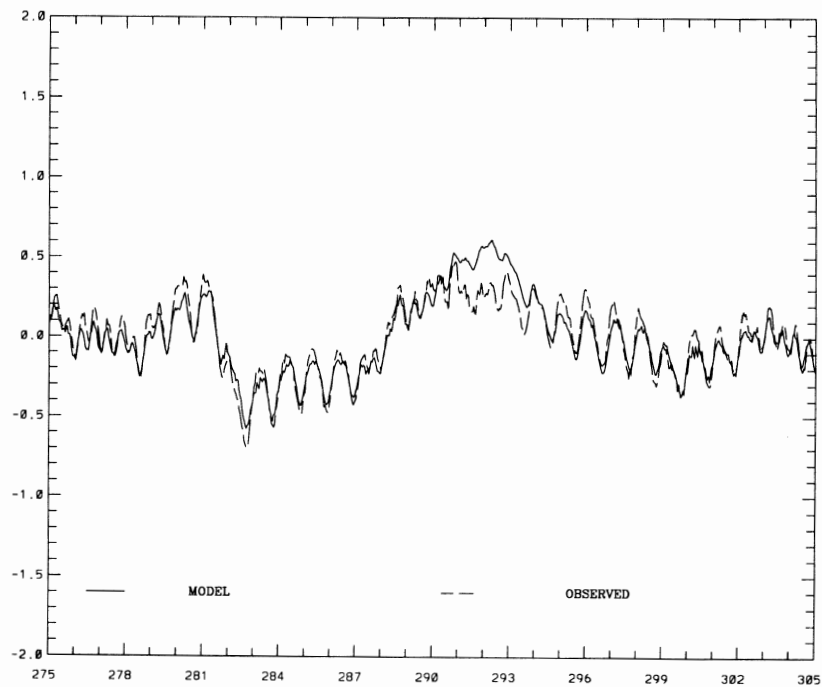
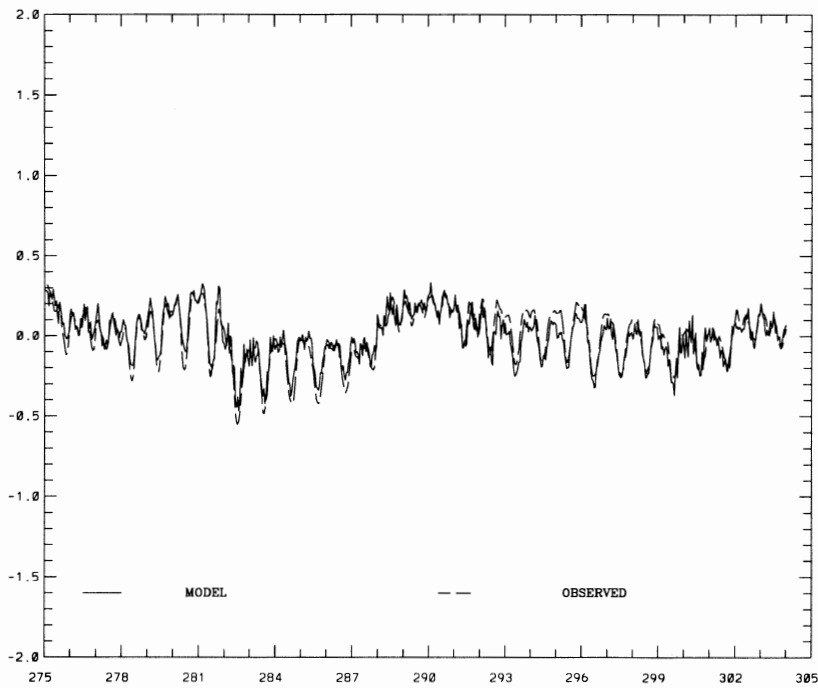


Figure 4.18. Experiment Set 2 Experiment 2 Water Level Time Series Response Comparisons at Morgans Point

NOS HINDCAST (0.01 FLOW + GOM) OCTOBER 1994 GALVESTON CHANNEL PIER 21

ELEVATION (M)

RMS ERROR = 0.07 IND AGRMT = 0.95



NOS HINDCAST OCTOBER 1994 GALVESTON CHANNEL PIER 21

ELEVATION (M)

RMS ERROR = 0.05 IND AGRMT = 0.97

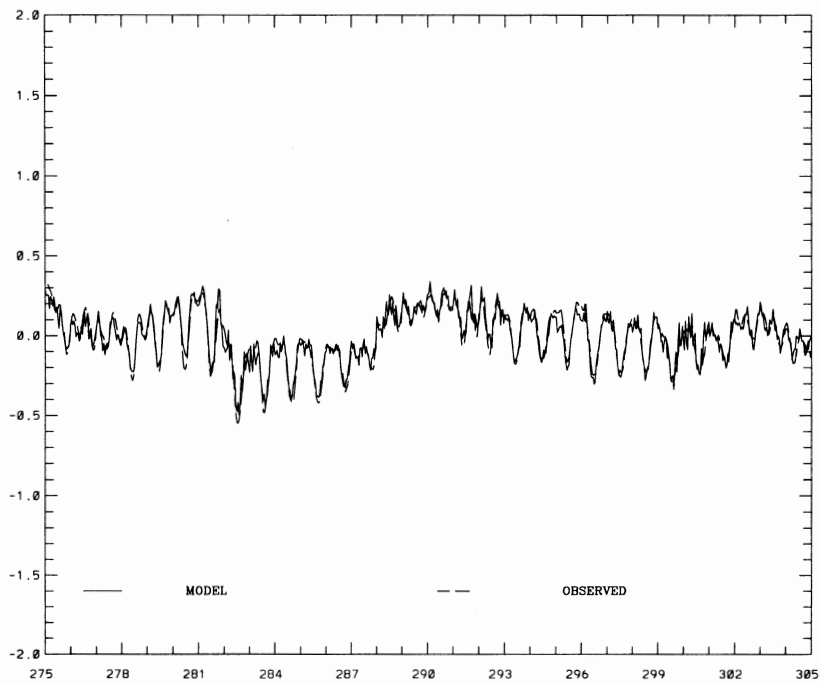
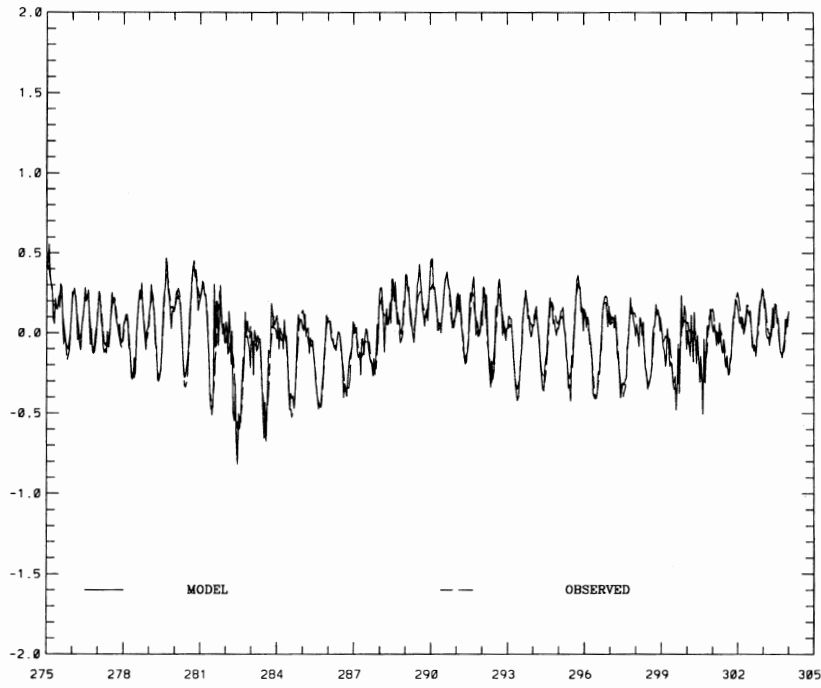


Figure 4.19. Experiment Set 2 Experiment 2 Water Level Time Series Response Comparisons at Galveston Pier 21

NOS HINDCAST (0.01 FLOW + GOM) OCTOBER 1994 GALVESTON PLEASURE PIER

ELEVATION (M)

RMS ERROR = 0.08 IND AGRMT = 0.96



NOS HINDCAST OCTOBER 1994 GALVESTON PLEASURE PIER

ELEVATION (M)

RMS ERROR = 0.08 IND AGRMT = 0.96

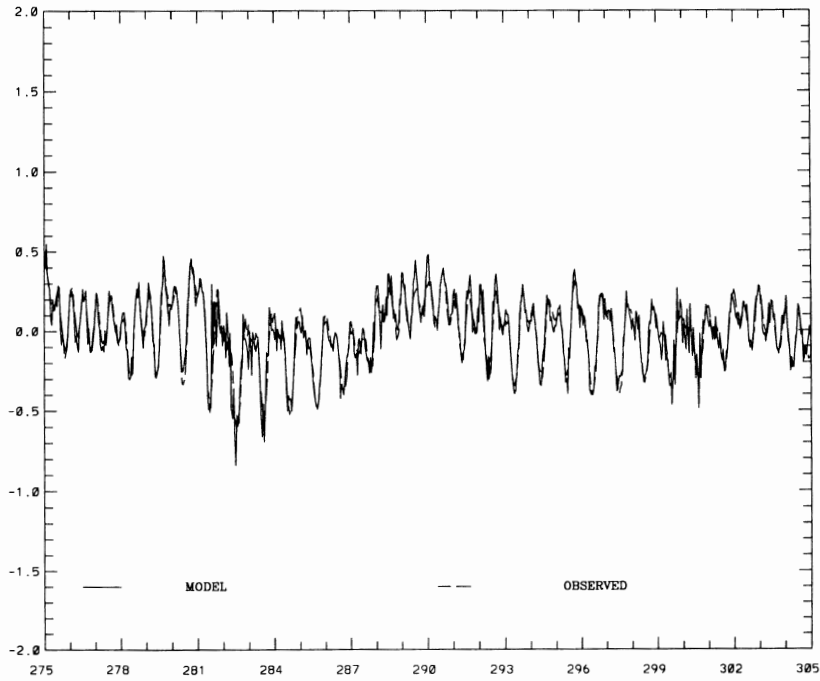
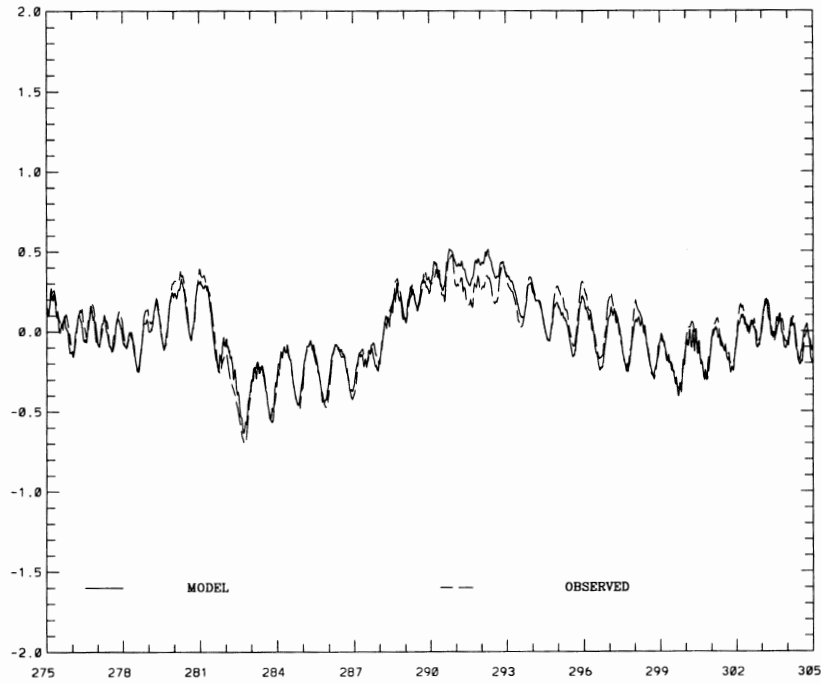


Figure 4.20. Experiment Set 2 Experiment 2 Water Level Time Series Response Comparisons at Galveston Pleasure Pier

NOS HINDCAST (TAMU WINDS) OCTOBER 1994 MORGANS POINT

ELEVATION (M)

RMS ERROR = 0.06 IND AGRMT = 0.98



NOS HINDCAST OCTOBER 1994 MORGANS POINT

ELEVATION (M)

RMS ERROR = 0.09 IND AGRMT = 0.96

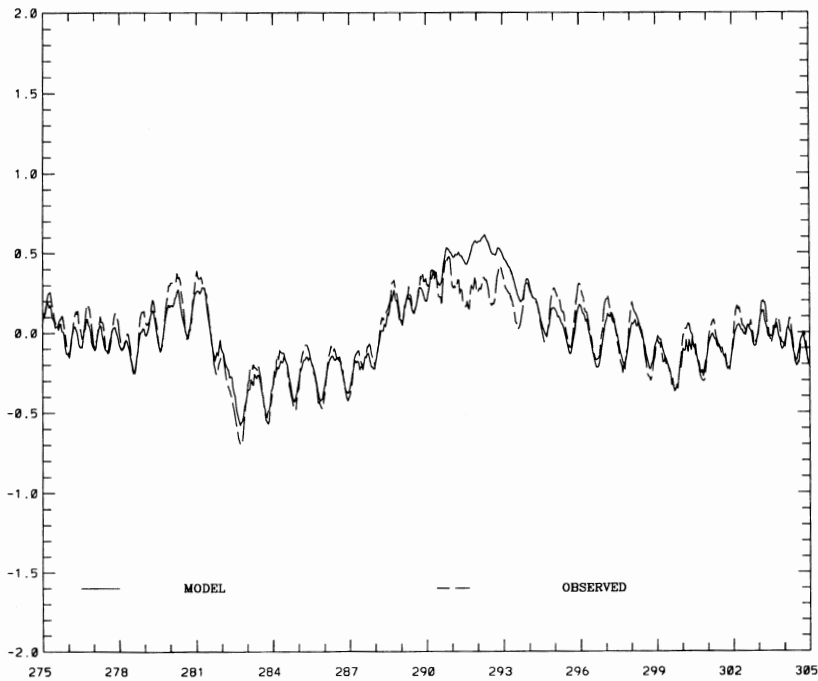
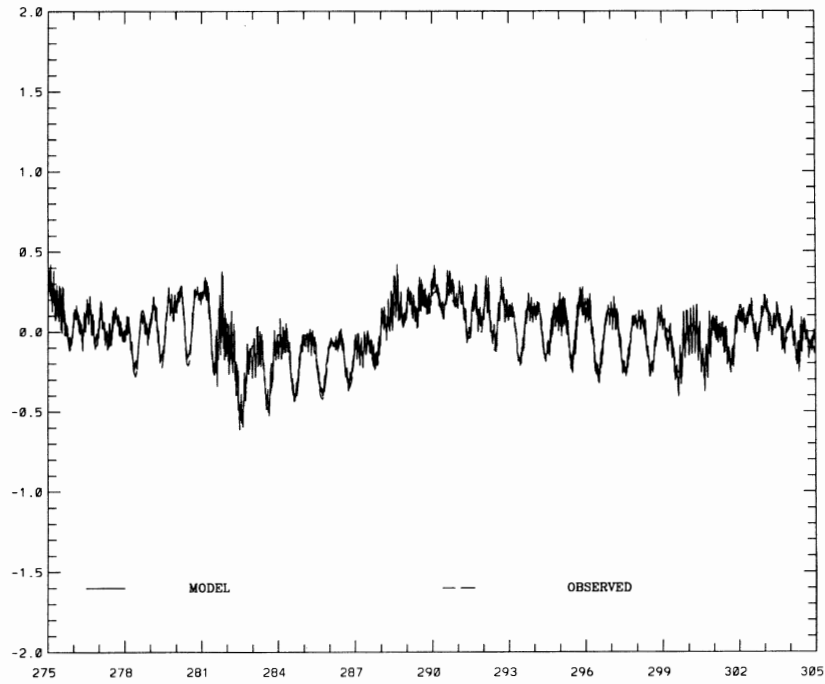


Figure 4.21. Experiment Set 2 Experiment 4 Water Level Time Series Response Comparisons at Morgans Point

NOS HINDCAST (TAMU WINDS) OCTOBER 1994 GALVESTON CHANNEL PIER 21

ELEVATION (M)

RMS ERROR = 0.06 IND AGRMT = 0.97



NOS HINDCAST OCTOBER 1994 GALVESTON CHANNEL PIER 21

ELEVATION (M)

RMS ERROR = 0.05 IND AGRMT = 0.97

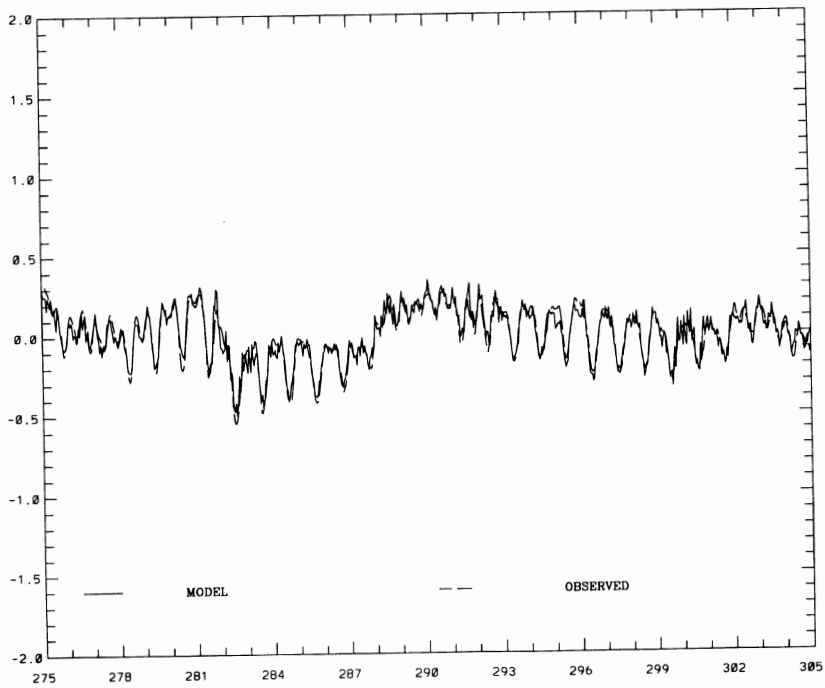
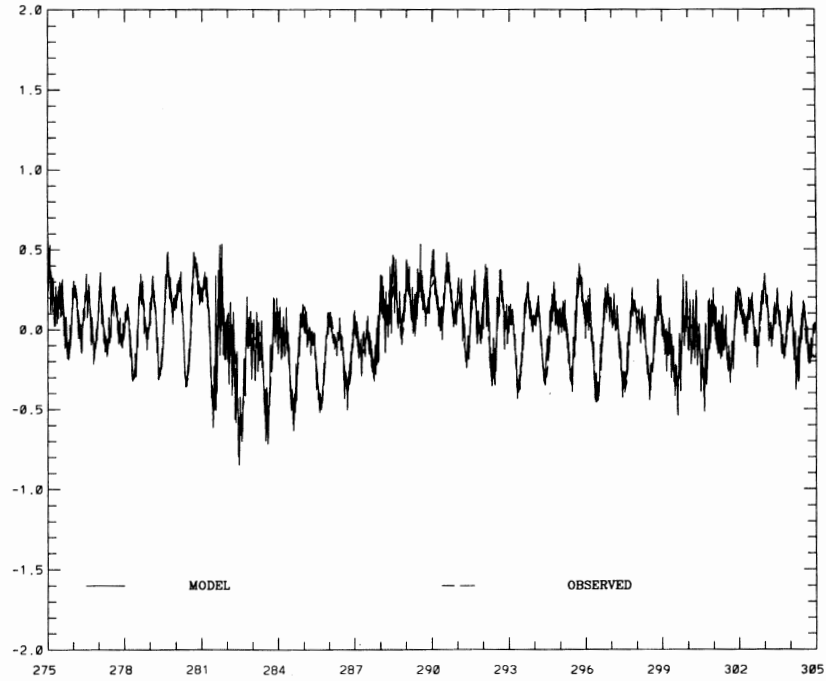


Figure 4.22. Experiment Set 2 Experiment 4 Water Level Time Series Response Comparisons at Galveston Pier 21

NOS HINDCAST (TAMU WINDS) OCTOBER 1994 GALVESTON PLEASURE PIER

ELEVATION (M)

RMS ERROR = 0.08 IND AGRMT = 0.96



NOS HINDCAST OCTOBER 1994 GALVESTON PLEASURE PIER

ELEVATION (M)

RMS ERROR = 0.08 IND AGRMT = 0.96

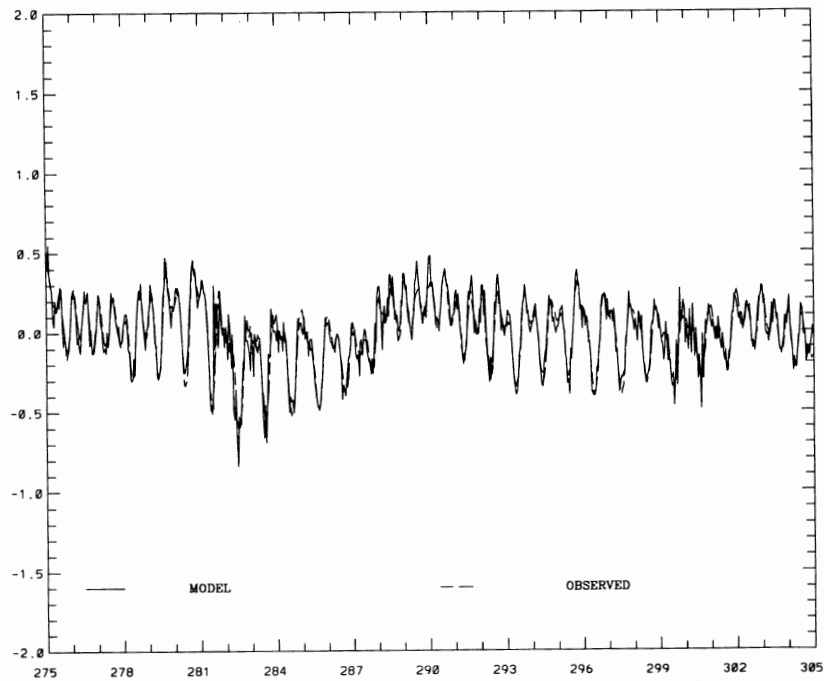


Figure 4.23. Experiment Set 2 Experiment 4 Water Level Time Series Response Comparisons at Galveston Pleasure Pier

5. ONE-WAY COUPLED BAY AND CHANNEL MODEL HINDCAST

During April 1996, all three PORTS current meters were in operation and thus this period was used to evaluate both the water level and current response of both models. Herein, we first consider the Galveston Bay Model (GBM) hindcast in terms of initial and boundary conditions and simulation results. We next consider the Houston Ship Channel Model (HSCM) hindcast in a similar manner. Then an assessment of the one-way coupling scheme is made. To end the chapter, an error budget is presented to partition the total model errors into astronomical tide and subtidal effects.

5.1. Galveston Bay Model

Since there was some evidence that the water level response in the previous two hindcasts was somewhat damped, bottom roughness, z_0 , was reduced from 1 cm to 2mm. The Smagorinsky horizontal eddy viscosity coefficient, C_H , was maintained at 0.005 for the April 1996 simulation (Mellor, 1996). To place the April 1996 period simulation results in context, initial and boundary condition development are first discussed.

Initial Conditions

Velocities and water surface elevations were set to zero. Texas Water Development Board (TWDB) salinity and temperature data were available at 90 minute intervals at approximate mid-depth (see Figure 3.1). These data were melded with climatological salinity and temperature data (Temple et al., 1977 ; Orlando et al., 1993), as previously, to form the initial salinity and temperature fields. Initial near surface salinity as shown in Figure 5.1 ranges from 21.9 to 32.6 PSU while near bottom initial salinity shown in Figure 5.2 ranges from 21.9 to 34.6 PSU with a vertical stratification of order 5 PSU. Initial near surface temperature fields are well mixed and are shown near the surface in Figure 5.3 (16.3 to 17.7 °C) and near the bottom in Figure 5.4 (15.4 to 17.8 °C), respectively. Since the initial Bay model fields represent tidal cycle average conditions, the salinity and temperature contours contain an uncertainty in location equal to the tidal excursion length. The problem is most severe in specifying the initial salinity field, which contains large horizontal gradients.

Boundary Conditions

River inflows, wind and atmospheric pressure fields, and water level residuals, were included. Average daily flows were obtained from USGS, Houston Office, for Buffalo Bayou at Piney Point, TX (USGS Gauge 0807 3700), for the Trinity River at Romayor, TX (USGS Gauge 0806 6800), and at Lake Houston near Sheldon, TX (USGS Gauge 0807 2000). The Buffalo Bayou streamflow is shown in Figure 5.5. Minor flow events on JD 104 and JD 114 are to be noted. The observed mean of 94 cfs is much less than the climatological flow of 620 cfs. In Figure 5.6, the Trinity River at Romayor, TX streamflow during April is shown. The observed mean of 2100 cfs is much less than the climatological flow of 8600 cfs. At Lake Houston near Sheldon, TX a stage vs discharge relation is used to convert water surface elevation at Lake Houston to released discharge. For the San Jacinto River, no releases at Lake Houston were made and the flow was zero over the entire month. At stream inflow locations salinity is assumed zero, while temperature is set equal to the temperature of the inflow point. April 1996 represented a period of very low freshwater inflow to Galveston Bay.

NDBC buoy 42020 (3m Discus) and 42035 (3m Discus) and C-MAN station S-2 Sabine and S-4 Port Aransas, TX observations were obtained along with NWS surface weather observations at Houston IAH, Port Arthur, and WSO Galveston, TX. Refer to Figure 2.1 for station locations. Wind and sea-level atmospheric pressure fields were developed at 3 hour intervals over the model domain via the two-step Barnes (1973) interpolation procedure discussed in Chapter 2.

Prior to performing the interpolation, all winds are adjusted to 10m. At overwater stations (42035, Galveston) wind speeds are converted to land values by inverting the formula given by Hsu (1988). At Galveston the conversion from overwater to overland wind is not performed if wind directions are greater than 225 and less than 45 degrees True; e.g. the wind is from the land. The interpolation is then performed on overland winds. The formula of Hsu (1988) and the GBM land/water mask are then used to adjust the overland values to overwater values for all water cells.

Daily average (8 fields per day) GBM grid cell minimum and maximum windspeed and atmospheric pressure are given in Table 5.1 for the resulting interpolations. Maximum wind strengths are order 25 kts. Reviewing the minimum atmospheric pressure column, one notes storm occurrences on April 12 - 14, 25 and 28 - 29. Windfields at hour zero CST on JD 101, 111, and 121 are shown in Figures 5.7, 5.9, and 5.11, respectively, with corresponding windspeed contours shown in Figures 5.8, 5.10, and 5.12, respectively. On JD 101 hour zero CST, winds are directed onshore at 8 to 12 kts. On JD 111 hour zero CST, winds are directed onshore at up to 14 kts. On JD 121 hour zero CST winds are directed offshore at 15 to 20 kts.

Subtidal water level at Galveston Pleasure Pier shown in Figure 5.13 with mean 8 cm and standard deviation of 12 cm was added to the astronomical tide at each cell along the entire GBM open boundary. The subtidal water level was obtained by subtracting the predicted astronomical tide (based on a one year least squares harmonic analysis) from the total observed water level and as shown exhibits considerable oscillation. No smoothing was performed. Major events occur on JD 106, 114, and 120, with excursions in subtidal water levels of up to 0.5 m.

Since surface water temperatures are available in the PORTS and that additional calibration of the heat flux algorithm is required, a SST specification was used in place of the heat flux formulation reported in Chapter 2. A sinusoidal varying daily heating cycle was assumed with a specified amplitude of 0.5 °C . Maximum surface temperature was assumed to occur at 1500 CST. Refer to Schmalz (1994) for details of this SST implementation.

For the salinity and temperature open boundary conditions, climatological values consistent with the above initial conditions were used. Again the assumption was made that the initial and boundary conditions were sufficient to allow the density field to dynamically adjust to a representative value over a single day. In actuality, the influence of the tidal cycle average based initial salinity conditions may require a longer adjustment time, which is dependent on the history of the freshwater inputs to the Bay.

Table 5.1. April 1996 Galveston Bay Model Barnes Interpolation Summary

Day	Wind Speed Minimum (m/s)	Wind Speed Maximum (m/s)	Air Pressure Minimum (mb)	Air Pressure Maximum (mb)
1	5.75	9.18	1019.18	1022.79
2	3.84	7.70	1019.75	1021.82
3	4.41	8.63	1014.52	1016.55
4	4.03	7.39	1012.82	1014.61
5	5.09	9.93	1014.60	1017.12
6	7.30	12.85	1016.13	1019.75
7	2.59	7.23	1015.47	1017.67
8	3.29	6.21	1013.40	1014.93
9	3.04	6.84	1014.17	1015.70
10	4.67	8.01	1017.44	1019.33
11	5.23	9.18	1015.79	1018.03
12	5.99	10.14	1009.73	1012.43
13	4.05	8.53	1007.69	1009.73
14	4.47	8.48	1007.81	1009.95
15	6.40	11.93	1015.01	1019.47
16	3.24	8.39	1020.98	1024.07
17	5.56	8.91	1016.54	1018.59
18	6.17	9.43	1012.70	1014.47
19	5.33	9.47	1010.27	1012.54
20	4.47	8.12	1010.40	1012.20
21	6.35	10.05	1011.99	1013.46
22	5.77	9.50	1011.35	1013.30
23	5.75	10.44	1018.35	1022.83
24	3.51	6.93	1020.65	1023.10
25	7.17	10.61	1010.46	1013.59
26	3.48	8.03	1009.99	1011.46
27	4.34	8.51	1012.49	1014.31
28	7.70	10.18	1009.80	1011.27
29	5.17	11.76	1013.46	1017.24
30	2.48	8.73	1018.19	1021.02

Simulation Results

For water levels both observed and simulated time series were demeaned. For salinity and temperature no demeaning was performed. As a result, error measures are expressed in terms of standard deviation (SD) for water levels and in terms of root mean square error (RMSE) for salinity and temperature. Note on all water surface elevation plots RMS ERROR corresponds to SD. The Willmott et al. (1985) dimensionless (0-1) average relative error (ARE) is also used to express the agreement in shape. For no error, this relative error is zero. Simulated hydrodynamics are discussed in terms of water surface elevation, current, salinity, and temperature responses in turn below

Water Surface Elevation

First consider the water level response throughout the month. After the one-day spin-up period, simulated water levels were demeaned and compared with demeaned observations in terms of standard deviation (SD) and the Willmott et al. (1985) dimensionless average relative error (ARE) as given in Table 5.2. The observed water level means are with respect to mean tide level adjusted to a tidal epoch based on only a single year's worth of data at the majority of stations with an associated error of 1.5 cm after Marmer (1951). Only the two Galveston stations have a full 19 year data record to determine a true epoch mean tide level. The simulated means are with respect to model datum, which represents a surface through the mean tide level; e.g., all model depths are adjusted to mean tide level. Since river flows are minor, they have insignificant effect on the monthly mean simulated water levels. Water level offsets were again added to the reconstructed tidal signals consistent with a northerly directed coastal current.

If one again assumes that the model datum approximates a true equipotential surface over Galveston Bay, we note that the mean water level rises by 7 cm from Galveston Pleasure Pier to Morgans Point. Observed means at Umbrella Point, Lynchburg Landing, and Manchester Dock 2 appear to be out of line with values at other stations. At these stations the tidal epoch MTL datum is based on only one month's data resulting in an error of order 3 cm according to Marmer (1951). Buffalo Bayou

Table 5.2. Galveston Bay Model April 1996 Hindcast Water Surface Elevation Comparisons. Note both series are demeaned and the standard deviation (SD) is computed and compared with the mean diurnal range (MDR).

Station Name	Observed Mean (cm)	Simulated Mean (cm)	SD, MDR (cm, cm)	ARE (-)
Galveston Pleasure Pier	12	21	9.5, 67	0.06
Galveston Pier 21	8	24	7.2, 43	0.06
Port Bolivar	11	23	7.3, 43	0.06
Eagle Point	10	26	4.8, 30	0.02
Clear Lake	9	28	6.9, 28	0.04
Morgans Point	12	28	5.4, 30	0.02
Umbrella Point	1	27	5.5, 30	0.02
Lynchburg Landing	1	29	6.1, 43	0.02
Manchester Dock 2	1	30	6.9, 43	0.02

and San Jacinto River influences appear to have further complicated the datum computation at these stations. With this in mind, we note that the observed means indicate no rise over the Bay occurring through the Entrance. Thus if epoch mean tide levels are assumed to constitute an equipotential surface, then this surface differs by order 7 cm from the model datum surface. Note the level of agreement in terms of SD is order 10 cm or better at all stations. Agreement in shape expressed in terms of ARE is order 0.05.

The demeaned simulated water level response at Galveston Pleasure Pier is compared with demeaned observations at six-minute intervals in Figure 5.14. One notes high frequency oscillations (noise) in the simulated water level on JD 97 and 120. Time series of demeaned simulated and observed water levels at Galveston Pier 21 are shown in Figure 5.15. Noise in the simulated water level response is present at Galveston Pier 21 at the times exhibited offshore. The observed reduction in tidal amplitude through the Galveston Bay Entrance again seems to be well replicated in the model. In Figure 5.16, the water level response at Port Bolivar is examined. Noise in simulated water levels is present at the same times as at Galveston Pier 21.

In Figure 5.17 the demeaned simulated water levels are compared with demeaned observations at Eagle Point. No noise is present in the simulated water level response. At Clear Lake shown in Figure 5.18, the agreement is 7 cm in SD with no cell width reduction factor applied in the grid cell at the entrance to Clear Lake. At Morgans Point the simulated water level response in Figure 5.19 is similar to that at Clear Lake but improves to a 5 cm in SD.

Simulated water level responses at Umbrella Point are compared with observations in Figure 5.20 and are very similar to those at Morgans Point. At Lynchburg Landing in Figure 5.21 and Manchester (Houston) Dock 2 in Figure 5.22, water level responses are in excellent agreement with observations (order 5 cm in SD and 0.02 in ARE) despite the coarseness of the grid.

Oscillations in simulated Galveston Bay water level response are not present at stations above Eagle Point. Noise in coastal water level response may be induced from the clamped water surface elevation offshore boundary condition or the subtidal water level boundary signal. The noise propagates through the Galveston Bay entrance channel and is damped out in lower to middle Galveston Bay.

Principal Component Direction Currents

Simulated principal component direction currents at NOS 4.6m prediction depth are assessed in terms of level of agreement in direction and root mean square error (RMSE). Model and observed principal component directions are compared in Table 5.3 at the three PORTS stations. Agreement in direction ranges from 14 degrees at Redfish Bar to 28 degrees at Morgans Point. Comparisons between observed and simulated principal component direction current (PCDC) means as well as RMSE and ARE are given in Table 5.4 over ten day intervals.

Table 5.3. Galveston Bay Model April 1996 Principal Flood Direction Comparison

PORTS Station	Observed Principal Flood Direction (deg T)	Model Principal Flood Direction (deg T)
Bolivar Roads	322	342
Redfish Bar	322	336
Morgans Point	341	313

Table 5.4. Galveston Bay Model April 1996 Principal Component Direction Current Comparisons. Note the flood direction is positive. Mean PCDC diurnal range (MDR) is also given for reference.

PORTS Station	Observed Mean (cm/s)	Simulated Mean (cm/s)	RMSE (cm/s)	MDR (cm/s)	ARE (-)
Bolivar Roads					
1-10	8.1	-0.1	21.3		0.04
11-20	0.7	-5.8	21.1		0.04
21-30	3.8	-4.8	25.7	195	0.07
Redfish Bar					
1-10	5.7	4.1	13.3		0.04
11-20	-3.1	-10.5	13.8		0.05
21-28	-5.7	-9.5	11.7	130	0.04
Morgans Point					
1-10	-0.2	-5.2	17.9		0.39
11-20	-5.9	-10.9	15.9		0.27
21-30	-5.0	-10.0	16.4	65	0.33

Simulated means at Redfish Bar and Morgans Point are in the same direction as observations. Such is not the case at Bolivar Roads. Differences in means are order 5 cm/s. AREs are order 0.04 for all three day intervals at Bolivar Roads with RMSE order 20 cm/s, which represents 10 percent of the principal component direction amplitude. At Redfish Bar, the shape agreement in terms of relative error is excellent at 0.05 and the RMSE is 13 cm/s, which represents 10 percent of the principal component direction amplitude. At Morgans Point, the shape agreement deteriorates to 0.30 with an RMSE of 16 cm/s, which represents 30 percent of the principal component direction amplitude.

The PCDC time series during the second ten day period are shown in Figure 5.23 at Bolivar Roads, in Figure 5.24 at Redfish Bar, and in Figure 5.25 at Morgans Point. It should be noted that observed and simulated currents have not been demeaned. At Bolivar Roads (Figure 5.23), we note the increased ebb current strength at JD 106 hour 9 due to the large negative (-0.5m) water level residual signal on the model open boundary. In general, the simulated ebb currents are in excellent agreement with observations. Simulated flood current strengths are underestimated by order 30 cm/s. At Redfish Bar (Figure 5.24), both simulated flood and ebb current strengths agree with observations except for the ebbs near JD 107 and JD 110 and for the flood on JD 110. At Morgans Point (Figure 5.25), simulated current strengths are under predicted, with good agreement on ebb but under estimation on flood of order 30 cm/s.

Salinity

Simulated mid-depth (level 3) salinity time series are compared with TWDB datasonde observed salinities in Table 5.5 in terms of RMSE and ARE. Observed means differ from simulated means by as little as 0.9 PSU at Dollar Point to over 6.0 PSU at Trinity Bay-DBC. The difference in means

contributes substantially to the RMS errors, which can be only reliably assessed at Hannah Reef and Red Bluff as discussed below. Relative errors are above 0.50 indicating substantial disagreement in shape.

Table 5.5. Galveston Bay Model April 1996 Mid-depth Salinity Comparisons

TWDB Station	Observed Mean (PSU)	Simulated Mean (PSU)	RMSE (PSU)	ARE (-)
Dollar Point	26.9	27.8	0.8	0.54
Trinity Bay-DBC	29.5	23.1	6.5	0.62
Hannah Reef	24.2	26.7	2.8	0.54
Red Bluff	23.5	26.5	3.2	0.62
Port Bolivar	28.5	30.6	4.3	0.62

If one considers the first portion of the time series at Trinity Bay-DBC in Figure 5.26, at Hannah Reef in Figure 5.27, at Red Bluff in Figure 5.28, and at Port Bolivar in Figure 5.29, one notes a problem with the initial condition determination only at Red Bluff. The simulated salinity response at Dollar Point appears to be reasonable and in agreement with observations, which are only available over the last four days. The observed salinity response at Trinity Bay-DBC (Figure 5.26) appears to be in error, since salinities of over 32 PSU are not physically realizable at this location. At Hannah Reef (Figure 5.27) the observed sinusoidal response at tidal period, indicative of the advection of a large horizontal salinity gradient, is not captured in the simulation. At Red Bluff (Figure 5.28) the model response tracks the observations with an offset of 3 PSU, which persists from initialization. At Port Bolivar (Figure 5.29) simulated salinities are in close agreement with observations over the first nine days and then diverge. The rapid decrease in the observed salinities indicates a possible biological fouling problem.

Temperature

Simulated mid-depth (level 3) temperature time series are compared with TWDB datasonde observations in Table 5.6 in terms of RMSE and ARE. Refer to Figure 3.1 for station locations. Simulated means differ from observed means by order 1 °C. RMSEs are order 1.5 °C and AREs are order 0.25 except for the short observation record at Dollar Point.

Table 5.6. Galveston Bay Model April 1996 Mid-depth Temperature Comparisons

TWDB Station	Observed Mean (deg C)	Simulated Mean (deg C)	RMSE (deg C)	ARE (-)
Dollar Point	23.2	20.3	1.4	0.71
Trinity Bay-DBC	19.9	19.3	1.8	0.29
Hannah Reef	20.3	20.1	1.7	0.26
Red Bluff	20.1	19.9	1.3	0.14
Port Bolivar	19.9	20.4	1.2	0.11

Simulated temperature responses are compared with observations at Trinity Bay-DBC in Figure 5.30, at Hannah Reef in Figure 5.31, at Red Bluff in Figure 5.32, and at Port Bolivar in Figure 5.33.

Note the daily atmospheric warming and cooling, which may exhibit changes in SST of order 1 to 2 °C, is the principal cause of sinusoidal behavior in observed temperatures rather than the advection of horizontal water temperature gradients at tidal period.

5.2. Houston Ship Channel Model

The GBM was used to provide boundary conditions to drive the HSCM via the one-way coupling scheme discussed in Chapter 2 during the April 1996 period. Bottom roughness, z_0 , was set equal to the GBM value of 2mm. No attempt was made to further reduce the Smagorinsky horizontal eddy viscosity coefficient, C_H , below 0.005 despite the order two increase in horizontal resolution in the HSCM. To place the simulation results in context, initial and boundary condition development are first discussed.

Initial Conditions

Velocities and water surface elevations were set to zero. A nearest neighbor horizontal interpolation and sigma coordinate to depth to sigma coordinate vertical interpolation were used to place the initial GBM salinity and temperature fields on the finer resolution HSCM grid.

Boundary Conditions

River inflows, wind and atmospheric pressure fields, and water level residual forcings were all included. The same inflows used in the GBM for the Buffalo Bayou and San Jacinto inflows were input. The Trinity River flow was not considered, since its inflow location was outside the HSCM.

NDBC buoy 42020 (3m Discus) and 42035 (3m Discus) and C-MAN station S-2 Sabine and S-4 Port Aransas, TX observations were obtained along with NWS surface weather observations at Houston IAH, Port Arthur, and WSO Galveston, TX. Wind and sea-level atmospheric pressure fields were developed at 3 hour intervals over the Channel model domain via the two-step Barnes (1973) interpolation procedure discussed in Chapter 2. Daily average (8 fields per day) Bay model grid cell minimum and maximum windspeed and atmospheric pressure are given in Table 5.7 for the resulting interpolations. Windfields at JD 101, 111, and 121 are shown in Figures 5.34, 5.36, and 5.38, respectively, with corresponding windspeed contours shown in Figures 5.35, 5.37, and 5.39, respectively. Note that the windfields developed over the HSCM are consistent with those previously developed over the GBM. Total water levels developed within the GBM were specified along the HSCM open boundaries. Note that at the entrance jetties a solid wall boundary was used; e.g., in Figure 2.8 only water surface elevations along the southwest to northeast offshore boundary are specified. A nearest neighbor horizontal interpolation was used to place GBM SST fields on the HSCM grid.

Table 5.7. April 1996 Houston Ship Channel Model Barnes Interpolation Summary

Day	Wind Speed Minimum (m/s)	Wind Speed Maximum (m/s)	Air Pressure Minimum (mb)	Air Pressure Maximum (mb)
1	5.39	8.04	1020.13	1022.28
2	4.53	6.20	1020.42	1021.43
3	5.10	7.46	1015.07	1016.00
4	4.70	6.00	1013.36	1014.33
5	5.40	8.35	1015.21	1017.13
6	6.54	11.10	1016.93	1019.53
7	3.03	5.90	1016.00	1017.32
8	3.62	5.47	1013.79	1014.71
9	3.78	5.91	1014.56	1015.53
10	5.44	7.15	1017.94	1019.11
11	5.92	8.30	1016.48	1017.43
12	7.04	9.12	1010.66	1011.60
13	4.79	6.93	1008.22	1009.35
14	4.93	7.73	1008.44	1009.57
15	7.18	10.15	1015.94	1019.10
16	3.59	6.80	1021.81	1023.53
17	5.92	7.77	1017.19	1018.03
18	6.86	8.18	1013.11	1014.02
19	6.31	8.52	1010.82	1012.01
20	5.44	7.25	1010.94	1011.96
21	7.32	8.86	1012.53	1013.08
22	6.04	8.15	1011.88	1013.18
23	5.73	8.73	1019.40	1022.37
24	4.03	5.91	1021.21	1022.63
25	7.70	9.40	1011.18	1012.78
26	3.93	6.35	1010.44	1011.28
27	5.32	7.10	1013.01	1014.01
28	8.14	9.48	1010.21	1010.87
29	5.53	9.72	1014.27	1016.94
30	2.82	6.62	1018.82	1020.62

Simulation Results

Water Surface Elevation

For water levels both observed and simulated time series were demeaned. For salinity and temperature no demeaning was performed. As a result, error measures are expressed in terms of standard deviation (SD) for water levels and in terms of root mean square error (RMSE) for salinity and temperature. Note on all water surface elevation plots RMS ERROR corresponds to SD. Simulated hydrodynamics are discussed in terms of water surface elevation, salinity, and temperature responses in turn below.

Water Surface Elevation

First consider the water level response throughout the month. After a one-day spin-up period, simulated water level were demeaned and compared with demeaned observations in terms of RMSE and ARE as given in Table 5.8. Note that the observed water level means are with respect to mean tide level adjusted to a tidal epoch based on only a single year's worth of data with an associated error of 1.5 cm after Marmer (1951) at all stations except at Galveston Pier 21, which has a full 19 year data record. The simulated means are with respect to model datum, which represents a surface through the mean tide level; e.g., all model depths are adjusted to mean tide level. Since river flows are included, one would expect that the mean simulated water levels would be above mean tide level. If one again assumes that the model datum approximates a true equipotential surface over Galveston Bay, we note that the mean water level rises by 4 cm from Galveston Pleasure Pier to Morgans Point.

Note that the observed means also indicate only a 4 cm rise over the Bay from Galveston Pier 21 to Morgans Point, but are order 16 cm less than the simulated means. Observed means at Lynchburg Landing and Manchester Dock as previously noted appear to be in error. The level of agreement in terms of RMSE is order 8 cm or better. Agreement in shape expressed in terms of ARE is order 0.05. Note the Houston Ship Channel Model water level results obtained are nearly identical in mean, RMSE, and ARE to those obtained in the Galveston Bay Model.

Table 5.8. Houston Ship Channel Model April 1996 Hindcast Water Surface Elevation Comparisons. Both time series are demeaned and the standard deviation (SD) is computed and compared with the mean diurnal range (MDR).

Station Name	Observed Mean (cm)	Simulated Mean (cm)	SD, MDR (cm, cm)	ARE (-)
Galveston Pier 21	8	24	7.6, 43	0.06
Port Bolivar	11	22	7.5, 43	0.06
Eagle Point	10	26	4.7, 30	0.02
Morgans Point	12	28	5.4, 30	0.02
Lynchburg Landing	1	29	6.5, 43	0.02
Manchester Dock 2	1	29	7.9, 43	0.03

Time series of demeaned simulated and observed water levels at Galveston Pier 21 and Port Bolivar are shown in Figure 5.40 and Figure 5.41, respectively. Oscillations in the simulated water level responses at both locations are present at the times exhibited offshore at Galveston Pleasure Pier and

are greater than those found in the Galveston Bay Model (see Figures 5.15 and 5.16) at the same locations. As in the Galveston Bay Model, as one proceeds up Galveston Bay, the water level oscillations are damped as indicated at Eagle Point (Figure 5.42) and Morgans Point (Figure 5.43). Despite the finer resolution, the water level responses at Lynchburg Landing (Figure 5.44) and at Manchester Dock 2 (Figure 5.45) are nearly identical to the corresponding responses in the Galveston Bay Model.

Principal Component Direction Currents

Principal component direction currents at NOS 4.6m prediction depth are assessed. Model and observed principal component direction currents are given in Table 5.9. Agreement in direction ranges from 1 degree at Bolivar Roads to 23 degrees at Morgans Point. Comparisons between observed and simulated principal component direction current (PCDC) means as well as RMSEs and AREs are given in Table 5.10 over ten day intervals to assess the variability of the mean currents over weather system influenced time scales. Simulated means at Redfish Bar and Morgans Point are mostly in the same direction as observations. Such is not the case at Bolivar Roads. Differences in means are order 5 cm/s. AREs are order 0.10 for all three day intervals at Bolivar Roads with RMSEs order 30 cm/s, which represents a 10 cm/s degradation from GBM results. At Redfish Bar, the shape agreement in terms of ARE is 0.07 and the RMSE is 15 cm/s, which represent a 0.02 and 2 cm/s degradation from GBM results. At Morgans Point, the shape agreement is order 0.10 ARE with an RMSE of 13 cm/s, which represent a 0.20 and 3 cm/s improvement over results obtained in the GBM.

Table 5.9. Houston Ship Channel Model April 1996 Principal Flood Direction Comparison

PORTS Station	Observed Principal Flood Direction (deg T)	Model Principal Flood Direction (deg T)
Bolivar Roads	322	321
Redfish Bar	322	331
Morgans Point	341	318

PCDC time series during the second ten day period are shown in Figure 5.46 at Bolivar Roads, in Figure 5.47 at Redfish Bar, and in Figure 5.48 at Morgans Point. It should be noted that observed and simulated currents have not been demeaned. At Bolivar Roads (Figure 5.46), we note the increased ebb current strength at JD 106 hour 9 due to the large negative (-0.5m) water level residual signal offshore. In general, the simulated ebb currents are in excellent agreement with observations but exhibit larger oscillations than the ebb currents generated in the GBM. Simulated flood current strengths are underestimated as in the GBM by order 30 cm/s and exhibit more oscillation. At Redfish Bar (Figure 5.47), both simulated flood and ebb current strengths agree closely with GBM results but again exhibit larger oscillations. At Morgans Point (Figure 5.48), simulated current strengths are much improved and are in good agreement on ebb and flood within order 10 cm/s.

Table 5.10. Houston Ship Channel Model April 1996 Principal Component Direction Current Comparisons. Note the flood direction is positive. Mean diurnal range (MDR) is also given for comparison.

PORTS Station	Observed Mean (cm/s)	Simulated Mean (cm/s)	RMSE (cm/s)	MDR (cm/s)	ARE (-)
Bolivar Roads					
1-10	8.1	0.3	27.4		0.08
11-20	0.7	-3.5	26.1		0.07
21-30	3.8	-5.2	30.2	195	0.10
Redfish Bar					
1-10	5.7	-0.3	17.0		0.07
11-20	-3.1	-10.1	15.5		0.07
21-28	-5.7	-6.3	13.5	130	0.06
Morgans Point					
1-10	-0.2	0.1	12.7		0.10
11-20	-5.9	-10.1	13.2		0.11
21-30	-5.0	-7.2	14.4	65	0.15

Salinity

Simulated mid-depth (level 3) salinity time series are compared with TWDB datasonde observed salinities in Table 5.11 in terms of RMSE and ARE. Observed means differ from simulated means by as little as 0.6 PSU at Dollar Point to over 2.5 PSU at Red Bluff. The difference in means contributes substantially to the RMSE. AREs are above 0.50 indicating substantial disagreement in shape.

If one considers the time series at Port Bolivar in Figure 5.49 and at Red Bluff in Figure 5.50, one notes a problem with the initial condition determination only at Red Bluff of order 2.5 PSU. At Port Bolivar in Figure 5.49, the simulated response is nearly equal to the Galveston Bay Model response and thus in agreement with observations over the first nine days, after which the observations seem to indicate a potential biological fouling problem.

The simulated salinity response at Dollar Point is nearly identical to the response of the Galveston Bay Model and appears to be in reasonable agreement with observations, which are only available over the last four days. At Red Bluff (Figure 5.50) the model response is close to that of the Galveston Bay Model tracking the observations, with an offset of approximately 3 PSU, which persists from initialization.

Table 5.11. Houston Ship Channel Model April 1996 Mid-depth Salinity Comparisons

TWDB Station	Observed Mean (PSU)	Simulated Mean (PSU)	RMSE (PSU)	ARE (-)
Port Bolivar	28.5	30.9	4.4	0.58
Dollar Point	26.9	27.5	1.4	0.66
Red Bluff	23.5	26.3	3.0	0.65

Temperature

Simulated mid-depth (level 3) temperature time series are compared with TWDB datasonde observed temperatures in Table 5.12 in terms of RMSE and ARE. Simulated means differ from observed means by order 1 °C. RMSEs are order 1.5 °C and AREs are order 0.25 except for the short observation record at Dollar Point. Simulated temperature responses are compared with observations at Port Bolivar in Figure 5.51 and at Red Bluff in Figure 5.52. Note the daily atmospheric warming and cooling, which may exhibit changes in SST of order 1 to 2 °C, is the principal cause of sinusoidal behavior in observed temperatures rather than the advection of large horizontal gradients at tidal period. Houston Ship Channel Model temperature responses are nearly identical to those of the Galveston Bay Model.

Table 5.12. Houston Ship Channel Model April 1996 Mid-depth Temperature Comparisons

TWDB Station	Observed Mean (deg C)	Simulated Mean (deg C)	RMSE (deg C)	ARE (-)
Port Bolivar	19.9	20.3	1.2	0.11
Dollar Point	23.2	20.3	1.2	0.62
Red Bluff	20.1	19.8	1.4	0.15

5.3. Coupling Mechanism Assessment

To assess the coupling mechanism, demeaned water level SDs for both models are compared in Table 5.13. SDs are nearly identical at common stations in the two models. As previously noted, salinity and temperature responses are also similar, tending to further confirm the coupling mechanics. With respect to currents, it was hoped that the current response would be improved within the Houston Ship Channel by employing the finer resolution HSCM.

With respect to the principal flood directions shown in Table 5.14, this appears to be the case. Near the entrance an improvement of order 10 to 20 degrees is obtained. At Redfish Bar and Morgans Point the improvements are order 5 degrees. Note from Table 5.14, the inclusion of meteorological effects does not significantly alter the principal flood directions in the GBM; e.g., compare line 2 to line 1.

Principal direction currents at prediction depth RMSEs for the two models are compared in Table 5.15. Below Redfish Bar, the agreement in currents is closer in the GBM, while at Morgans Point, the Houston Ship Channel model is in closer agreement to observations

To investigate the source of the discrepancy in the lower Bay, the bathymetry was reviewed in each model. In Table 5.16, grid cell depths with respect to MLLW are given at several grid cell locations corresponding to different deployment locations for the PORTS current meters. During April 1996 all locations were located at deployment 1. At Bolivar Roads, one notes that there is considerable difference in depths at corresponding model grid cells. The Houston Ship Channel Model depths appear to be considerably smaller than those found in the Galveston Bay Model except during the

Table 5.13. Demeaned Water Level GBM and HSCM Model vs April 1996 Intercomparisons

Station	Galveston Bay Model SD (cm)	Houston Ship Channel Model SD (cm)	Galveston Bay Model ARE (-)	Houston Ship Channel Model ARE (-)
Galveston Pleasure Pier: 677-1510	9.5	-	0.06	-
Galveston Pier 21: 677-1450	7.2	7.6	0.06	0.06
Port Bolivar: 677-1328	7.3	7.5	0.06	0.06
Eagle Point: 677-1013	4.8	4.7	0.02	0.02
Clear Lake: 677-0933	6.9	-	0.04	-
Morgans Point: 677-0613	5.4	5.4	0.02	0.02
Lynchburg Landing: 877-0733	6.1	6.5	0.02	0.02
Manchester Dock 2: 877-0777	6.9	7.9	0.02	0.03

Table 5.14. Galveston Bay Model vs Houston Ship Channel Model April 1996 Principal Component Direction Comparison. Note line 1 corresponds to Galveston Bay Model May 1995 calibration results.

Station	Houston Ship Channel Model PCD (deg T)	Galveston Bay Model PCD (deg T)	Observation (deg T) / Date
Galveston Reference	- 282	282 290	- 273 / August 1988
HSC Secondary	- 332	340 343	- 313 / October 1988
Bolivar Roads PORTS	- 321	350 342	- 322/ April 1996
Redfish Bar PORTS	- 331	336 336	- 322/ April 1996
Morgans Point PORTS	- 318	317 313	- 341/ April 1996

Table 5.15. Principal Direction Current at Prediction Depth GBM and HSCM Model vs April 1996 Intercomparisons

PORTS Station	Galveston Bay Model RMSE (cm/s)	Houston Ship Channel Model RMSE (cm/s)	Galveston Bay Model ARE (-)	Houston Ship Channel Model ARE (-)
Bolivar Roads	21	26	0.04	0.07
Redfish Bar	14	16	0.05	0.07
Morgans Point	16	13	0.27	0.11

Table 5.16. Galveston Bay Model and Houston Ship Channel Model Bathymetry Comparison

PORTS Station/ Dplmt No	Latitude (deg N)	Longitude (deg W)	Bay Model Grid Cell	Bay Model Depth (m)	Channel Model Grid Cell	Channel Model Depth (m)
Bolivar Roads /1	29.362	94.792	(87,36)	4.5	(44,40)	6.6
Bolivar Roads /2	29.359	94.792	(86,35)	12.3	(43,39)	6.6
Bolivar Roads /3	29.345	94.782	(86,34)	12.3	(40,34)	8.2
Bolivar Roads /4	29.343	94.781	(86,34)	12.3	(39,33)	5.7
Redfish Bar /1	29.506	94.874	(94,50)	12.2	(44,99)	12.2
Redfish Bar/2	29.506	94.872	(95,50)	3.2	(44,99)	12.2
Redfish Bar /3	29.507	94.872	(95,50)	3.2	(44,99)	12.2
Redfish Bar/4	29.507	94.875	(94,51)	12.2	(44,100)	12.2
Morgans Point /1	29.679	94.981	(80,76)	12.2	(33,150)	12.2
Morgans Point /2	29.679	94.981	(80,76)	12.2	(33,150)	12.2
Morgans Point/3	29.679	94.981	(80,76)	12.2	(33,150)	12.2

first deployment.

It appears that a review of the bathymetry in the lower Bay on the HSCM grid is warranted. The present approach is heuristic and attempts to assign the nearest 15 sec grid cell average depth to the given model grid cell. The approach does not compute (assign) the true nearest 15 sec grid cell average to every model grid cell in order to reduce computer time. Once a 15 sec grid cell has been assigned, it cannot be assigned to any other grid cell. This approach assumes that the spacings of model grid cells are order the 15 sec spacings of approximately 500m. This assumption holds for the GBM grid but is violated over some portions of the finer resolution HSCM grid.

In addition, a 15 sec grid cell average may be assigned to a model grid cell, if it is within a critical distance set to 2 km. This distance is order the grid spacing for the GBM grid but is larger than the majority of spacings on the HSCM grid. For the HSCM grid, the critical distance should be reduced to order 500m. In the heuristic, one runs the risk that if the critical distance is reduced sufficiently small very few model grid cells will be assigned a 15 sec grid cell average depth.

In principle, one would like to have the spacing of the bathymetric gridded data on the same order as the spacings of the hydrodynamic grid. Such is the case for the GBM. For the HSCM, a finer resolution bathymetric dataset would appear to be required. However, if one uses two different resolution gridded bathymetric datasets, they should be consistent; e.g., the grid cell averages of the finer resolution dataset with respect to the coarser grid should be equal to the coarse grid cell values.

5.4. Error Budget

Harmonic analyses (Schureman, 1958) of both water surface elevations and principal direction component series were performed to partition the error into astronomical and nontidal components. We consider each in turn in summary form below with the reader referred to Hess et al. (1999) Appendix C for individual constituent comparisons.

Water Levels

The results of NOS standard 29-day harmonic analysis (Shureman, 1958) of water level for the May 1995 and April 1996 Galveston Bay Model simulations are given in Table 5.17 for offshore, West, and East Bay stations and in Table 5.18 at Galveston Bay stations. The weighted gain corresponds to the ratio of model to observation harmonic constituent weighted by the observation constituent amplitude averaged over each of the standard 24 constituents. The weighted phase corresponds to the difference in model phase minus observation phase weighted by observation constituent amplitude averaged over each of the standard 24 constituents. Thus for negative phase values, the model lags the observation. Based upon the difference of the constituent amplitudes and phases, an RMSE may be estimated (Hess, 1994).

If we consider the results shown in Table 5.17, we note that offshore the tidal amplitudes appear to be damped immediately off Galveston by 10 percent and by 20 percent at Rollover Pass further to the north. The results at High Island near Rollover Pass near the northern grid boundary are excellent. Further to the south inside West Bay at Alligator Point and Christmas Bay, the tidal amplitudes are over excited by 10 percent.

Table 5.17. Galveston Bay Model Offshore, West Bay, and East Bay 29-day Harmonic Analysis Results. Line 1 corresponds to April 1996 and line 2 to May 1995 calibration results. Mean Diurnal Range (MDR) is also given for reference.

Station	Weighted Gain (-)	Weighted Phase (hr)	RMSE (cm)	MDR (cm)
Galveston Pleasure Pier: 877-1510	0.87	0.05	4	67
	0.85	-0.10	4	
Galveston Pleasure Pier: 677-1510	0.96	-0.10	3	67
	0.91	-0.25	3	
Galveston, GPS Buoy: 877-1624	0.87	0.04	4	67
	0.86	-0.11	4	
Rollover Pass: 877-0971	0.83	-2.03	8	41
	0.81	-1.98	7	
High Island: 877-0923	0.98	0.31	3	67
	0.96	0.09	2	
Christmas Bay: 677-2132	1.07	1.27	4	28
	1.07	1.63	5	
Alligator Point: 877-1801	1.10	-0.02	2	28
	1.08	0.14	2	

Considering the results given in Table 5.18, we observed that the gain is reduced by an additional 5 percent as one proceeds through the Bay entrance. This 15 percent damping is maintained up the Bay to Morgans Point.

GBM water level harmonic analysis results for April 1996 are compared with the corresponding HSCM results over April 1996 in Table 5.19. Results are nearly identical in both models and indicate a water level damping of 10 to 20 percent. Above Lynchburg Landing, the HSCM water level response is less damped. Phase lags are generally less than 0.5 hour at most stations in both models.

Based upon the results of Table 5.19 and those previously presented in Tables 5.2 and 5.8, the meteorological RMSE, $rmse_m$, is reported in Table 5.20. It is derived from the total RMSE, $rmse_t$, and the astronomical tide RMSE, $rmse_a$, using the relation, $(rmse_t)^2 = (rmse_m)^2 + (rmse_a)^2$. The estimated meteorological error are nearly identical in both models and are order of the astronomical tide error component at all stations. It appears that by improving the astronomical tide response in the Galveston Bay Model, a corresponding level of improvement would be achieved via the one-way coupling mechanism with the Houston Ship Channel Model.

Table 5.18. Galveston Bay Model Galveston Bay 29-day Harmonic Analysis Results. Line 1 corresponds to April 1996 and line 2 to May 1995 calibration results. Mean Diurnal Range (MDR) is also given for reference.

Station	Weighted Gain (-)	Weighted Phase (hr)	RMSE (cm)	MDR (cm)
Galveston Pier 21: 877-1450	0.79	0.25	4	43
	0.82	0.08	3	
Galveston Pier 21: 677-1450	0.85	0.13	3	43
	0.87	-0.04	3	
Port Bolivar: 677-1328	0.86	-0.43	3	43
	0.86	-0.72	3	
Smith Point: 877-0931	0.83	1.01	4	30
	0.89	0.31	2	
Eagle Point: 677-1013	0.91	0.98	4	30
	0.97	0.32	3	
Trinity River Channel Platform: 877-1021	0.87	0.72	3	30
	0.92	0.16	2	
Clear Lake: 677-0933	0.96	-1.25	4	28
	1.00	-1.89	5	
Morgans Point: 677-0613	0.87	0.01	3	30
	0.89	-0.68	3	
Round Point: 877-0559	0.81	0.64	4	30
	0.90	-0.32	3	

Table 5.19. Galveston Bay Model vs Houston Ship Channel Model April 1996 Galveston Bay 29-day Harmonic Analysis Results. Line 1 corresponds to Galveston Bay Model and line 2 to Houston Ship Channel simulation results. Mean Diurnal Range (MDR) is also given for reference.

Station	Weighted Gain (-)	Weighted Phase (hr)	RMSE (cm)	MDR (cm)
Galveston Pier 21: 877-1450	0.79	0.25	4	43
	0.81	0.26	3	
Galveston Pier 21: 677-1450	0.85	0.13	3	43
	0.88	0.04	3	
Port Bolivar: 677-1328	0.86	-0.43	3	43
	0.90	-0.66	3	
Eagle Point: 677-1013	0.91	0.98	4	30
	0.90	0.79	4	
Morgans Point : 677-0613	0.87	0.01	3	30
	0.87	0.08	3	
Lynchburg Landing: 877-0733	0.95	-0.02	2	43
	0.82	-0.27	4	
Manchester Dock 2: 877-0777	0.66	-0.69	7	43
	0.83	-0.22	4	

Table 5.20. April 1996 Water Surface Elevation RMSE Budget. Line 1 corresponds to Galveston Bay Model and line 2 to Houston Ship Channel simulation results.

Station	Astronomical Tide RMSE (cm)	Meteorological RMSE (cm)	Total RMSE (cm)
Galveston Pl. Pier: 877-1510	4 -	8 -	9 -
Galveston Pier 21: 677-1450	4 3	6 7	7 8
Port Bolivar: 677-1328	3 3	6 6	7 7
Eagle Point: 677-1013	4 4	3 3	5 5
Morgans Point : 677-0613	3 3	4 4	5 5
Lynchburg Landing: 877-0733	2 4	5 4	6 6
Manchester Dock 2: 877-0777	7 4	0 7	7 8

Currents

Principal component direction currents (level 3) harmonic analysis results are given in Table 5.21 in terms of weighted gain and phase as defined previously. To determine current components along the principal direction, the simulated principal component directions were used. In Table 5.21 results are presented for the May 1995 astronomical tide calibration of the GBM (line 1) as well as for the April 1996 completely meteorologically forced GBM and HSC (lines 2 and 3). Similar results are obtained for the two different periods for the GBM. In the entrance and lower Bay, GBM principal current component strengths are damped by 10 percent. As one proceeds further up the Bay, strengths are further reduced by an additional 20 percent. At the head of Galveston Bay at Morgans Point, the response is damped by 70 percent. In the HSCM, the current strengths appear to be more uniformly damped throughout at order 30 percent. Phase lags are order 0.5 to 1.0 hour in both models.

Based upon the results of Table 5.21 and those previously presented in Tables 5.4 and 5.10, the meteorological error is estimated as previously and is reported in Table 5.22. This error is very small relative to the astronomical tide error in the lower Bay. However, at Morgans Point in the upper Bay, the meteorological error is nearly equal to the astronomical tide error component.

Table 5.21. Galveston Bay Current Station 29-day Harmonic Analysis Principal Component Direction at Prediction Depth. Note line 1 corresponds to the May 1995 Galveston Bay Model calibration, line 2 corresponds to April 1996 Galveston Bay Model, and line 3 corresponds to the April 1996 Houston Ship Channel Model results. Mean Diurnal Range (MDR) is also given.

Station	Weighted Gain (-)	Weighted Phase (hr)	RMSE (cm/s)	MDR (cm/s)
Galveston Reference	0.84	-1.02	19.8	200
	0.78	-0.33	19.4	
	0.49	-0.44	31.3	
HSC Secondary	0.99	0.41	12.0	200
	0.91	0.75	14.2	
	0.75	0.08	15.9	
Bolivar Roads PORTS	0.86	-0.50	17.8	195
	0.78	0.36	17.0	
	0.63	-0.27	26.8	
Redfish Bar PORTS	0.72	0.06	19.7	130
	0.70	-0.17	14.4	
	0.70	-0.66	16.6	
Morgans Point PORTS	0.32	-1.45	16.0	65
	0.42	-0.77	13.1	
	0.68	-0.49	8.6	

Table 5.22. April 1996 Principal Component Direction Current at Prediction Depth RMSE Budget. Line 1 corresponds to Galveston Bay Model and line 2 to Houston Ship Channel simulation results.

PORTS Station	Astronomical Tide RMSE (cm/s)	Meteorological RMSE (cm/s)	Total RMSE (cm/s)
Bolivar Roads	17	12	21
	27	0	27
Redfish Bar	14	0	14
	16	0	16
Morgans Point	13	9	16
	9	9	13

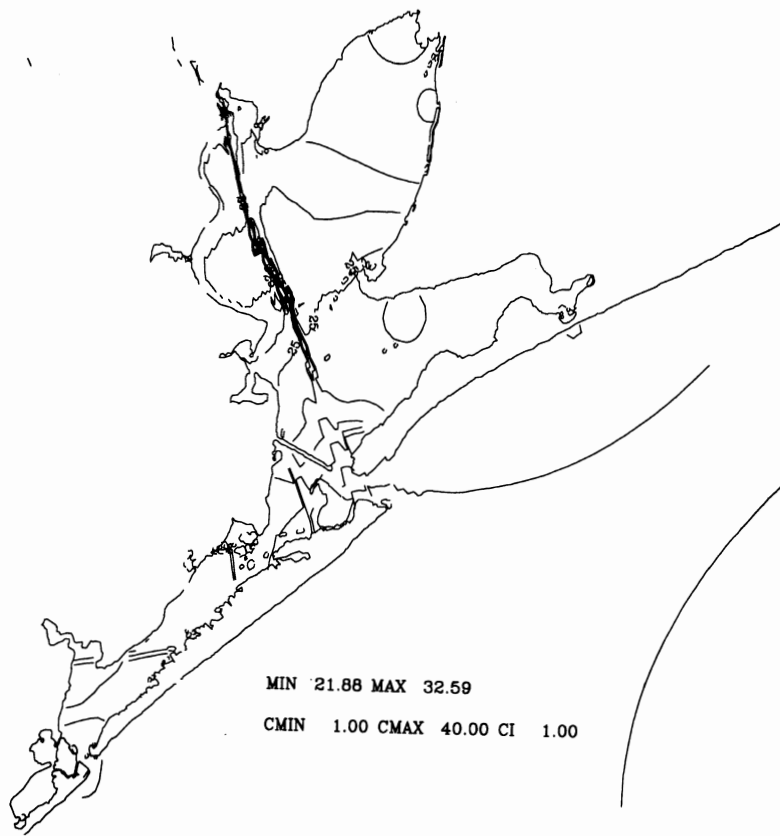


Figure 5.1. Initial Near-surface Salinity Field (PSU) 1 April 1996

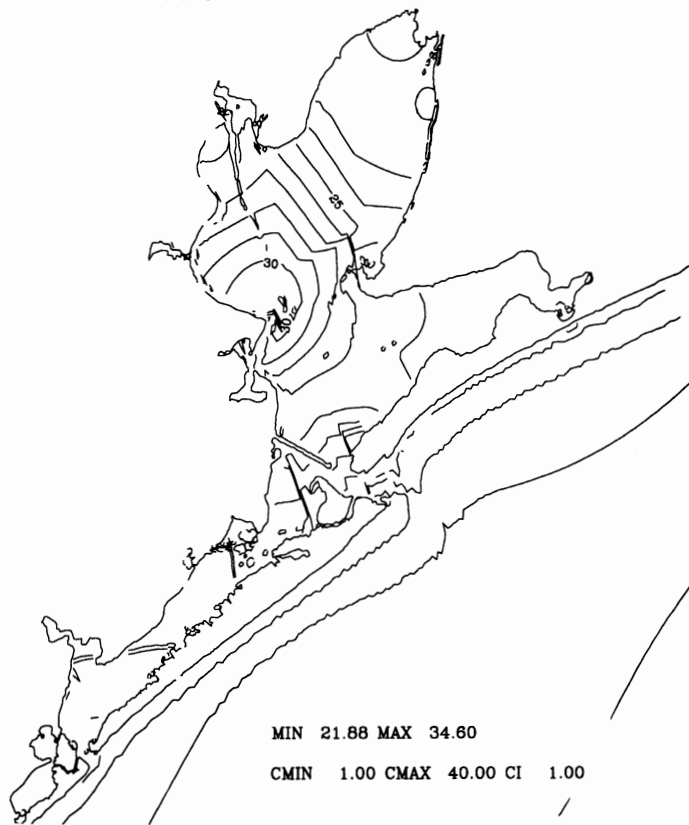


Figure 5.2. Initial Near-bottom Salinity Field (PSU) 1 April 1996

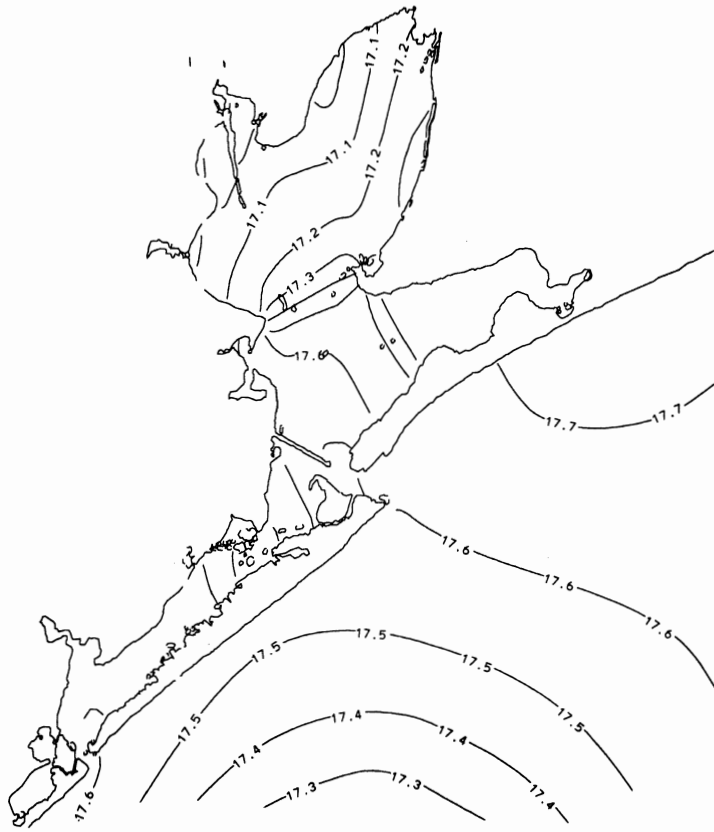


Figure 5.3. Initial Near-surface Temperature Field (°C) 1 April 1996

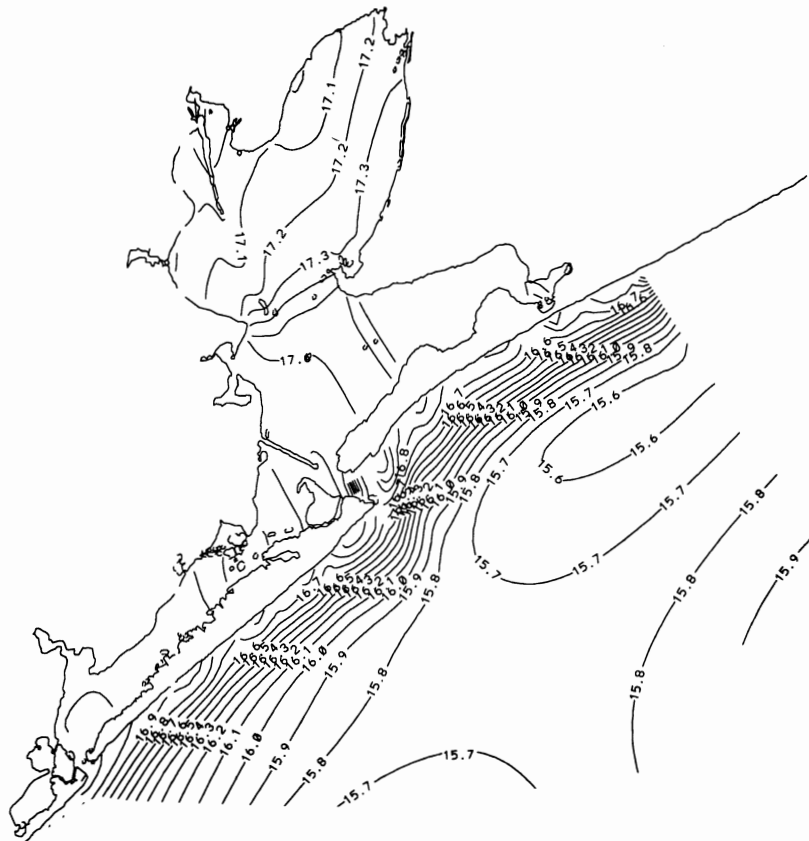


Figure 5.4. Initial Near-bottom Temperature Field (°C) 1 April 1996

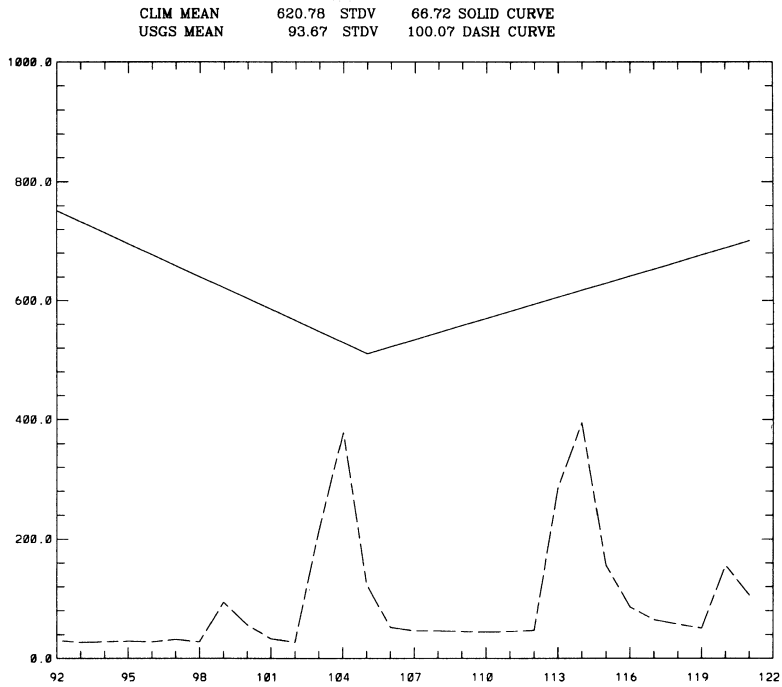


Figure 5.5. USGS Average Daily Flows (Cfs) Buffalo Bayou at Piney Point, TX in April 1996

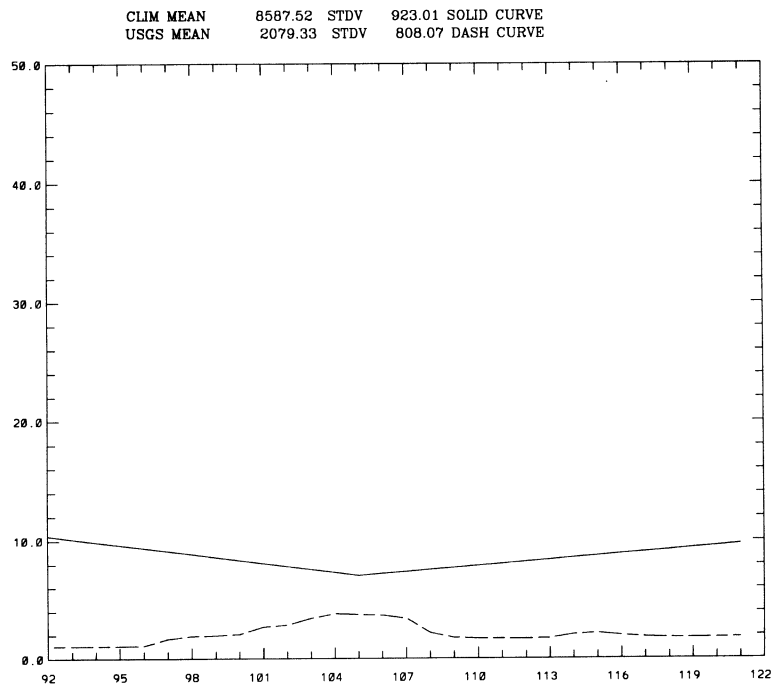


Figure 5.6. USGS Average Daily Flows (10^3 Cfs) Trinity River at Romayor, TX in April 1996

WIND

Data Source NOS
wmin = 3.88 wmax = 6.72
Julian Date = 101.000
April 10 1996

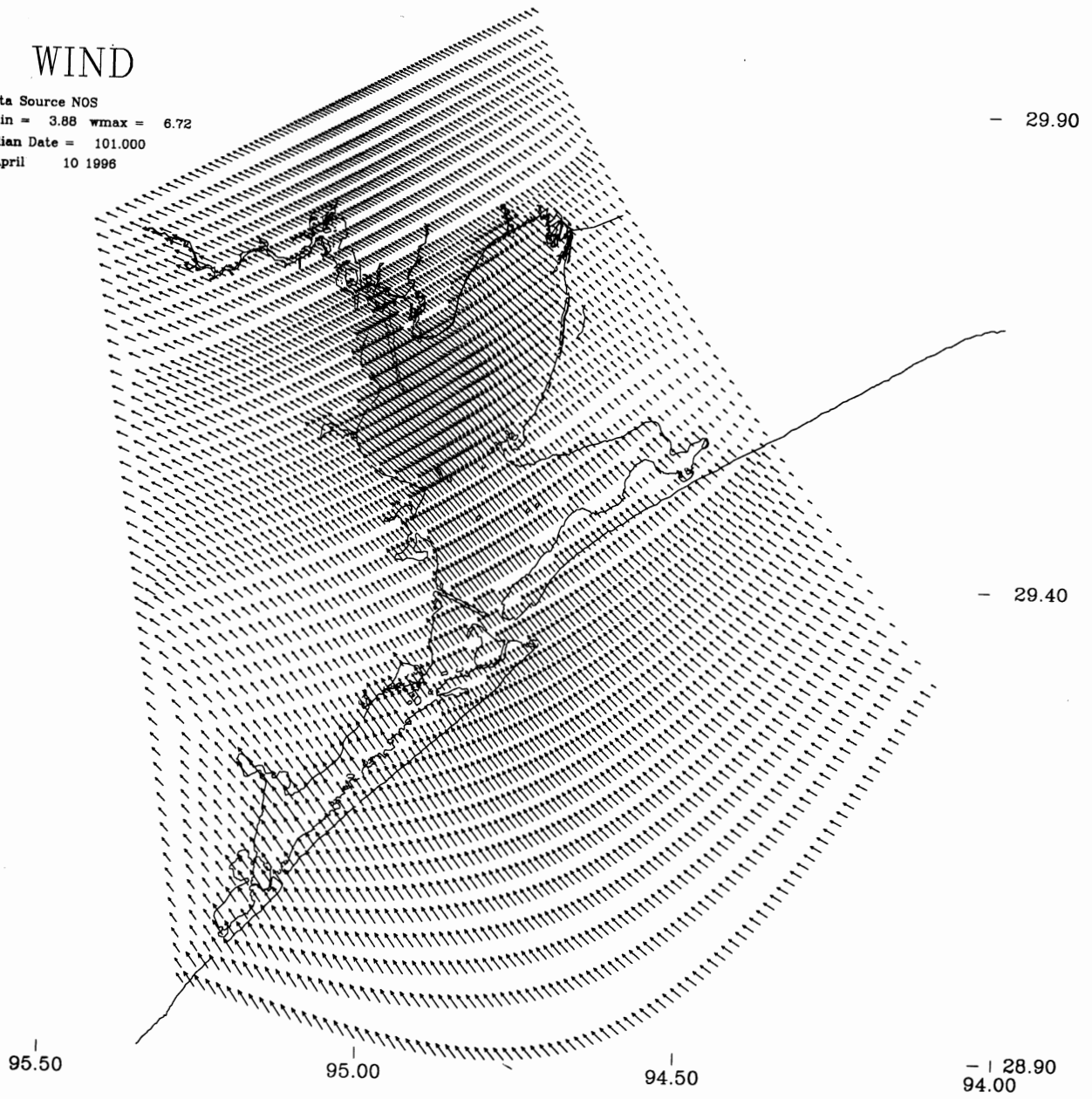


Figure 5.7. JD 101 Barnes Interpolation Windfield

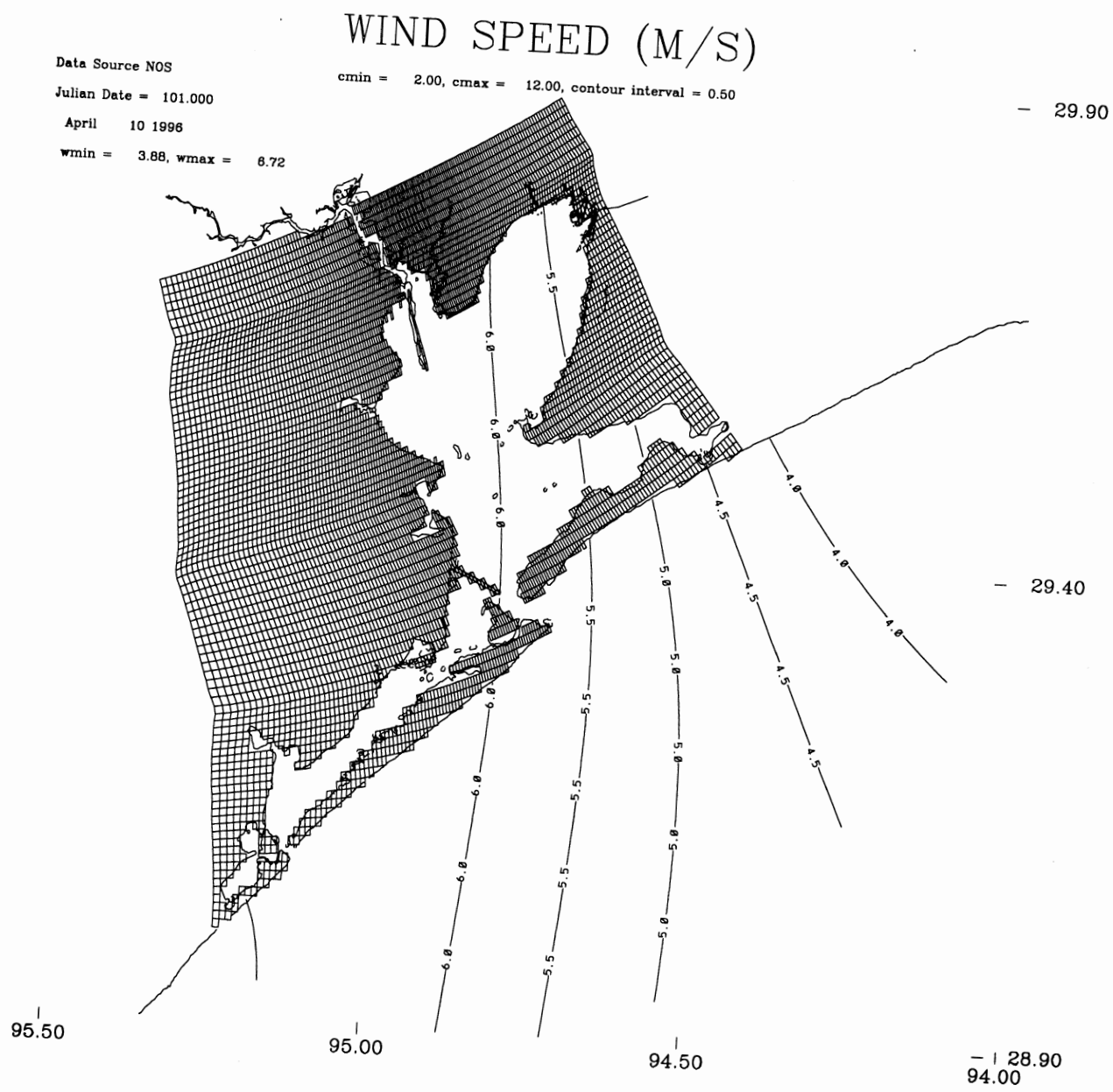


Figure 5.8. JD 101 Barnes Interpolation Windspeed Contours

WIND

Data Source NOS
wmin = 5.31 wmax = 7.62
Julian Date = 111.000
April 20 1996

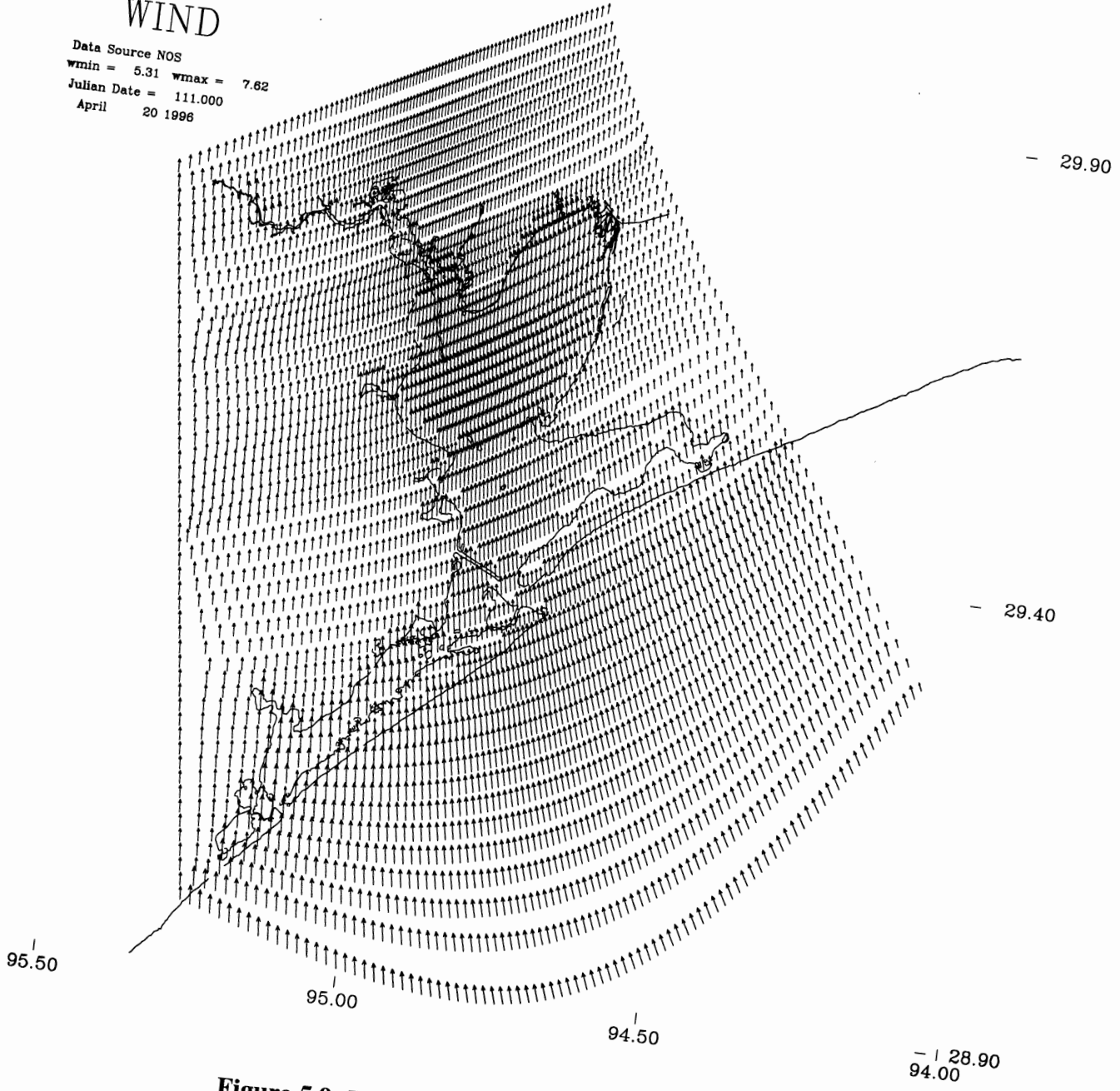


Figure 5.9. JD 111 Barnes Interpolation Windfield

WIND SPEED (M/S)

Data Source NOS

cmin = 2.00, cmax = 12.00, contour interval = 0.50

— 29.90

Julian Date = 111.000

April 20 1996

wmin = 5.31, wmax = 7.62

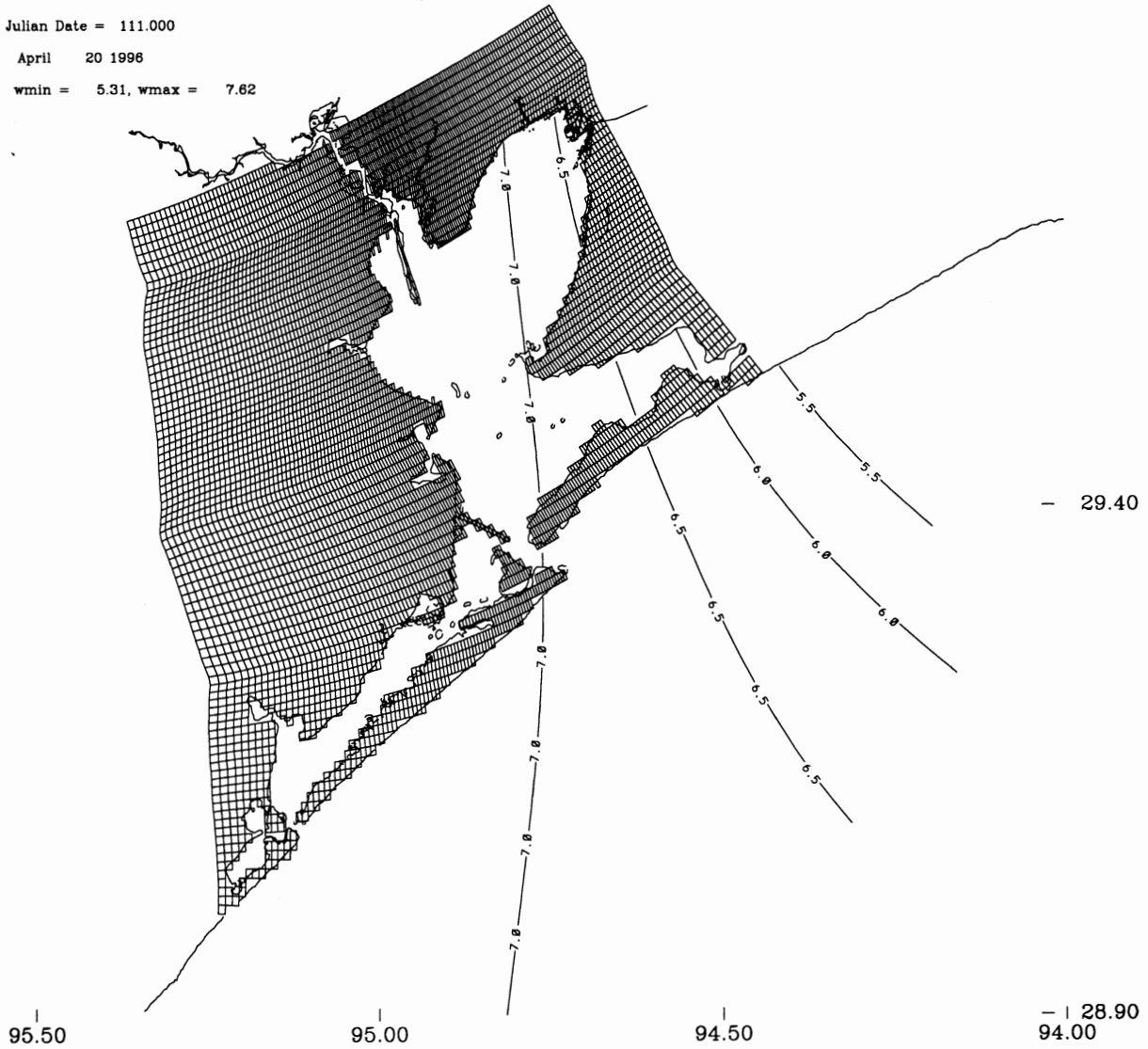
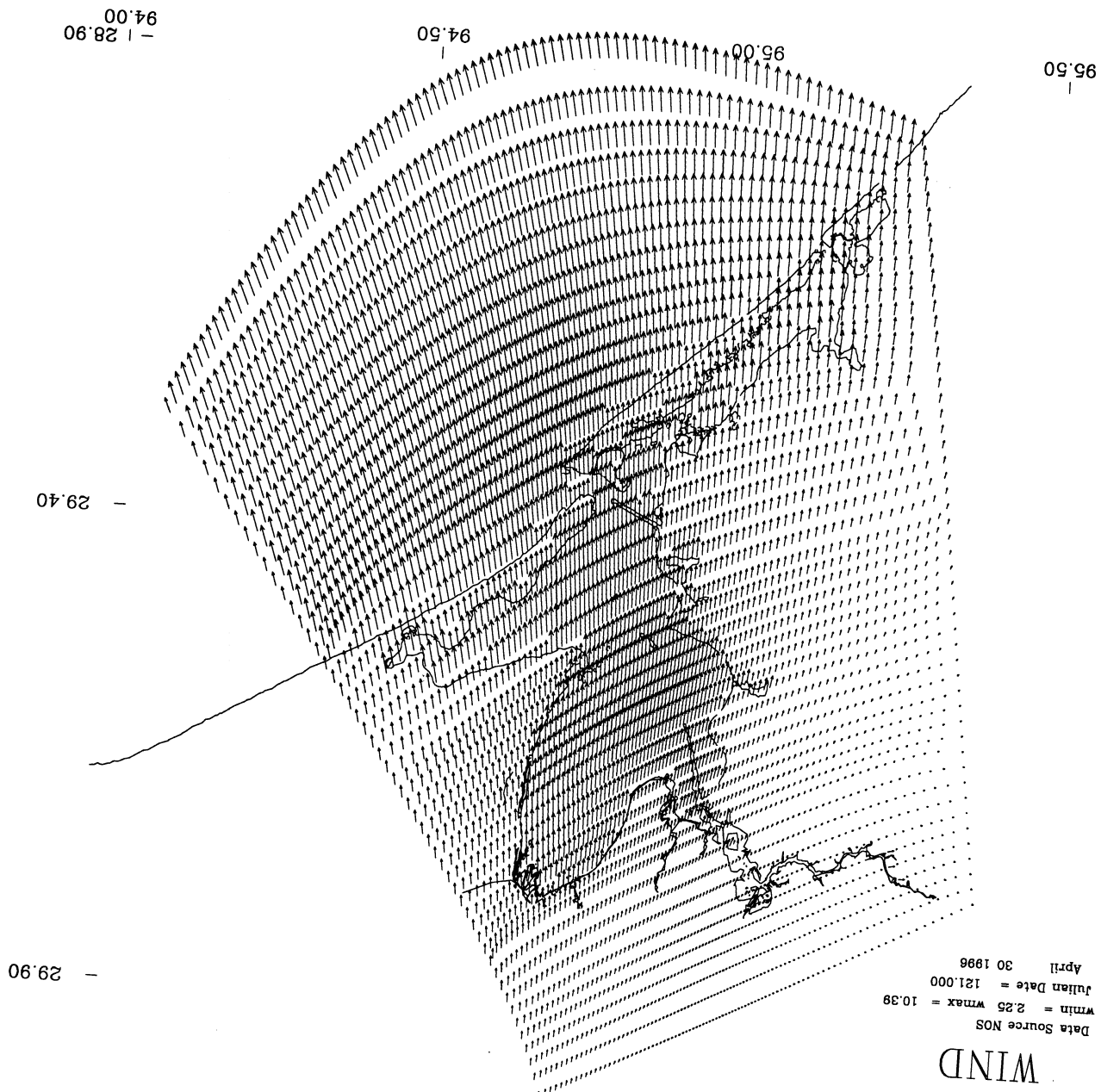


Figure 5.10. JD 111 Barnes Interpolation Windspeed Contours

Figure 5.11. JD 121 Barnes Interpolation Windfield



WIND SPEED (M/S)

Data Source NOS

cmin = 2.00, cmax = 12.00, contour interval = 0.50

- 29.90

Julian Date = 121.000

April 30 1996

wmin = 2.25, wmax = 10.39

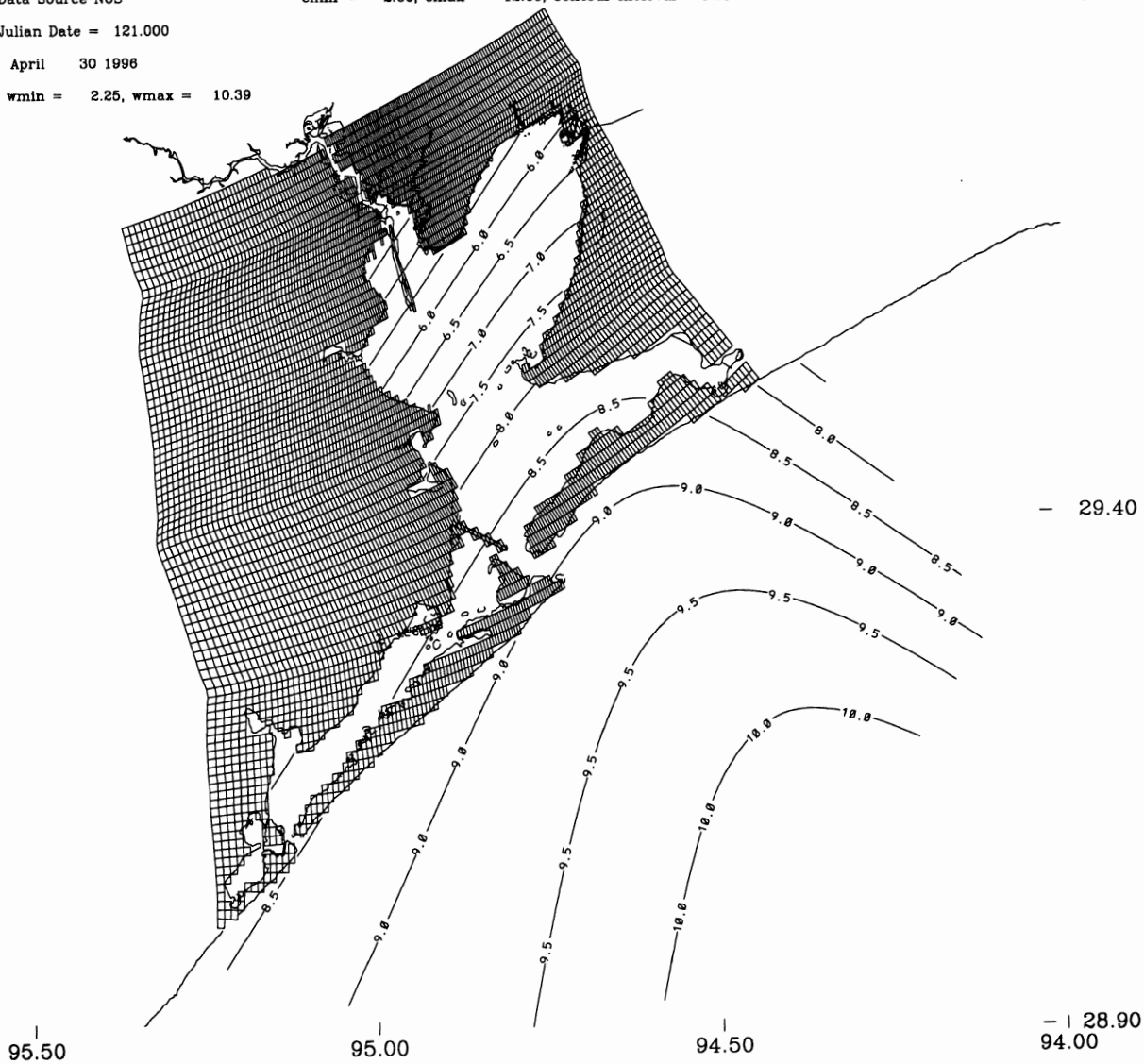


Figure 5.12. JD 121 Barnes Interpolation Windspeed Contours

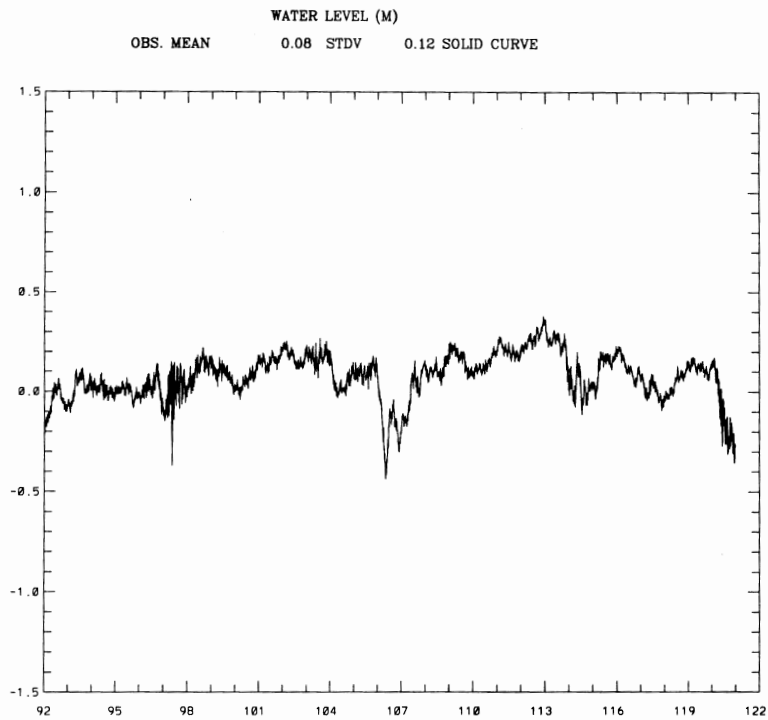


Figure 5.13. Galveston Pleasure Pier Subtidal Water Level Signal during April 1996

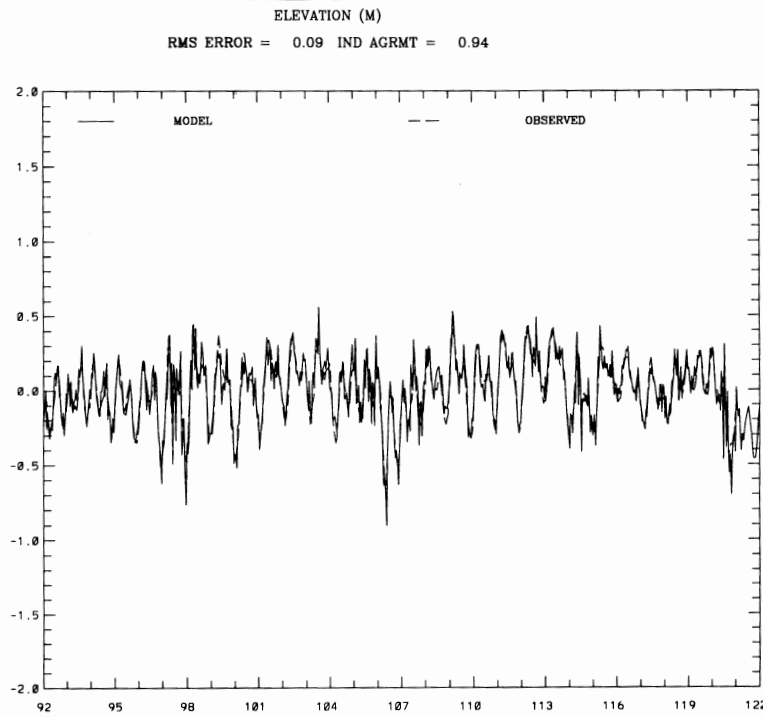


Figure 5.14. GBM: Galveston Pleasure Pier Simulated vs Observed Water Level Comparison during April 1996

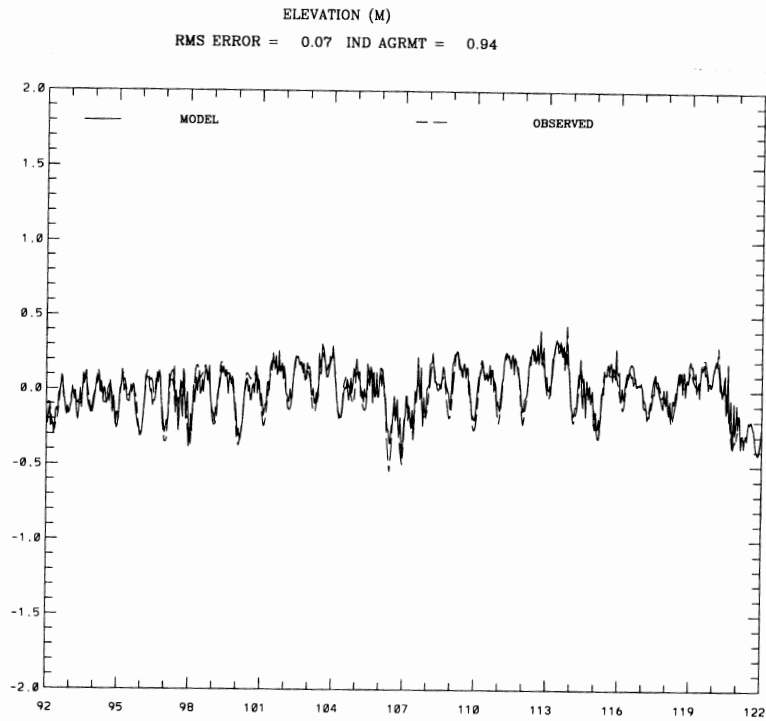


Figure 5.15. GBM: Galveston Pier 21 Simulated vs Observed Water Level Comparison during April 1996

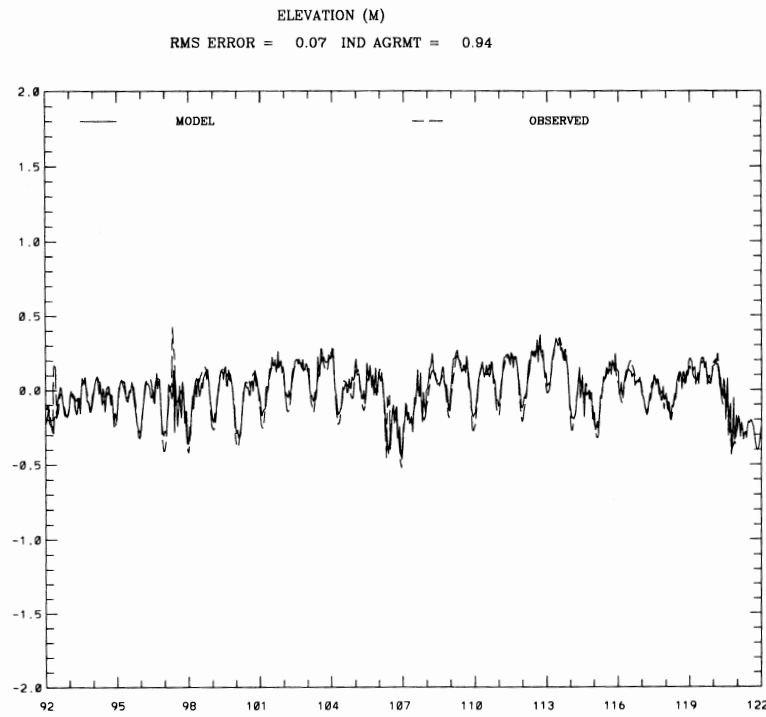


Figure 5.16. GBM: Port Bolivar Simulated vs Observed Water Level Comparison during April 1996

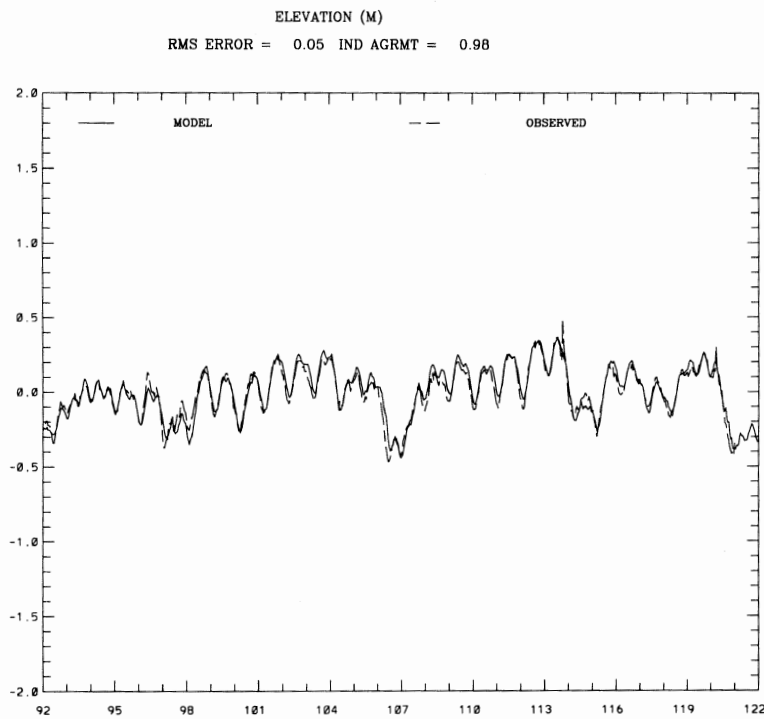


Figure 5.17. GBM: Eagle Point Simulated vs Observed Water Level Comparison during April 1996

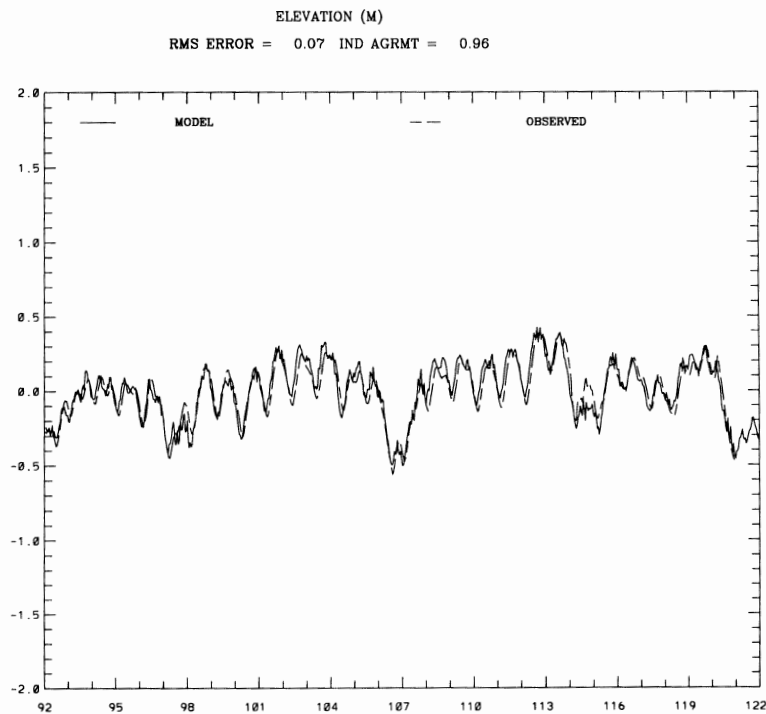


Figure 5.18. GBM: Clear Lake Simulated vs Observed Water Level Comparison during April 1996

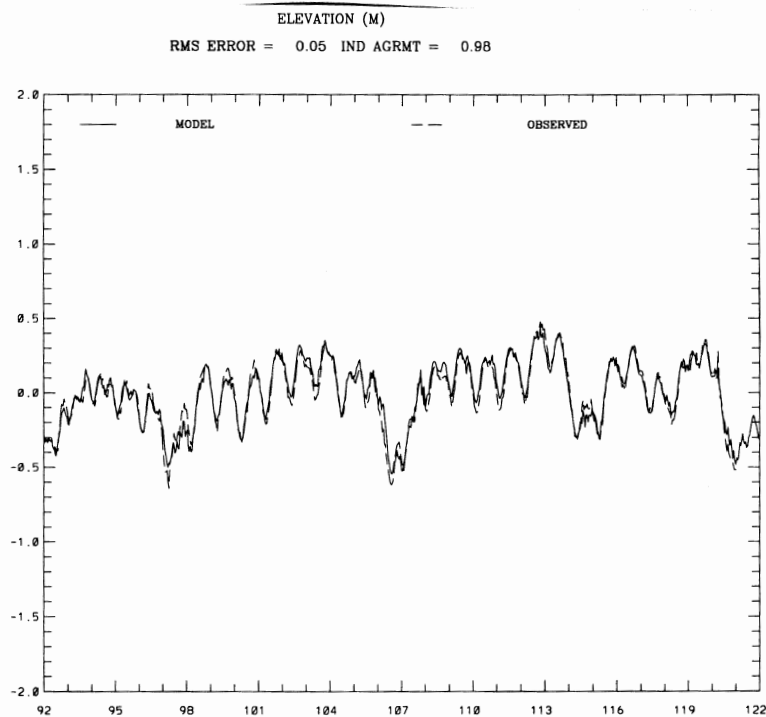


Figure 5.19. GBM: Morgans Point Simulated vs Observed Water Level Comparison during April 1996

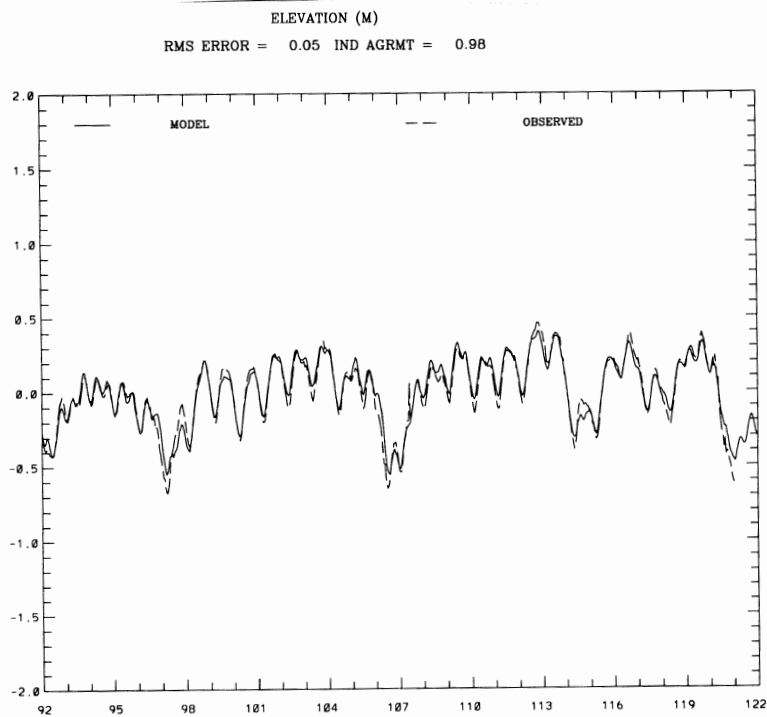


Figure 5.20. GBM: Umbrella Point Simulated vs Observed Water Level Comparison during April 1996

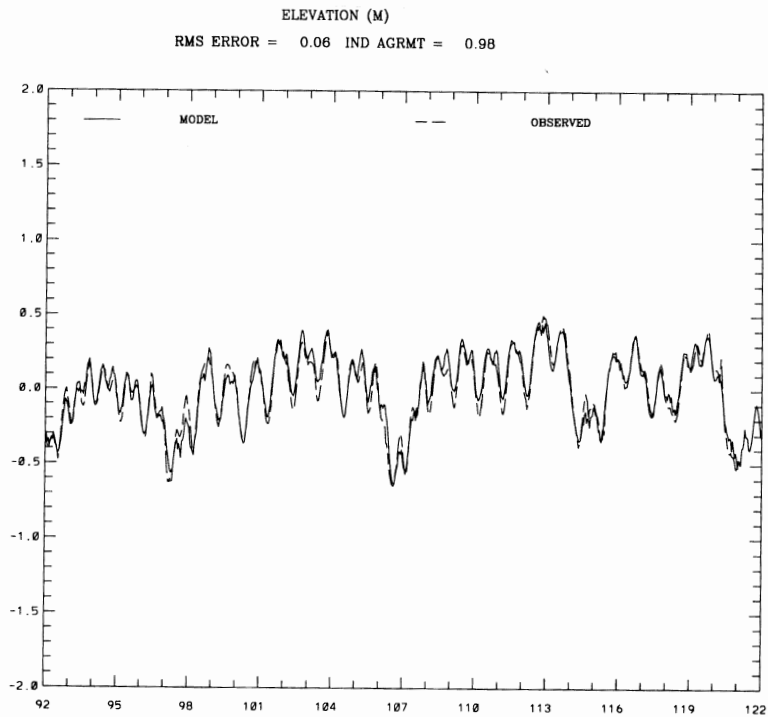


Figure 5.21. GBM: Lynchburg Landing Simulated vs Observed Water Level Comparison during April 1996

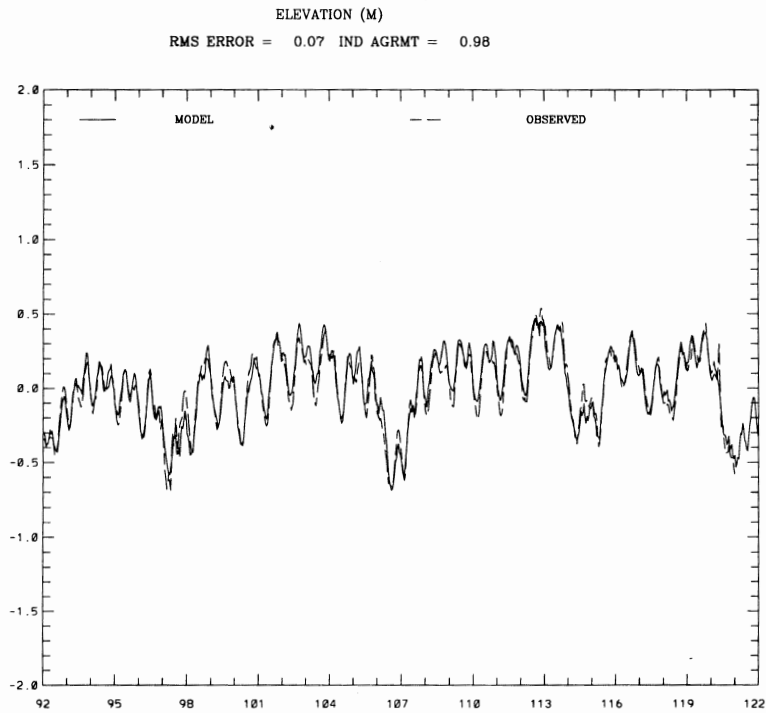


Figure 5.22. GBM: Manchester Dock 2 Simulated vs Observed Water Level Comparison during April 1996

PD CURRENT (CM/S) - (FLOOD +)
RMS ERROR = 21.11 IND AGRMT = 0.96

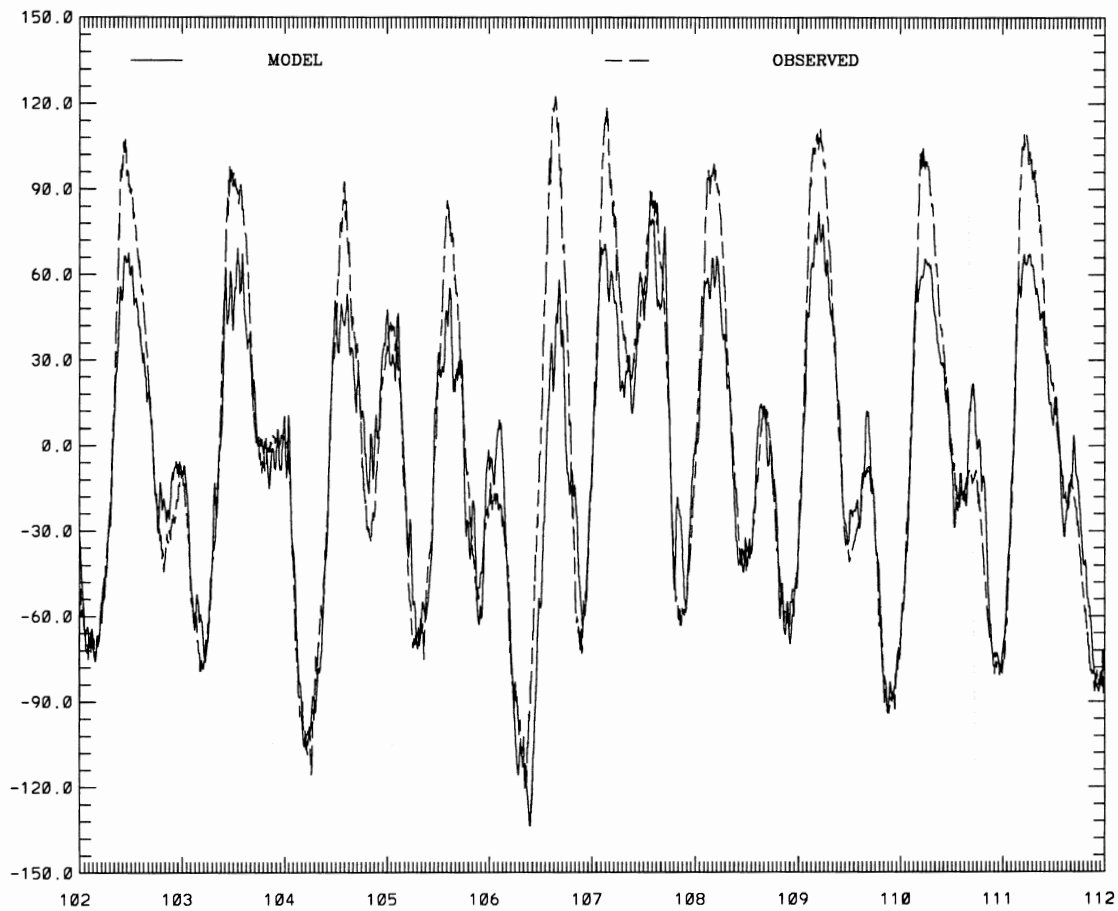


Figure 5.23. GBM: Bolivar Roads (PORTS) Simulated vs Observed Principal Component Direction Current Comparison during April 1996

PD CURRENT (CM/S) - (FLOOD +)
RMS ERROR = 13.83 IND AGRMT = 0.95

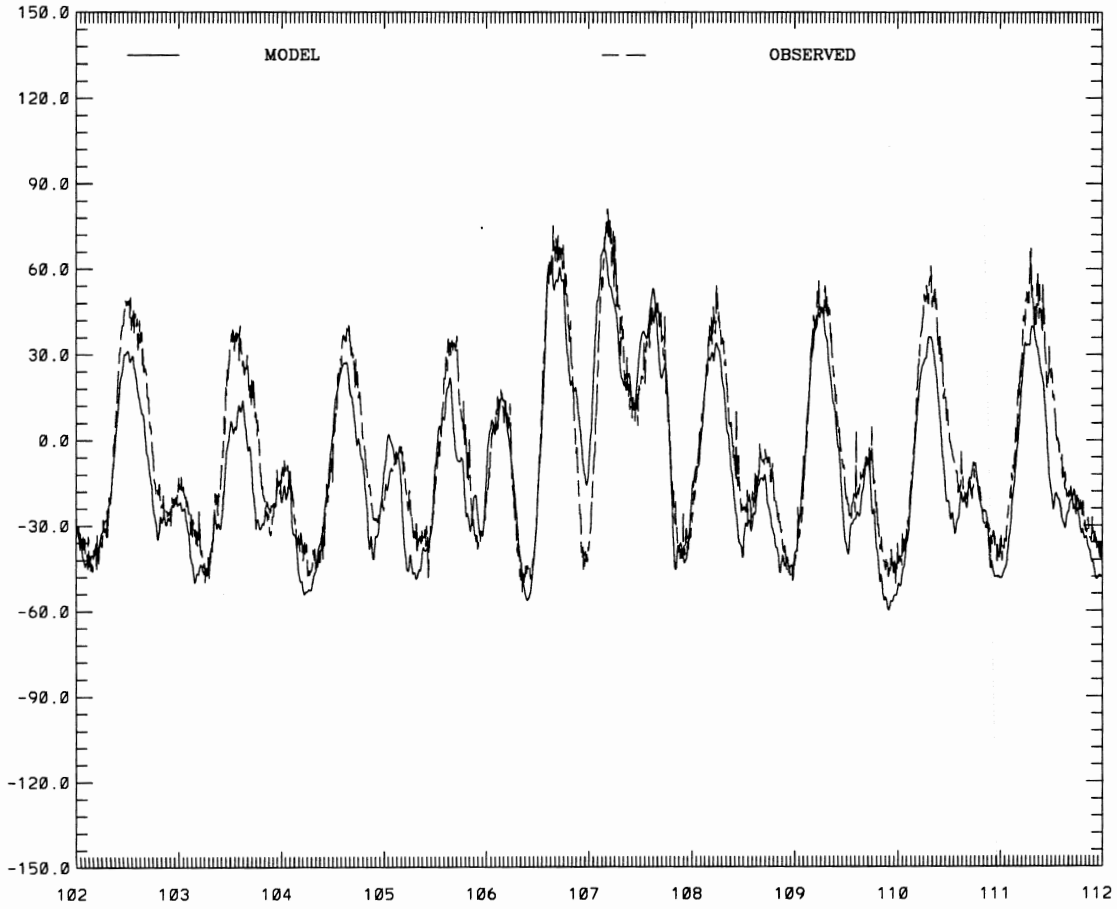


Figure 5.24. GBM: Redfish Bar (PORTS) Simulated vs Observed Principal Component Direction Current Comparison during April 1996

PD CURRENT (CM/S) - (FLOOD +)
RMS ERROR = 15.90 IND AGRMT = 0.73

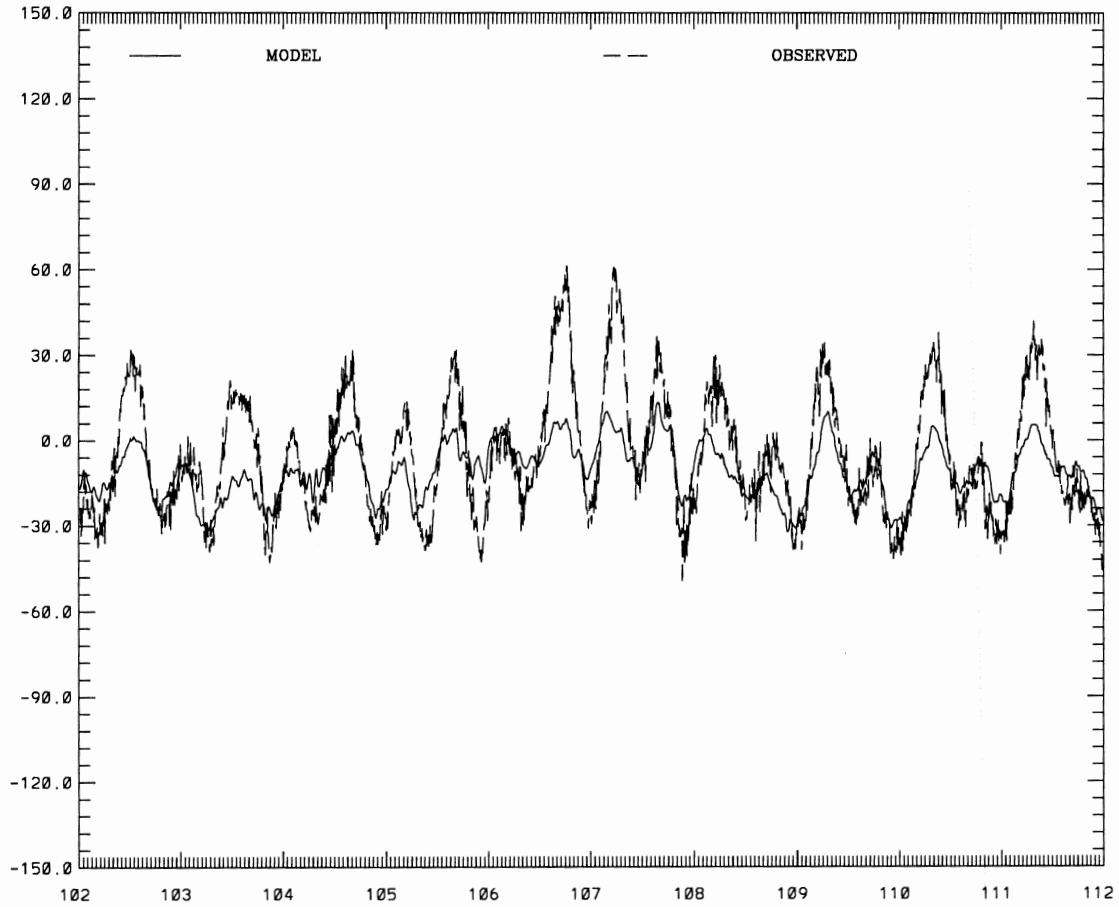


Figure 5.25. GBM: Morgans Point (PORTS) Simulated vs Observed Principal Component Direction Current Comparison during April 1996

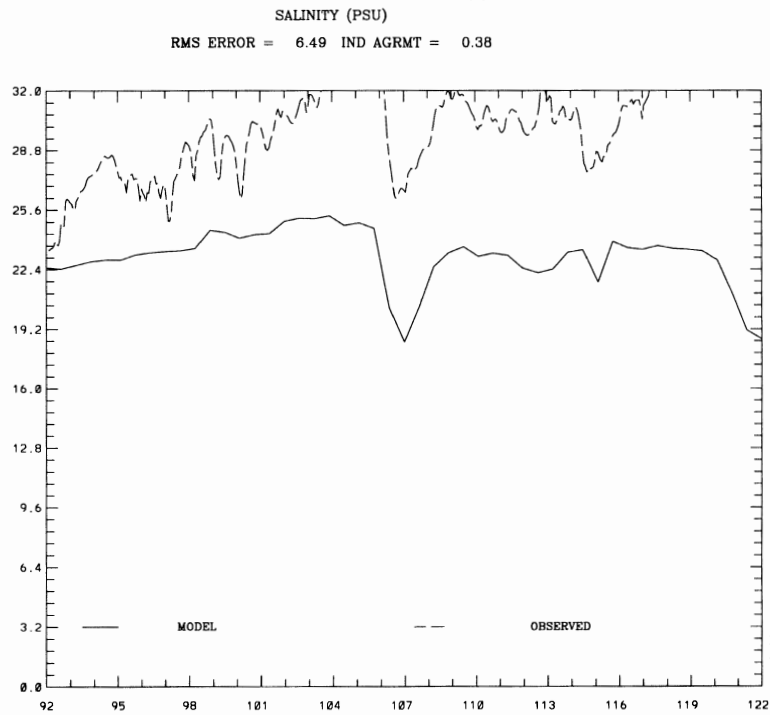


Figure 5.26. GBM: Trinity Bay (DBC) Simulated vs Observed Salinity Comparison during April 1996

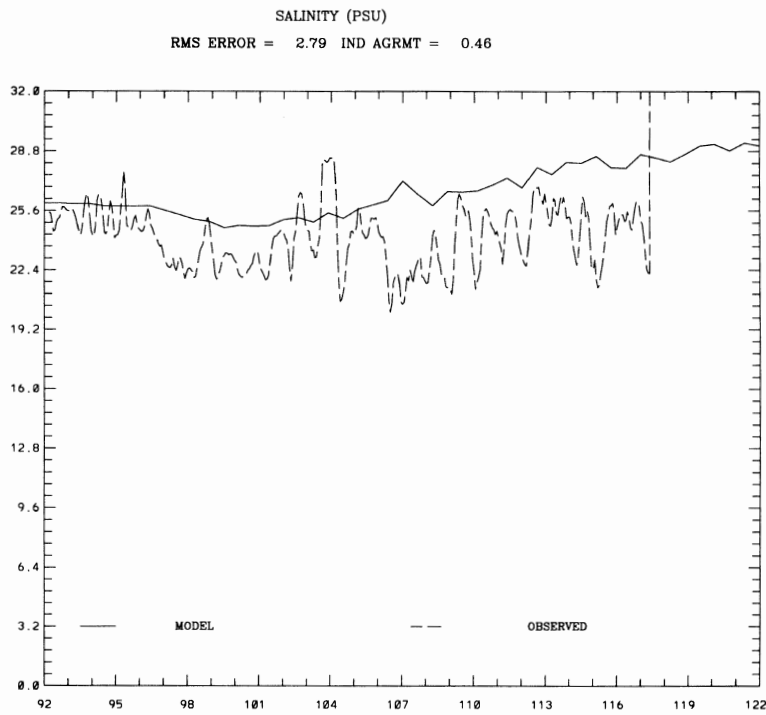


Figure 5.27. GBM: Hannah Reef Simulated vs Observed Salinity Comparison during April 1996

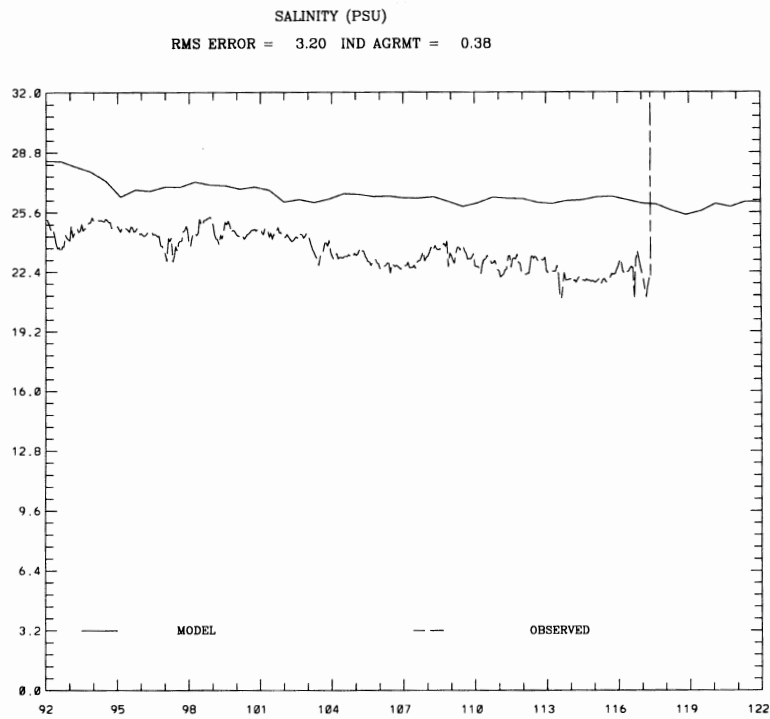


Figure 5.28. GBM: Red Bluff Simulated vs Observed Salinity Comparison during April 1996

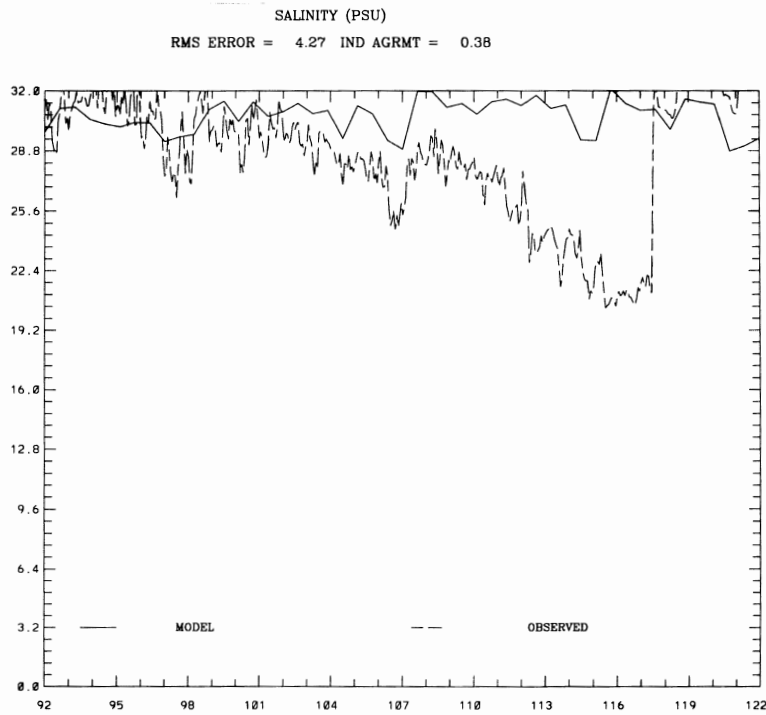


Figure 5.29. GBM: Port Bolivar Simulated vs Observed Salinity Comparison during April 1996

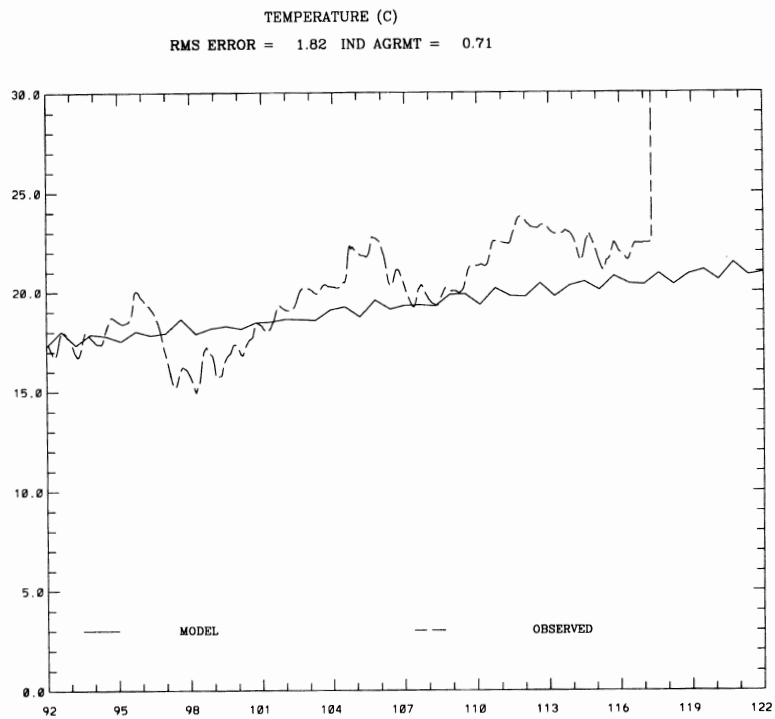


Figure 5.30. GBM: Trinity Bay (DBC) Simulated vs Observed Temperature Comparison during April 1996

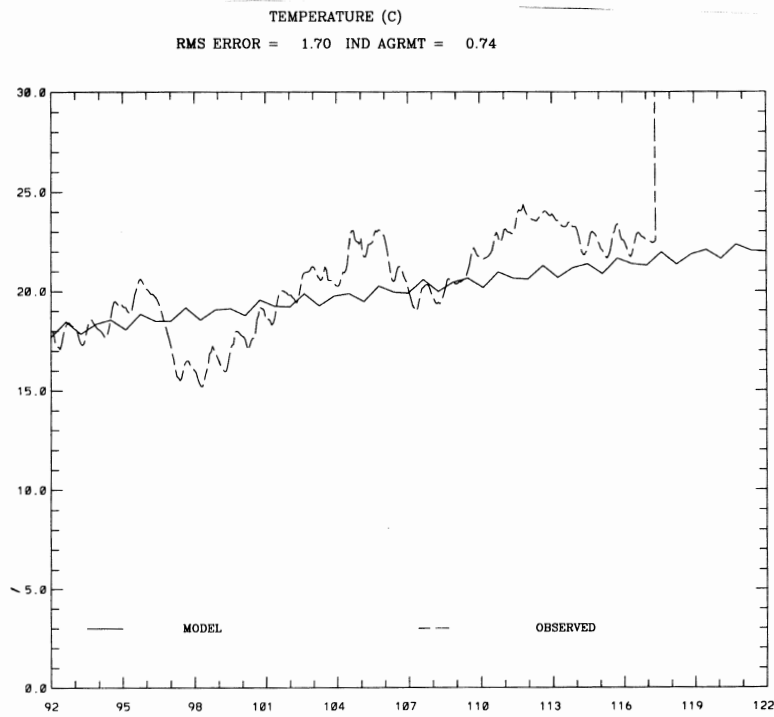


Figure 5.31. GBM: Hannah Reef Simulated vs Observed Temperature Comparison during April 1996

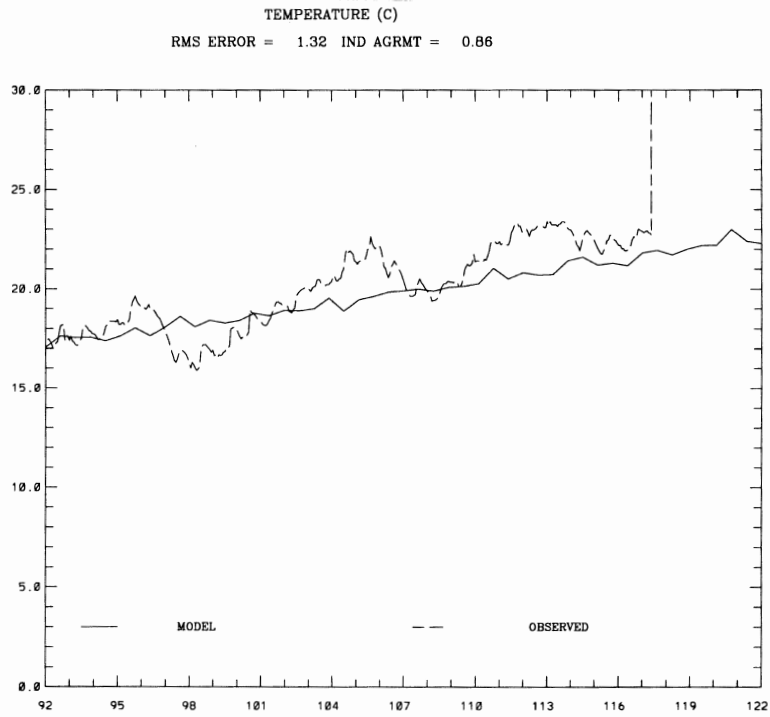


Figure 5.32. GBM: Red Bluff Simulated vs Observed Temperature Comparison during April 1996

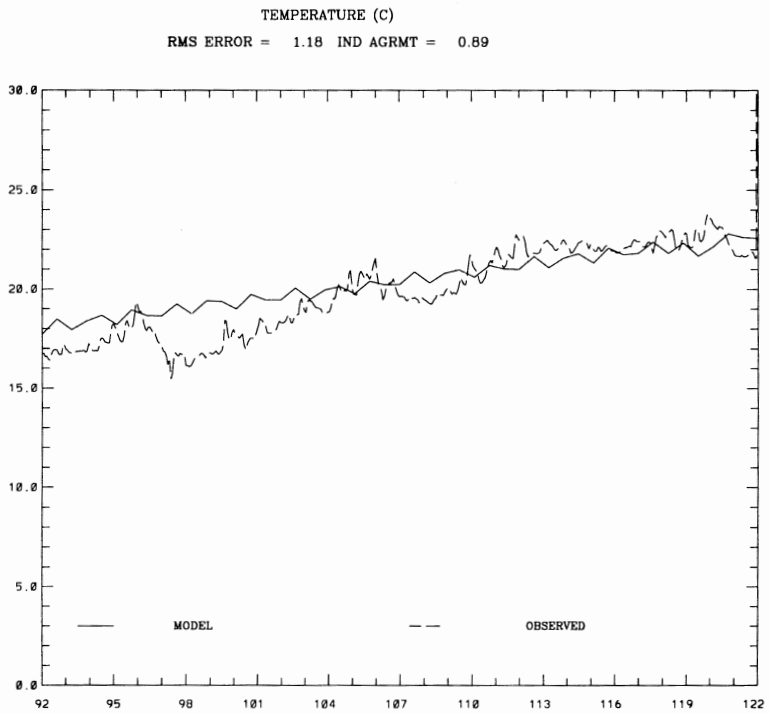


Figure 5.33. GBM: Port Bolivar Simulated vs Observed Temperature Comparison during April 1996

WIND

Data Source NOS
wmin = 4.74 wmax = 6.23
Julian Date = 101.000
April 10 1998

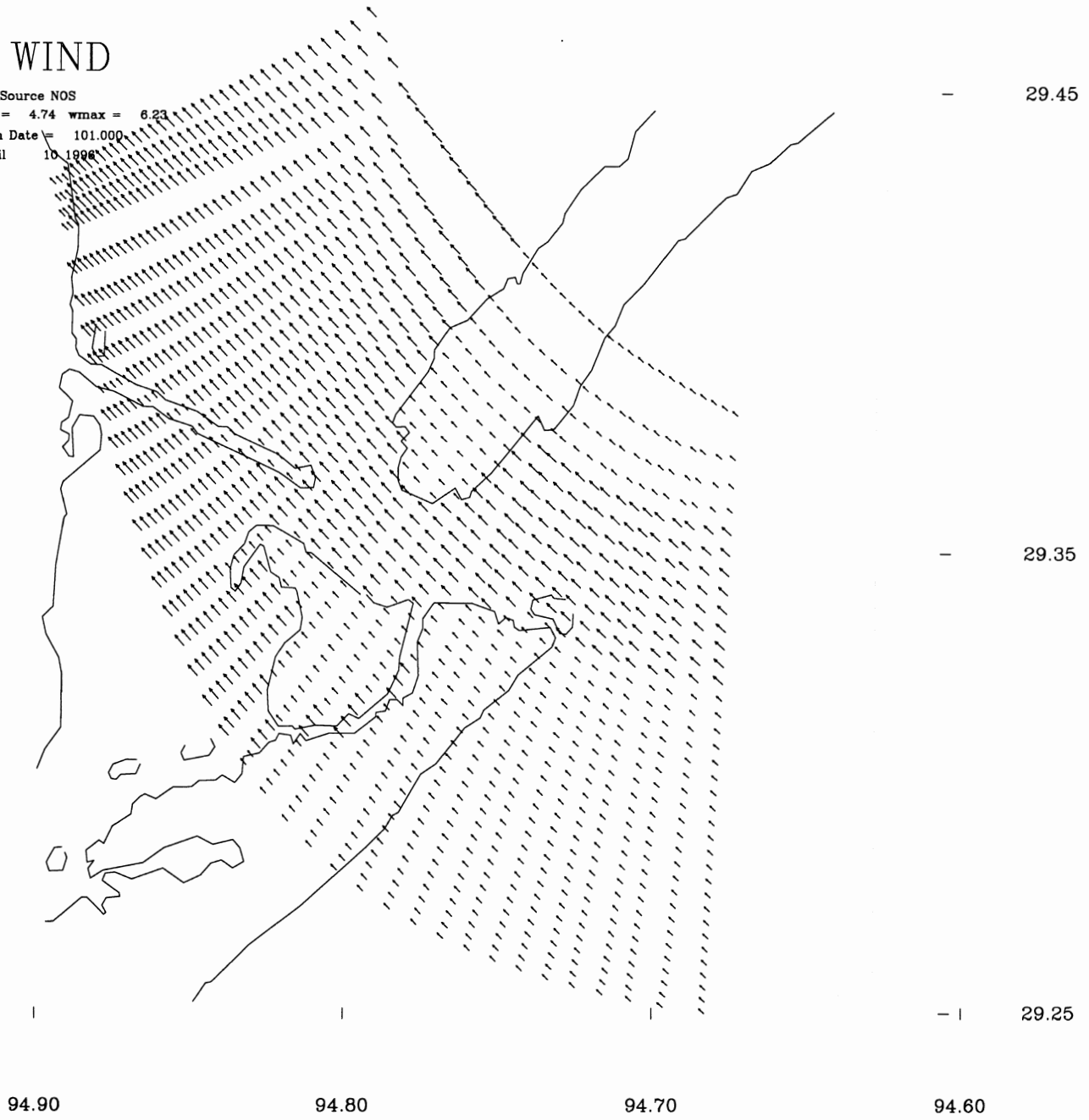


Figure 5.34. HSCM: JD 101 Barnes Interpolation Windfield

WIND SPEED (M/S)

Data Source NOS

cmin = 1.00, cmax = 10.00, contour interval = 0.50

29.45

Julian Date = 101.000

April 10 1996

wmin = 4.74, wmax = 8.23

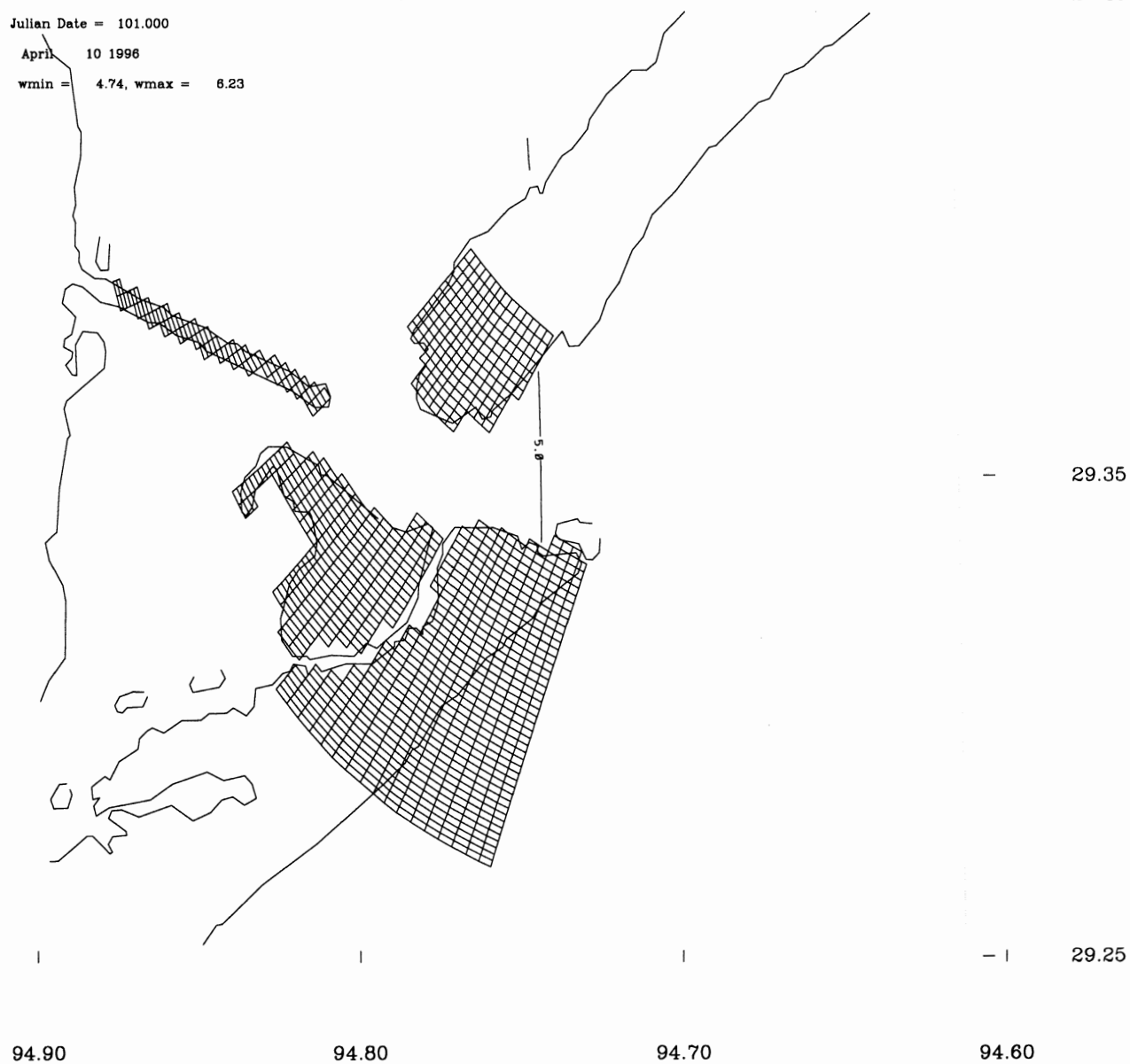


Figure 5.35. HSCM: JD 101 Barnes Interpolation Windspeed Contours

WIND

Data Source NOS
wmin = 6.16 wmax = 7.99
Julian Date = 111.000
April 20 1996

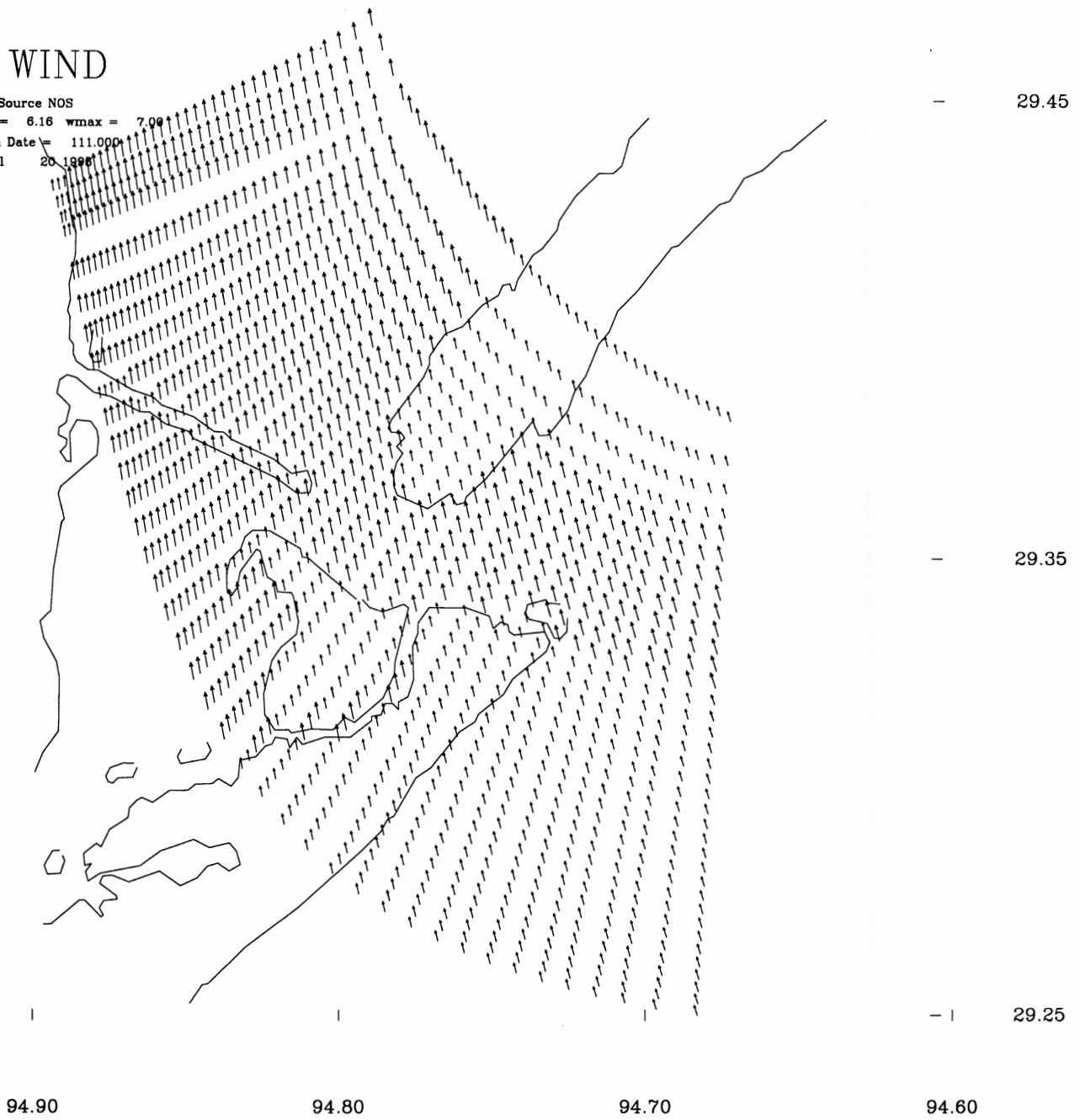


Figure 5.36. HSCM: JD 111 Barnes Interpolation Windfield

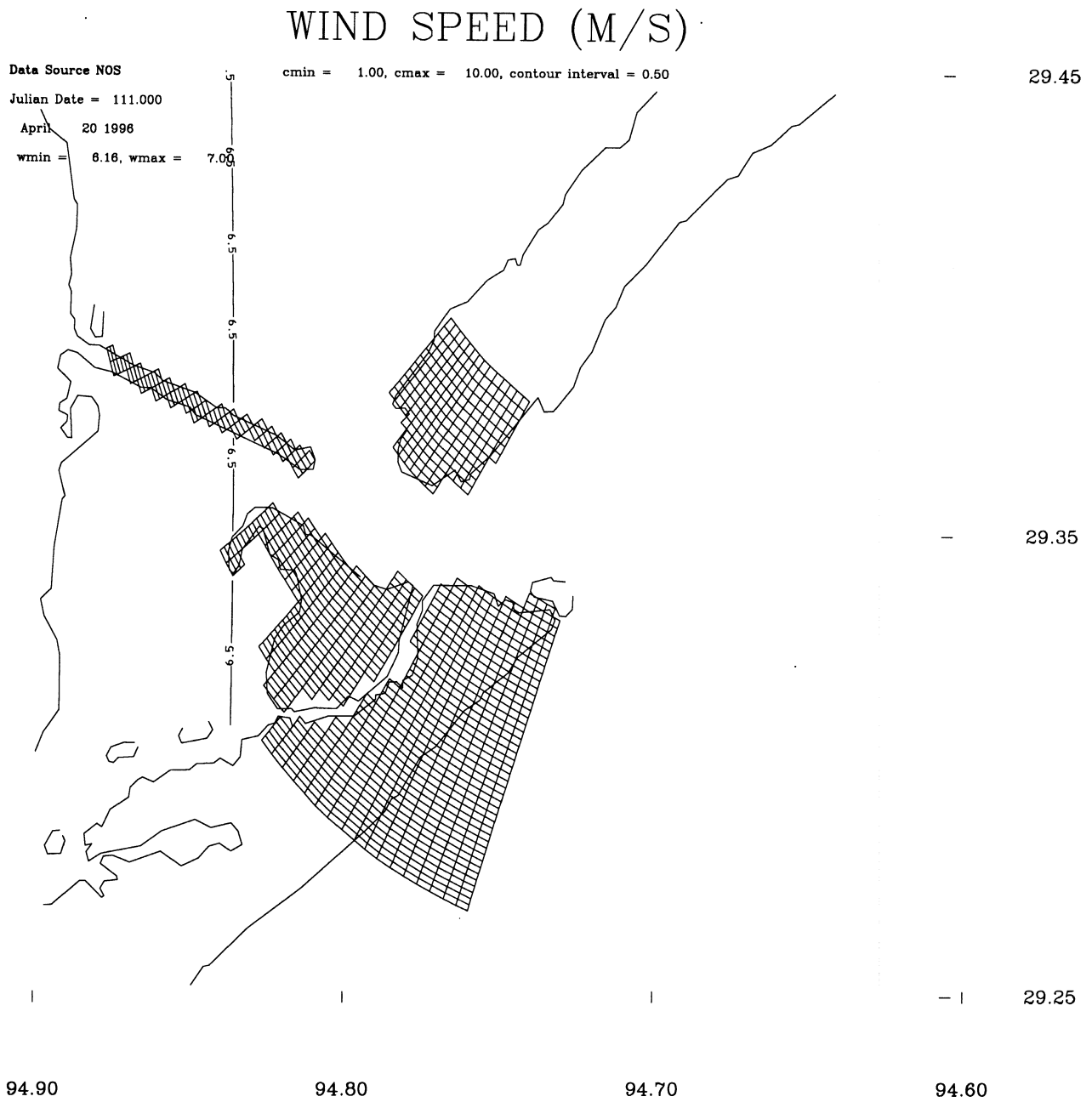
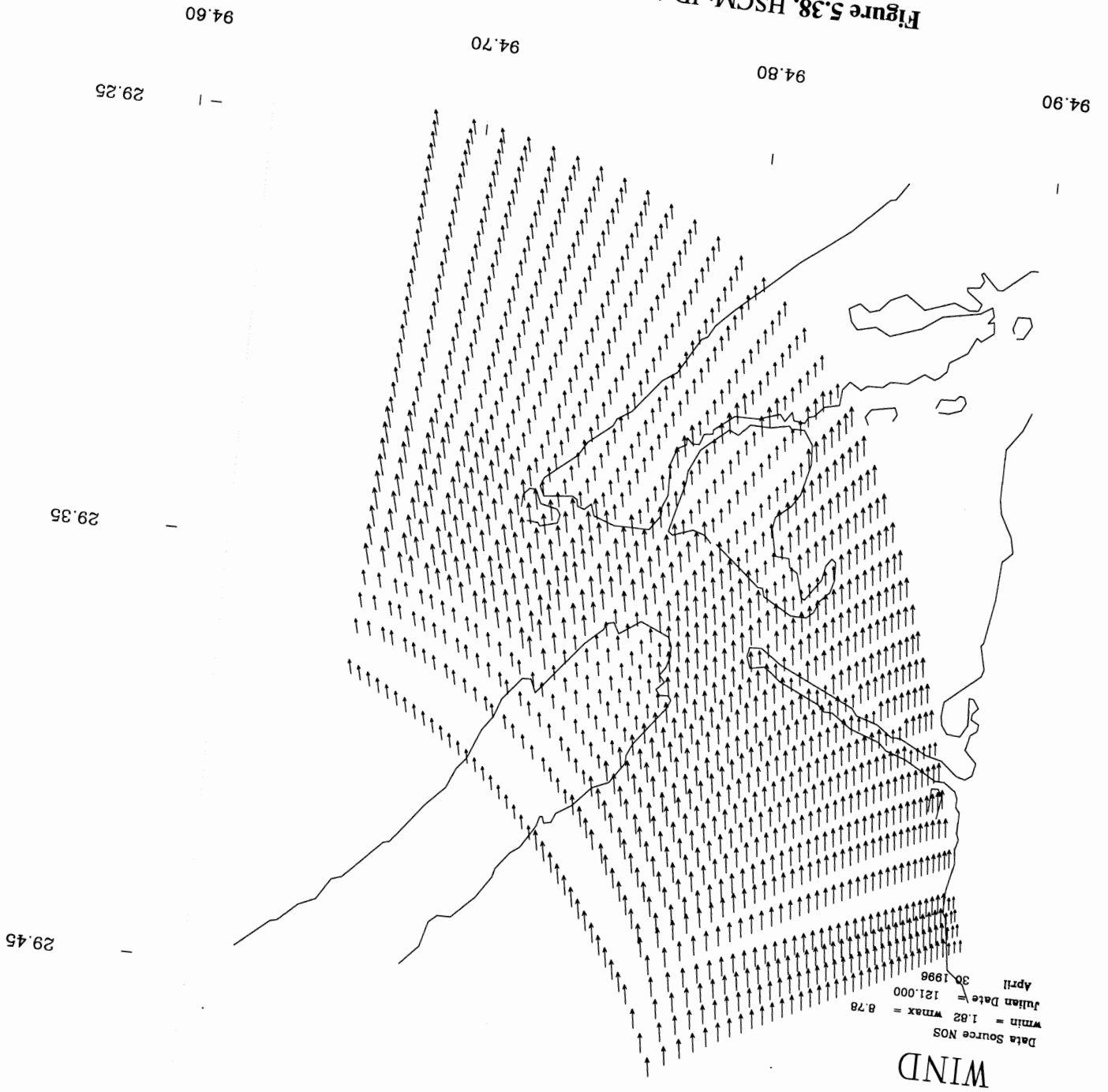


Figure 5.37. HSCM: JD 111 Barnes Interpolation Windspeed Contours

Figure 5.38. HSCM: JD 121 Barnes Interpolation Windfield



WIND SPEED (M/S)

Data Source NOS
Julian Date = 121.000
April 30 1996
wmin = 1.82, wmax = 8.78

cmin = 1.00, cmax = 10.00, contour interval = 0.50



Figure 5.39. HSCM: JD 121 Barnes Interpolation Windspeed Contours

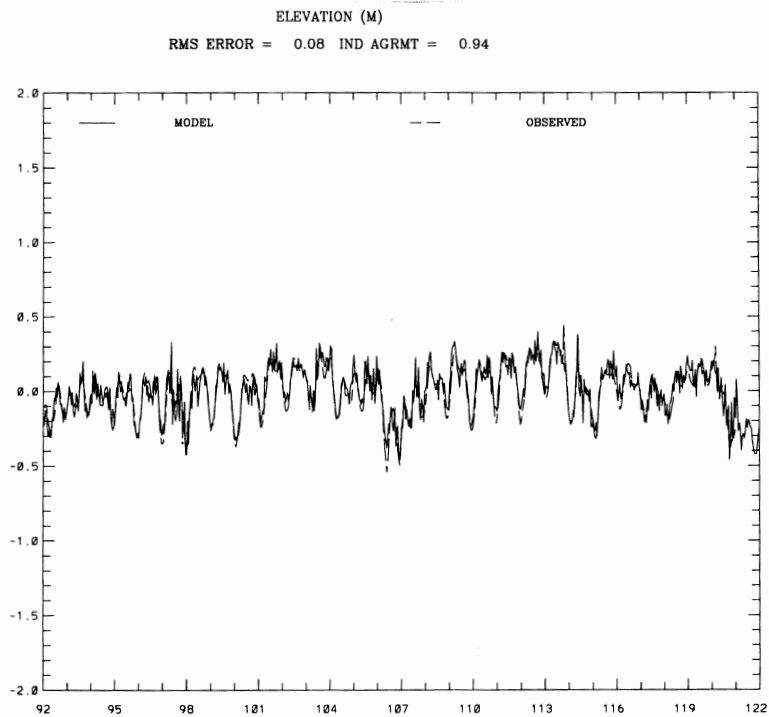


Figure 5.40. HSCM: Galveston Pier 21 Simulated vs Observed Water Level Comparison during April 1996

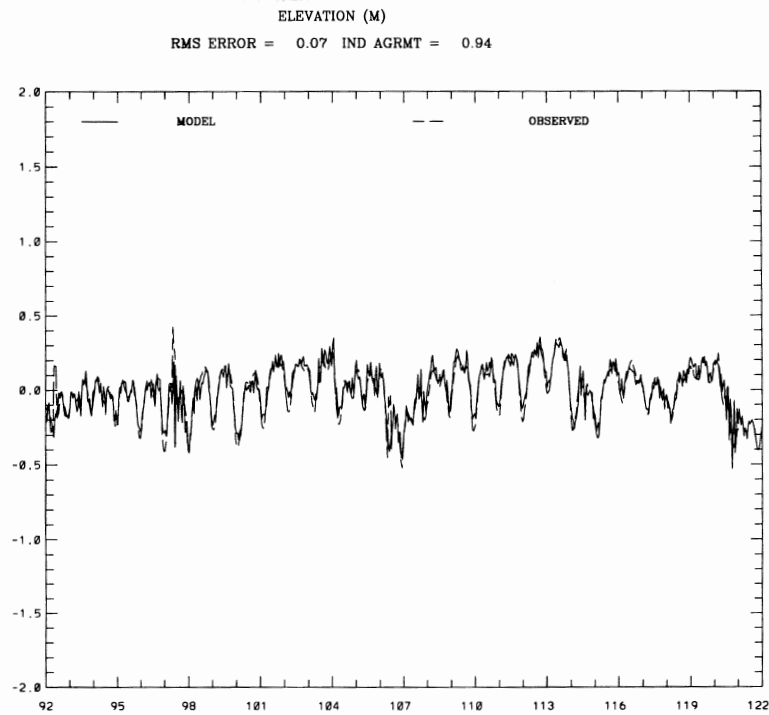


Figure 5.41. HSCM: Port Bolivar Simulated vs Observed Water Level Comparison during April 1996

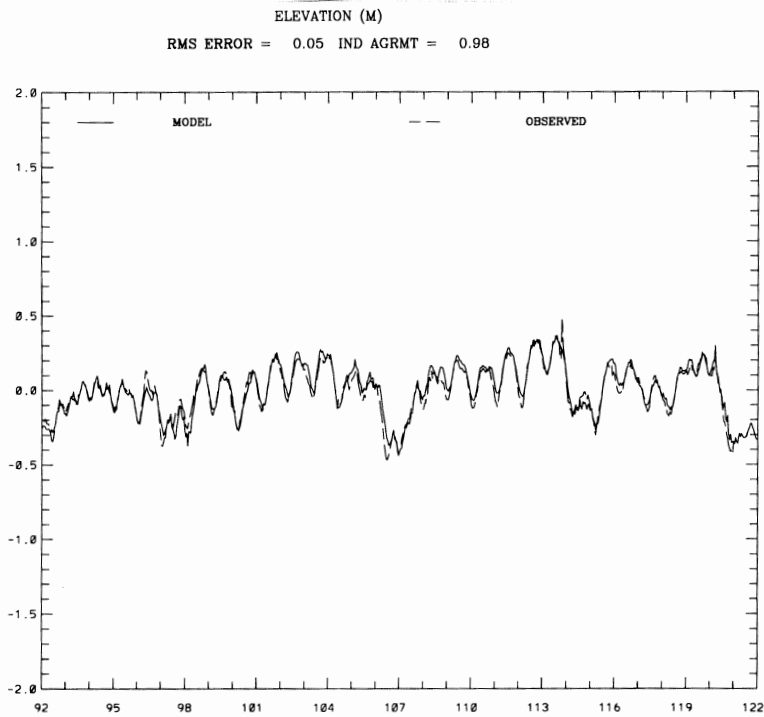


Figure 5.42. HSCM: Eagle Point Simulated vs Observed Water Level Comparison during April 1996

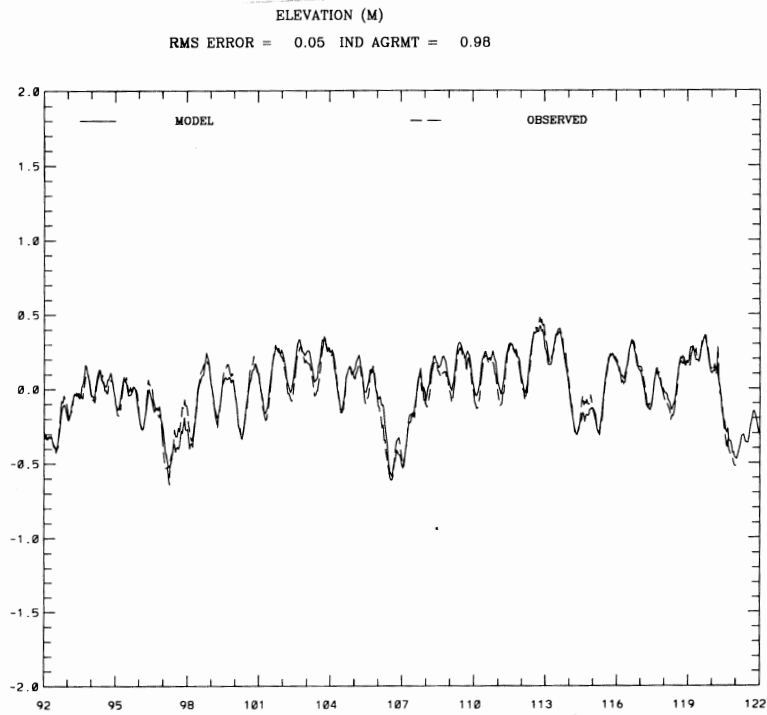


Figure 5.43. HSCM: Morgans Point Simulated vs Observed Water Level Comparison during April 1996

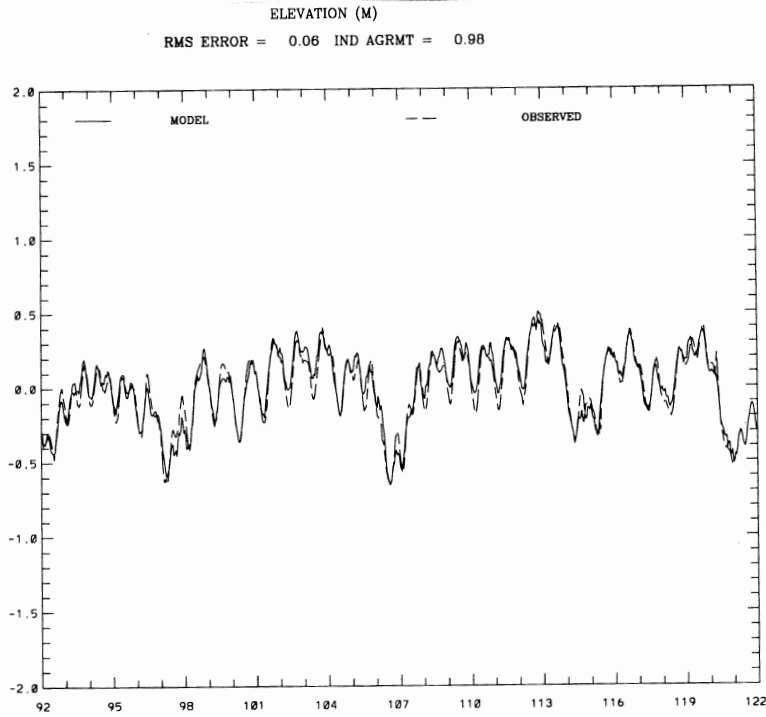


Figure 5.44. HSCM: Lynchburg Landing Simulated vs Observed Water Level Comparison during April 1996

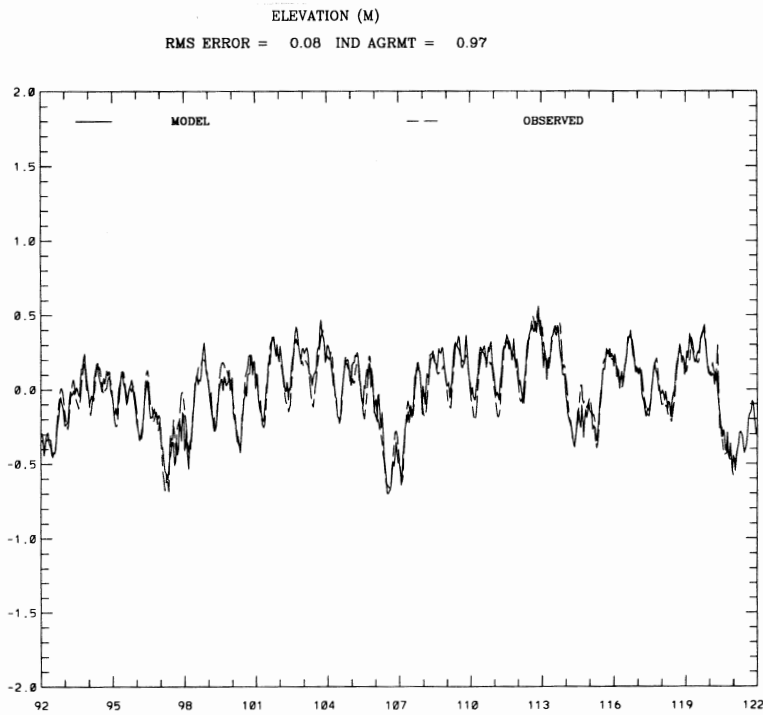


Figure 5.45. HSCM: Manchester Dock 2 Simulated vs Observed Water Level Comparison during April 1996

PD CURRENT (CM/S) - (FLOOD +)
RMS ERROR = 26.08 IND AGRMT = 0.93

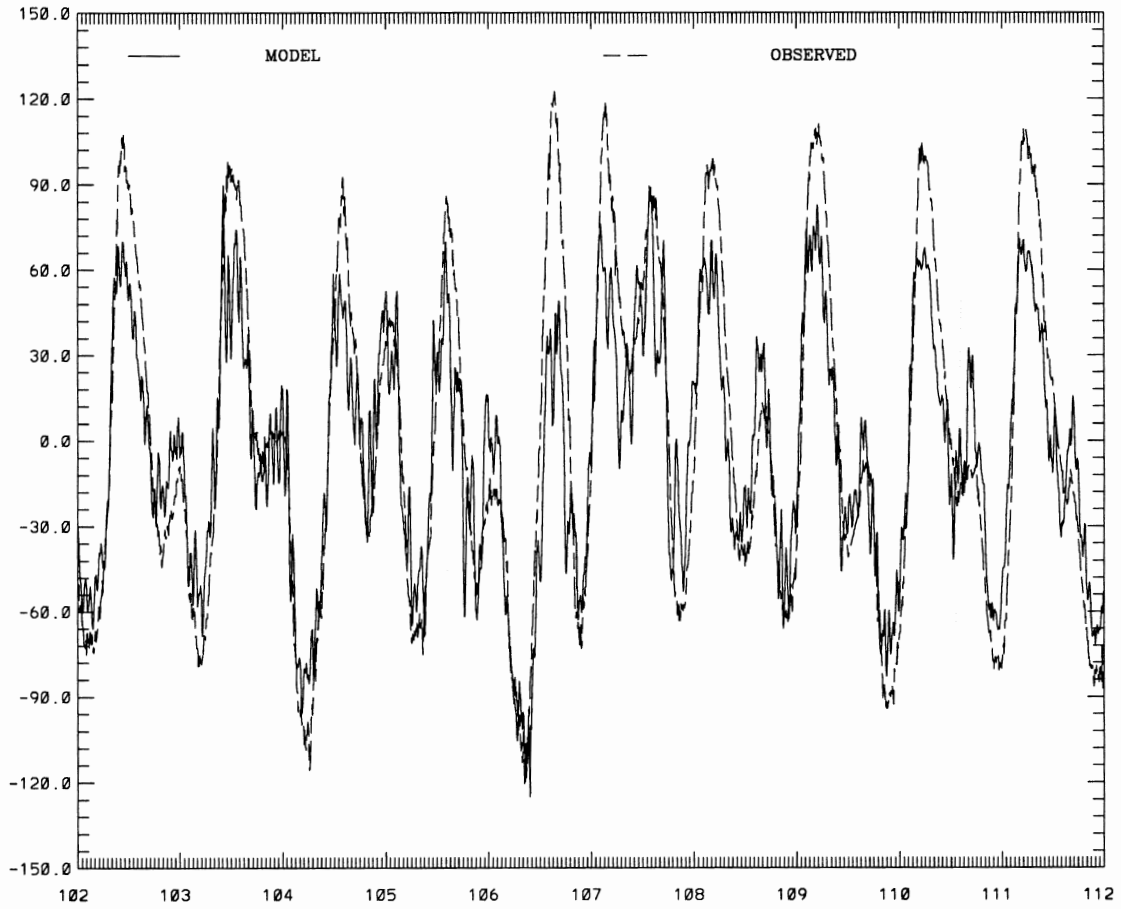


Figure 5.46. HSCM: Bolivar Roads (PORTS) Simulated vs Observed Principal Component Direction Current Comparison during April 1996

PD CURRENT (CM/S) - (FLOOD +)
RMS ERROR = 15.45 IND AGRMT = 0.93

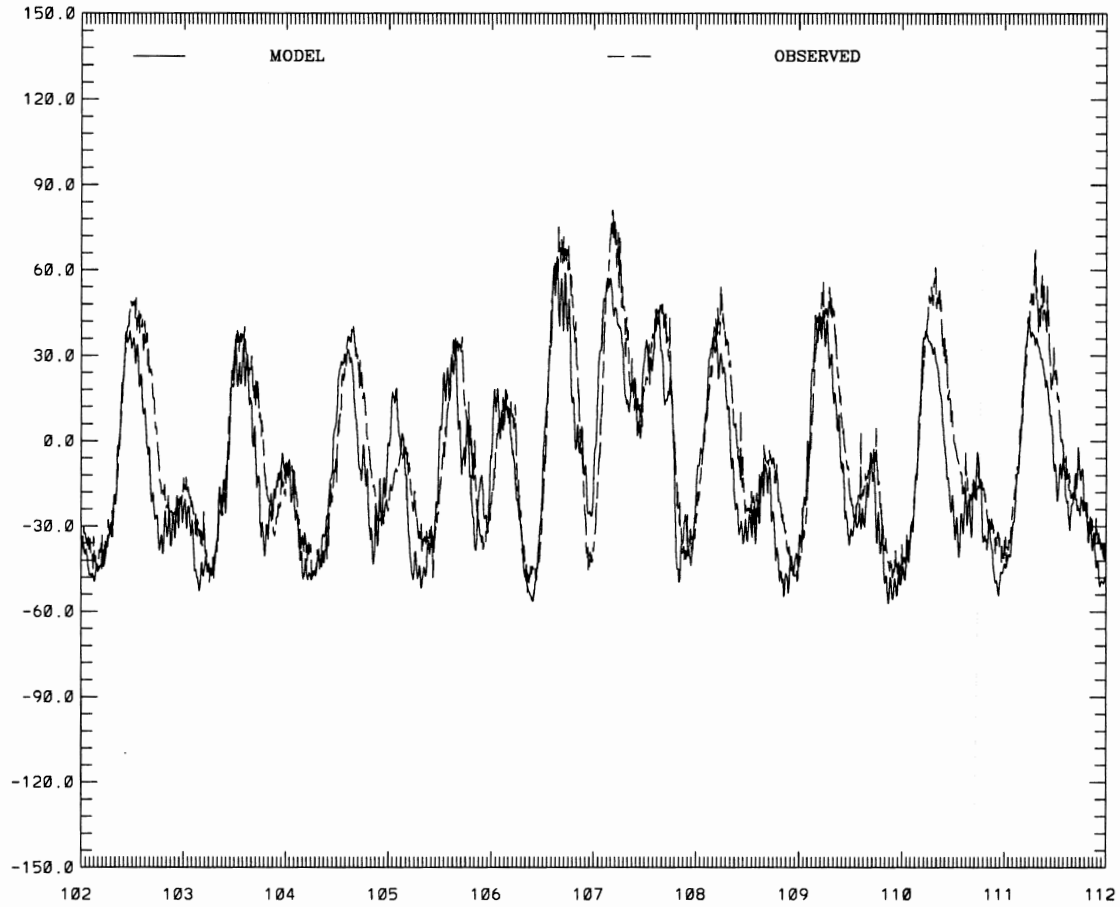


Figure 5.47. HSCM: Redfish Bar (PORTS) Simulated vs Observed Principal Component Direction Current Comparison during April 1996

PD CURRENT (CM/S) - (FLOOD +)
RMS ERROR = 13.15 IND AGRMT = 0.89

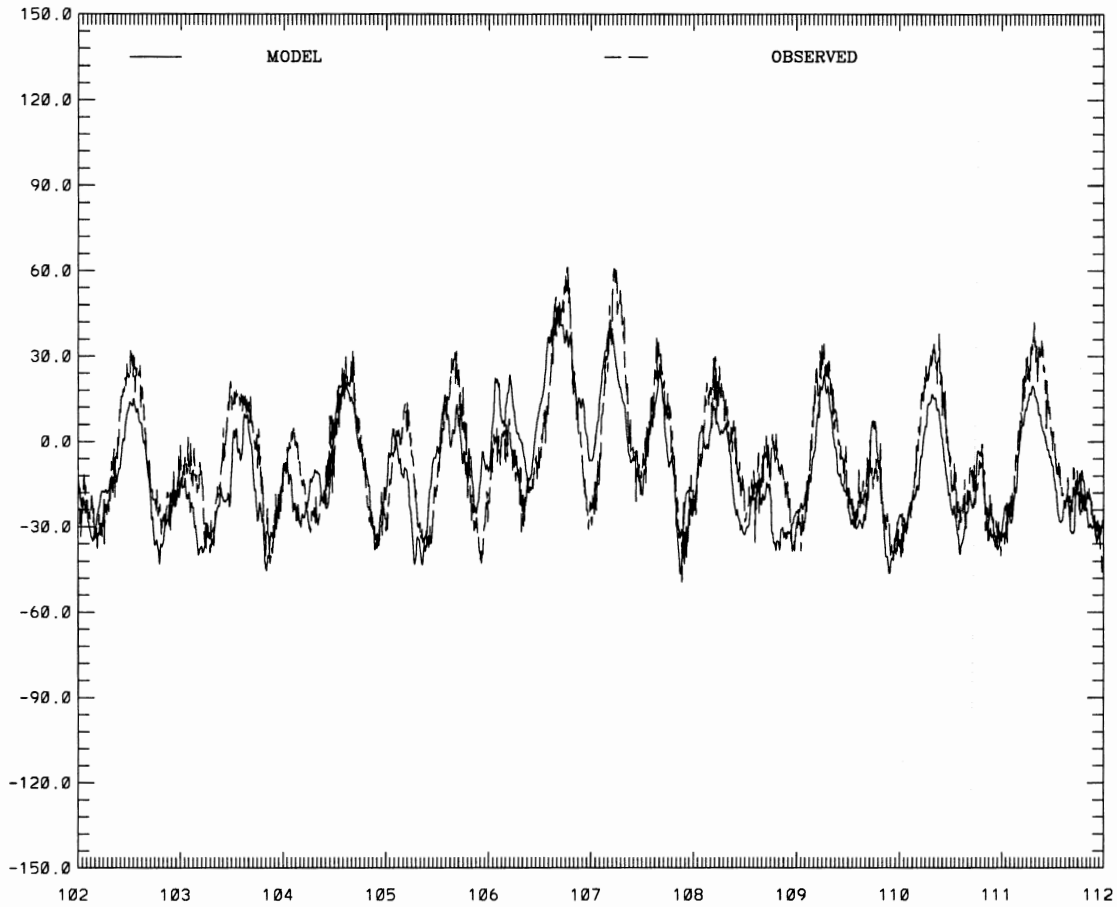


Figure 5.48. HSCM: Morgans Point (PORTS) Simulated vs Observed Principal Component Direction Current Comparison during April 1996

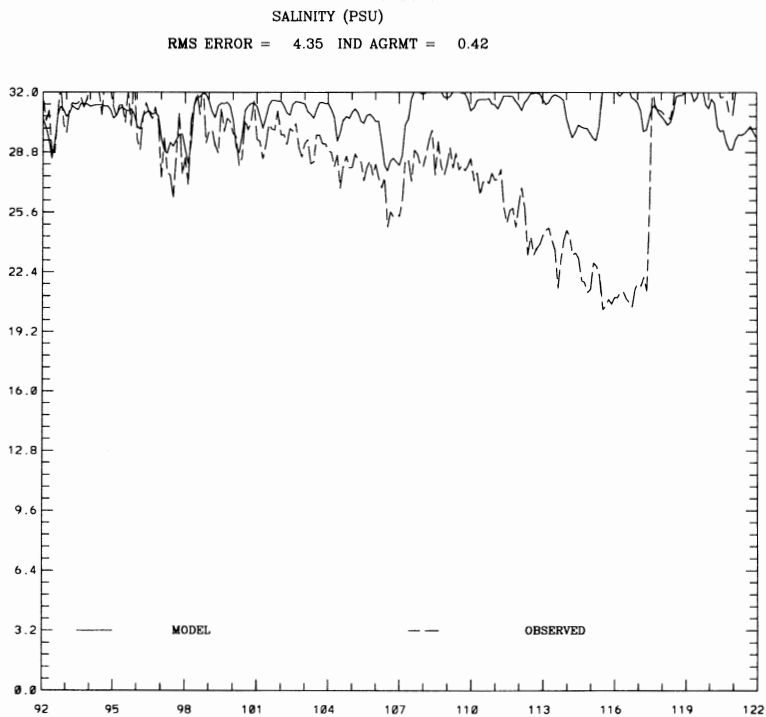


Figure 5.49. HSCM: Port Bolivar Simulated vs Observed Salinity Comparison during April 1996

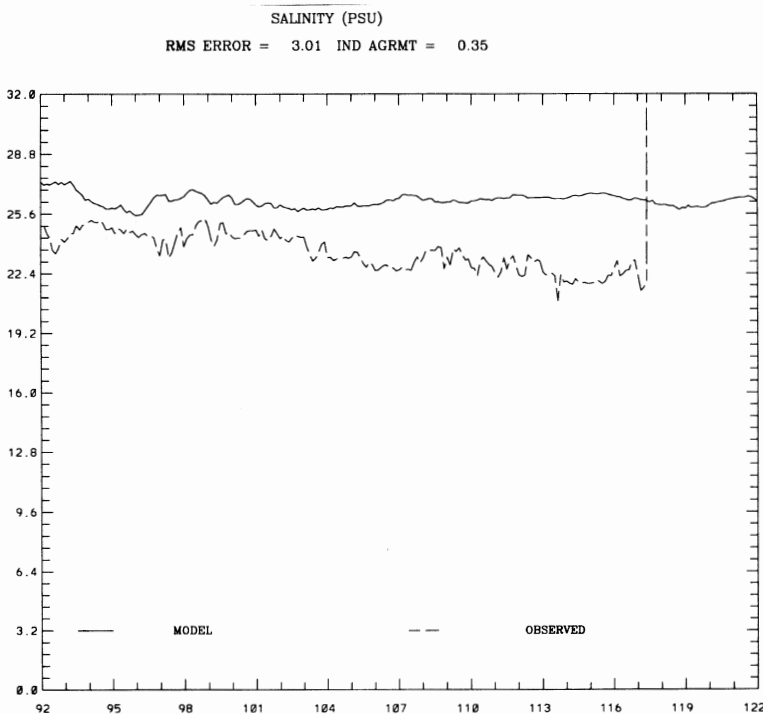


Figure 5.50. HSCM: Red Bluff Simulated vs Observed Salinity Comparison during April 1996

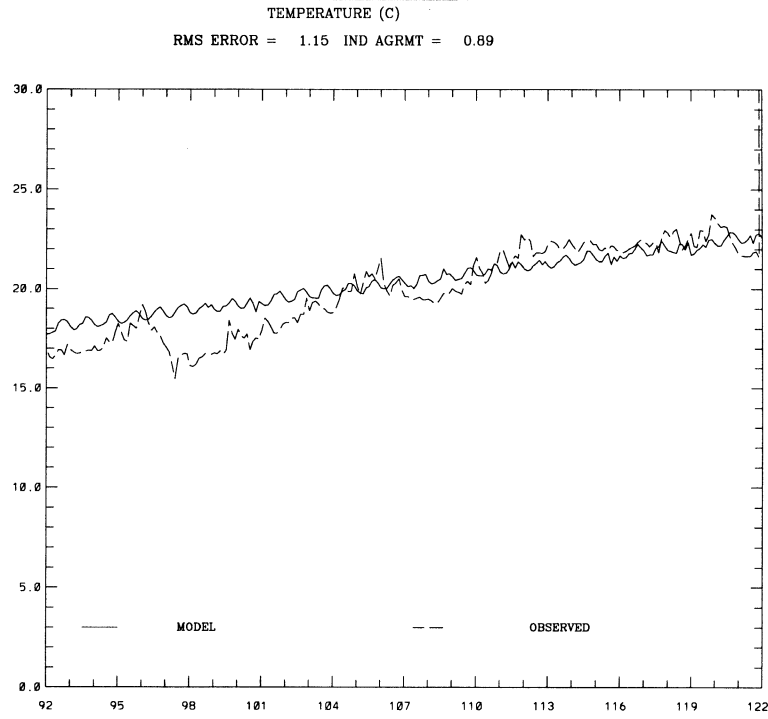


Figure 5.51. HSCM: Port Bolivar Simulated vs Observed Temperature Comparison during April 1996

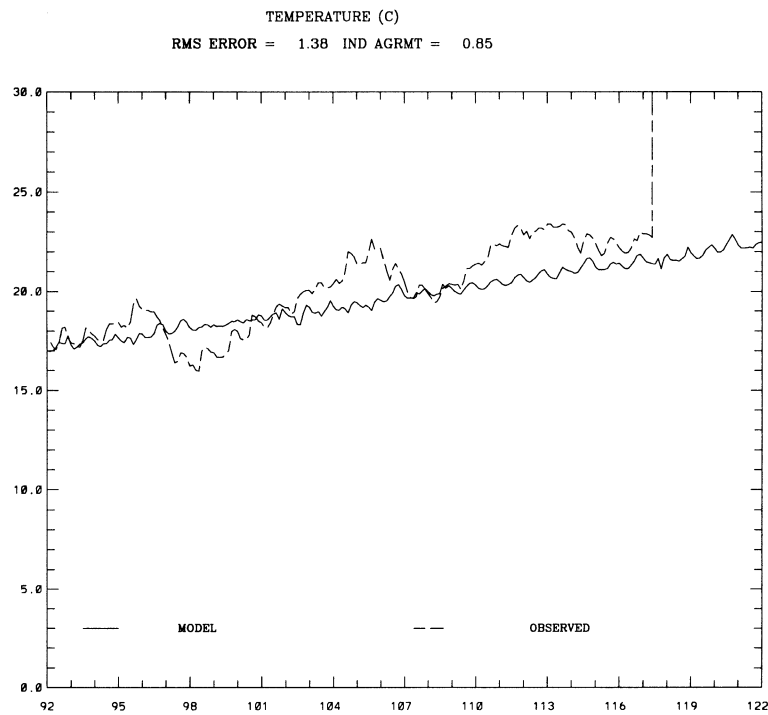


Figure 5.52. HSCM: Red Bluff Simulated vs Observed Temperature Comparison during April 1996

6. CONCLUSIONS AND RECOMMENDATIONS

The NOS Galveston Bay hydrodynamic model (Schmalz, 1996) developed within the NOS Partnership Program has been extended to include bottom emergence/submergence, salinity flux-corrected transport, and atmospheric heat flux. A Barnes (1973) interpolation technique has been developed to provide the model with wind, atmospheric pressure, and additional meteorological fields needed for heat flux (dry and wet bulb temperature and cloud cover). The incorporation of these extensions marked the completion of the development phase of the Galveston Bay hindcast model.

The hindcast model was applied to the October 1994 flood of record and demeaned simulated water levels were in agreement with demeaned observations to order 8 cm in standard deviation (SD), which was in line with the order 10 cm objective. The simulated salinity response exhibited no over or under shooting and was positive definite, indicating the effectiveness of the flux-corrected transport scheme in handling the large horizontal salinity gradient.

Next, the hindcast model was applied to the January 1995 "Northers", during which observed water depths at Round Point went to zero. Simulated water depths remained nonzero. Demeaned simulated water levels were in agreement with demeaned observations to order 8 cm in SD. Additional hindcast studies are needed to further evaluate the emergence/submergence scheme and to aid in the potential development of a over land flooding scheme.

Both the October 1994 and January 1995 hindcast water temperatures appeared to be order 2 to 3 °C cooler than observations. It is recommended that the incoming solar radiation mechanics be further studied: in particular the transmissivity of the earth's atmosphere.

A water level sensitivity analysis to winds and freshwater inflows was performed using the Bay hindcast model. The pursuit of additional improvements in Bay windfields using local high resolution atmospheric models is warranted based on these results. However, NOS and TAMU windfield interpolation techniques are consistent and provide reasonably accurate nowcast windfields; e.g., water levels are generated in agreement with observations in the Upper Bay to order RMSE of 10 cm. It appears that the Galveston Bay nowcast/forecast system represents an extremely challenging problem. Accurate subtidal water level forecasts, Bay windfield forecasts, and streamflow forecasts are all necessary requirements for the system.

A fine resolution Houston Ship Channel Model was developed and one-way coupled to the Galveston Bay hindcast model. The two models combined are used to form the initial hydrodynamic component of the nowcast/forecast system. They were applied using a SST specification to the April 1996 PORTS test period to simulate water levels and currents. Simulated water temperatures were within 1 to 2 °C RMS of observations. The SST specification appears to be sufficient for the nowcast/forecast studies, thereby eliminating the need for further calibration of the heat flux algorithm.

Principal flood direction accuracies were improved in the Houston Ship Channel Model relative to the Galveston Bay Model. However, the current speed accuracies are improved in the Channel model only above Redfish Bar. Simulation results in both models generally met the 20 cm/s RMSE and the 25 degree direction objectives.

There is some indication, that the bathymetry used in the Channel model may be inappropriate through the lower Bay. It is recommended that the more recent 1988 hydrographic datasets for Galveston Bay be used to update both model bathymetries.

Based upon the results of the error budget, a significant portion of the water level and current errors is in the astronomical tidal component in both models. As a result, it is recommended (after the refined bathymetries have been incorporated) that additional experiments be performed focusing on improving tidal response. Refined tidal boundary conditions and further adjustment of bottom friction should be considered. Since the Galveston Bay Model appears to be damped an increase of tidal amplitude of order 10 percent should be investigated. Within the Houston Ship Channel Model, a velocity/transport boundary condition might be explored in addition to further adjustments of the present internal mode radiation scheme.

Additional work on specifying the subtidal signal along the Galveston Bay Model open boundary should also be undertaken. There is some indication that a smoothing of the subtidal signal would reduce the oscillations in simulated coastal water levels.

Of concern is the availability of measurements to assess these three-dimensional models. For water surface elevation, this may be less of a problem than for currents and density. One approach towards alleviating this concern would be to broaden the PORTS system philosophy. Several mobile instrument packs (Mobile-PORTS) might be incorporated to allow for the acquisition of additional data throughout the system in non realtime.

The basic navigational sensors (Navigational-PORTS) would be stationary and could of course be increased, but the mobile sensors would be used to continually obtain additional data and to assess future additional navigational sensor sites. As the model development and PORTS matured, the Mobile-PORTS sensors would either migrate into the Navigational-PORTS or be discontinued for use elsewhere.

ACKNOWLEDGEMENTS

Dr. Bruce B. Parker, Chief of the Coast Survey Development Laboratory, conceived of this project and provided leadership and critical resources. Dr. Parker suggested the performance of the water level sensitivity analysis to aid in the construction of the nowcast/forecast system. Mr. Philip H. Richardson is especially acknowledged for assistance in implementing the meteorological field interpolation algorithms and for developing the wind field and pressure field plots as well as providing overall technical support. Dr. Kurt W. Hess supplied a wealth of information on modeling shallow bay systems. Dr. John G.W. Kelley supplied his versions of the Barnes interpolation over

Lake Erie and was of great assistance. Discussions with Drs. Eugene J. Wei and William P. O'Connor were very useful in evaluating model performance and behaviors.

REFERENCES

Appell, G. F., T. N. Mero, T. D. Bethem, and G. W. French, 1994: The development of a real-time port information system, **IEEE, Journal of Oceanic Engineering**, 19,149-157.

Barnes, S. L., 1973: Mesoscale objective map analysis using weighted time-series observations, **NOAA Technical Memorandum ERL NSSL-62**, National Severe Storms Laboratory, Norman, OK.

Bethem, T. D., and H. R. Frey, 1991: Operational physical oceanographic real-time data dissemination. **Proceedings, IEEE Oceans 91**, 865 - 867.

Blumberg, A. F., and G. L. Mellor, 1987: A description of a three-dimensional coastal ocean circulation model. **Three-Dimensional Coastal Ocean Models**, (ed. Heaps), American Geophysical Union, Washington, DC., 1 - 16.

Buck, A.L., 1981: New equations for computing vapor pressure and enhancement factor, **Journal of Applied Meteorology**,20,1527-1532.

Hess, K. W., R. A. Schmalz, C. E. Zervas, and W. Collier, 1999: Tidal Constituent and Residual Interpolation (TCARI): A New Method for the Tidal Correction of Bathymetric Data. NOAA, National Ocean Service, Coast Survey Development Laboratory, **NOAA Technical Report NOS CS 4**, Silver Spring, MD.

Hess, K. W., 1994: Tampa Bay Oceanography Project: Development and application of the numerical circulation model. NOAA, National Ocean Service, Office of Ocean and Earth Sciences, **NOAA Technical Report NOS OES 005**, Silver Spring, MD.

Hsu, S. A., 1988: **Coastal Meteorology**, Academic Press, Inc., NY.

Ives, D. C. and R. M. Zacharias, 1987: Conformal mapping and orthogonal grid generation, Paper No. 87-2057, **AIAA/SAE/ASME/ASEE 23rd Joint Propulsion Conference**, San Diego, CA.

Kondo, J., 1975: Air-sea bulk transfer coefficients in diabatic conditions, **Boundary-Layer Meteorology**, 9, 91-112.

Large, W.C. and S. Pond, 1981: Open ocean momentum flux measurements in moderate to strong winds, **Journal of Physical Oceanography**,11,324-326.

Lin, S-J., W. C. Chao, Y. C. Sud, and G. K. Walker, 1994: A class of the van-Leer transport schemes and its application to the moisture transport in a general circulation model, **Monthly Weather Review**, 122, 1575-1593.

List, R. J., 1951: Smithsonian Meteorological Tables, **Smithsonian Institution Publication 4014**, Washington, DC.

Marmer, H. A., 1951: Tidal Datum Planes. **U.S. Department of Commerce, Coast and Geodetic Survey, Special Publication No. 135 [revised 1951 edition, reprinted 1977]**, Rockville, MD.

Martin, P. J., 1985: Simulation of the mixed layer at OWS November and Papa with several models, **Journal of Geophysical Research**, 90, C1, 903-916.

Mellor, G. L., 1996: Princeton Ocean Model Users Guide, Program in Oceanic and Atmospheric Sciences, Princeton University.

National Geophysical Data Center, 1987. NOS hydrographic survey data - U.S. Coastal Waters - 15-second gridded data, Data Announcement 87-MGG-12, Boulder, CO.

Orlando, S. P., L. P. Rozas, G. H. Ward, and C. J. Klein, 1993: Salinity characterization of Gulf of Mexico estuaries, **NOAA Tech Memorandum, Office of Ocean Resources Conservation and Assessment**, Silver Spring, MD.

Parker, B. B., 1996 Monitoring and modeling of coastal waters in support of environmental preservation, **Journal of Marine Science and Technology**, 1,75-84.

Payne, R. E., 1972: Albedo of the sea surface, **Journal of the Atmospheric Sciences**,72, 959-970.

Schmalz, R. A., 1994: Long Island Sound Oceanography Project Summary Report, Volume 1: application and documentation of the Long Island Sound three-dimensional circulation model. NOAA, National Ocean Service, Office of Ocean and Earth Sciences, **NOAA Technical Report NOS OES 03**, Silver Spring, MD.

Schmalz, R. A., 1996: National Ocean Service Partnership: DGPS-supported hydrosurvey, water level measurement, and modeling of Galveston Bay :development and application of the numerical circulation model. NOAA, National Ocean Service, Office of Ocean and Earth Sciences, **NOAA Technical Report NOS OES 012**, Silver Spring, MD.

Schureman, P., 1958: Manual of harmonic analysis and prediction of tides. **U.S. Department of Commerce, Coast and Geodetic Survey, Special Publication No. 98 [revised 1940 edition, reprinted 1988]**, Rockville, MD.

Temple, R. F., D. L. Harrington, J. A. Martin, 1977: Monthly temperature and salinity measurements of continental shelf waters of the northwestern Gulf of Mexico, 1963-1965., **NOAA Technical Report NMFS SSRF-707**, Rockville, MD.

Wilken, J. L., 1988: A computer program for generating two-dimensional orthogonal curvilinear coordinate grids, Woods Hole Oceanographic Institution (unpublished manuscript), Woods Hole, MA.

Willmott C. J., S. G. Ackleson, R. E. Davis, J. J. Feddema, K. M. Klink, D.R. Legates, J. O'Donnell, and C. M. Rowe, 1985: Statistics for the evaluation and comparison of models, **Journal of Geophysical Research**, 90, 8995-9005.